ISRES
Publishing

The Eurasia Proceedings of Science, Technology, Engineering & Mathematics

EPSTEM

VOLUME 25 ICBAST CONFERENCE
ISSN: 2602-3199
ISBN: 978-625-6959-30-9

ICBAST 2023: 3rd International Conference on Basic Sciences and Technology (ICBAST)

November 16 - 19, 2023
Antalya, Turkey
Edited by: Prof.Dr. Mehmet Özaslan - Gaziantep University, Turkey

ICBAST 2023 NOVEMBER

Volume 25, Pages 1-195 (November 2023)

The Eurasia Proceedings of Science, Technology, Engineering & Mathematics (EPSTEM)

e-ISSN: 2602-3199

Address: Istanbul C. Cengaver S. No 2 Karatay/Konya/TURKEY

Website: www.isres.org

Contact: isrespublishing@gmail.com

Conference: ICBAST2023 : 3rd International Conference on Basic Sciences and Technology (ICBAST)
Conference website: https://www.2023.icbast.net
Dates: November 16 – 19, 2023
Location: Antalya, Turkey
Edited by: Prof. Dr. Mehmet Özaslan

About Editor
Prof Dr. Mehmet Ozaslan
Department of Biology, Gaziantep University, Turkey
Website: mehmetozaslan.com
Email: ozaslanmd@gantep.edu.tr

Language Editor
Assoc. Prof. Dr. Kagan Buyukkarci
Department of English Language Education, Suleyman Demirel University, Turkey
Email: kaganbuyukkarci@sdu.edu.tr

CONFERENCE PRESIDENT
Prof Dr. Mehmet Ozaslan

Jose Manuel Lopez Guede - University of Basque Country, Spain
Marija STANIĆ - University of Kragujevac, Serbia
Mehmet Ozaslan - Gaziantep University, Turkey
M. Hanefi CALP - Karadeniz Technical University, Turkey
Mohamed Ahmed - Mansoura University, Egypt
Nicu BIZON - Pitesti University, Romania
Pandian VASANT - Teknology Petronas University, Romania
Rajnalkar LAXMAN - Gulbarga University, India
Sanaa AL-DELAIMY - Mosul University, Iraq
Servet YATİN - Quincy College, United States
Shynar BAIMAGANBETOVA - Nazarbayev University, Kazakhstan
Yiyang Chen - Soochow University (CN), China
Zairi Ismael Rizman - MARA University of Technology, Malaysia
Zipporah Pewat DUGURYIL - Federal College of Education, Nigeria

ORGANIZING COMMITTEE

Besnik Hajdari - University "isa Boletini" Mitrovica, Kosovo
Cemil Aydogdu - Hacettepe University
Danielle Gonçalves de Oliveira Prado-Federal Technological University of Paraná, Brazil
Dariusz Jacek Jakóbczak - Technical University of Koszalin, Poland
Halil SNOPCE - South East European University, Macedonia
Jaya Bishnu Pradhan-Tribhuvan University, Mahendra Ratna Campus, Nepal
Mehmet Ozaslan - Gaziantep University, Turkey
Mohammad Sarwar - Scialert, Dubai, United Arab Emirates
Murat Beytur - Kafkas University
M. Hanefi CALP - Karadeniz Technical University, Turkey
Shaymaa Fadhel Abbas Albaayit - Baghdad University, Iraq
Zairi Ismael Rizman - MARA University of Technology, Malaysia

Editorial Policies

ISRES Publishing follows the steps below in the procedings book publishing process.
In the first stage, the papers sent to the conferences organized by ISRES are subject to editorial oversight. In the second stage, the papers that pass the first step are reviewed by at least two international field experts in the conference committee in terms of suitability for the content and subject area. In the third stage, it is reviewed by at least one member of the organizing committee for the suitability of references. In the fourth step, the language editor reviews the language for clarity.

Review Process

Abstracts and full-text reports uploaded to the conference system undergo a review procedure. Authors will be notified of the application results in three weeks. Submitted abstracts will be evaluated on the basis of abstracts/proposals. The conference system allows you to submit the full text if your abstract is accepted. Please upload the abstract of your article to the conference system and wait for the results of the evaluation. If your abstract is accepted, you can upload your full text. Your full text will then be sent to at least two reviewers for review. The conference has a double-blind peer-review process. Any paper submitted for the conference is reviewed by at least two international reviewers with expertise in the relevant subject area. Based on the reviewers' comments, papers are accepted, rejected or accepted with revision. If the comments are not addressed well in the improved paper, then the paper is sent back to the authors to make further revisions. The accepted papers are formatted by the conference for publication in the proceedings.

Aims & Scope

Technology and basic sciences are closely related fields. Developments and innovations in one of them affect the other. Therefore, the focus of the conference is on studies related to these two fields. Studies in the fields of technology and basic sciences are accepted to the conference even if they are not associated with other field. The conference committee thinks that a study in only one field (for example, mathematics, physics, etc.) will contribute to other field (such as technology) in future studies, even if it is not associated with the presentation at the conference. In line with this perspective, studies in the following fields are accepted to the conference: Biology, Chemistry, Physics, Mathematics and Technology.

The aim of the conference is to bring together researchers and administrators from different countries, and to discuss theoretical and practical issues in all fields of technology and basic science.

Articles: 1-20

CONTENTS

Thermal Oxidation Kinetics of Nickel and Dilute (Ni-Al) Alloys / Pages: 187 - 195
Nacer HALEM, Zohra HALEM, Petot Ervas GEORGETTE

The Eurasia Proceedings of Science, Technology,
Engineering & Mathematics (EPSTEM)
ISSN: 2602-3199

The Eurasia Proceedings of Science, Technology, Engineering & Mathematics (EPSTEM), 2023

Volume 25, Pages 1-7

ICBAST 2023: International Conference on Basic Sciences and Technology

Determination of the Coefficient of Thermal Expansion in a Non-Linear Elastic Rod of Two Concentric Layers

Victor Rizov
University of Architecture

Abstract: The present theoretical paper treats the problem of determination of the coefficient of thermal expansion of a rod with two concentric longitudinal layers. The layers exhibit non-linear elastic behaviour. Besides, the layers have different thickness. The rod is exposed to temperature influence. The coefficient of thermal expansion of the rod is derived by analysing the thermal strains in the two layers. Since the layers are connected, the strains in the layers are equal (this fact is used to work out an equation for determining the coefficient of thermal expansion of the rod). The case when the two layers are continuously inhomogeneous along the rod length is also considered. In this case the material properties of the layers vary continuously in longitudinal direction. Here again the layers have non-linear elastic mechanical behaviour. Analysis of the distribution of strains along the length of the rod is carried-out when deriving the coefficient of thermal expansion of the rod. A comparison with the coefficient of thermal expansion of a rod having linear-elastic mechanical behaviour is performed for check-up of the solutions obtained in the present paper.

Keywords: Concentric layers, Rod, Circular section, Coefficient of thermal expansion

Introduction

Layered material systems find wide application in different sectors of modern technics (components of load-carrying structures, electronics, optical devices, sport facilities, engineering infrastructure, aeronautics, aerospace, car industry, etc.) (Dolgov, 2005; Kim et al., 1999; Nguyen et al., 2015). The increased usage of layered material systems in recent decades can be explained mainly by their excellent properties like high strength-to-weight and stiffness-to-weight ratios and very good processability (Rzhanitsyn, 1986; Rizov, 2017). The layered material systems represent combinations of layers made of different engineering materials (Kaul, 2014; Lloyd & Molina Aldareguia, 2003; Rizov, 2018). This fact is a premise for developing of diverse systems which combine in a highly efficient manner the advantages of the constituent materials. Besides, the layers may have different thickness.

In many practical applications in various areas of contemporary engineering layered components are subjected to temperature influence during their life-time. Besides, some layered material systems have non-linear elastic mechanical behaviour, i.e. their stress-strain constitutive law is non-linear. In such cases the Hook's law is not applicable. Also, the coefficients of thermal expansion of the layers are different. Besides, the layers may be manufactured by using inhomogeneous materials like functionally graded materials (the latter represent advanced continuously inhomogeneous composites (Gururaja Udupa et al., 2014; Radhika et al., 2020; Rizov, 2020; Toudehdehghan et al., 2017). In cases when layers are inhomogeneous, the material properties of a layer including the coefficient of thermal expansion change continuously along one or more directions.

The purpose of the present paper is to develop an analytical approach for determination of the coefficient of thermal expansion of a rod with two concentric longitudinal layers which have non-linear elastic mechanical behaviour. The moduli of elasticity and the coefficients of thermal expansion of layers are different. First, the case of homogeneous layers is treated. Then a solution is obtained also for a rod whose layers are continuously

- Selection and peer-review under responsibility of the Organizing Committee of the Conference

inhomogeneous in longitudinal direction. Comparisons with known solutions for the coefficient of thermal expansion are performed for check-up of the solutions derived in this paper.

Coefficient of Thermal Expansion Determination

Consider a rod of circular cross-section with radius, R. The rod is made of two concentric longitudinal layers. The radius of cross-section of the internal layer is r as shown in Fig. 1. The rod is subjected to uniform heating by temperature, Δt. The coefficients of thermal expansion of layers 1 and 2 of the rod are denoted by α_{t1} and α_{t2}, respectively. The layers are homogeneous.

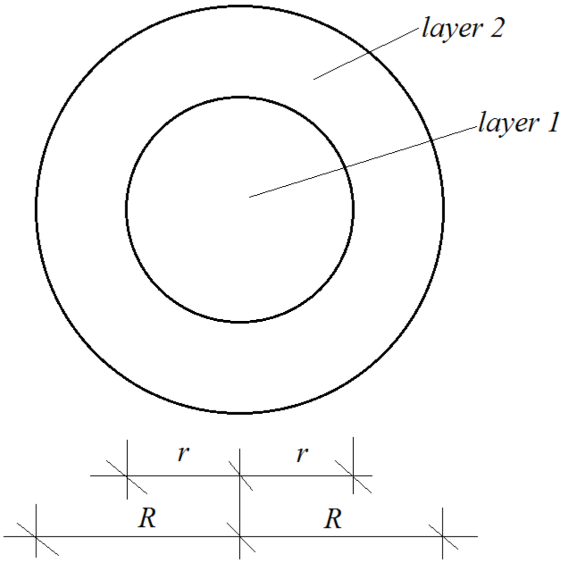

Figure 1. Cross-section of the rod.

The mechanical behaviour of the layers is non-linear elastic. The non-linear constitutive law of layer 1 is expressed by formula (1) (Lukash, 1997), i.e.

$$\sigma_1 = \frac{E_1 \varepsilon}{\sqrt{1 + s_1 \varepsilon^2}}, \tag{1}$$

where σ_1 is the stress, ε is the strain, E_1 is the modulus of elasticity, s_1 is a material property of this layer. Similarly, for the constitutive law of layer 2 of the rod we have

$$\sigma_2 = \frac{E_2 \varepsilon}{\sqrt{1 + s_2 \varepsilon^2}}. \tag{2}$$

Here σ_2 is the stress, ε is the strain, E_2 is the modulus of elasticity, s_2 is a material property. The purpose of the present analysis is to derive the coefficient of thermal expansion, α_{tc}, of the rod. As known, the prolongation, Δl_t, of the rod due to heating can be calculated by applying formula (3), i.e.

$$\Delta l_t = \alpha_{tc} \Delta t\, l, \tag{3}$$

where l is length of the rod.

The following approach is used here to derive α_{tc}. If the layers of the rod are not connected their prolongation can calculated by formulas (4) and (5), i.e.

$$\Delta l_{t1} = \alpha_{t1}\,\Delta t\,l\,, \tag{4}$$

$$\Delta l_{t2} = \alpha_{t2}\,\Delta t\,l\,, \tag{5}$$

where α_{t1} and α_{t2} are the coefficients of thermal expansion of layers 1 and 2, respectively. However, the rod layers are connected. As a result of this the prolongations of the layers are equal. This induces axial forces in layers 1 and 2 denoted by N_{t1} and N_{t2}, respectively. The prolongations, Δl_{Nt1} and Δl_{Nt2}, of the layers due to axial forces are found by formulas (6) and (7), i.e.

$$\Delta l_{Nt1} = \varepsilon_1 l\,, \tag{6}$$

$$\Delta l_{Nt2} = \varepsilon_2 l\,, \tag{7}$$

where the strains, ε_1 and ε_2, are found as

$$\varepsilon_1 = \frac{\sigma_1}{\sqrt{E_1^2 - s_1\sigma_1^2}}\,, \tag{8}$$

$$\varepsilon_2 = \frac{\sigma_2}{\sqrt{E_2^2 - s_2\sigma_2^2}}\,. \tag{9}$$

Formulas (8) and (9) are obtained by solving (1) and (2) with respect to strain. By using formulas (4) – (9), the prolongations of layers 1 and 2 of the rod due to heating and to axial forces are written as

$$\Delta l_1 = \Delta l_{t1} + \Delta l_{Nt1} = \alpha_{t1}\Delta t l + \frac{l\sigma_1}{\sqrt{E_1^2 - s_1\sigma_1^2}}\,, \tag{10}$$

$$\Delta l_2 = \Delta l_{t2} + \Delta l_{Nt2} = \alpha_{t2}\Delta t l + \frac{l\sigma_2}{\sqrt{E_2^2 - s_2\sigma_2^2}}\,. \tag{11}$$

Since the layers of the rod are connected, their prolongations are equal, i.e.

$$\Delta l_1 = \Delta l_2\,. \tag{12}$$

From (10), (11) and (12), we obtain

$$\alpha_{t1}\Delta t l + \frac{l\sigma_1}{\sqrt{E_1^2 - s_1\sigma_1^2}} = \alpha_{t2}\Delta t l + \frac{l\sigma_2}{\sqrt{E_2^2 - s_2\sigma_2^2}}\,. \tag{13}$$

The stresses, σ_1 and σ_2, in equation (13) are unknowns. One complementary equation is written by considering the equilibrium of the axial forces, N_{t1} and N_{t2}, in the layers of the rod, i.e.

$$N_{t1} = N_{t2}\,. \tag{14}$$

Since

$$N_{t1} = \sigma_1 A_1 \tag{15}$$

and

$$N_{t2} = \sigma_2 A_2 \tag{16}$$

formula (14) takes the following form

$$\sigma_1 A_1 = \sigma_2 A_2, \tag{17}$$

where the areas, A_1 and A_2, of the cross-sections of layers 1 and 2 are found as

$$A_1 = \pi r^2, \tag{18}$$

$$A_2 = \pi(R^2 - r^2). \tag{19}$$

The stresses are derived from equations (13) and (17) by MatLab. In order to determine α_{tc} we equalize Δl and Δl_{t1}, i.e.

$$\Delta l = \Delta l_{t1}. \tag{20}$$

Finally, by inserting of (3) and (10) in (20), we obtain the following equation with unknown, α_{tc} :

$$\alpha_{tc} \Delta t\, l = \alpha_{t1} \Delta t\, l + \frac{l \sigma_1}{\sqrt{E_1^2 - s_1 \sigma_1^2}}. \tag{21}$$

Equation (21) is solved with respect to α_{tc}, i.e.

$$\alpha_{tc} = \alpha_{t1} + \frac{\sigma_1}{\Delta t \sqrt{E_1^2 - s_1 \sigma_1^2}}. \tag{22}$$

Expression (22) is checked-up in the following way. It is clear from formulas (1) and (2) that at $s_1 = s_2 = 0$ the non-linear constitutive laws transform into the Hook’s law, i.e.

$$\sigma_1 = E_1 \varepsilon, \tag{23}$$

$$\sigma_2 = E_2 \varepsilon. \tag{24}$$

This fact indicates that at $s_1 = s_2 = 0$ formula (22) for the coefficient of thermal expansion of the non-linear elastic rod derived in this paper should transform into the formula for the coefficient of thermal expansion of the linear-elastic rod. We are going to check-up this. For this purpose, we substitute $s_1 = s_2 = 0$ in (13) and (22) and by carrying-out some mathematical transformations we derive

$$\alpha_{tc} = \frac{\alpha_{t1} E_1 A_1 + \alpha_{t2} E_2 A_2}{E_1 A_1 + E_2 A_2}. \tag{25}$$

By inserting of (18) and (19) in (25), we have

$$\alpha_{tc} = \frac{\alpha_{t1} E_1 r^2 + \alpha_{t2} E_2 \left(R^2 - r^2\right)}{E_1 r^2 + E_2 \left(R^2 - r^2\right)}. \tag{26}$$

The fact that (26) coincides with the expression for the coefficient of thermal expansion of a linear-elastic rod published in (Hoa et al., 2003) is a check-up of (22).

The case of a non-linear elastic rod with two concentric layers which are continuously inhomogeneous in longitudinal direction is also considered. The rod cross-section is shown in Fig. 1. The moduli of elasticity and the coefficients of thermal expansion of the two layers change continuously along the rod length, i.e.

$$E_1 = E_1(x), \tag{27}$$

$$E_2 = E_2(x), \tag{28}$$

$$\alpha_{t1} = \alpha_{t1}(x), \tag{29}$$

$$\alpha_{t2} = \alpha_{t2}(x), \tag{30}$$

where

$$0 \le x \le l. \tag{31}$$

In formulas (27) – (30) x is the longitudinal centroidal axis of the rod. The prolongations of the two layers due to heating are written as

$$\Delta l_{t1} = \int_0^l \alpha_{t1} \Delta t \, dx, \tag{32}$$

$$\Delta l_{t2} = \int_0^l \alpha_{t2} \Delta t \, dx. \tag{33}$$

The prolongations of the two layers induced by the axial forces are expressed as

$$\Delta l_{Nt1} = \int_0^l \varepsilon_1 dx, \tag{34}$$

$$\Delta l_{Nt2} = \int_0^l \varepsilon_2 dx. \tag{35}$$

By combing of (8), (9), (32), (33), (34) and (35) we derive the following expressions for the prolongations of layers 1 and 2 of the continuously inhomogeneous rod due to heating and to axial forces:

$$\Delta l_1 = \int_0^l \alpha_{t1} \Delta t dx + \int_0^l \frac{\sigma_1}{\sqrt{E_1^2 - s_1 \sigma_1^2}} dx, \tag{36}$$

$$\Delta l_2 = \int_0^l \alpha_{t2} \Delta t dx + \int_0^l \frac{\sigma_2}{\sqrt{E_2^2 - s_2 \sigma_2^2}} dx. \tag{37}$$

The prolongations of the layers are equal, i.e.

$$\int_0^l \alpha_{t1} \Delta t dx + \int_0^l \frac{\sigma_1}{\sqrt{E_1^2 - s_1 \sigma_1^2}} dx = \int_0^l \alpha_{t2} \Delta t dx + \int_0^l \frac{\sigma_2}{\sqrt{E_2^2 - s_2 \sigma_2^2}} dx. \tag{38}$$

Equations (17) and (38) are solved with respect to stresses, σ_1 and σ_2.
By equalizing of (3) and (36) we have

$$\alpha_{tc}\,\Delta t\, l = \int_0^l \alpha_{t1}\Delta t dx + \int_0^l \frac{\sigma_1}{\sqrt{E_1^2 - s_1\sigma_1^2}} dx\,. \tag{39}$$

From equation (39) we determine

$$\alpha_{tc} = \frac{1}{\Delta t\, l}\left(\int_0^l \alpha_{t1}\Delta t dx + \int_0^l \frac{\sigma_1}{\sqrt{E_1^2 - s_1\sigma_1^2}} dx \right). \tag{40}$$

It should be mentioned that when α_{t1} and E_1 are constants (i.e., α_{t1} and E_1 do not change along the length of the rod) formula (40) transforms into expression (25) for the coefficient of thermal expansion of a non-linear elastic rod with two concentric layers which are homogeneous in longitudinal direction.

Conclusion

The problem for determination of the coefficient of thermal expansion of a rod with two concentric layers is considered theoretically. The rod has non-linear elastic behaviour that is treated by using a smooth stress-strain relationship. First, the case of a rod with two homogeneous layers is analyzed. Equations for determination of the coefficient of thermal expansion are worked out by analyzing the strains in the rod and by considering the equilibrium of axial forces in the two layers. The expression for the coefficient of thermal expansion obtained in the present paper is checked-up by comparing with a known formula for the coefficient of thermal expansion of a rod having linear-elastic behaviour (it is shown that the expression derived transforms into the known formula by substituting of $s_1 = s_2 = 0$ in the equations for obtaining the coefficient of thermal expansion. The problem of determination of the coefficient of thermal expansion of a non-linear elastic rod with two concentric layers which are made of materials that are continuously inhomogeneous in longitudinal direction is also treated. The coefficients of thermal expansions determined in the present paper can be applied for calculating the prolongations of non-linear elastic rods under heating. The equations worked out can also be used for analyzing the stressed and strained state of the rod layers due to heating. It should be noted that the approach for determining the coefficient of thermal expansion presented in this paper can be developed further by considering various non-linear stress-strain relationships and laws for distributions of material properties of the inhomogeneous layers in longitudinal direction.

Recommendations

The theoretical approach presented in this paper can be used for determination of the coefficient of thermal expansion of rods with two concentric layers having non-linear elastic behavior.

Scientific Ethics Declaration

The author declares that the scientific ethical and legal responsibility of this article published in EPSTEM journal belongs to the author.

Acknowledgements or Notes

* This article was presented as an oral presentation at the International Conference on Basic Sciences and Technology (www.icbast.net) held in Antalya/Turkey on November 16-19, 2023.

References

Dolgov, N. (2005). Determination of stresses in a two-layer coating. *Strength of Materials, 37, 422-431.*

Hoa, S.V., Gay, D., & Tsai, S W. (2003). *Composite materials* (1st ed.). Boca Raton: CRC Press.

Kaul, A. B. (2014). Two-dimensional layered materials: Structure, properties, and prospects for device applications, *Journal of Material Research*, *29*, 348-361.

Kim, J. S., Paik, K.W., & Oh, S. H. (1999). The multilayer-modified Stoney's formula for laminated polymer composites on a silicon substrate. *Journal of Applied Physics, 86*, 5474–5479.

Lloyd, S.J., & Molina-Aldareguia, J. M. (2003), Multilayered materials: a palette for the materials artist. *Phil. Transactions R. Soc. Lond. A, 361*(1813), 2931-2940.

Lukash, P. (1997). *Fundamentals of non-linear structural mechanics*. Science.

Nguyen, S. N., Lee, J., & Cho, M. (2015). Efficient higher-order zig-zag theory for viscoelastic laminated composite plates. *International Journal of Solids and Structures, 62, 174-185.*

Radhika, N., Sasikumar, J., Sylesh, J. L., & Kishore, R. (2020). Dry reciprocating wear and frictional behaviour of B4C reinforced functionally graded and homogenous aluminium matrix composites. *Journal of Materials Research and Technology*, *9*(2), *1578-1592.*

Rizov, V. I. (2020). Longitudinal vertical crack analysis in beam with relaxation stresses. *World Journal of Engineering, 18*(3), 452-457.

Rizov, V.I. (2017). Analysis of longitudinal cracked two-dimensional functionally graded beams exhibiting material non-linearity. *Frattura ed Integrita Strutturale, 11*(41), *498-510.*

Rizov, V.I. (2018). Analysis of cylindrical delamination cracks in multilayered functionally graded non-linear elastic circular shafts under combined loads. *Frattura ed Integrità Strutturale, 12*(46), 158-17.

Rzhanitsyn, A.R. (1986). *Built-up bars and plates*. Stroyiizdat.

Toudehdehghan, J., Lim, W., Foo1, K. E., Ma'arof, M. I. N., & Mathews J. (2017). A brief review of functionally graded materials. *MATEC Web of Conferences, 131.*

Udupa, G., Rao, S. S., & Gangadharan, K. V. (2014). Functionally graded composite materials: An overview. *Procedia Materals Science, 5,* 1291-1299.

Author Information

Victor Rizov
University of Architecture
Sofia, Bulgaria
Contact e-mail: *v_rizov_fhe@uacg.bg*

To cite this article:

Rizov, V. (2023). Determination of the coefficient of thermal expansion in a non-linear elastic rod of two concentric layers. *The Eurasia Proceedings of Science, Technology, Engineering & Mathematics (EPSTEM), 25,* 1-7.

The Eurasia Proceedings of Science, Technology, Engineering & Mathematics (EPSTEM), 2023

Volume 25, Pages 8-16

ICBAST 2023: International Conference on Basic Sciences and Technology

Synthesis and Characterization of 3,6 - Disubstituted Carbazole Containing Fluorene and DSSC Applications

Betul Derince
University of Eskisehir Osmangazi

Kamuran Gorgun
University of Eskisehir Osmangazi

Evrim Hur
University of Eskisehir Osmangazi

Yasemin Caglar
Eskisehir Technical University

Mujdat Caglar
Eskisehir Technical University

Abstract: Heterocyclic compounds containing nitrogen are regarded as essential structural motifs present in numerous natural products and organic materials. Within this group, carbazoles are important hetero-aromatic molecules which play a significant role in the development of materials with various functionalities. Carbazole derivatives play a crucial role in various organic electronic devices such as organic transistors (OTFTs), organic light-emitting diodes (OLEDs), and organic solar cells. In this study, the solubility of the carbazole nucleus, which initially had limited solubility in organic solvents, was increased by adding an octyl group. Next, a carbazole-based compound 3,6-di(fluorene-9)-9-octyl-9H-carbazole (IV) was synthesized via the Suzuki-Miyaura cross-coupling reaction (Figure 1). The photophysical and thermal properties of this compound were determined by UV-Vis, thermogravimetric analysis (TGA) and differential thermal analysis (DTA). The HOMO and LUMO energy levels and the optical band gap (E_g,opt) were obtained by cyclic voltammetry (CV) and absorption bands. TiO_2-based dye-sensitized solar cells (DSSCs) were fabricated using compound IV. The photoelectrochemical properties of the resulting TiO_2-DSSCs were measured.

Keywords: Carbazole, Suzuki-Miyaura cross-coupling reactions, Cyclic Voltammetry, DSSC.

Introduction

Carbazole is a class of aromatic ring compounds with the molecular formula $C_{12}H_9N$, containing nitrogen, and is associated with conjugated structures known for their electron and charge transfer properties (Bouaziz et al., 2015; Behrens, 1900). Carbazole was first discovered by Graebe and Glaser in 1872 when they isolated it from coal tar (Bouaziz et al., 2015). Carbazole exhibits strong fluorescence when exposed to ultraviolet (UV) light, a characteristic that makes it frequently used in the production of photographic plates and in paint manufacturing (Drechsel, 1858). This compounds can be substituted at the nitrogen position, and they can be substituted at the 3- and 6-positions to yield 3,6-carbazoles or at the 2- and 7-positions to yield 2,7-carbazoles (Doskocz et al., 2006). Fluorene is a white crystalline hydrocarbon compound known for its strong fluorescence properties. Additionally, fluorene is found in small quantities in coal tar and can also be synthetically produced, with a chemical formula of $C_{13}H_{10}$. Fluorene belongs to a group of chemicals known as polycyclic aromatic

---

hydrocarbons (PAHs), and its derivatives can be modified and used in advanced materials. It is also commonly used in paints and optical brightening agents. Furthermore, fluorene is widely used as a ligand (Zou et al., 2007; Han & Wang, 2009). Due to its high donor and acceptor properties, various applicable methods have been developed for the synthesis of fluorene derivatives in organometallic chemistry and various coordination mechanisms (Xu et al., 2015). The literature also mentions the creation of a series of oligofluorenes (OFs) with increasing conjugation lengths, which can be attached at the 2- and 7-positions (Abbel et al., 2009). Fluorene exhibits a planar structure due to the freedom of rotation around the biphenyl bond (Abbel et al., 2009).

According to research by Venkateswararao and colleagues, incorporating the phenyl/fluorene/carbazole unit has allowed for the modification of the conjugation bridge between the donor and acceptor in organic solar cells. Fluorene and carbazole, as electron-rich units, have improved the redox stability of dyes and their dye regeneration tendencies. In this study, they used carbazole compounds as donors in organic solar cells due to their good thermal and electrochemical stability and their hole-transporting properties. They assumed that adding fluorene units would effectively enhance conjugation and serve as an effective charge-delocalizing segment, especially when compared to 3,6-substituted carbazoles. The newly developed dyes outperformed their counterparts with simple phenyl spacer units in terms of optical and electrochemical properties. Experimentally determined values included a V_{oc} value of 634-636 mV and efficiency percentages of 4.20-4.62. The results suggested that the addition of fluorene and carbazole units provided benefits to optical and electrochemical processes, and it was also observed that fluorene units generally increased molar extinction coefficients in absorption (Venkateswararao et al., 2012).

In this study, 3,6-disubstituted carbazole compound containing fluorene was synthesized using bromination, alkylation, and Suzuki-Miyaura cross-coupling reactions. In these reactions, fluorene, known for its high fluorescence and electron-deficient properties at the -3 and -6 positions of carbazole, was used with fluorene boronic acid, enhancing conjugation. The structural characterizations of this synthesized compound were determined using FT-IR, ^{1}H-NMR, ^{13}C-NMR, and elemental analysis, and photophysical and thermal gravimetric analyses were conducted using UV-Vis, FL, TGA-DTA spectra. After elucidating the structure of the synthesized carbazole derivative, its potential use as a dye in TiO_2-based Dye-Sensitized Solar Cells (DSSCs) with a new electron donor-hole system was investigated.

Materials and Method

Instruments and Measurements

All chemicals and solvents used in the reactions were sourced from Sigma Aldrich (Turkey) and abcr. Organic solvents were of HPLC grade or purified using standard procedures. Milli-Q grade water (18.2 MΩ cm) was used for all experiments. FT-IR spectra of all compounds were obtained using a Bruker FT-IR Spectrophotometer (4000-400 cm^{-1}). NMR spectra were recorded in $CDCl_3$ with TMS as the internal standard for ^{1}H-NMR (500 MHz) or an appropriate solvent as the internal standard for ^{13}C-NMR (125 MHz) using a Jeol ECZ500R (11.75 Tesla) NMR instrument. The UV-Vis absorption spectra of the target compound were acquired using a SHIMADZU UV2450 UV-Vis scanning spectrophotometer, while fluorescence spectra were obtained with a Perkin–Elmer LS-55 spectrophotometer. Thermal analyses were conducted using a Perkin Elmer STA 8000 instrument (25°C-1600°C) in the Central Research Laboratory Application and Research Center (ARUM). The current-voltage characteristics of the Dye-Sensitized Solar Cells (DSSCs) were recorded using a FYTRONIX OPTOSENSE solar cell measurement system, with a voltage sweep rate of 0.01V/s under AM1.5G conditions.

Synthesis of Sensitizer IV

The synthesis method and scheme used to achieve the target compound are summarized in Scheme 1

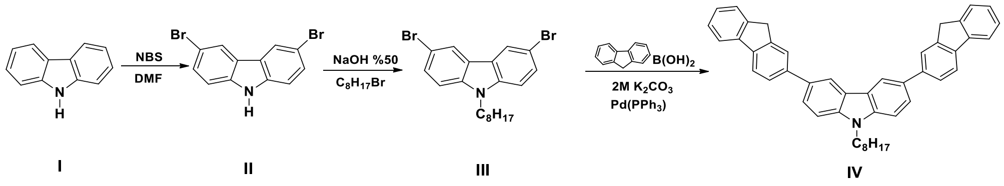

Figure 1. Synthesis scheme of compounds II, III and IV

.Synthesis of 3,6-dibromo-9H-carbazole (II) and Synthesis of 3,6-dibromo-9-octyl-9H-carbazole (III) (Derince et al., 2022). Bromination (II) and alkylation (III) reactions were carried out, as in our previous studies (Derince et al., 2022), to activate the 9H-carbazole and enhance its solubility, and these reactions were characterized.

Synthesis of 3,6-di(9H-fluorene-2-yl)-9-octyl-9H-carbazole (IV)

Reaction of Suzuki Miyaura coupling (Miyaura, 2004) 3,6-dibromo-9-octyl-9H-carbazole (1 eq.) with of fluorene-2-boronic acid (2.2 eq.) catalyzed by 2% Pd(PPh$_3$)$_4$ and 2M K$_2$CO$_3$ (7.5 eq.) was carried out in a mixture of water and 1,2-dimethoxyethane (2:1, DME/H$_2$O, v/v). Reaction mixture was continued at 80°C for 24h. in N$_2$ atmosphere. Crude product was washed with DCM and water. It was obtained which the residue was purified by column chromatography (silica gel, petroleum ether: DCM (5:1), affording 3,6-di(9H-fluorene-2-yl)-9-octyl-9H-carbazole (IV) as a yellowish powder. Isolated yield: (75%) ^{1}H-NMR (500 MHz, CDCl$_3$, δ ppm): 8.45 (qz s, 2H), 7.91(s, 2H), 7.87 (d, 2H *J*=7.96 Hz), 7.81 (d, 2H, *J*=7.63Hz), 7.79(dd, 2H, *J*=8.48Hz), 7.76 (dd, 2H, *J*=8.00 Hz), 7.56 (d, 2H, *J*=7.44 Hz), 7.49 (d, 2H, *J*=8.89 Hz), 7.39 (t, 2H *J*=8.16 Hz), 7.30(t, 2H, *J*=8.46 Hz), 4.24 (t, 2H), 4.00 (s, 4H), 1.82 (m, 2H), 1.20-1.30 (m, 10H), 0.85 (t, 3H). ^{13}C NMR (125 MHz, CDCl$_3$, δ ppm): 143.971, 141.610, 140.803, 140.362, 132.644, 126.799, 126.511, 125.407, 125.042, 123.890, 123.545, 120.137, 119.859, 118.947, 109.089, 37.051, 31.820, 29.420, 29.209, 27.366, 22.624, 14.100.

TiO$_2$-DSSC Fabrication

Commercially available TiO$_2$ photoanodes (were kept in the dark for 1 day in a chloroform solution containing the new 3,6-disubstituted carbazole compound containing fluorene sensitizer (IV) with a concentration of 1x10^{-3} M. It was observed that the photoanodes absorbed the dyes during this 24-hour period. After 24 hours, these electrodes were removed from the solution, washed with ethanol, dried on a 100°C heater, and then covered with Meltonix (a transparent sealing film). Iodine solution [iodide/triiodide (I$^-$/I^{-3})] was injected onto the films, and they were sealed with a platinum-coated electrode. Thus, the fabrication of Dye-Sensitized Solar Cells (DSSCs) was completed.

Results and Discussion

Absorption and Emission Properties of Synthesized IV

To determine the photophysical properties of the compound synthesized for dye-sensitized solar cells (DSSC), different polarity solvents (THF, DMF, DCM, DMSO, and TOLUEN) were selected and used to measure the maximum absorption and emission wavelengths. In studies conducted with the Fluorene fluorophore, Wang and colleagues (Chen et al., 2022) observed bathochromic shifts in the emission spectra with increasing solvent polarity (TOLUEN < THF < EtOH < H$_2$O). Compound number IV, which we synthesized, also contains both carbazole and fluorene groups, and it has been observed that bathochromic shifts occur with increasing solvent polarity. The UV-Vis absorption and emission spectra of this compound in various polar solvents are shown in Figure 2(a) and Figure 2(b).

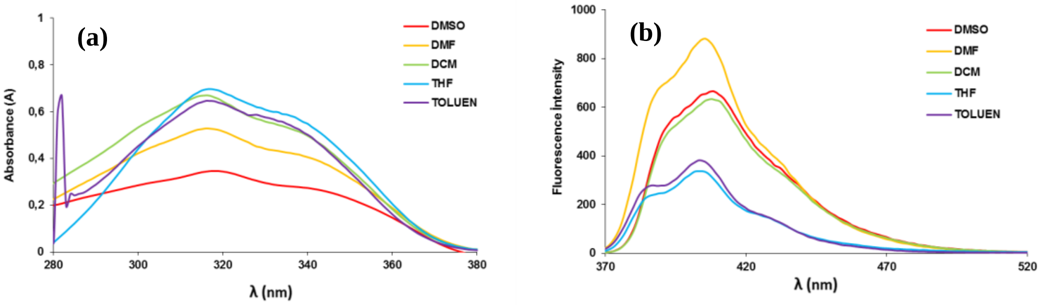

Figure 2. (a) UV-Vis (Ultraviolet-Visible) Spectrum of 3,6-di(9H-fluoren-2-yl)-9-octyl-9H-carbazole (10^{-5} M) (b) Fluorescence Spectrum of 3,6-di(9H-fluoren-2-yl)-9-octyl-9H-carbazole (10^{-7} M)

When the photophysical properties of the π-conjugated systems were examined based on the UV-Vis absorption spectra, it was observed that the absorption values of the π-π* transitions in the synthesized molecules, influenced by the carbazole groups, varied between 294.0 nm and 306.0 nm (Figure 2(a)). According to the absorption spectra of compound IV in different solvents, the absorptions observed between 316.0 nm in DCM shifted to 318.0 nm in DMSO solvent. This can be explained as a bathochromic shift in the chromophore substitution absorption due to the increase in solvent polarity.

When the emission spectra of compound IV in different solvents were examined, a bathochromic shift was observed at 405.5 and 400.0 nm in DMSO solvent, respectively, while a hypsochromic shift was observed in the emission spectra at 388.5 and 389.0 nm in toluene solvent with decreasing solvent polarity. Additionally, the solvatochromic effect of these compounds was calculated using the Stokes shift value, which demonstrated a bathochromic shift in DMSO solvent (Table 1).

Table 1. Absorption and emission data of compounds IV in various solvents.

Compound	Solvent	$\lambda_{(max)\ abs}$ (nm)	$\lambda_{(max)\ ems}$ (nm)	Stokes shift ($cm^{-1}\,M^{-1}$)	□ ($cm^{-1}\,M^{-1}$)
IV	DMSO	318	408	6937	34634
	DMF	316	405	6954	52869
	DCM	316	408	7135	64987
	THF	317	403	6732	69703
	TOLUEN	316	404	6893	64644

Thermal Stability of Synthesized IV

The thermal stability of the compound with the determined IV number, synthesized in accordance with the target, was investigated using thermal gravimetric analysis (TGA) and differential thermal analysis (DTA), and these data are presented in Figure 3.

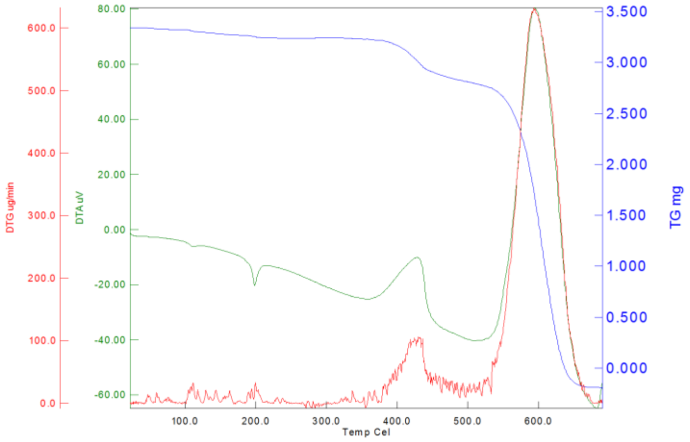

Figure 3. TGA mass loss and DTA plots of compounds IV taken under N_2 atmosphere.

The temperature data for this compound was observed to be 285.72˚C, which corresponds to the temperature of thermal decomposition with a 5% mass loss. Based on the thermal stability data of the synthesized compound IV, it was found to exhibit good thermal stability.

FT-IR Spectra of Synthesized II, III and IV Compounds

All spectra were displayed in Figure 4 for determining the functional groups in the synthesized compounds. In the synthesis of a new conjugated system containing donor and π-spacer groups, a bromination reaction was carried out using *N*-bromosuccinimide with carbazole as the starting material, resulting in the formation of 3,6-dibromocarbazole (II). According to the FT-IR spectrum, the characteristic N-H stretching band of carbazole appeared at 3421 cm^{-1}, the N-H bending signal at 1564 cm^{-1}, and the signal of C-Br groups at 562 cm^{-1}. In the second stage of the reaction, 3,6-dibromo-9-octylcarbazole (III) was synthesized through an alkylation reaction of 3,6-dibromocarbazole (II), and the characteristic N-H stretching signal of carbazole at 3421 cm^{-1} disappeared. Additionally, C-H stretching bands related to the aliphatic group were observed at 2957, 2922, and 2851 cm^{-1}. For the targeted compound, 3,6-bis(3,5-bis(fluorene)phenyl)-9-octyl-9H-carbazole (IV), a Suzuki-Miyaura cross-coupling reaction was performed with palladium catalysis. In the FT-IR spectra of the synthesized compound, the characteristic signal of the C-Br group, as observed in compound III at 562 cm^{-1}, was found to be absent. Furthermore, in the synthesized compound, it was observed that the signals at 1164 cm^{-1} and 797 cm^{-1} belong to the strong bending signals of the 1,4-disubstituted phenyl ring. Additionally, in the synthesized compounds, aromatic C-H stretching vibrations were observed just above 3000 cm^{-1}, while aliphatic C-H stretching vibrations were observed just below 3000 cm^{-1}.

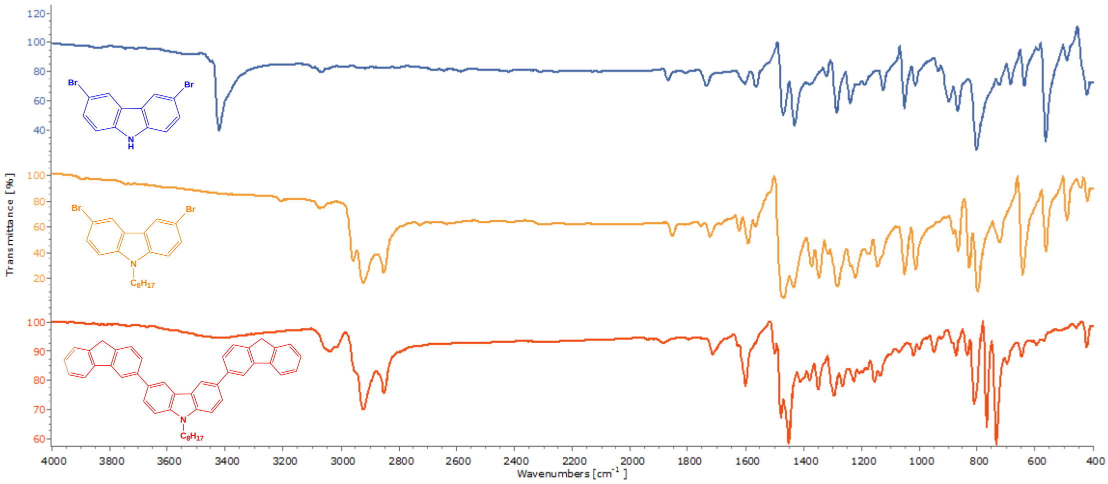

Figure 4. FT-IR spectra of compounds I, III and IV.

^{1}H-NMR Spectra of Synthesized II, III and IV Compounds

The structures of the synthesized compounds II and III were elucidated using ^{1}H-NMR and ^{13}C-NMR spectra obtained in CDCl$_3$, and it was observed that these spectra were in accordance with the literature (Li et al., 2004). The targeted compound IV has a total of 30 protons. The presence of these protons was observed in the ^{1}H-NMR spectrum, and the relevant spectrum is provided in Figure 5.

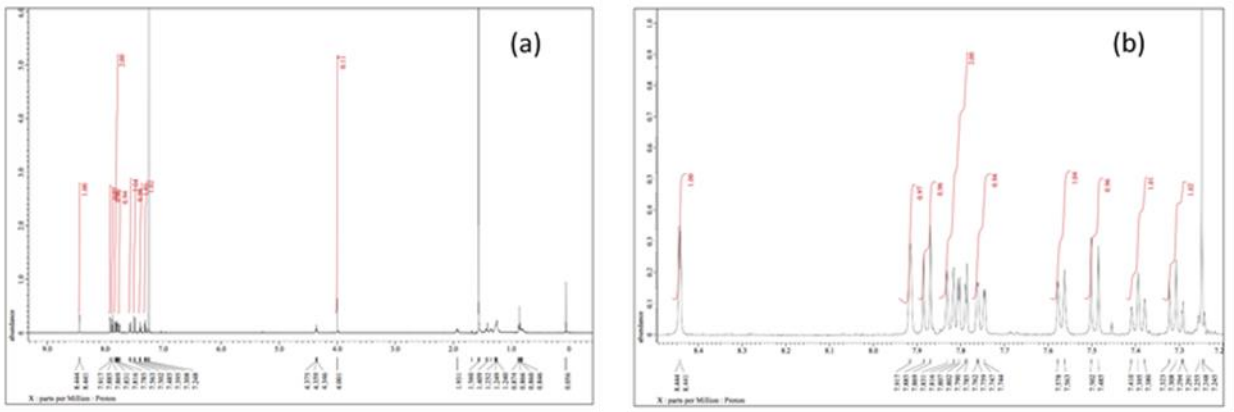

Figure 5. The ^{1}H NMR spectrum of compound IV in CDCl$_3$.

According to the signals observed in this spectrum, it was determined that the aromatic region protons belong to the phenyl rings within the carbazole and fluorene moieties, accounting for a total of 20 protons calculated in the ^{1}H-NMR spectrum. Additionally, in Figure 5, the presence of alkyl groups is indicated by the triplet of two protons at 4.39 ppm, multiple signals of two protons at 1.93 ppm, multiple signals of ten protons at 1.28-1.25 ppm, and triplets of three protons observed at 0.86 ppm, which are attributed to the aliphatic octyl group.

Electrochemical Study

The electrochemical properties of the I, III and IV were investigated using CV using DCM solution containing NBu$_4$PF$_6$ as the supporting electrolyte and ferrocene as the internal standard. The obtain CV voltomograms are shown in Figure 7, and corresponding data are summarized in Table 2. The onset oxidation potential was observed in range of 0.998, 1.292 and 0.896 V for I, III and IV, respectively. The HOMO energy levels were calculated using these onset value as negatively 5.58, 5.76 and 5.32 eV for I, III and IV, respectively. Also, the LUMO energy levels of molecules were calculated according to estimate from the onset wavelength of the optical absorption bands (Figure 6). Additionally, the HOMO energy levels of carbazole-derived compounds used in solar cells were determined as -5.67 and -6.02 eV (Agarwal et al., 2011). Therefore, it can be concluded that the HOMO energy level of the carbazole derivative molecule “IV” synthesized in our study, is suitable for use as an active material in solar cells.

Table 2. Optical and electrochemical properties synthesized compounds

	E^{ox}_{onset} [a] (V)	HOMO[b] (eV)	LUMO[c] (eV)	λ_{onset} [d] (nm)	Eg_{opt} [e] (V)
I	0.998	-5.58	-2.46	397	3.12
III	1.292	-5.76	-2.43	372	3.33
IV	0.896	-5.32	-2.09	384	3.23

[a] Determined from cyclic voltammetry experiments vs. Fc/Fc^+ in DCM.

[b] Calculated based on HOMO= - [E^{ox}_{onset} - $E_{1/2,\ Fc,Fc+}$ + 4.8] eV (Sathiyan et al., 2016)

[c] Obtained from LUMO = HOMO + $E_g$opt (Yang et al., 2018)

[d] Calculated from the cross point of absorption onset line and corrected base line.

[e] Estimated from the onset wavelength of the optical absorption bands.

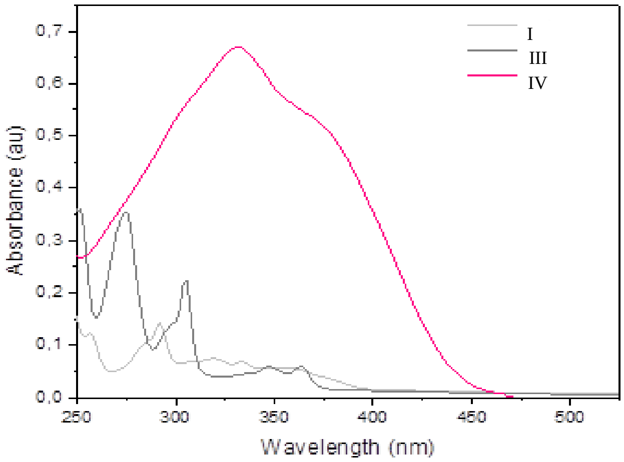

Figure 6. Absorption spectra of compounds I, III, and IV in DCM solution (10^{-5} M)

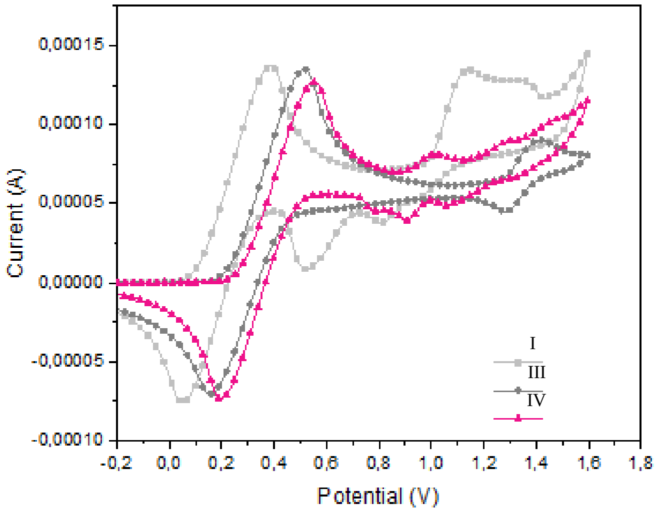

Figure 7. Cyclic voltammograms of compounds II, III and IV under room conditions; Au as working electrode; scan rate ν = 50 mV/s, 0.1 M Bu_4NPF_6 in DCM.

Photovoltaic Properties of TiO_2-DSSC

We were used in the fabrication of dye-sensitized solar cells (DSSC) of compound IV, alongside commercially available TiO_2 nanopowders (TiO_2-DSSC). These DSSCs were constructed on FTO substrates, and electrical measurements were conducted. The performance values obtained are presented in Table 3. Additionally, current density-voltage graphs of the prepared TiO2-DSSC, and the commercially available ones are depicted in Figure 8.

Table 3. The photovoltaic parameters of TiO_2-DSSCs

DSSC	**V_{oc} (V)**	**FF**	**n (%)**
TiO_2-Ru(535)bis TBA	0.631	0.520	0.570
TiO_2-**IV**	0.490	0.370	0.253
TiO_2-**IV**-Ru(535)bis TBA	0.650	0.630	5.572

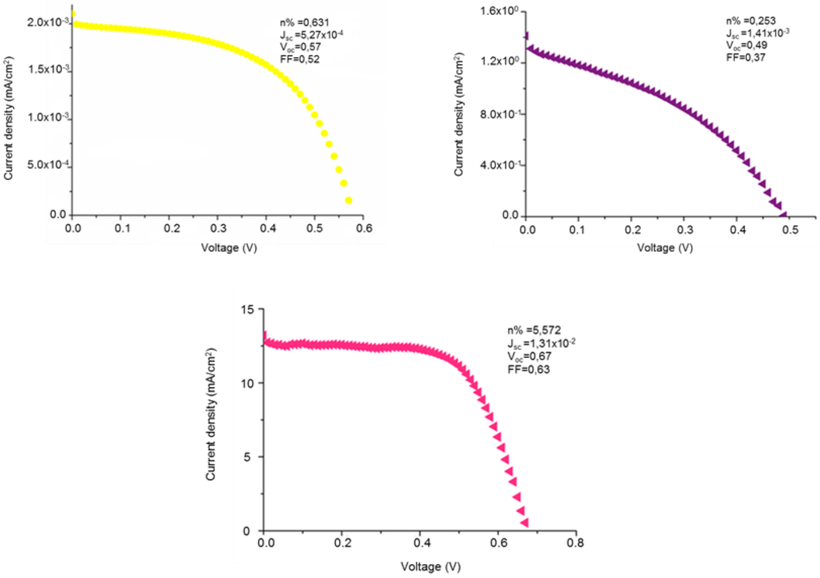

Figure 8. J-V graph of TiO_2-DSSCs

The electrical measurements showed that the power conversion efficiencies (PCE) of the cells fabricated with the prepared using the commercially available TiO_2 nanopowders exhibited power conversion efficiencies ranging from 0.253 to 5.572%, with V_{oc} values varying between 0.370 and 0.630V. In addition, fluorenes are part of intramolecular charge transfer dyes (ICT or push-pull). In these compounds, the π-conjugated systems typically consist of multiple bonds (olefin or acetylene), aromatic rings (such as fluorene or benzenoids), heteroaromatics (e.g., thiophenes), or combinations of these. Besides being categorized as D-π-A systems, there are other arrangements like quadrupolar (D-π-A-π-D) and octupolar ((D-π)3-A) systems. The significant spectroscopic properties and the linear characteristics of the carbazole-fluorene compound (IV) we used as a π-conjugated system may contribute to V_{oc} values ranging from 0.37 to 0.65 and PCE values between 0.253 and 5.572.

Conclusion

In this study, 3,6-dibromo-9-octylcarbazole and aryl boronic acids containing the fluorene group were used to synthesize 3,6-bis(3,5-bis(fluorene)phenyl)-9-octyl-9H-carbazole (IV) through a Suzuki-Miyaura cross-coupling reaction. Prior to the reaction, 3,6-dibromocarbazole (II) and 3,6-dibromo-9-octylcarbazole (III) were synthesized through bromination and alkylation reactions. The synthesized carbazole derivative compounds (II, III, and IV) were characterized using FT-IR, ^{1}H NMR and ^{13}C NMR, analysis techniques. Additionally, the UV-Vis absorption and emission spectra of these compounds were obtained in different solvents (DMSO, DMF, DCM, THF, and TOLUEN). It was observed that the π-π* transitions shifted towards longer wavelengths (red-shifted) with increased conjugation within the carbazole group. Thermal gravimetric analyses were conducted to assess the thermal stability of the synthesized compounds, and the temperature value for 5% mass loss of compound IV was found to be 285.72°C. Dye-sensitized solar cells (DSSC) were fabricated using compound IV on FTO-coated TiO_2. The efficiencies of the prepared TiO_2-DSSC-Ru(535)bis TBA, TiO_2-DSSC-IV, and TiO_2-DSSC-IV-Ru(535)bis TBA dye-sensitized solar cells were found to be in the range of 0.253-5,572. The V_{oc} values were found to be in the range of 0.28-0.63V. The fluorene groups linked through the 3,6- positions of the carbazole unit can lead to the reduction of the hole injection barrier, thereby facilitating the injection of positive charge carriers. The fluorene groups linked through the 3,6- positions of the carbazole unit can lead to the reduction of the hole injection barrier, thereby facilitating the injection of positive charge carriers.

Scientific Ethics Declaration

The authors declare that the scientific ethical and legal responsibility of this article published in EPSTEM journal belongs to the authors.

Acknowledgements or Notes

* We would like to thank Dr. Merve Yandımoğlu for all her contributions.

* This article was presented as an oral presentation at the International Conference on Basic Sciences and Technology (www.icbast.net) held in Antalya/Turkey on November 16-19, 2023.

References

Abbel, R., Schenning, A. P., & Meijer, E. W. (2009). Fluorene-based materials and their supramolecular properties. *Journal of Polymer Science Part A: Polymer Chemistry, 47*(17), 4215-4233.

Agarwal, N., Nayak, P. K., Ali, F., Patankar, M. P., Narasimhan, K. L., & Periasamy, N. (2011). Tuning of HOMO levels of carbazole derivatives: New molecules for blue OLED. *Synthetic Metals, 161*(5-6), 466-473.

Behrens, T. H. (1900). Microchemical distinction of the hydrocarbons of coal tar. Recl Trav. *Chim Pays-Bas, 19*, 386-397.

Bouaziz, Z., Issa, S., Gentili, J., Gratz, A., Bollacke, A., Kassack, M., & Le Borgne, M. (2015). Biologically active carbazole derivatives: focus on oxazinocarbazoles and related compounds. *Journal of Enzyme Inhibition and Medicinal Chemistry, 30*(2), 180-188.

Chen, H., Wang, X., Ren, H., Lu, M., Cui, X., Wang, L., & Tang, Q. (2022). Fluorene-based polymers of intrinsic microporosity as fluorescent probes for metal ions. *Reactive and Functional Polymers*, *181*

Derince, B., Gorgun, K., Caglar, Y., & Caglar, M. (2022). Architectural design of new conjugated systems carrying donor-π-acceptor groups (carbazole-CF3): Characterizations, optical, photophysical properties and DSSC's applications. *Journal of Molecular Structure, 1250.*

Doskocz, J., Doskocz, M., Roszak, S., Soloducho, J., & Leszczynski, J. (2006). Theoretical studies of symmetric five-membered heterocycle derivatives of carbazole and fluorene: precursors of conducting polymers. *The Journal of Physical Chemistry A, 110*(51), 13989-13994.

Drechsel, E. (1858). Borsche-Drechsel cyclization. *J. Prakt. Chem, 38*(2), 69-72.

Han, Y., & Wang, Z. (2009). Solubility of fluorene in benzene, chloroform, acetone, 1-propanol, isobutanol, and methylbenzene from (283 to 323) K. *Journal of Chemical & Engineering Data, 54*(1), 148-149.

Li, Y., Ding, J., Day, M., Tao, Y., Lu, J., & D'iorio, M. (2004). Synthesis and properties of random and alternating fluorene/carbazole copolymers for use in blue light-emitting devices. *Chemistry of Materials*, *16*(11), 2165-2173.

Miyaura, N. (2004) *Metal-catalyzed cross-coupling reactions of organoboron com- pounds with organic halides, in: Metal-catalyzed cross-coupling reactions* (pp. 41-123).WILEY-VCH Verlag GmbH & Co. KGaA, Sathiyan, G., Thangamuthu, R., & Sakthivel, P. (2016). Synthesis of carbazole-based copolymers containing carbazole-thiazolo [5, 4-d] thiazole groups with different dopants and their fluorescence and electrical conductivity applications. *RSC advances, 6*(73), 69196-69205.

Venkateswararao, A., Thomas, K. J., Li, C. T., & Ho, K. C. (2015). Functional tuning of organic dyes containing 2, 7-carbazole and other electron-rich segments in the conjugation pathway. *RSC Advances, 5*(23), 17953-17966.

Yang, T., Xu, H., Wang, K., Tao, P., Wang, F., Zhao, B., & Xu, B. (2018). Bipolar host materials based on diphenylphosphine oxide and carbazole derivatives with high triplet energy: Synthesis, characterization and photoelectronic performance in PhOLEDs. *Dyes and Pigments, 153*, 67-73.

Xu, S., Shangguan, X., Li, H., Zhang, Y., & Wang, J. (2015). Pd (0)-catalyzed cross-coupling of 1, 1-diboronates with 2, 2′-dibromobiphenyls: Synthesis of 9 H-fluorenes. *The Journal of Organic Chemistry, 80*(15), 7779-7784.

Zou, Z., Dang, L., Liu, P., & Wei, H. (2007). Solubility of fluorene in different solvents from 278.98 K to 338.35 K. *Journal of Chemical & Engineering Data, 52*(4), 1501-1502.

Author Information

Kamuran Gorgun
University of Eskisehir Osmangazi
Eskisehir, Turkey
Contact e-mail: *kgorguntr@gmail.com*

Betul Derince
University of Eskisehir Osmangazi
Eskisehir, Turkey

Evrim Hur
Department of Chemistry
University of Eskisehir Osmangazi
Eskisehir, Turkey

Yasemin Caglar
Eskisehir Technical University
Eskisehir, Turkey

Mujdat Caglar
Eskisehir Technical University
Eskisehir, Turkey

To cite this article:

Derince, B., Gorgun, K., Hur, E., Caglar, Y., & Caglar, M. (2023). Synthesis and characterization of 3,6-disubstituted carbazole containing fluorene and DSSC applications. *The Eurasia Proceedings of Science, Technology, Engineering & Mathematics (EPSTEM), 25,* 8-16.

The Eurasia Proceedings of Science, Technology,
Engineering & Mathematics (EPSTEM)
ISSN: 2602-3199

The Eurasia Proceedings of Science, Technology, Engineering & Mathematics (EPSTEM), 2023

Volume 25, Pages 17-25

ICBAST 2023: International Conference on Basic Sciences and Technology

Bibliometric Analysis in Scientific Articles on Nitrogen Fixation of Legumes

Aybegun Ton
Cukurova University

Abstract: Legumes has a great important in sustainable agriculture because roots are aerate and improve the physical, chemical and biological properties of soil. Legumes also enrich soil for nitrogen throughout symbiotic nitrogen fixation by rhizobia bacteria in nodules on roots and they provide products with low input. There are many studies about nitrogen fixation in legumes. However, indicating status and trends of researches are great important by bibliometric analysis. Bibliometric analysis is a useful method in literature review that reveals where research is done on a topic, models and mapping of research fields. In this study, 356 publications on nitrogen fixation of legumes between 1980-2023 were investigated using Web of Science (WoS) data and VOS viewer programme by bibliometric analysis methods. The highest number of publication on nitrogen fixation of legumes was produced in 1987, while the lowest one was in 1989. The most citation was achieved from year of 2021 with 1038 while the lowest was in 1980. Peoples, M., Sprent, J. and Urquiga, S. had highest number of publication. Plant and Soil has the most record count of publications. The organization with most publications was CSIRO. Swedish University of Agricultural Sciences had 438 citations with 6 documents while CSIRO had the 400 citations with 14 documents. USA and Australia had the highest numbers of publications. As a results, the study revealed fields of research, identify the main journal, authors, countries, research trends on nitrogen fixation of legumes by bibliometric analysis methods.

Keywords: Bibliometric analysis, Legumes, Nitrogen fixation

Introduction

Legumes (*Leguminoceae*) one of the most important plant familia and are used for human diet, livestocks feeding, medical, paper and furniture industry, fuel at the worldwide. Legumes roots prevent erosion and improve the physical, chemical and biological properties of soil (Jensen & Hauggard Nielsen, 2003). Legumes also enrich soil for nitrogen throughout symbiotic nitrogen fixation by rhizobium bacteria that form nodules on roots. Nitrogen is essential plant nutrient for plant growth. Yield can be increased by chemical fertilizer, but different problems occured in soil. Chemical fertilizer production is difficult and expensive. Therefore, production cost for crop increases and fertilizer degrades physical properties of soil. Importance of symbiotic nitrogen fixation in agriculture is increasing due to environmental problems arised in the use and production of nitrogen fertilizer. Amount of biological nitrogen fixation in the world is about 175 million ton year. About 50% of nitrogen fixed is provided through symbiotic of legume-rhizobium (Sarıoglu et al., 1993). Legumes can be used as green manure in cropping system. It provides nitrogen mineral matter and humus contents in soil. Legumes should be considered in the development of future agroecosystem (Jensen et al., 2012). Nitrogen fixation is affected different environmental condions (Rao & Rupela, 1998). Nitrogen fixed by pulses ranges from 65 to 224 kg ha^{-1} (Nutman,1976). Nearly 30-40 kg of N is fixed on plant for each ton dry matter produced by legume crops (Peoples et.al., 2009). There are many studies about nitrogen fixation by various legumes under different environmental conditions (Gibson et al., 1982; Zahran,1999; Pampana et al., 2018; Fenta et al., 2020). However, indicating status of research and trends are great important by bibliometric analysis. Bibliometric analysis is a useful method in literature reviews that reveals where research is done on a topic, models and

---

- Selection and peer-review under responsibility of the Organizing Committee of the Conference

mapping of research field (Şimşir, 2021; Silva et al., 2022; Akşahin & Gülser, 2022; Akşahin & Ortaş, 2022). Many studies were conducted in legume mycorrhiza field (Xu, 2021), maize–soybean intercropping (Feng et al., 2022), various legumes such as chickpea, common beans (Jinfeng et al., 2015; Antunes et al., 2019; Magrini et al., 2019; Spatti et al., 2021; Bhat et al., 2022) by using bibliometric analysis methods for determining the trends of researches.

In this study, publications on nitrogen fixation by legumes between 1980-2023 were revealed using WoS data and VOS viewer programm throughout bibliometric analysis. The aim of the study is determine fields of research, identify the main journal, authors, countries, research trends conducted on nitrogen fixation by bibliometric analysis methods. The results of bibliometric analysis on nitrogen fixation will be guiding to researchers for future studies.

Materials and Methods

Analysis of Data

Dataset was provided from the Web of science (WoS) database. The WoS is one of the most resources evaluated in bibliometric analysis in the World (Magrini et al., 2019). The Wos ‘‘corre collection’’ includes about million records. In this research, 356 publications between 1980-2023 years in 23.04.2023 were found by considering title of legume and nitrogen fixation in the database. Data reached from WoS database were investigated according to name of publication, co- authors of author citation, journal, country, organization, keywords. The bibliometric analysis steps was identifiying keywords, selection of search results, recording and control of WoS files, entering data into vosviewer, creating data maps respectively (Aksahin & Ortas, 2022). Bibliometric analysis map was created for the foremost authors with minimum number of documents and citations. Bibliometric analyzed by using the VOS- viewer, 1.6.19 software (Vosviewer, 2023).

Results and Discussion

The Number of Publications and Citations on Nitrogen Fixation by Legumes

Scientific publications on legumes and nitrogen fixation the years between 1980-2023 were evaluated. (Figure 1). The highest number of publication was produced in 1987 with 16 while the lowest one is in 1989 with 2. Number of citations are 356 during 43- years and it increased in the recently. The highest number of citation was achieved from year of 2021 with 1038 while the lowest was in 1980 with 1. Generally, number of citation increased due to increasing publications.

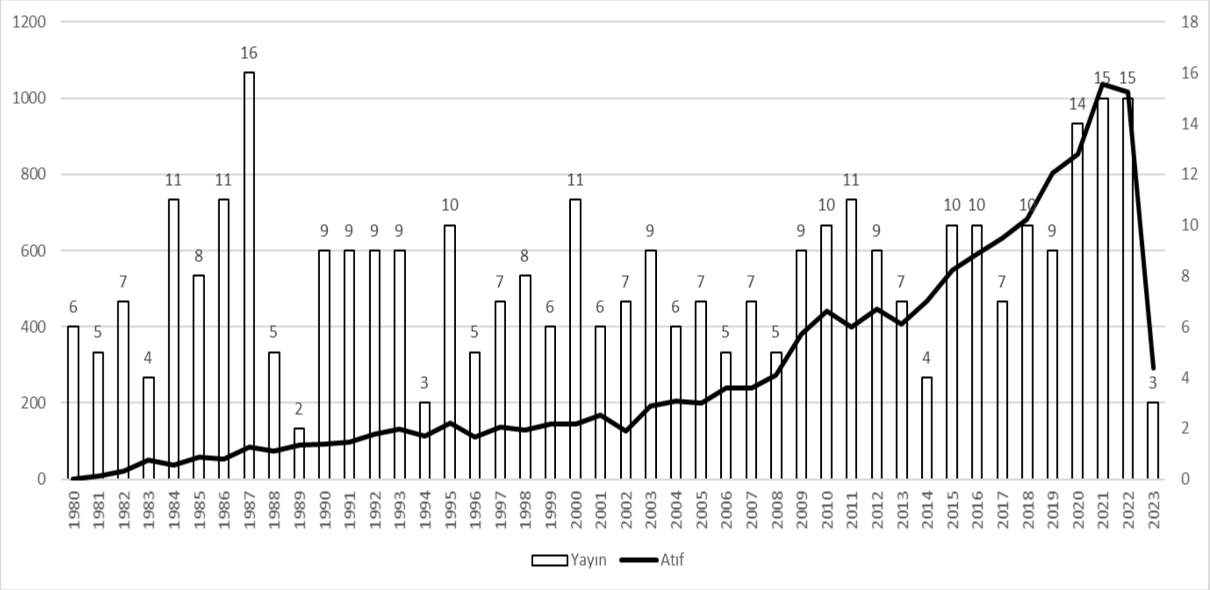

Figure 1. The number of publications and citations produced during last 43- year period.

Journals with the most Publications on Nitrogen Fixation by Legumes

In the 10 top ranking Journal Plant and Soil has the most record count of publications with 43 (12.08%) followed by Field crops Research with 12 record count (3.37 %) between 1980-2023 (Table 1).

Table 1. The top 10 ranking by number of journal between years 1980-2023

No	Publication titles	Record count	Percentage*
1	Plant and Soil	43	12.08
2	Field Crops Research	12	3.37
3	Frontiers in Plant Science	9	2.53
4	New Phytologist	8	2.25
5	Australian Journal of Agriculture Research	7	1.97
6	Biology and Fertiliy of Soils	7	1.97
7	Soil Biology Biochemistry	7	1.97
8	Agronomy Journal	6	1.69
9	Nutrient Cycling in Agroecosystems	6	1.69
10	Annals of Botany	5	1.40

*Percentage of total publications between 1980-2023 years (23.04.2023)

Co-Authorship and Authors with the most Publications on Nitrogen Fixation by Legumes

Bibliometric analysis map for the 10 top authors with at least 1 or more publications was presented in Table 2. Peoples, M., Sprent, J. and Urquiga, S. had highest publication with 6 in the top 10 ranking. Citation number of Ledgard, S with 462 was more than Peoples, M with 393, however documents of People, M was higher than Ledgard, S (Table 2).

Table 2. Co-authorship and authors with the most publications and citations

No	Author	Documents	Citations
1	Peoples, M	6	393
2	Sprent, J	6	211
3	Urquiga, S	6	78
4	Ledgard, S	5	462
5	Herridge, D	5	310
6	Bergersen, F	5	125
7	Sheehy, J	5	119
8	Giller, KE	5	39
9	Serraj, R	4	145
10	Rupela O	4	141

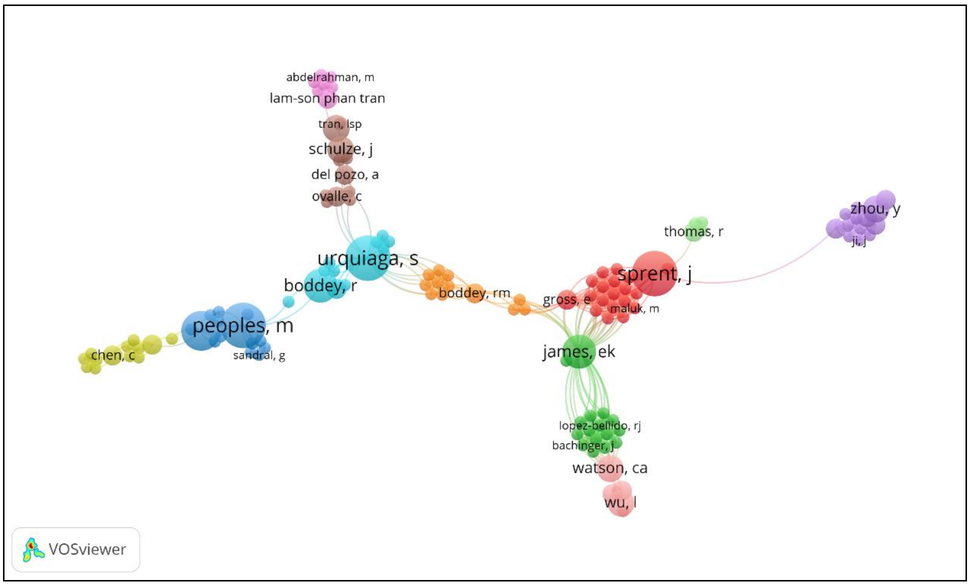

Figure 2. Bibliometric analysis map for foremost co-authorhsip and authors

Authors were grouped into 11 various cluster for the most publications. Cluster 1 included to have highest number of publication author (Figure 2). Each clusters shows that there are related to between publication and authors with same color in graph (Ponomariov & Boardman, 2016; Cevik, 2021). Glänzel and Schubert (2004) reported that co-authorship is showing research collaboration between regions, institutions and countries. Co-authorship is content measure of research collaboration that is two and more individuals are listed as co-authors on the same publication (Ponomariov & Boardman, 2016)

Most used Keywords used on Nitrogen Fixation and Legume

Keywords show the study fields in the researches of nitrogen fixation by legumes and their changes in various periods. Keywords used at least 2 in publications on legume and nitrogen fixation was given in Table 3. Nitrogen fixation was used the most keywords with 46 occurences followed by legumes and legume with 33 and 22, respectively (Table 3 and Figure 3). Keywords were grouped into 14 various clusters (Figure 3). Each cluster shows that relationship between key words. The components with same color used same keywords. Keyword is essential that reach to information about scienfitic research (Su & Lee, 2010; Tripathi et al., 2018; Deka & Sarmah, 2020).

Table 3. Keywords used at least 2 times

No	Keyword	Occurences
1	Nitrogen fixation	46
2	Legumes	33
3	Legume	22
4	Symbiosis	19
5	Nodulation	19
6	Rhizobia	18
7	Biological nitrogen fixation	17
8	N_2 fixation	12
9	Symbiotic nitrogen fixation	10
10	n15	10

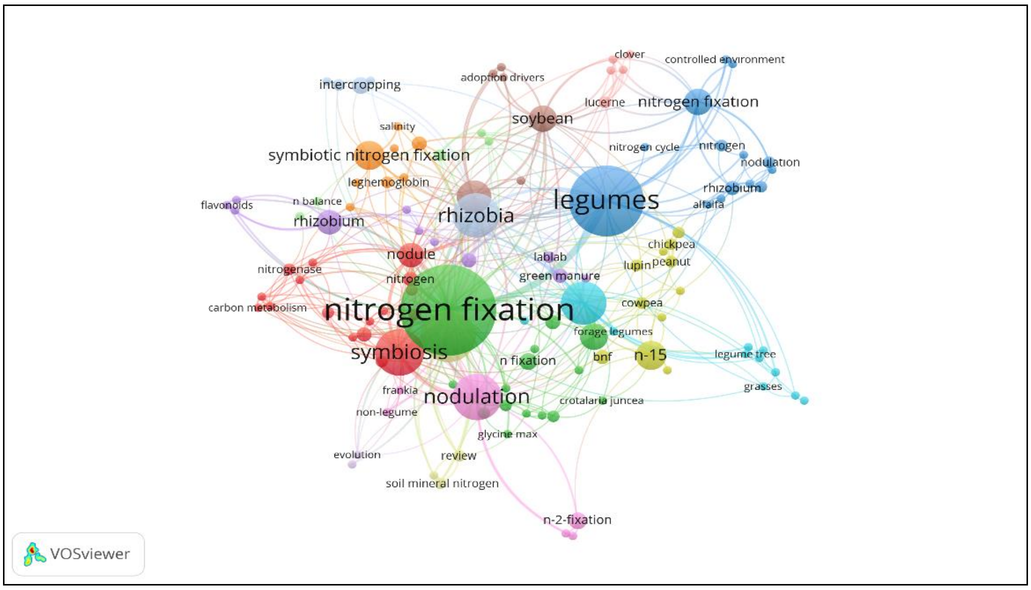

Figure 3. Bibliometric analysis map for foremost keywords used at least 2 times.

Countries with the most Publications on Nitrogen Fixation by Legumes

Bibliometric analysis map for the countries was shown in Figure 4. Countries with highest with publications was USA with 68 followed by with Australia 67. Other most productive countries were United Kingdom with 33 China with 25, Brazil and India with 22 about nitrogen fixation by legumes, respectively.

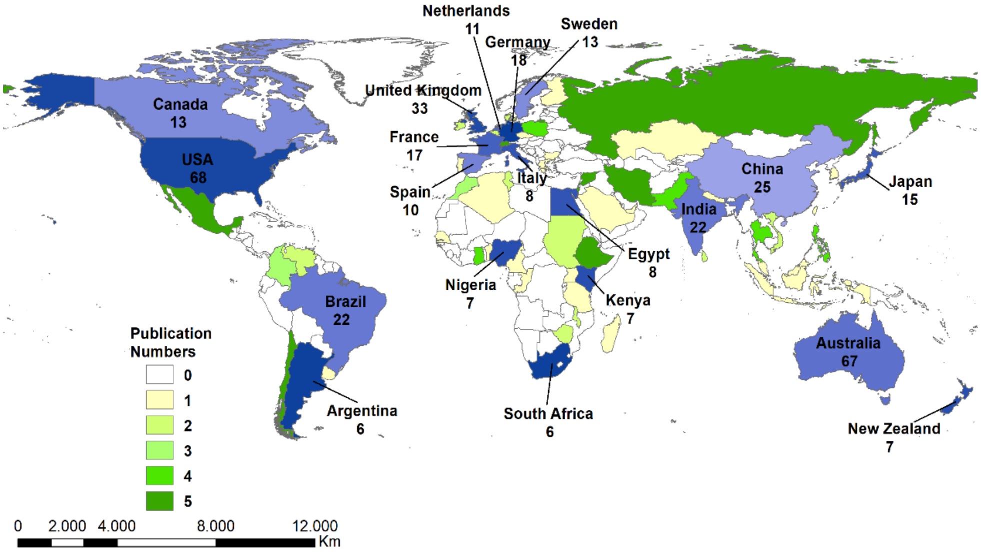

Figure 4. Bibliometric analysis map for the countries for number of publication.

Organization with the most Publications and Citations on Nitrogen Fixation by Legumes

Bibliometric analysis for the 10 top organization with at least 1 or more publications and citations was presented during the 43-years in Table 4. The organization with most publications was CSIRO and Chinese acad sci with 14 and 10 publications respectively. Swedish University of Agricultural Sciences had 438 citations with 6 documents while CSIRO had the 400 citations with 14 documents.

Table 4. The top 10 ranking citations and publications by number of organization

No	Organization	Documents	Citations
1	Csıro	14	400
2	Chinese acad sci	10	138
3	Embrapa agrobiol	7	130
4	Nsw agr	7	267
5	Swedish univ agr sci	6	438
6	Murdoch univ	6	229
7	Univ western australia	6	184
8	Univ adelaide	5	129
9	Univ chinese acad sci	5	107
10	Univ minnesota	5	93

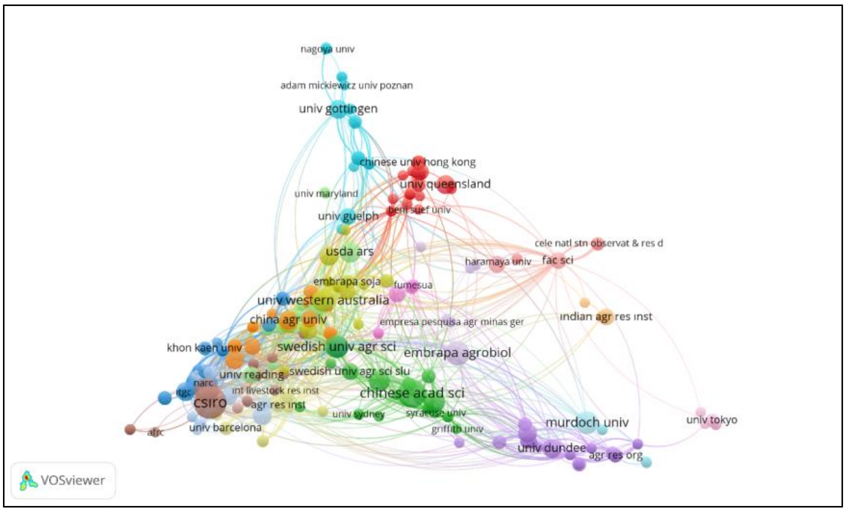

Figure 5. Bibliometric analysis map for foremost the organization with at least 1 or more publications and citations

Organization were grouped into 18 various clusters for most citation. Clusters with same color show that relationship among the cited organization and shows how they are distributed (Van Eck and Waltman, 2014; Van Eck and Waltman, 2017). Cluster 1 included to have highest number of cited organization followed by cluster 2 (Figure 5).

Publications with the Highest Citations on Nitrogen Fixation by Legumes

Bibliometric analysis for the 10 top publications with at least 1 or more citations was presented during the 43-years in Table 5. Zahran (1999) had citations with 954 on nitrogen fixation of legumes followed by Santi (2013) with 343 cited (Table 5).

Table 5. Top 10 ranking publication for citations

No	Publication	Citations
1	Zahran (1999)	954
2	Santi (2013)	343
3	Lodwig (2003)	338
4	Ledgard (1992)	328
5	Unkovıch (1994)	318
6	Carlsson (2003)	308
7	Chen (2003)	275
8	Ott (2005)	260
9	Van kessel (2000)	235
10	Roy (2020)	229

Author were grouped into 19 various clusters for the most citation. Cluster group shows the connection between cited publications. Cluster 1 included to have highest number of cited publications followed by cluster 2 (Figure 6).

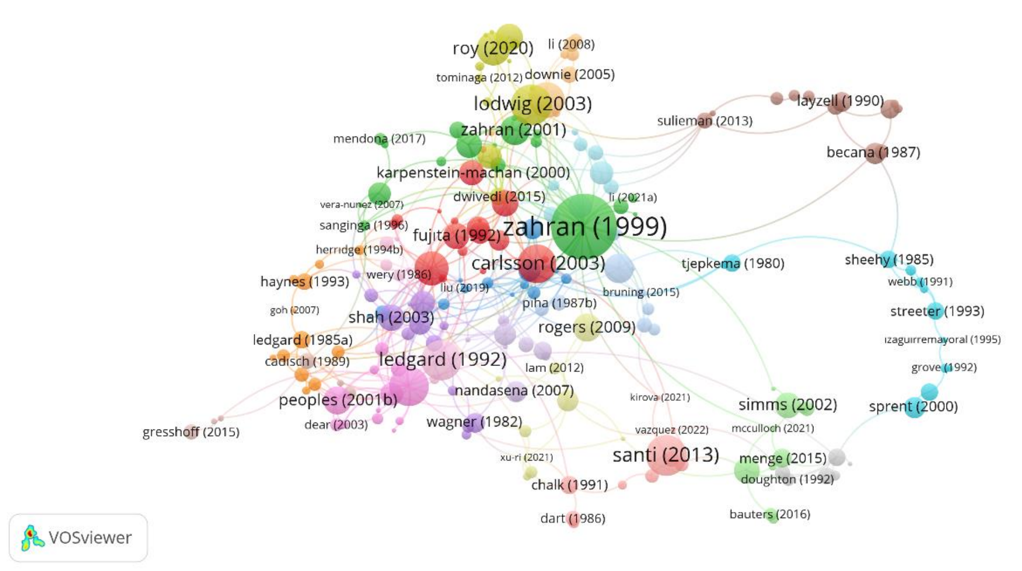

Figure 6. Bibliometric analysis map for foremost the publications with at least 1 or more Citations

Bibliographic Coupling Analysis

Bibliographic coupling analysis for the 10 top organizations with at least 1 or more publications and citations was presented during the 43-years in Figure 7. CSIRO had most citations on nitrogen fixation of legumes followed by Chinese Acad SCI (Figure 7). Organizations were grouped into 14 various clusters for the bibliographic coupling analysis. Cluster analysis shows the connection between cited organizations for bibliographic coupling. Cluster 1 included to highest number of collaboration organization with 119 for bibliographic coupling followed by cluster 2 with 60 (Figure 7). Bibliographic coupling analysis measures co-citations in two different publications (Cevik, 2021). Bibliographic coupling is the opposite of co-citation (Al et al., 2010; Van Eck & Watman, 2014). Two publications are bibliographically coupled if there is a third publication that is cited by both publications (Kessler, 1963).

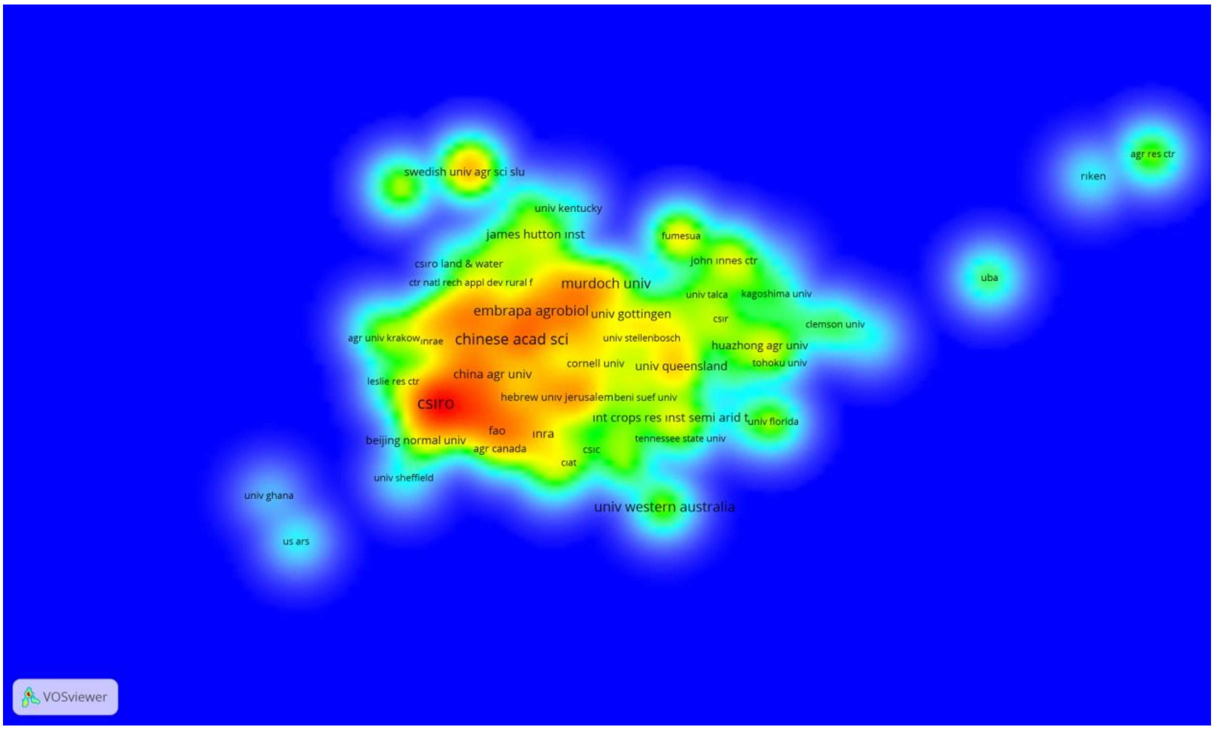

Figure 7. Bibliographic coupling analysis map for foremost organization.

Funding Agencies

Looking at the 23 year data, National Natural Science Foundad had most supporting organization on nitrogen fixation of legumes followed by National Science Foundadition Nsf (Table 6).

Table 6. Top 10 ranking organizations for funding agencies

No	Funding Agencies
1	National Natural Science Foundation Of China Nsfc
2	National Science Foundation Nsf
3	Australian Research Council
4	Grains R D Corp
5	Grants In Aid For Scientific Research Kakenhi
6	Japan Society For The Promotion Of Science
7	Ministry Of Education Culture Sports Science And Technology Japan Mext
8	Conselho Nacional De Desenvolvimento Cientifico E Tecnologico Cnpq
9	Cgiar
10	China Scholarship Council

Conclusions

In this study, 356 publications on nitrogen fixation of legumes between 1980-2023 were investigated using Web of Science (WoS) data and VOS viewer programm by bibliometric analysis methods. The highest number of publication was produced in 1987 the lowest one is in 1989. Peoples, M had highest number of publication followed by Sprent, J. The highest number of citation was achieved from year of 2021 with 1038 while the lowest was in 1980. Plant and Soil has the most record count of publications. The organization with most publications was CSIRO. Swedish University of Agricultural Sciences had 438 citations with 6 documents while CSIRO had the 400 citations with 14 documents. The publication of Zahran (1999) had highest citations on nitrogen fixation by legumes. USA and Australia had highest the numbers of publications. As a results, the study revealed fields of research, identify the main journal, authors, countries, research trends conducted on nitrogen fixation of legumes by bibliometric analysis methods.

Scientific Ethics Declaration

The author declares that the scientific ethical and legal responsibility of this article published in EPSTEM journal belongs to the author.

Acknowledgements or Notes

This article was presented as an oral presentation at the International Conference on Basic Sciences and Technology (www.icbast.net) held in Antalya/Turkey on November 16-19, 2023.

References

Aksahin, V. & Gulser, F. (2022). Tarımsal acıdan 2000-2022 yılları arasında yapılan havuc bitkisi ile ilgili yayınların bibliyometrik analizi. M.Z. Karipcin, (Eds.), *Sebzecilikte farklı yaklasımlar* (pp. 21-44). Ankara, Turkey: Iksad Publishing.

Aksahin, V., & Ortas I. (2022). Bibliometric analysis of scientific research articles on water and drought between 2000-2022. Proccedings of *International Congress and Workshop on Agricultural Structures and Irrigation*. Diyarbakır, Turkey.

Al, U., Soydal, I., & Yalcın, H. (2010). Bibliyometrik ozellikleri acısından bilig'in degerlendirilmesi. Bilig, *55*, 1-20.

Antunes, A. R., Elias, G. A., Pezente, G., & Dos Santos, R. (2019). Scientific literature on Inga (Fabaceae) from Santa Catarina state, Southern Brazil (1983-2017). *Revista de Biología Tropical*, *67*(6), 1247-1256.

Bhat, S., Aditya, K. S., Kumari, B., Acharya, K. K., & Sendhil, R. (2022). Pulses production, trade and policy imperatives: A global perspective. In *Advances in legumes for sustainable intensification* (pp. 639-656). Academic Press.

Cevik I. (2021). Bibliyometrik arastırmalarda analiz tekniklerinin uygulanması.. In O. Ozturk & G. Gurler (Eds.), *Bir literatur incelemesi aracı olarak bibliyometrik analiz*. Ankara, Turkey: Nobel Bilimsel Eserler.

Deka, P., & Sarmah, M. (2020). Co-occurrence of keywords in ecocriticism research publications: An analytical approach. *Library Philosophy and Practice*, *4452*.

Feng, L., Tang, H., Pu, T., Chen, G., Liang, B., Yang, W., & Wang, X. (2022). Maize–soybean intercropping: A bibliometric analysis of 30 years of research publications. *Agronomy Journal*, *114*, 3377-3388.

Fenta, B. A., Beebe, S. E., & Kunert, K. J. (2020). Role of fixing nitrogen in common bean growth under water deficit conditions. *Food and Energy Security*, *9*(1).

Gibson, A. H., Dreyfus, B. L., & Dommergues, Y. R. (1982). *Nitrogen fixation by legumes in the tropics.* Microbiology of tropical soils and plant productivity (pp.37-73).

Glanzel, W., & Schubert, A. (2004). Analysing scientific networks through co-authorship. In H. F. MoedW. Glanzel &U.Schmoch (Eds.), *Handbook of quantitative science and technology research: The use of publication and patent statistics in studies of S&T systems* (pp. 257-276).Kluwer Academic Publishers.

Jensen, E. S., & Hauggaard-Nielsen, H. (2003). How can increased use of biological N 2 fixation in agriculture benefit the environment?. *Plant and Soil*, *252*, 177-186.

Jensen, E. S., Peoples, M. B., Boddey, R. M., Gresshoff, P. M., Hauggaard-Nielsen, H., JR Alves, B., & Morrison, M. J. (2012). Legumes for mitigation of climate change and the provision of feedstock for biofuels and biorefineries. A review. *Agronomy for Sustainable Development*, *32*(2), 329-364.

Jinfeng, Y., Junsheng, L., & Xiaoyun Z. (2015). Bibliometric analysis of Chickpea research. *Chinese Agricultural Science Bulletin, 31*(18), 96-110.

Kessler, M. M. (1963). Bibliographic coupling between scientific papers. *American Documentation*, *14*(1), 10-25.

Magrini, M. B., Cabanac, G., Lascialfari, M., Plumecocq, G., Amiot, M. J., Anton, M., ... & Wery, J. (2019). Peer-reviewed literature on grain legume species in the WoS (1980–2018): A comparative analysis of soybean and pulses. *Sustainability*, *11*(23), 6833.

Nutman, P. S. (1976). *Symbiotic nitrogen fixation in plants*. Cambridge, London: Cambridge University Press,

Pampana, S., Masoni, A., Mariotti, M., Ercoli, L., & Arduini, I. (2018). Nitrogen fixation of grain legumes differs in response to nitrogen fertilisation. *Experimental Agriculture*, *54*(1), 66-82.

Peoples, M. B., Brockwell, J., Herridge, D. F., Rochester, I. J., Alves, B. J. R., Urquiaga, S., & Jensen, E. S. (2009). The contributions of nitrogen-fixing crop legumes to the productivity of agricultural systems. *Symbiosis*, *48*, 1-17.

Ponomariov, B., & Boardman, C. (2016). What is co-authorship?. *Scientometrics*, *109*(3), 1939-1963.

Rao, J.V. D. K. K., & Rupela, O. P. (1998). Factors affecting biological nitrogen fixation and residual effects of legumes in the Indo-Gangetic *Plain.* In: *Residual effects of legumes in rice and wheat cropping systems of the indo-gangetic plain* (pp.82-104). New Delhi: Oxford & IBH Publishing.

Sarıoglu, G.Ozcelik, S., & Kaymaz, S. (1993). Selection of effective nodosity bacteria (*Rhizobium leguminosarum* biovar. viceae) from lentil grown in Elazıg. *Turkish Journal Agriculture Foestry, 17,* 569-573.

Silva, G. G. B. S., Ferraz, P. F. P., Damasceno, F. A., Zotti, M. L. A. N., & Barbari, M. (2022). Compost barns: A bibliometric analysis. *Animals*, *12*(19), 2492.

Spatti, A. C., Bezerra, L. M. C., Bin, A., Fredo, C. E., & Carbonell, S. A. M. (2021). Bibliometric indicators to measure the internationalization of Brazilian research: A case study on common beans. 18 th International Conference on Scientometrics & Infrometrics- ISSI2021. Leuven, Belgium.

Su, H. N., & Lee, P. C. (2010). Mapping knowledge structure by keyword co-occurrence: A first look at journal papers in technology foresight. *Scientometrics*, *85*(1), 65-79.

Tripathi, M., Kumar, S., Sonker, S. K., & Babbar, P. (2018). Occurrence of author keywords and keywords plus in social sciences and humanities research: A preliminary study. *COLLNET Journal of Scientometrics and Information Management*, *12*(2), 215-232.

Simsir, I. (2021). Bibliyometri ve bibliyometrik analize iliskin kavramsal cerceve. In O. Ozturk & G. Gurler (Eds.), *Bir literatur incelemesi aracı olarak bibliyometrik analiz.* Ankara, Turkey: Nobel Bilimsel Eserler.

Van Eck, N. J., & Waltman, L. (2014). Visualizing bibliometric networks. In Y. Ding R. Rousseau & D. Wolfram (Eds.), *Measuring scholarly impact: Methods and practice* (pp. 285-320). Springer.

Van Eck, N. J., & Waltman, L. (2017). Citation-based clustering of publications using CitNetExplorer and VOSviewer. *Scientometrics*, *111*(2), 1053-1070.

VOSviewer. (2023). VOSviewer software. Retrieved from https://www.vosviewer.com/

Xu, S. X. (2021). Bibliometricanalysis of the research characteristics and trends in legume mycorrhiza field. *Legume Research-An International Journal*, *44*(11), 1301-1307.

Zahran, H. H. (1999). Rhizobium-legume symbiosis and nitrogen fixation under severe conditions and in an arid climate. *Microbiology and Molecular Biology Reviews*, *63*(4), 968-989.

Author Information

Aybegun Ton
Department of Field Crops, Faculty of Agriculture,
Cukurova University, 01330
Adana, Turkey
Contact e-mail: *aybeguntoncu@gmail.com*

To cite this article:

Ton, A. (2023). Bibliometric analysis in scientific articles on nitrogen fixation of legumes. *The Eurasia Proceedings of Science, Technology, Engineering & Mathematics (EPSTEM), 25,* 17-25.

**The Eurasia Proceedings of Science, Technology,
Engineering & Mathematics (EPSTEM)
ISSN: 2602-3199**

The Eurasia Proceedings of Science, Technology, Engineering & Mathematics (EPSTEM), 2023

Volume 25, Pages 26-34

ICBAST 2023: International Conference on Basic Sciences and Technology

In-silico Identification of Natural Compounds as Pesticides against Plutella Xylostella

Nergiz Gurbuz-Colak
Izmir Institute of Technology

Abstract: Plutella xylostella (diamondback moth), a major invasive pest of Brassica crops, feeds on cruciferous plants and causes serious economic loss. The moth has spread worldwide owing to its short life cycle, high fecundity, and capability to migrate long distances. Chlorantraniliprole is a human-made insecticide widely used to control P. xylostella. On the other hand, resistance to chlorantraniliprole was reported in the literature. The use of natural compounds as pesticides can eliminate resistance and reduce potential harm to humans. In the present study, natural compounds were identified as potential pesticide candidates *in silico*. To achieve this goal, the binding potentials of over 3000 natural compounds found in the MPD3 database to the diamondback moth ryanodine receptor N-terminal domain (PDB:5y9v) were scanned using AutoDock Vina. The active sites of the target proteins were identified using PyMOL software. The first filtration was applied according to the binding energies, with a threshold of -6,0 kcal/mol. Second, the binding affinities to the N-terminal region of the human ryanodine receptor 2 (PDB:4jkq) of the candidates were checked. Candidates were then filtered according to the ADME properties based on Lipinski's rule of five using DruLiTo software. Finally, toxicity (oral toxicity, hepatotoxicity, carcinogenicity, immunotoxicity, mutagenicity, and cytotoxicity) was evaluated using ProTox II online server. In addition, the binding energy and toxicity of chlorantraniliprole were compared. Chlorantraniliprole binds to 5y9v with a binding energy of -3,5 kcal/mol while binds to 4jkq with higher affinity (-6,8 kcal/mol). Moreover, it may cause hepatotoxicity. Dorsmanin B, chartaceone B, and 7-O-galloyltricetifavan bind to 5y9v with a binding energy of -6,1 kcal/mol, -6,0 kcal,/mol, -6,1 kcal/mol, respectively while binding to 4jkq with lower affinity (0,1 kcal/mol, -2,4kcal,/mol, -2,9 kcal/mol, respectively). In addition, these candidates did not show any toxicity. These natural compounds can be used instead of chlorantraniliprole to control *Plutella xylostella*.

Keywords: Plutella xylostella, Natural compounds, Pesticide

Introduction

Invasive insect species have a destructive effect on various aspects of human well-being, including health, food security, ecosystems, biodiversity, and the economy. The diamondback moth, scientifically known as *Plutella xylostella*, belongs to the order Lepidoptera and is one of the most notorious offenders. This moth causes significant losses worldwide by feeding on *Brassica* plants, resulting in yield losses of up to 90% and economic losses of up to US$ 5 billion. Managing this pest costs approximately $1 billion annually (Kapinder et al., 2022). Diamide pesticides have been used to control diamondback moths. Chlorantraniliprole is an effective broad-spectrum anthranilic diamide pesticide that targets ryanodine receptors (RyRs) in insects, including lepidopterians. Diamondback moths have developed resistance to this pesticide because of the excessive use of chlorantraniliprole due to its high efficiency and selectivity (Gong et al., 2014). Therefore, efforts to develop new pesticides to control diamondback moth have increased.

Ryanodine receptors in insects are crucial intracellular calcium channels that regulate muscle contraction (Sattell et al., 2008). These receptors are targets of diamide insecticides, which have been effective against lepidopterans. However, their overuse has led to a decrease in their efficacy and insects have developed resistance to them (Sun & Xu, 2019). Humans have three isoforms of RyRs (RyRs1, RyRs2, and RyRs3) expressed in different tissues (Leeb & Brening, 1998), whereas insects have only one. Despite their shared functions, there are significant differences in the amino acid sequences of these receptors. In fact, ryanodine receptors in mammals and insects differ by approximately 45% in their sequences. This structural divergence makes them attractive targets for developing insecticides that can selectively eliminate insect populations without harming mammals. By exploiting these structural differences, scientists may develop more effective and eco-friendly insecticides to control the spread of harmful insect-borne diseases and protect crops from damage (Prestle et al., 2003).

Excessive use of chemical pesticides has been linked to numerous detrimental effects on the environment and inhabitants. In addition to harming humans and animals, they also have a negative impact on soil fertility. Moreover, their overuse has led to the emergence of pesticide resistance in insects, making them less effective in combating pest infestations (Kapinder et al., 2022). Recently, concerns regarding the harmful effects of chemical pesticides on the environment and human health have been growing. This has led researchers to explore the use of natural compounds as alternative pesticides. Natural compounds offer several advantages, including being environmentally friendly, sustainable, target-specific, inexpensive, and safer (Borges et al., 2021). However, it is challenging to evaluate the biological activity of the vast number of secondary metabolites produced by plants.

In the current study, the insecticidal properties of natural compounds present in the MPD3 database were assessed for their ability to interact with the ryanodine receptor of the diomandback moth. Through rigorous screening, a group of candidates was selected based on multiple criteria. This study identified natural pesticides that may be effective in combating diomandback moths. These compounds should be further evaluated to determine their efficacy as pesticides. The findings of this study underscore the value of computational techniques for the discovery of pesticides and highlight the potential of natural compounds as a source of novel insecticides.

Method

This study aimed to analyze the binding energies of natural compounds using molecular docking. A total of 3,150 compounds used in this study were obtained from the MPD3 database in .sdf format and subjected to docking studies with the diamondback moth ryanodine receptor N-terminal domain (PDB:5y9v). AutoDock Vina in PyRx virtual screening software was used to determine the binding energies of these compounds. The ligand files (compound files) were then converted to. pdbqt format after energy minimization. The crystal structure of the N-terminal domain of the ryanodine receptor of diamondback moth and human ryanodine receptor 2 (RyR2) (PDB: 4jkq) were obtained from the "RCSB Protein Data Bank" and used as a rigid molecule after protein preparation using "BIOVIA Discovery Studio 2021" software. PyRx virtual screening software was employed to conduct docking studies, and the candidates were filtered based on their binding energies with a threshold of -6 kcal/mol. The drug-likeness of the compounds was evaluated using the DruLiTo software according to Lipinski's Rule of Five (Ro5). Moreover, their physicochemical properties were evaluated to ensure their suitability as pesticide candidates. The toxicity of the compounds was assessed using the ProTox II online server to ensure safety for agricultural use. In addition, the binding energies and toxicities of chlorantraniliprole and the candidate molecules were compared. LigPlot+ software was used to evaluate the interaction of the pesticide candidates with the target protein.

Results and Discussion

In the present study, the N-terminal domain of the ryanodine receptor of the diamondback moth was used to identify candidate pesticides derived from natural compounds. Given the crucial function of ryanodine receptors in muscle contractions and the significant dissimilarity in amino acid sequences between insects and humans, they have become attractive targets for pesticides (Prestle et al., 2003). To identify potential candidates, a molecular docking technique was employed with a binding energy threshold of -6 kcal/mol. The binding energies of the candidates were compared those with of human RyR2 and chlorantraniliprole insecticides already used in the management of diamondback moths. Candidates that showed higher affinity for RyRs than human RyR2 and chlorantraniliprole are presented in Table 1. A total of 92 out of 3,150 natural compounds bound to the N-terminal domain of RyRs with a binding energy of -6 kcal/mol or lower.

Table 1. Candidates after the first filtration based on binding energies.

	Binding energies (kcal/mol)			Binding energies (kcal/mol)	
Compound name	5y9v	4jkq	Compound name	5y9v	4jkq
Chlorantraniliprole	-3.5	-6.8	Chushizisin I	-6.2	17.2
Chartaceone B	-6.0	-2.4	Epoxyazadiradione	-6.0	2.6
7-O-galloyltricetifavan	-6.1	-2.9	Chrotacumine C	-6.1	-2.2
Alvaradoin J	-6.0	9.8	Eucalmaidin B	-6.0	-2.2
Cepharadione B	-6.2	-5.7	Eucalmaidin E	-6.1	6.7
23,24-Dihydrocucurbitacin B	-6.2	11.5	Sibiricaxanthone A	-6.5	2.2
23,24-Dihydrocucurbitacin E	-6.0	10.4	Kadcoccilactone D	-6.0	1.2
28-deoxonimbolide	-6.3	-2.6	Kadcoccilactone G	-6.6	13.3
Rhinacanthin N	-6.7	5.5	Fuscaxanthone G	-6.1	-3.1
Rhinacanthin Q	-6.5	-3.6	Garcihombronane D	-6.7	-0.5
Artobiloxanthone	-6.2	-0.9	Garcihombronane E	-6.2	-1.4
Longikaurin B	-6.1	-4.9	Rhinacanthin B	-6.3	-5.7
Bruceantin	-6.0	5.9	Ovaliflavanone C	-6.4	-6.3
Calceolarioside A	-6.3	-2.5	Vittarin F	-6.1	-3.1
Calceolarioside B	-6.2	2.5	Styraxlignolide B	-6.1	3.4
Isorhoifolin	-6.4	13.8	Withanolide F	-6.5	1.4
Maytenfolone-A	-6.2	17.7	Isoglycyrol	-6.4	-6.0
Melianin C	-6.4	19.5	Cudraflavanone A	-6.2	5.5
Nigrasin D	-6.0	0.7	Physalin H	-6.2	25.0
Neodiosmin	-6.2	16.3	Geyerline	-6.1	16
Prochaetoglobosin I	-6.0	0.2	Withanolide E	-6.8	-1.7
Solamargine	-6.2	24.0	Newbouldiaquinone A	-6.6	-4.7
Withaferin A	-6.4	-1.5	Enantiomultijugin	-6.0	-4.7
(R)-cryptopleurine	-6.0	-5.3	Azadirachtin I	-6.1	4.9
4',5'-Dihydro-11,5'-dihydroxy-4'-Methoxytephrosin	-6.3	0.9	Bartericin B	-6.0	6.2
Mansonone H	-6.0	-5.7	Alvaradoin L	-6.1	-3.4
Tephrosin	-6.3	2.2	Nigrolineaxanthone I	-6.0	-5.5
Acumitin	-6.0	-4.7	Salvianolic acid J	-6.6	3.8
Alpha-Toxicarol	-6.5	-0.8	Physalin F	-6.1	6.5
Antofine	-6.1	-5.4	Sophoraisoflavanone C	-6.0	-4.8
Chicoric acid	-6.0	-3.7	Quresimine A	-6.2	12.2
Inophyllum E	-6.1	2.0	Daphnodorin F	-6.7	3.6
Sanggenon M	-6.0	0.5	Ponganone V	-6.1	-4.8
Subtrifloralactone A	-6.1	6.5	Physangulide	-6.8	26.6
Subtrifloralactone B	-6.0	3.3	6-Farnesyl-3',4',5,7-tetrahydroxyflavanone	-6.0	7.3
Subtrifloralactone C	-6.0	7.2	Dorsmanin B	-6.1	0.1
Subtrifloralactone D	-6.7	-5.5	Tanariflavanone B	-6.0	6.1
Subtrifloralactone E	-6.3	-5.6	Lumaflavanone A	-6.2	8.6
Subtrifloralactone F	-6.4	-4.6	Physalin J	-6.0	18.9
Subtrifloralactone G	-6.3	-5.0	(2S)-5,7,3',4'-Tetrahydroxyflavanone 7-glucuronide	-6.0	-2.9
28-hydroxyisoiguesterin	-6.2	-0.4	5,7,3',4'-Tetrahydroxyflavanone 7-alpha-L-arabinofuranosyl-(1->6)-glucoside	-6.2	8.5
Gedunin	-6.1	7.4	Ergotamine	-6.9	35.8
Salannin	-6.0	14.8	Desmodianone A	-6.3	0.8
Chaetoglobosin V	-6.3	23.9	Bolusanthol C	-6.1	-5.1
Lysicamine	-6.1	-5.8	Daphnodorin M	-6.2	24.2
Nimocinol	-6.2	-3.3	Balsaminone B	-6.8	1.2

The biological activity of an insecticide depends on its intrinsic activity and bioavailability, which are in turn influenced by its structural properties. The relationship between the structure and biological activity of an experimentally designed pesticide is contingent on its bioavailability. While absorption, distribution, metabolism, and excretion (ADME) properties and mammalian toxicity are typically utilized as criteria for evaluating pharmaceuticals, they may also be applied to pesticides. Understanding and evaluating the parameters that limit the bioavailability of a pesticide during its development provides critical information for the selection of pesticide candidates (David, 2016). Thus, the second filtering process was conducted based on the ADME properties, considering Lipinski's Rule of Five (Ro5). Ro5 is used to determine the oral bioavailability and membrane permeability of a compound. Molecular descriptors are incorporated into this rule. Therefore, the candidate's molecular weight must be less than 500 Da, its LogP (hydrophobicity) must be less than 5, the number of hydrogen bond donors (HBD) must be less than 5, and the number of hydrogen bond acceptors (HBA) must be less than 10. Candidates that comply with these criteria were deemed to have acceptable solubility and cell permeability (Avram et al., 2014). The ADME properties of the filtered candidates are presented in Table 2.

Table 2. ADME properties of the candidates.

Compound Name	MW (g/mol)	LogP	HBA	HBD
Chlorantraniliprole	483,15	4,72	20	2
Chartaceone B	458,5	4,54	6	3
7-O-galloyltricetifavan	442,37	2,7	10	7
Alvaradoin J	528,51	1,07	39	5
Cepharadione B	323,33	3,23	20	0
23,24-Dihydrocucurbitacin B	560,72	3,72	56	3
23,24-Dihydrocucurbitacin E	558,7	4,41	54	3
28-deoxonimbolide	452,54	4,22	37	0
Rhinacanthin N	460,48	4,86	31	2
Rhinacanthin Q	474,5	5,16	33	1
Artobiloxanthone	464,44	4,68	28	4
Longikaurin B	406,47	0,95	37	3
Bruceantin	548,58	1,15	47	3
Calceolarioside A	478,45	0,13	37	7
Calceolarioside B	478,45	0,13	37	7
Isorhoifolin	578,52	-1,1	43	8
Maytenfolone-A	470,68	5,94	50	1
Melianin C	620,77	6,46	56	0
Nigrasin D	454,47	3,08	34	4
Neodiosmin	608,55	-1,9	46	8
Prochaetoglobosin I	482,66	6,8	41	2
Solamargine	868,06	1,14	89	9
Withaferin A	470,6	3,35	44	2
(R)-cryptopleurine	377,48	4,87	31	0
4',5'-Dihydro-11,5'-dihydroxy-4'-methoxytephrosin	474,46	1,85	36	3
Mansonone H	258,27	2,33	18	1
Tephrosin	410,42	3,11	29	1
Acumitin	466,48	5,47	27	3
Alpha-Toxicarol	410,42	3,71	29	1
Antofine	363,45	4,48	29	0
Chicoric acid	474,37	1,23	30	6
Inophyllum E	402,44	5,24	26	0
Sanggenon M	436,45	4,19	31	3
Subtrifloralactone A	454,56	3,18	40	1
Subtrifloralactone B	454,56	3,18	40	1
Subtrifloralactone C	470,56	2,3	41	2
Subtrifloralactone D	456,57	3,01	42	2
Subtrifloralactone E	456,57	3,01	42	2
Subtrifloralactone F	472,57	1,98	43	3
Subtrifloralactone G	472,57	1,98	43	3
28-hydroxyisoiguesterin	420,58	6,14	39	2
Gedunin	482,57	4,56	40	0
Salannin	596,71	5,29	52	0

Chaetoglobosin V	528,64	4,67	42	4
Lysicamine	291,3	3,46	17	0
Nimocinol	452,58	5,21	40	1
Chushizisin I	476,52	4,39	35	3
Epoxyazadiradione	466,57	4,63	39	0
Chrotacumine C	499,51	3,12	38	2
Eucalmaidin B	498,48	0,02	42	7
Eucalmaidin E	512,59	0,88	50	5
Sibiricaxanthone A	538,46	-1,96	39	9
Kadcoccilactone D	512,63	5,46	47	0
Kadcoccilactone G	530,65	3,21	50	2
Fuscaxanthone G	478,58	6,7	39	2
Garcihombronane D	470,68	6,58	50	2
Garcihombronane E	470,68	6,58	50	2
Rhinacanthin B	408,49	5,12	33	0
Ovaliflavanone C	352,38	4,34	25	1
Vittarin F	436,45	4,05	31	3
Styraxlignolide B	532,49	0,2	40	4
Withanolide F	470,6	3,54	44	3
Isoglycyrol	366,36	4,51	22	1
Cudraflavanone A	422,47	5,2	32	3
Physalin H	562,99	0,97	41	2
Geyerline	710,81	1,95	63	2
Withanolide E	486,6	2,75	45	3
Newbouldiaquinone A	410,38	4	20	1
Enantiomultijugin	422,43	4,01	28	0
Azadirachtin I	618,67	1,1	54	3
Bartericin B	408,49	4,58	33	3
Alvaradoin L	470,47	1,4	35	5
Nigrolineaxanthone I	392,4	4,73	25	2
Salvianolic acid J	538,46	2,73	34	6
Physalin F	526,53	0,77	40	1
Sophoraisoflavanone C	476,6	6,91	41	3
Quresimine A	502,64	3,2	49	2
Daphnodorin F	542,49	3,99	32	6
Ponganone V	382,41	4,48	28	0
Physangulide	522,63	0,86	51	5
6-Farnesyl-3',4',5,7-tetrahydroxyflavanone	492,6	7,18	42	4
Dorsmanin B	392,5	4,9	4	1
Tanariflavanone B	490,59	6,93	40	3
Lumaflavanone A	506,59	5,05	41	2
Physalin J	526,53	0,77	40	1
(2S)-5,7,3',4'-Tetrahydroxyflavanone 7-glucuronide	464,38	-0,22	32	7
5,7,3',4'-Tetrahydroxyflavanone 7-alpha-L-arabinofuranosyl-(1->6)-glucoside	528,51	-1,85	45	9
Ergotamine	581,66	2,2	44	3
Desmodianone A	436,5	5,38	34	3
Bolusanthol C	408,49	5,18	33	3
Daphnodorin M	542,49	3,6	32	5
Balsaminone B	506,46	1,55	31	4

A crucial step in the development of pesticides is to conduct risk assessment to evaluate their potential adverse effects on human health. In this study, an *in silico* toxicity analysis was conducted to assess the toxicity of the identified pesticide candidates. Oral toxicity was evaluated to determine the acute toxicity of the compounds and hepatotoxicity was evaluated to determine whether they could cause liver failure. Additionally, carcinogenicity was evaluated to determine whether the compounds could trigger tumor formation, and immunotoxicity was evaluated to determine whether they could have adverse effects on the immune system. Mutagenicity was evaluated to determine whether the compounds caused DNA or cell damage. Finally, cytotoxicity of the candidates was evaluated to determine whether they could cause any deficits. The toxicity profiles of the pesticide candidates are presented in Table 3 (Banerjee et al., 2018).

Table 3. Toxicity assessment of the candidates.

Compound Name	Oral Toxicity	Hepatoxicity	Carcinognity	Immunotoxicity	Mutagenity	Cytotoxicty
Chlorantraniliprole	🟨	🟥	🟩	🟩	🟩	⬛
Chartaceone B	🟨	⬛	🟩	⬛	🟩	⬛
7-O-galloyltricetifavan	🟩	⬛	🟩	⬛	⬛	⬛
Alvaradoin J	🟥	🟩	🟩	🟥	🟩	🟩
Cepharadione B	🟨	🟥	🟩	🟥	🟥	🟥
23,24-Dihydrocucurbitacin B	🟧	⬛	🟩	🟩	⬛	🟩
23,24-Dihydrocucurbitacin E	🟧	⬛	🟩	🟥	⬛	🟩
28-deoxonimbolide	🟨	⬛	🟥	🟥	⬛	⬛
Rhinacanthin N	🟨	🟩	🟩	🟥	🟩	🟥
Rhinacanthin Q	🟨	🟩	🟩	🟥	🟩	🟥
Artobiloxanthone	🟩	🟩	🟩	🟥	🟩	⬛
Longikaurin B	🟧	⬛	⬛	🟥	🟩	🟥
Bruceantin	🟥	⬛	🟩	🟥	🟩	⬛
Calceolarioside A	🟩	⬛	⬛	🟥	⬛	⬛
Calceolarioside B	🟩	⬛	⬛	🟥	⬛	⬛
Isorhoifolin	🟩	⬛	⬛	🟥	🟩	🟩
Maytenfolone-A	🟩	🟩	🟩	🟥	⬛	🟩
Melianin C	🟩	⬛	🟥	🟥	⬛	⬛
Nigrasin D	🟥	🟩	🟩	🟥	🟥	⬛
Neodiosmin	🟩	⬛	⬛	🟥	⬛	🟥
Prochaetoglobosin I	🟧	⬛	🟩	🟥	🟩	⬛
Solamargine	🟨	⬛	🟩	🟥	⬛	🟥
Withaferin A	🟧	⬛	🟩	🟥	⬛	🟥
(R)-cryptopleurine	🟧	⬛	🟩	🟥	🟩	🟥
4',5'-Dihydro-11,5'-dihydroxy-4'-methoxytephrosin	🟧	⬛	🟩	🟥	🟩	⬛
Mansonone H	⬛	⬛	🟩	🟥	🟩	⬛
Tephrosin	🟥	⬛	🟩	🟥	🟩	⬛
Acumitin	🟨	⬛	🟩	🟥	🟥	⬛
Alpha-Toxicarol	🟥	⬛	🟩	🟥	🟩	⬛
Antofine	🟧	⬛	🟩	🟥	🟩	🟥
chicoric acid	🟩	🟩	🟩	🟥	⬛	⬛
Inophyllum E	🟨	⬛	🟩	🟥	🟩	⬛
Sanggenon M	🟥	🟩	🟩	🟥	🟥	⬛
Subtrifloralactone A	🟨	⬛	🟥	🟥	🟩	🟩
Subtrifloralactone B	🟩	⬛	🟥	🟥	🟩	🟩
Subtrifloralactone C	🟨	⬛	🟩	🟥	🟩	🟩
Subtrifloralactone D	🟨	⬛	🟩	🟥	🟩	⬛
Subtrifloralactone E	🟩	⬛	🟩	🟥	🟩	⬛
Subtrifloralactone F	🟩	⬛	🟩	🟥	🟩	⬛
Subtrifloralactone G	⬛	⬛	🟩	🟥	🟩	⬛
28-hydroxyisoiguesterin	🟨	⬛	🟩	🟥	⬛	⬛
Gedunin	🟧	⬛	🟩	🟥	⬛	⬛
Salannin	🟨	⬛	🟩	🟥	⬛	⬛
Chaetoglobosin V	🟨	⬛	🟩	🟥	🟩	🟩
Lysicamine	🟨	🟥	🟩	🟥	🟥	⬛
Nimocinol	🟨	⬛	🟥	🟥	⬛	⬛
Chushizisin I	🟩	⬛	🟩	🟥	🟩	⬛
Epoxyazadiradione	🟨	⬛	🟩	🟥	⬛	🟩
Chrotacumine C	🟨	⬛	🟩	🟥	🟩	⬛
Eucalmaidin B	🟩	⬛	⬛	⬛	⬛	⬛

Eucalmaidin E	🟧	⬛	⬛	⬛	⬛	⬛
Sibiricaxanthone A	🟨	⬛	⬛	🟥	🟩	⬛
Kadcoccilactone D	🟥	⬛	🟥	🟥	⬛	⬛
Kadcoccilactone G	🟥	🟩	⬛	🟥	⬛	🟥
Fuscaxanthone G	🟨	⬛	🟩	🟥	🟩	⬛
Garcihombronane D	🟨	⬛	🟥	⬛	⬛	🟥
Garcihombronane E	🟨	⬛	🟥	⬛	⬛	🟥
Rhinacanthin B	🟨	🟩	🟩	🟩	⬛	⬛
Ovaliflavanone C	🟨	⬛	🟩	🟥	🟥	⬛
Vittarin F	🟨	⬛	🟩	🟥	⬛	⬛
Styraxlignolide B	🟨	⬛	⬛	🟥	🟩	⬛
withanolide F	🟨	⬛	🟩	🟩	⬛	⬛
Isoglycyrol	🟨	⬛	🟩	🟥	🟥	⬛
Cudraflavanone A	🟨	🟩	🟩	🟥	🟩	⬛
Physalin H	🟩	⬛	🟩	🟥	⬛	🟩
Geyerline	🟥	🟩	🟩	🟥	⬛	🟩
Withanolide E	🟥	⬛	🟩	🟥	⬛	🟥
Newbouldiaquinone A	🟨	🟩	🟩	⬛	🟥	⬛
Enantiomultijugin	🟩	⬛	🟥	🟥	🟩	🟩
Azadirachtin I	🟨	⬛	🟥	🟥	⬛	🟥
Bartericin B	🟨	🟩	🟩	🟥	🟥	⬛
Alvaradoin L	🟩	🟩	🟩	🟥	🟩	⬛
Nigrolineaxanthone I	🟩	⬛	🟩	🟥	🟥	⬛
Salvianolic acid J	🟩	⬛	🟩	🟥	🟩	⬛
Physalin F	🟩	⬛	🟩	🟥	⬛	🟩
Sophoraisoflavanone C	🟨	⬛	🟩	🟥	🟩	⬛
Quresimine A	🟥	⬛	🟩	🟥	⬛	🟥
Daphnodorin F	🟥	⬛	🟩	🟥	🟩	⬛
Ponganone V	🟨	⬛	🟩	🟥	⬛	⬛
Physangulide	⬛	⬛	🟩	🟥	⬛	🟥
6-Farnesyl-3',4',5,7-tetrahydroxyflavanone	🟨	⬛	🟩	🟥	🟩	⬛
Dorsmanin B	🟨	🟩	🟩	⬛	🟩	⬛
Tanariflavanone B	🟨	⬛	🟩	🟥	🟩	⬛
Lumaflavanone A	🟨	⬛	🟩	🟥	🟩	⬛
Physalin J	🟩	⬛	🟩	🟥	⬛	🟩
(2S)-5,7,3',4'-Tetrahydroxyflavanone 7-glucuronide	🟩	⬛	🟩	🟥	🟩	⬛
5,7,3',4'-Tetrahydroxyflavanone 7-alpha-L-arabinofuranosyl-(1->6)-glucoside	⬛	⬛	⬛	🟥	⬛	⬛
Ergotamine	🟧	⬛	🟥	🟥	⬛	🟩
Desmodianone A	🟨	⬛	🟩	🟥	🟩	⬛
Bolusanthol C	🟩	⬛	⬛	🟥	🟩	⬛
Daphnodorin M	🟥	🟩	🟥	🟥	🟩	⬛
Balsaminone B	🟩	⬛	⬛	🟥	🟥	⬛

*Color code; dark green and green: non-toxic, yellow: acceptable, orange and red: toxic

When their binding energies, ADME properties, and toxicity were evaluated, dorsmanin B, chartaceone B, and 7-O-galloyltricetifavan were the leading candidates in the fight against the diamondback moth. The interaction of these compounds with the N-terminal domain of the diamondback moth ryanodine receptor is shown in Figure 1A-C. Dorsmanin B binds to RyRs through hydrophobic interactions with amino acids Gln69, Leu71, Leu79, Val80, and Arg96 on RyRs. Chartaceone B binds to RyRs through hydrogen bonding with His95 and Thr97 on RyRs and hydrophobic interactions with the amino acids Thr19, Glu20, Glu68, Gln69, and Arg96. 7-O-galloyltricetifavan binds to RyRs through hydrogen bonding with Gln69 and Arg96 on RyRs, and hydrophobic interactions with amino acids Leu71, Leu79, His95, Thr97, and Leu99.

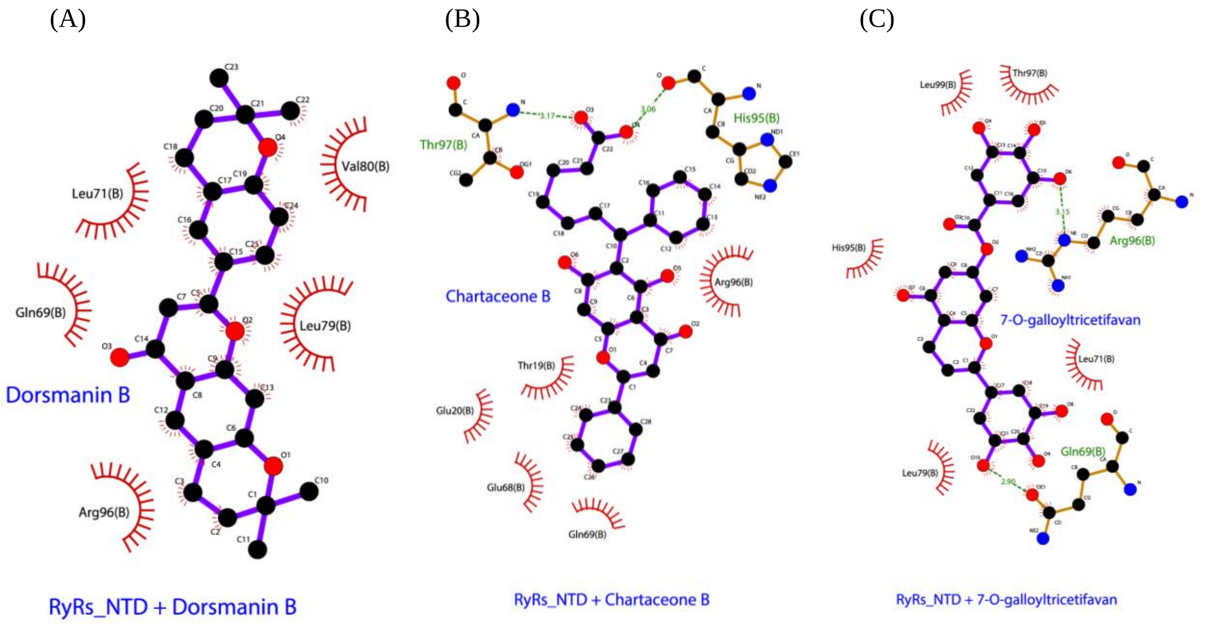

Figure 1. Interactions between candidates and diamondback moth RyRs N terminal domain (A) Dorsmanin B and RyRs NTD (B) Chartaceone B and RyRs NTD and (C) 7-O-galloyltricetifavan and RyRs NTD

Conclusion

The diamondback moth is a destructive insect species that causes significant losses to agriculture and human well-being. To manage this pest, researchers have developed new pesticides, including chlorantraniliprole, an effective broad-spectrum anthranilic diamide pesticide that targets insect ryanodine receptors. However, excessive use of chlorantraniliprole has led to the development of resistance in diamondback moths. To address this issue, researchers are exploring the use of natural compounds as alternative pesticides. This study aimed to identify natural compounds that may be effective in combating diamondback moths by assessing their binding energies with the ryanodine receptor of diamondback moths using molecular docking. A total of 3,150 compounds were screened, and 28 candidates were selected based on their binding energies and other criteria. These compounds showed promising insecticidal properties and were evaluated as potential pesticides. Three natural compounds, including dorsmanin B, chartaceone B, and 7-O-galloyltricetifavan, have demonstrated potential as pesticide candidates against diamondback moth.The study highlights the potential of natural compounds as a source of novel insecticides and the value of computational techniques for the discovery of pesticides.

Recommendations

This study was conducted using computational models, rather than practical trials. The next step involves the formulation of conclusive pesticide compositions based on the candidates identified in the investigation. These compositions will then be evaluated for efficacy in a controlled laboratory setting through in vitro testing.

Scientific Ethics Declaration

The author declares that the scientific ethical and legal responsibility of this article published in EPSTEM journal belongs to the author.

Acknowledgements or Notes

* This article was presented as an oral presentation at the International Conference on Basic Sciences and Technology (www.icbast.net) held in Antalya/Turkey on November 16-19, 2023.

References

Avram, S., Funar-Timofei, S., Borota, A., Chennamaneni, S.R., Manchala, A.K., & Muresan, S. (2014). Quantitative estimation of pesticide-likeness for agrochemical discovery. *Journal of Cheminformatics, 6*(1*)*, 42.

Banerjee, P., Eckert, A.O., Schrey, A.K., & Preissner, R. (2018). ProTox-II: A webserver for the prediction of toxicity of chemicals. *Nucleic Acids Research, 46*(1), 257-263.

Borges, S., Alkassab, A. T., Collison, E., Hinarejos, S., Jones, B., McVey, E., Roessink, I., Steeger, T., & Sultan, M., Wassenberg, J. (2021). Overview of the testing and assessment of effects of microbial pesticides on bees: Strengths, challenges and perspectives. *Apidologie, 52*, 1256–1277.

David, M. D. (2017). Insecticide ADME for support of early-phase discovery: Combining classical and modern techniques. *Pest Management Science, 73*(4), 692-699.

Gong, W., Yan, H. H., Gao, L., Guo, Y. Y., & Xue, C. B. (2014). Chlorantraniliprole resistance in the diamondback moth (Lepidoptera: Plutellidae). *Journal of Economic Entomology*, *107*(2), 806-814.

Kapinder, B., Kriti, S., & Savita, T. (2022). Biofabricated nanoparticles: Their delivery and utility in *Plutella xylostella* management. *Indian Journal of Biochemistry and Biophysics, 59*(4), 399-404.

Leeb, T., & Brenig, B. (1998). Ryanodine receptors and their role in genetic diseases. *International Journal of Molecular Medicine*, *2*(3), 293-593.

Prestle, J., Quinn, F. R., & Smith, G. L. (2003). Ca$^{(2+)}$-handling proteins and heart failure: Novel molecular targets? *Current Medicinal Chemistry*, *10*(11), 967-981.

Sattell, D. B., Cordova, D., & Cheek, T. R. (2008). Insect ryanodine receptors: Molecular targets for novel pest control chemicals. *Invertebrate Neuroscience*, *8*(3), 107-119.

Sun, Z., & Xu, H. (2019). Ryanodine receptors for drugs and insecticides: An overview. *Mini-Reviews in Medicinal Chemistry*, *19*(1), 22-33.

Author Information

Nergiz Gurbuz Colak
Izmir Institute of Technology
Izmir, Turkey
Contact e-mail: *nergizgurbuz@iyte.edu.tr*

To cite this article:

Gurbuz-Colak, N. (2023). *In-silico* identification of natural compounds as pesticides against plutella xylostella. *The Eurasia Proceedings of Science, Technology, Engineering & Mathematics (EPSTEM), 25,* 26-34.

The Eurasia Proceedings of Science, Technology,
Engineering & Mathematics (EPSTEM)
ISSN: 2602-3199

The Eurasia Proceedings of Science, Technology, Engineering & Mathematics (EPSTEM), 2023

Volume 25, Pages 35-41

ICBAST 2023: International Conference on Basic Sciences and Technology

The Effect of Food Labels on Consumers' Choice of Milk and Dairy Products

Fatma Hazan Gul
Mersin University

Ayse Saltekin
Mersin University

Abstract: The information on food labels helps consumers to make conscious and correct choice. The aim of this study is to determine how information on milk and dairy product labels influences consumer preferences. Subjects participating in the study were randomly divided into two homogeneous groups. Subjects in group 1 (n=19) tasted only the test foods without looking food labels, subjects in group 2 (n=19) tasted by looking food labels. After tasting, subjects were asked about their general dietary habits, to rate the tasted foods using the visual analog scale (VAS), and, their health literacy level was determined using the newest vital signs (NVS) test. 63.2% (n=12) of subjects in group 1 and 52.6% (n=10) of group 2 were female. 52.6% of individuals in group 1 and 57.9% of individuals in group 2 ate three main meals per day. It is noteworthy that the most frequently skipped main meal in both groups is lunch, and individuals eating outside generally prefer dinner on weekends. The VAS value of group 1 was 6±0.9; VAS value of group 2 was 7.4±0.36. The study power was 0.99, effect size was 2.04 (Cohen's d) and a margin of error was 0.05 (α=0.05), calculated according to t-test performed with the VAS results. While individuals in group 1 have adequate health literacy (4.8±1.7), individuals in group 2 have limited health literacy (3.8±2.4). This indicates that food label information is an effective factor in evaluating the visual appeal, odor, taste, aftertaste, and flavor of food products. In this context, labeling seems to be very effective in the selection of healthy foods that form the basis of an adequate and balanced diet. It is believed that the results of this study may provide a new perspective for the development of strategies for the selection of healthy foods by individuals.

Keywords: Food labels, Milk and dairy products, Food choice

Introduction

Food labels are intended to facilitate consumers' purchasing behavior and help them make more conscious and healthier choices (Egnell et al., 2018). From an individual and public health perspective, food labels are critical to addressing the global increase in diet-related diseases (Crockett et al., 2018). A randomized controlled trial found a significant association between the use of labels and the health value of the products purchased (Mhurchu et al., 2018).

Taste and smell perception increases people's intention to buy (Bialkova et al., 2016). Perceptions of health, taste, and aroma can be influenced by both the internal and external characteristics of the product. Package design, brands, colors, labels, and other visual elements are among the factors that influence consumer expectations and dietary preferences (Mazzù et al., 2021). Taste-based labeling is offered as an alternative to health-based labeling, which primarily emphasizes the health attributes of foods (e.g., low calorie, low fat, or low sugar). One study has shown that taste-oriented labeling increases healthy food choices by 38% (Turnwald & Crum, 2019).

Improving the knowledge of some consumer groups about nutrition may increase their motivation in this regard. A potential benefit of adequate nutrition information is that it may encourage individuals to make healthier choices by improving their ability to use nutrition labels. For example, knowledge of the link between diet and cancer may lead consumers to focus on fiber claims on the nutrition label and whole grain products on the ingredient list. This is consistent with the notion that the long-term working memory provided with nutritional information promotes both frequencies of label use and understanding of food labeling (Miller & Cassady, 2015). The more consumers know about nutrition, the more likely they are to read and understand the nutrition information on food labels. Nutrition labels are an important source of nutrition information, but the information contained on labels can be complex and not used appropriately by consumers. Food labels can raise expectations about the sensory or hedonic properties of a product (Li & Dando, 2019).

The purpose of this study is to determine how information on milk and dairy product labels (brand, nutrition declaration, nutrition and health claims, etc.) influences consumers' sensory and hedonic perceptions. Previous studies have mostly been cross-sectional, surveying people's reading habits and purchasing behavior regarding food labels, but unlike other studies, this study identifies the parameters by which people make their food choices.

Method

This study, designed to investigate how nutrition labels affect consumer preferences, followed the principles of the Declaration of Helsinki. Prior to the study, individuals were fully informed of the purpose and method of the study, and verbal consent was obtained from those individuals who agreed to participate. Furthermore, the study was approved by the Ethics Committee of the University of Mersin for Social and Human Sciences with a decision dated 28.08.2023 and number 199.

Participants

The study involved educated individuals aged 18 to 65 years who did their own shopping, had no chronic or metabolic diseases, were not lactose intolerant, were not pregnant or breastfeeding, and were women who were not menstruating. Before starting the survey, a mini questionnaire was conducted to determine whether the participants met the inclusion criteria. First, a homogeneous group was formed by considering the inclusion and exclusion criteria. Then, simple random sampling was used to determine which group the participants belonged to. The sample size was calculated using the G-power 3.1.9.2 program, considering $\alpha=0.05$, effect size=0.5, and $1-\beta=0.8$. It was sufficient to conduct the study with a total of 38 subjects, 19 subjects in each group.

Data Collection

Sociodemographic Characteristics and General Dietary Habits

The survey questionnaire asking for sociodemographic characteristics and general eating habits was prepared by the researcher. In the sociodemographic characteristics section, gender, age, education level, marital status, income level, disease status, smoking, and alcohol consumption were queried. Regarding general dietary habits, subjects were asked about the number of main meals and snacks, skipping meals, which meal those who skip meals generally skip, frequency of eating away from home, use of dietary supplements, and amount of physical activity.

Visual Analogue Scala (VAS)

In this study, subjects tasted the same foods from different brands. After tasting, the different characteristics of the foods were rated using a visual analog scale. Participants were asked to rate the visual stimulus, odour, taste, aftertaste, and aroma of the tested foods on the scale. Water was drunk between each assessment to ensure that the assessments of test nutrients consumed did not influence each other. The evaluation results were calculated using the following formula: [visual stimulus+odour+taste+flavour+(100-aftertaste)/5] (Gonzalez-Anton et al., 2015).

Newest Vital Sign (NVS)

The NVS, first developed by Weiss et al. (2005), consists of six questions and measures reading and comprehension of a food label. The NVS test consists of questions about the information found on the nutrition label of a carton of ice cream, and the correct answer to each question in the test, which requires basic reading and math skills, is worth 1 point. Those who score between 4 and 6 points on the NVS test are considered adequate, those who score between 2 and 3 points are considered limited, and those who score 0 to 1 point are most likely to be considered a person with limited health literacy.

Study Design

The subjects were randomly divided into two groups, group 1 and group 2, and were given the following foods from milk and dairy products:

- Plain milk
- Chocolate milk
- Fortified milk
- Yoghurt
- Fruit yoghurt
- Plain kefir
- Fruit kefir
- Plant-based milk

After the study, the sociodemographic characteristics and general dietary habits of all subjects participating in the study were obtained. Group 1 participants sampled and evaluated without seeing the nutrition label. Group 2 participants looked at the food labels and then tasted. Both groups answered VAS and NVS tests, respectively, after tasting.

Statistical Analysis

Data obtained from the study were analyzed using the SPSS (Statistical Package for Social Science) program. Normality test was performed using the Shapiro-Wilk test. Non-parametric statistical methods were used for non-normally distributed values. Mean and standard deviation were used for normally distributed variables, and median (and minimum-maximum) were used for non-normally distributed variables. Nonparametric statistical methods were used for skewed distributed values. Mann Whitney U test was used to compare two independent groups that were not normally distributed. The Wilcoxon signed test was used for comparison of two dependent groups that were not normally distributed. To analyze the correlation between two continuous variables that were not normally distributed Spearman's rho correlation analysis was used.

Results

Table 1. Sociodemographic characteristics

Gender (%)	Group 1	Group 2
Female	63.2	52.6
Male	36.8	47.4
Age (x̄±SD)	36.8±12.4	38.6±12.1
BMI (kg/m^2)	26.5	24.7
Education level (%)		
Primary-secondary school	15.8	15.8
High school	31.5	15.8
Associate degree	15.8	0.0
Bachelor	31.6	52.6
Master and above	5.3	15.8
Smoking status (%)		
No	57.9	52.6
Yes	42.1	47.4
Alcohol consumption (%)		
No	94.7	68.4
Yes	5.3	31.6

In this study, which included 19 subjects in each group and a total of 38 subjects, 63.2% of the subjects in the group 1 and 52.6% of the subjects in group 2 were women. The average age of the group 1 is 36.8±12.4 years, that of the group 2 is 38.6±12.1 years. The average BMI of the group 1 is 26.5 kg/m^2, that of the group 2 is 24.7 kg/m^2. The majority of participants in both groups have a bachelor degree (31.6% of group 1; 52.6% of group 2). The majority of participants in both groups are nonsmokers (57.9% of group 1; 52.6% of group 2). 94.7% of individuals in group 1 and 68.4% of individuals in group 2 do not consume alcohol (Table 1).

For all food groups, the VAS rating of those who tasted by examining the nutrition labeling (group 2) was higher than the VAS rating for those who tasted without looking at the nutrition labeling (group 1). The highest VAS score in group 1 belongs to yoghurt (x̄: 7.0 point), while the highest VAS score in group 2 belongs to fruit yoghurt (x̄: 7.9 point). The lowest VAS score in group 1 belongs to fortified milk (x̄: 4.8 point), while the lowest VAS score in group 2 belongs to plant-based milk (x̄: 7.0 point) (Figure 2).

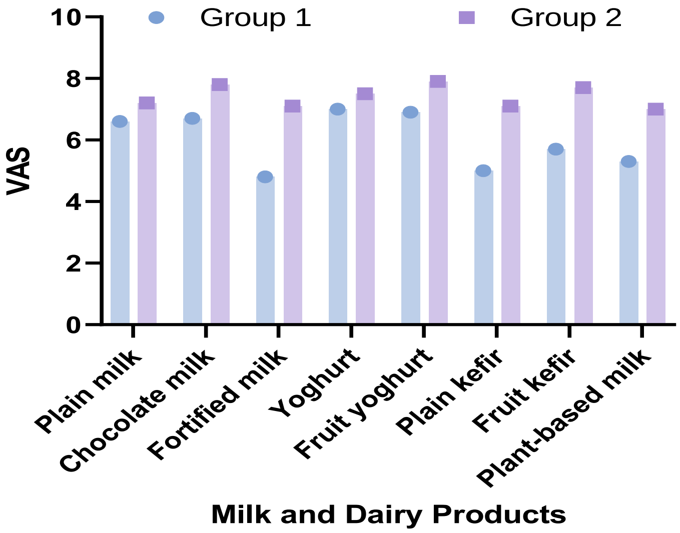

Figure 2. Visual analogue scale

The Newest Vital Sign is a new tool designed to quickly and simply assess a patient's health literacy skills. It can be administered in only 3 minutes and is available in English. The patient is given a specially designed ice cream nutrition label to review and is asked a series of questions about it. Based on the number of correct answers, health care providers can assess the patient's health literacy level and adjust the way they communicate to ensure patient understanding. In this study, health literacy of both groups is adequate literacy. The NVS score of group 1 (x̄: 4.8 point) is higher than the NVS score of group 2 (x̄: 3.8 point) (Figure 3).

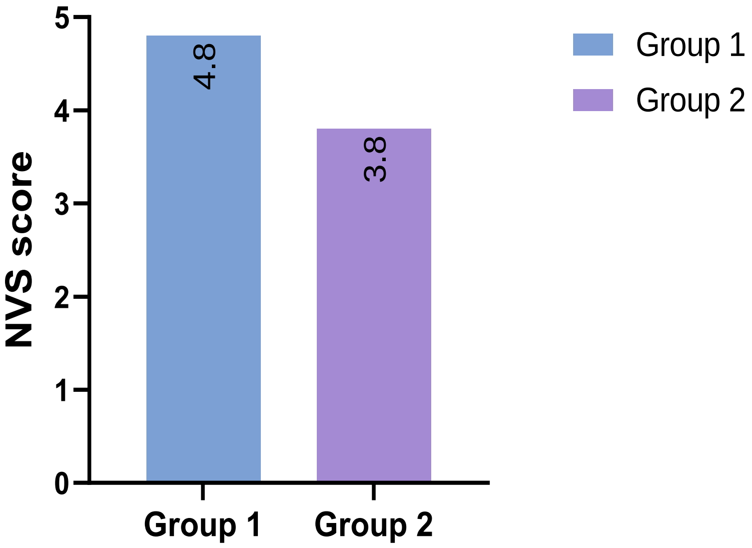

Figure 3. NVS score

Discussion

Individuals have some basic needs to continue their lives and improve their quality of life. Nutrition is at the forefront of these needs, and nutrients must be provided. The information that companies provide about the product when providing nutrients is an important issue because it affects consumers' decision-making processes. The most important and common form of this information transfer is labels, product composition, price, expiration date and origin. In particular, nutrition labeling, which provides information about nutritional value, makes it easy for consumers to make healthy and informed choices. The common goal of the national and international programs developed in this regard is to inform consumers so that they can make healthy food choices and to provide nutrition labeling according to scientific principles.

This study is the first to investigate how information on milk and dairy product labels (brand, nutrition declaration, nutrition and health claims, etc.) affects consumers' sensory and hedonic perceptions. The results of the current study showed that people who look at food labels are deceived by the label and believe that the food is more delicious, regardless of the taste of that food. People who tasted food without seeing the nutrition label gave a different rating because they focused only on the taste of the food. While both groups had adequate levels of health literacy, this did not affect how individuals rated food groups.

Nutrition labelling is a recognised strategy that influences consumers to make healthier food choices (WHO 2004; Ikonen et al., 2020). Consumers generally believe that food with good labels and high quality is better, regardless of the taste of the food. They have a different opinion when they taste foods that they believe will taste good because their labels are very good without seeing the labels. Many even believe that food products from some origins are of higher quality, safer, more environmentally friendly, and otherwise superior to food products from other origins (Thøgersen, 2023). In this study, subjects found foods with better labeling more delicious, even when they were produced in the same country of origin.

According to a study, people pay the most attention to the labels of milk and dairy products when shopping for food (Cecchini & Warin., 2015). In this study, individuals in group 2 examined food labels more carefully when the foods tasted were from the milk and dairy products group. The subjects in Group 1 had a biased attitude toward food because they tasted it without seeing the food label. Therefore, they gave low scores when evaluating the taste of foods. In group 2, subjects were fooled by the attractiveness of the nutrition label and gave high scores in evaluating taste. The comparison of these two situations shows that nutrition labeling is very important for consumer preferences and that nutrition labeling influences people's purchasing preferences more than food taste.

Health literacy is the ability to obtain, process, and understand basic information in order to make appropriate health-related decisions. In order for individuals to protect their own health and improve their nutritional status, they must properly understand and apply the information available (Shah et al., 2010). The health literacy test is used to assess the ability of individuals to understand the information on the label when purchasing packaged foods, to interpret this information correctly, and to select appropriate foods. According to the National Adult Literacy Assessment in America, 53% of the adult population was found to have moderate health literacy, 36% had inadequate health literacy, and 22% had basic health literacy (Me et al., 2003). In the Health Literacy Survey (2012) conducted in eight member countries of the European Union (Austria, Bulgaria, Germany, Spain, Ireland, Netherlands, Poland, Greece), the level of health literacy in these countries is most likely limited, as follows: Austria 12.9%; Bulgaria 28.8%; Germany 15.8%; Spain 34.3%; Ireland 19.9%; Netherlands 8.9%; Poland 32.3%; Greece 17.7%. The most likely limited health literacy of these eight countries was 21.44%, and the adequate health literacy was 55%. The average NVS score of these countries is as follows: Austria, 4.1±0.81; Bulgaria, 3±1.9; Germany, 3.9±2.1; Spain, 2.6±2; Ireland, 3.6±2.1; Netherlands, 4.5±1.8; Poland, 2.9±2.1; Greece, 3.6±2 (Consortium et al., 2012). In this study, individuals in group 1 have adequate health literacy (4.8±1.7), individuals in group 2 have limited health literacy (3.8±2.4).

Conclusion

The study, conducted to assess the impact of nutrition labels on consumer preferences regarding milk and milk groups, yielded the following results: Most participants in both groups were women. The average age is 36.8±12.4 years in group 1 and 38.6±12.1 years in group 2. The educational level of the majority of both groups is a university degree. Most of the study participants do not smoke or consume alcohol. The average VAS score of group 2 was higher than that of group 1. Health literacy of both groups is adequate literacy. The NVS score of group 1 ($\bar{x}$: 4.8 point) is higher than the NVS score of group 2 ($\bar{x}$: 3.8 point).

Recommendations

This food labeling study differs from previous studies in the literature because it is an intervention study. While it is important to develop individuals' reading habits when reading nutrition labels to ensure a healthy diet, studies of what individuals understand from what they read are also very important. For this reason, it is believed that individuals' health literacy, and especially nutrition, literacy, is effective in helping them understand what they read and make decisions about their own health, especially when making healthy food choices. The regulations to be made in the Turkish Food Codex are intended to eliminate labeling problems, make labeling more understandable, and focus on consumer safety. It is assumed that the visibility and comprehensibility of nutritional information on packaging will make a significant contribution to consumers' healthy food choices.

Scientific Ethics Declaration

The authors declare that the scientific ethical and legal responsibility of this article published in EPSTEM journal belongs to the authors.

Acknowledgements or Notes

* This article was presented as an oral presentation at the International Conference on Basic Sciences and Technology (www.icbast.net) held in Antalya/Turkey on November 16-19, 2023.

References

Bialkova, S., Sasse, L., & Fenko, A. (2016). The role of nutrition labels and advertising claims in altering consumers' evaluation and choice. *Appetite, 96,* 38-46.

Cecchini, M., & Warin, L. (2016). Impact of food labelling systems on food choices and eating behaviours: a systematic review and meta-analysis of randomized studies. *Obesity Reviews*, *17*(3), 201-210.

Consortium H-E.(2012). *Comparative report of health literacy in eight EU member states. The European Health Literacy Survey HLS-EU.* http://www.health-literacy.eu/

Crockett, R. A., King, S. E., Marteau, T. M., Prevost, A. T., Bignardi, G., Roberts, N. W., ... & Jebb, S. A. (2018). Nutritional labelling for healthier food or non-alcoholic drink purchasing and consumption. *Cochrane Database of Systematic Reviews*, (2). https://doi.org/10.1002/14651858.CD009315.pub2

Egnell, M., Talati, Z., Hercberg, S., Pettigrew, S., & Julia, C. (2018). Objective understanding of front-of-package nutrition labels: an international comparative experimental study across 12 countries. *Nutrients*, *10*(10), 1542.

Gonzalez-Anton, C., Rico, M. C., Sanchez-Rodriguez, E., Ruiz Lopez, M. D., Gil, A., & Mesa, M. D. (2015). Glycemic responses, appetite ratings and gastrointestinal hormone responses of most common breads consumed in Spain. A randomized control trial in healthy humans. *Nutrients*, *7*(6), 4033-4053.

Ikonen, I., Sotgiu, F., Aydinli, A., & Verlegh, P. W. (2020). Consumer effects of front-of-package nutrition labeling: An interdisciplinary meta-analysis. *Journal of the Academy of Marketing Science*, *48*(3), 360-383.

Li, T., & Dando, R. (2019). Impact of common food labels on consumer liking in vanilla yogurt. *Foods*, *8*(11), 584.

Mazzù, M. F., Marozzo, V., Baccelloni, A., & de’Pompeis, F. (2021). Measuring the effect of blockchain extrinsic cues on consumers’ perceived flavor and healthiness: A cross-country analysis. *Foods, 10*(6), 1413.

Kutner, M., Greenburg, E., Jin, Y., & Paulsen, C. (2006). *The health literacy of America's adults: Results from the 2003 national assessment of adult literacy. NCES 2006-483. National Center for Education statistics*. Retrieved from https://nces. ed.gov/pubs2006/2006483.pdf

Mhurchu, C. N., Eyles, H., Jiang, Y., & Blakely, T. (2018). Do nutrition labels influence healthier food choices? Analysis of label viewing behaviour and subsequent food purchases in a labelling intervention trial. *Appetite*, *121*, 360-365.

Miller, L. M. S., & Cassady, D. L. (2015). The effects of nutrition knowledge on food label use. A review of the literature. *Appetite*, *92*, 207-216.

Shah, L. C., West, P., Bremmeyr, K., & Savoy Moore, R. T. (2010). Health literacy instrument in family medicine: the “newest vital sign” ease of use and correlates. *The Journal of the American Board of Family Medicine*, *23*(2), 195-203.

Thøgersen, J. (2023). How does origin labelling on food packaging influence consumer product evaluation and choices? A systematic literature review. *Food Policy*, *119*, 102503.

Turnwald, B. P., & Crum, A. J. (2019). Smart food policy for healthy food labeling: Leading with taste, not healthiness, to shift consumption and enjoyment of healthy foods. *Preventive Medicine*, *119*, 7-13.

Weiss, B. D., Mays, M. Z., Martz, W., Castro, K. M., DeWalt, D. A., Pignone, M. P., ... & Hale, F. A. (2005). Quick assessment of literacy in primary care: the newest vital sign. *The Annals of Family Medicine*, *3*(6), 514-522.

World Health Organization. (2004). Global strategy on diet, physical activity and health. Retrieved from https://www.who.int/publications/i/item/9241592222.

Author Information

Fatma Hazan Gul
Mersin University
Mersin, Turkey
Contact e-mail: hazanngul@gmail.com

Ayse Saltekin
Mersin University
Mersin, Turkey

To cite this article:

Gul, F. H., & Saltekin, A. (2023). The effect of food labels on consumer’s choice of milk and dairy products. *The Eurasia Proceedings of Science, Technology, Engineering & Mathematics (EPSTEM), 25,* 35-41.

The Eurasia Proceedings of Science, Technology, Engineering & Mathematics (EPSTEM), 2023

Volume 25, Pages 42-49

ICBAST 2023: International Conference on Basic Sciences and Technology

Investigation of Total Phenolic, Flavonoid Content and Antioxidant Activity of *Onobrychis Megataphros* Leaf Extract

Salih Muvakit
Gaziantep University

Mehmet Ozaslan
Gaziantep University

Abstract: This study aims to determine the total phenolic, flavonoid and antioxidant activity levels of *Onobrychis megataphros* plant leaves. The *O.megataphros* (Sainfoin) samples were collected, laid on blotting papers in shady places away from sunlight and dried. After that, the dried plant samples were pulverized. The powdered samples were extracted with methanol using Soxhlet device. The methanol was removed by evaporation in a rotary evaporator and stored at +4ºC until the experiment starts. Phenolic and flavonoid content and antioxidant activity properties of *O.megataphros* plant leaf extracts were examined. The determination of the Phenolic and flavonoid performed according to Zengin et al. (2015a). The sample and blank absorbance was read at 415 nm after 10 min incubation at room temperature. Absorbance of the blank was subtracted from that of the sample. Total flavonoid content was expressed as equivalent to routine. Total antioxidant activity of the samples was evaluated by phosphor molybdenum method. Sample solution (0.2mL) was combined with 2mL of reagent solution (0.6M sulfuric acid, 28mM sodium phosphate and 4mM ammonium molybdate). The sample absorbance was read at 695nm after 90 min incubation at 95°C. As a result, it was determined that the total phenolic content in *O.megataphros* plant leaf extracts was 20.62±0.15 mg GAE/g extract and total flavonoid content was 24.55±0.22 mg QE/g extract. At the end of this research work, it is concluded that TAS and TOS levels increased with the increase in concentration.

Keywords: Onobrychis megataphros, Total phenolic content, Total flavonoid content, TOS, TAS

Introduction

Many plant species have been used for various purposes among humans for many years across the world. According to the World Health Organization (WHO), pharmacopoeias of 91 countries and some publications on medicinal plants, the number of medicinal plants used for therapeutic purposes is over 20.000. The important properties of plants for human health have been investigated in the laboratory since 1926 (Toroglu & Cenet, 2006). The genus *Onobrychis*, which grows naturally in Turkiye consists of two subgenera, *Onobrychis* and *Sisyrosema*. Among these subgenera, *Onobrychis* is known to be divided into 3 different sections as *Dendobrychis*, *Laphobrychis* and *Onobrychis*. Fabaceae family is the second largest family after Asteraceae in Turkiye and has various uses among the people. For example, *Onobrychis gracilis* is used in the treatment of cold and flu, *Vicia faba* in gastrovascular diseases, *Vicia cracca* subsp. *stenophylla* in cold and *Vicia ervilia* in the treatment of diabetes (Demirci & Ozhatay, 2012; Sargın et al., 2013; Hayta et al., 2014).

Free radicals are formed during the functioning of normal metabolic pathways in the organism or by environmental agents such as pesticides, aromatic hydrocarbons, toxins, solvents or under the influence of various external factors such as stress and radiation (Pham Huy et al., 2008). Oxygen-centered free radicals and

---

- Selection and peer-review under responsibility of the Organizing Committee of the Conference

reactive oxygen species, which are continuously produced in the body, can cause tissue destruction and then cell death. Oxidative damage caused by free radicals can cause aging and some diseases (Phaniendra et al., 2015). Fruits and vegetables rich in phenolic compounds protect the human body against free oxygen radicals. Epidemiological studies have shown that phytonutrients in plant sources are beneficial against reactive oxygen species and the protective effects of fruits and vegetables are due to natural compounds such as ascorbic acid (vitamin C), α-tocopherol (vitamin E), carotenoids, glutathione, flavonoids and phenolic acids (Halvorsen et al., 2002). When free radicals and reactive oxygen species cause oxidation in foods or biological systems, antioxidants can prevent or delay this process by various mechanisms (Ulusoy et al., 2010). With the measurement of antioxidant capacity in foods, people's interest in the use of natural products in pharmaceutical and cosmetic products for health purposes is increasing day by day (Lopez Alarcon & Lissi, 2006).

In recent years, indiscriminate use of antibiotics all over the world and drug resistance are closely related (Celik et al., 2010). It has been observed that the treatment of diseases and infections such as AIDS and cancer, which weaken the immune system, has become difficult due to drug-resistant pathogenic fungi and bacteria (Zazharskyi et al., 2019). This situation has encouraged scientists to search for new antimicrobial compounds from different sources. Since plants constitute a source from which new antimicrobial chemotherapeutic substances can be obtained, research has been particularly focused on medicinal plants (Zazharskyi et al., 2019). Although there is literature information that different *Onobrychis* species are used in the treatment of various diseases among humans (Demirci & Ozhatay, 2012; Sargın et al., 2013; Hayta et al., 2014), it is the first in terms of investigating the antioxidant, antimicrobial, total phenolic content of *O.megataphros* plant and bringing it to the literature.

Method

Collection and Extraction of Plant Samples

Onobrychis megataphros plant used in the study was collected from (Siverek- Hilvan) Şanlıurfa and the surrounding areas between 2021 and 2022 during the vegetation periods. After the plant samples were dried in the shade, the leaves were pulverized. The samples were subjected to methanol extraction for 6-8 hours in a Soxhlet apparatus. The extract was then filtered with Whatman blue band filter paper and evaporated at 40 °C to remove the solvent.

Biological Activity Determination

Determination of Total Phenolic Content: For total phenolic content, the sample solution (0.25 mL) was mixed with diluted Folin - Ciocalteu reagent (1 mL, 1:9) and shaken strongly. After 3 min, Na_2CO_3 solution (0.75 mL, 1%) was added and sample absorbance was read at 760 nm after incubation for 2 h at room temperature. Total phenolic content was expressed as Gallic acid equivalent (Zengin et al., 2015a).

Determination of Total Flavonoid Content: For total flavonoid content, the sample solution (1 mL) was mixed with the same volume of aluminum trichloride (2%) in methanol. Similarly, a blank was prepared by adding the sample solution (1 mL) to methanol (1 mL) without AlCl3. After incubation at room temperature for 10 min, the absorbance of the sample and the blank was read at 415 nm. The absorbance of the blank was subtracted from that of the sample. Total flavonoid content was expressed as routine equivalents (Zengin et al., 2015a).

Determination of Total Antioxidant Activity:

Total antioxidant activity of the samples was evaluated by phosphor molybdenum method. Sample solution (0.2 mL) was combined with 2 mL reagent solution (0.6 M sulfuric acid, 28 mM sodium phosphate and 4 mM ammonium molybdate). After incubation at 95°C for 90 min, the absorbance of the sample was read at 695 nm (Zengin et al., 2015b). For 1,1-diphenyl-2-picrylhydrazyl (DPPH) radical scavenging activity, sample solution (1 mL) was added to 4 mL 0.004% methanol DPPH solution. After incubation for 30 min at room temperature in the dark, the absorbance of the sample was read at 517 nm (Kocak et al., 2016; Tepe et al., 2011).

For ABTS cation radical trapping activity, $ABTS^{\cdot +}$ radical cation was directly produced by reacting 7 mM ABTS solution with 2.45 mM potassium persulfate and allowing the mixture to stand in the dark for 12-16 h at room temperature. Before starting the analysis, the ABTS solution was diluted with methanol to obtain an absorbance of 0.700 ± 0.02 at 734 nm. The sample solution (1 mL) was added to the ABTS solution (2 mL) and mixed. After incubation at room temperature for 7 min, the absorbance of the sample was read at 734 nm (Kocak et al., 2016).

For metal chelating activity on ferrous ions, briefly sample solution (2 mL) was added to FeCl2 solution (0.05 mL, 2 mM). The reaction was initiated by adding 5 mM ferrozine (0.2 mL). Similarly, a blank was prepared by adding sample solution (2 mL) to FeCl2 solution (0.05 mL, 2 mM) and ferrozine-free water (0.2 mL). After incubation at room temperature for 10 min, the absorbances of the sample and the blank were read at 562 nm (Tepe et al., 2011).

For copper ion reduction activity (CUPRAC), sample solution (0.5 mL) was added to a premixed reaction mixture containing CuCl2 (1 mL, 10 mM), neo cuproin (1 mL, 7.5 mM) and NH_4Ac buffer (1 mL, 1 M, pH 7.0). Similarly, a blank was prepared by adding sample solution (0.5 mL) to a premixed reaction mixture (3 mL) without CuCl2. Then, after incubation at room temperature for 30 min, the absorbance of the sample and the blank were read at 450 nm (Apak et al., 2006). For ferric reducing antioxidant power (FRAP), sample solution (0.1 mL) was added to FRAP reagent (2 mL) containing acetate buffer (0.3 M, pH 3.6), 2,4,6-tris(2-pyridyl)-s-triazine (TPTZ) and ferric chloride (20 mM) in a ratio of 10:1:1:1 (v/v/v) in 40 mM HCl.

Inhibitory activity on α-amylase was carried out using the Caraway-Somogyi iodine/potassium iodide (IKI) method. Sample solution (25 µL) was mixed with α-amylase solution (50 µL) in phosphate buffer (pH 6.9 with 6 mM sodium chloride) in a 96-well micro plate and incubated at 37°C for 10 min. After pre-incubation, starch solution (50 µL, 0.05%) was added and the reaction was initiated. Similarly, a blank was prepared by adding sample solution to all reaction reagents without enzyme solution (α-amylase). The reaction mixture was incubated at 37°C for 10 min. The reaction was then stopped by adding HCl (25 µL, 1 M). This was followed by adding iodine-potassium iodide solution (100 µL). The absorbance of the sample and the blank was read at 630 nm. The absorbance of the blank was subtracted from that of the sample.

Tyrosinase inhibitory activity was measured using a dopachrome method modified with L-DOPA as substrate. Sample solution (25 µL) was mixed with tyrosinase solution (40 µl) and phosphate buffer (100 µl, pH 6.8) in a 96-well microplate and incubated at 25°C for 15 min. The reaction was then initiated by adding L-DOPA (40 µl). Similarly, a blank was prepared by adding sample solution to all reaction reagents without enzyme (tyrosinase) solution. Sample and blank absorbance were read at 492 nm after 10 min incubation at 25°C (Sarikurkcu et al., 2018).

Cholinesterase (ChE) inhibitory activity was measured using Ellman's method. The sample solution (50 µL) was mixed with DTNB (125 µL) and AChE solutions (25 µL) in Tris-HCl buffer (pH 8.0) in a 96-well micro plate and incubated at 25°C for 15 min. The reaction was then initiated by adding acetylthiocholine iodide (ATCI) (BTCI) (25 µL). Similarly, a blank was prepared by adding sample solution to all reaction reagents without enzyme solutions (AChE). The absorbance of the sample and the blank was read at 405 nm after 10 min incubation at 25°C. The absorbance of the blank was subtracted from the absorbance of the sample (Sarikurkcu et al., 2018).

For enzyme inhibition, radical scavenging and metal chelating assays, the sample concentration reducing the initial concentration by 50% was defined as IC50, while EC50 values were calculated as the sample concentration providing an absorbance of 0.500 for reducing power and phosphor molybdenum assays and 50% concentration providing initial inhibition for radical scavenging and metal chelation assays. The biological activities of the extracts were expressed as mg standard equivalents/g extract and compared with those of standards including trolox, ethylene di-amine tetra acetic acid (disodium salt) (EDTA), galantamine, Kojic acid and Acarbose used as positive controls.

Phyto Chemical Analysis

Phyto chemical analysis of the extract was carried out by a sensitive, rapid, simple and reproducible method previously developed and validated using LC-ESI-MS/MS (Cittan & Celik, 2018). An Agilent Technologies 6420 Infinity liquid chromatography system coupled to a 1260 triple Quadra pole mass spectrometer was used for quantitative analyses. Chromatographic separation was performed on a Poro-shell 120 EC-C18 (100 mm x 4.6 mm inner diameter, 2.7 µm) column. The mobile phase configuration (0.1% formic acid/methanol) was chosen on the basis of better chromatographic resolution of isomeric compounds. On the other hand, the selected mobile phase configuration also provided higher sensitivity for many phenolic compounds. Consequently, the mobile phase was made of solvent A (0.1%, v/v formic acid solution) and solvent B (methanol). The gradient profile was set as follows: 0.00 min 2% B fluent, 3.00 min 2% B fluent, 6.00 min 25% B fluent, 10.00 min 50% B fluent, 14.00 min 95% B fluent, 17.00 min 95% B and 17.50 min 2% B fluent. The column temperature was maintained at 25°C. The flow rate was 0.4 mL min-1 and the injection volume was 2.0 µL.

The tandem mass spectrometer was interfaced to the LC system via an ESI source. The electro spray source of the MS was operated in negative and positive multiple reaction monitoring (MRM) mode, and the interface conditions were as follows: -3.5 kV capillary voltage, 300°C gas temperature and 11 L min-1 gas flow. The nebulizer pressure was 40 psi.

Results

Total Phenolic and Flavonoid Substance Content

Total phenolic content was 20.62±0.15 mg GAE/g extract and total flavonoid content was 24.55±0.22 mg QE/g extract (Table 1). The concentrations of selected phenolic compounds in *Onobrychis megataphros* extract are shown in Table 2. Accordingly, (+)-Catechin, Taxifolin, 2-Hydroxycinnamic acid, Luteolin and Apigenin were not detected.

Table 1. Total phenolic and flavonoid contents of *Onobrychis megataphros* extract

Total phenolics (mgGAE/g extract)	20.62±0.15
Total flavonoids (mgQE/g extract)	24.55±0.22

GAE: Gallic acid equivalent

Table 2. Concentrations of selected phenolic compounds in *Onobrychis megataphros* extract

RT	Compounds	Concentration (µg/g extract)
8.7829	Gallic acid	25.8±0.8
10.5569	Protocatechuic acid	73.1±0.4
10.8157	Pyrocatechol	13.5±1.0
10.8352	3,4-Dihydroxyphenylacetic acid	5.24±0.19
11.2863	(+)-Catechin	nd
11.7605	Chlorogenic acid	43.6±0.3
11.9714	2,5-Dihydroxybenzoic acid	6.37±0.15
12.0643	4-Hydroxybenzoic acid	42.9±0.1
12.2281	(-)-Epicatechin	9.65±0.04
12.6006	Caffeic acid	7.37±0.14
12.6904	Syringic acid	11.4±0.8
12.8289	3-Hydroxybenzoic acid	3.97±0.32
13.0044	Vanillin	7.25±0.32
13.4183	Verbascoside	0.21±0.01
13.6707	Taxifolin	nd
13.7506	p-Coumaric acid	18.5±0.1
13.8236	Sinapic acid	5.20±0.19
13.8837	Ferulic acid	39.9±0.7
14.2311	Luteolin 7-glucoside	29.8±0.3
14.4193	2-Hydroxycinnamic acid	nd
14.4289	Hesperidin	2263±2
14.4634	Hyperoside	2580±5
14.4915	Rosmarinic acid	5.84±0.14
14.7066	Apigenin 7-glucoside	93.6±1.8
14.9445	Pinoresinol	12.2±0.3
15.0470	Eriodictyol	nd
15.5459	Quercetin	2.58±0.04
15.7763	Luteolin	nd
16.0729	Kaempferol	3.34±0.11
16.2364	Apigenin	nd

RT: Retention time, nd: not detected

Antioxidant Capacity

The results of the antioxidant activities of *Onobrychis megataphros* extracts are shown in Table 3. TEs and EDTAEs refer to the equivalents of trolox and ethyl enediaminetetetra acetic acid (disodium salt), respectively. ACEs, GALAEs and CAEs refer to acarbose, galantamine and kojic acid equivalents, respectively. Values shown with the same superscripts are not significantly different after Tukey's hoc test at the 5% significance level (Table 4).

Table 3. Antioxidant activities of *Onobrychis megataphros* extract

Assays	*Onobrychis megataphros*	Trolox	EDTA
Phospho molybdenum (EC_{50}: mg/mL)	2.03±0.07	0.49±0.04	
CUPRAC Reducing (EC_{50}: mg/mL)	1.76±0.03	0.11±0.001	
FRAP Reducing (EC_{50}: mg/mL)	1.45±0.01	0.04±0.002	
DPPH Scavenging (IC_{50}: mg/mL)	6.11±0.33	0.06±0.001	
ABTS Scavenging (IC_{50}: mg/mL)	2.40±0.02	0.11±0.001	
Ferrous ion chelating (IC_{50}: mg/mL)	2.12±0.02		0.03±0.001
Phospho molybdenum (mg TEs/g extract)	242±8		
CUPRAC Reducing (mg TEs/g extract)	62.6±1.2		
FRAP Reducing (mg TEs/g extract)	30.4±0.2		
DPPH Scavenging (mg TEs/g extract)	9.34±0.51		
ABTS Scavenging (mg TEs/g extract)	45.8±0.4		
Ferrous ion chelating (mg EDTAEs/g extract)	15.6±0.2		

Table 4. Enzyme inhibition activity of *Onobrychis megataphros* extracts.

Assays	*Onobrychis megataphros*	Galanthamine	Kojic acid	Acarbose
AChE inhibition (IC_{50}: mg/mL)	1.58±0.04	0.003±0.0001		
Tyrosinase inhibition (IC_{50}: mg/mL)	2.54±0.22		0.08±0.001	
α-Amylase inhibition (IC_{50}: mg/mL)	1.60±0.01			0.79±0.01
AChE inhibition (mg GALAEs/g extract)	1.7±0.04			
Tyrosinase inhibition (mg KAEs/g extract)	31.9±2.8			
α-Amylase inhibition (mg ACEs/g extract)	490±1			

In our study, TAS, TOS and OSI values increased according to the dose (Table 5).

Table 5. TAS/TOS and OSI index results of methanol extract of *Onobrychis megataphros*

µg/ml	TAS mmol/ml	TOS µmol/ml	OSI
50	2,685	23,84	0,888
100	3,102	37,01	1,193
150	3,208	48,68	1,517
200	3,221	56,22	1,745
250	3,237	72,80	2,249
300	3,255	75,56	2,321
350	3,290	81,79	2,486
400	3,300	87,27	2,644
450	3,336	91,88	2,754
500	3,313	93,53	2,823

Discussion and Conclusion

This study aims to determine the total phenolic, flavonoid and antioxidant activity levels of *Onobrychis megataphros* plant leaves. Therefore, firstly, *O.megataphros* (Sainfoin) samples were collected, laid on blotting papers in shady places away from sunlight and dried. The completely dried plant samples were pulverized. The powdered samples were extracted with methanol using Soxhlet device. The methanol was removed by evaporation in a rotary evaporator and stored at +4ºC until the experiment starts. Phenolic and flavonoid content and antioxidant activity properties of *O.megataphros* plant leaf extracts were investigated. To determine total phenolic content, sample solution (0.25 mL) was mixed with diluted Folin Ciocalteu reagent (1 mL, 1:9) and shaken strongly. After 3 min, Na_2CO_3 solution (0.75 mL, 1%) was added and the sample absorbance was read at 760 nm after 2 h incubation at room temperature. Total phenolic content was expressed as equivalents of gallic acid. For total flavonoid content, sample solution (1mL) was mixed with the same volume of aluminum trichloride (2%) in methanol. Similarly, a blank was prepared by adding sample solution (1mL) to methanol (1mL) without $AlCl_3$. The sample and blank absorbance were read at 415 nm after 10 min incubation at room temperature. Absorbance of the blank was subtracted from that of the sample. Total flavonoid content was expressed as equivalents of routine. Total antioxidant activity of the samples was evaluated by phosphor molybdenum method. Sample solution (0.2mL) was combined with 2mL of reagent solution (0.6M sulfuric acid, 28mM sodium phosphate and 4mM ammonium molybdate). The sample absorbance was read at 695nm after 90 min incubation at 95°C. As a result, it was determined that the total phenolic content in *O.megataphros* plant leaf extracts was 20.62±0.15 mg GAE/g extract and total flavonoid content was 24.55±0.22 mg QE/g extract.

As a result of our study, it was determined that TAS and TOS levels increased with the increase in concentration. Similar with our results Benchadi et al. (2022) determined that the total oxidant (TOS) and antioxidant status (TAS) levels of *O.crista-galli* increases with the concentration. Total phenolic content in our study was 20.62±0.15 mg GAE/g extract and total flavonoid content was 24.55±0.22 mg QE/g extract. Karakoca et al. (2013) investigated the phenolic compounds, biological and antioxidant activities of *Onobrychis armena* and found total phenolic content as 87.32 mg GAE/g and 128.23 mg GAE/g in flower and root methanol extracts, respectively. In a study conducted by Butkutė et al. (2016) on perennial legumes, reported that plant parts of the genus Trifolium and *Onobrychis viciifolia* contained more phenolics than Astragalus and Medicago species.

In another study investigating the phenolic content of *Onobrychis hypargyrea*, 83.25 mg GAE/g in ethyl acetate extract, 73.20 mg GAE/g in methanol extract and 69.38 mg GAE/g in water extract were determined (Zengin et al., 2015c). Godevac et al. (2008) investigated the antioxidant capacity of nine species belonging to the Fabaceae family collected from the mountains of Serbia and Montenegro. Antioxidant tests with various reaction mechanisms, including total phenolic content with Folin-Ciocalteu, DPPH radical scavenging capacity, Trolox equivalent antioxidant capacity (TEAC) values with ABTS radical cation, and inhibition of liposome peroxidation, were used in the study. As a result of the study, it was determined that the plant samples examined exhibited strong antioxidant capacity in all methods. Godevac et al (2008), determined the total phenolic content of *Onobrychis scardica* as 115.23 mg/GAE/g, which is higher than *O.megataphros* used in our study.

In our study the tyrosine inhibition and α-Amylase inhibition (IC_{50}) values were found respectively as 2.54±0.22 and 1.60±0.01 mg/mL. Similar with our results Aliyazıcıoğlu et al. (2017), in their study examining *Onobrychis oxyodonta* methanolic extract using the DPPH method, found the α-Amylase inhibition IC50 value as 1.333±0.0026 mg/mL.

In our study DPPH scavenging activity (IC_{50}) was determined as 6.11±0.33 mg/mL. Zengin et al. (2015c) investigated the antioxidant properties of *Onobrychis hypargyrea* and found DPPH activity as 0.31 ± 0.003 IC50 (mg/mL) in ethyl acetate extract, 0.29 ± 0.002 IC50 (mg/mL) in methanol extract and 0.27 ± 0.001 IC50 (mg/mL) in water extract.

Scientific Ethics Declaration

The authors declare that the scientific ethical and legal responsibility of this article published in EPSTEM journal belongs to the authors.

Acknowledgements or Notes

* This article was presented as an oral presentation at the International Conference on Basic Sciences and Technology (www.icbast.net) held in Antalya/Turkey on November 16-19, 2023.

References

Aliyazıcıoglu, R., Akkaya, S., Korkmaz, N., Sener, S. O., Badem, M., Ozgen, U., & Alpay Karaoglu, S. (2017). *Onobrychis Oxyodonta*; nın toprakustu kısmında antioksidan, antimikrobiyal ve tirozinaz inhibitor aktivitesi. *F.U. Sag. Bil. Tıp Dergisi, 31*(1), 25-31.

Apak, R., Guclu, K., Ozyurek, M., Esin Karademir, S., & Ercag, E. (2006). The cupric ion reducing antioxidant capacity and polyphenolic content of some herbal teas. *International Journal of Food Sciences and Nutrition*, *57*(2-6), 292-304.

Benchadi, W., Haba, H., Queiroz, E. F., Marcourt, L., Wolfender, J. L., Bensouici, C., & Benkhaled, M. (2020). Chemical composition, antioxidant, and anti-inflammatory activities of whole parts of onobrychis crista-galli (L.) lam. *The Natural Products Journal*, *10*(5), 642-654.

Butkutė, B., Lemežienė, N., Dagilytė, A., Cesevičienė, J., Benetis, R., Mikaliūnienė, J., Rodovičius, H. (2016). Mineral element and total phenolic composition and antioxidant capacity of seeds and aerial plant parts of perennial legumes. *Communications in Soil Science and Plant Analysis*, *47,* 36-45.

Celik, A., Herken, E. N., Arslan, I., Ozel, M.Z., & Mercan, N. (2010). Screening of the constituents, antimicrobial and antioxidant activity of endemic Origanum hypericifolium. *Natural Product Research, 24*(6), 1568-1577.

Cittan, M., & Celik, A. (2018). Development and validation of an analytical methodology based on liquid chromatography–electrospray tandem mass Spectrometry for the simultaneous determination of phenolic compounds in olive leaf extract. *Journal of Chromatographic Science* , *56*(4), 336-343.

Demirci, S., & Ozhatay, N. (2012). An ethnobotanical study in Kahramanmaras, (Turkiye); wild plants used for medicinal purpose in *Andirin, Kahramanmaras. Turkish Journal of Pharmceutical Science*, *9*(2), 75-92.

Godevac, D., Zdunic, G., Savikin, K., Vajs, V., & Menkovic N. (2008). Antioxidant activity of nine Fabaceae species growing in Serbia and Montenegro, *Fitoterapia*, *79*(3), 185-187.

Halvorsen, B.L., Holte, K., Myhrstad, M. C. W. (2002). A systematic screening of total antioxidants in dietary plants. *The Journal of Nutrition*,*132*(3), 461-471.

Hayta, S., Polat, R., & Selvi, S. (2014). Traditional uses of medicinal plants in Elazıg (Turkiye). *Journal of Ethnopharmacoogy*, *154*(3), 613-623.

Karakoca, K., Asan-Ozusaglam, M., Cakmak, Y. S., & Teksen, M. (2013). Phenolic compounds, biological and antioxidant activities of *Onobrychis armena* Boiss. & Huet flower and root extracts, *Chiang Mai Journal of Science*, *42*(2), 376-392.

Kocak, M. S., Sarikurkcu, C., Cengiz, M., Kocak, S., Uren, M. C., &Tepe, B. (2006). Salvia cadmica: Phenolic composition and biological activity. *Industrial Crops and Products*, *85*, 204-212.

Lopez Alarcon, C., & Lissi. E. (2006). A novel and simple ORAC methodology based on the interaction of Pyrogallol Red with peroxyl radicals. *Free Radical Research, 40*(9), 979-985.

Pham Huy, L. A., He, H., & Pham Huy, C. (2008). Free radicals, antioxidants in disease and health. *International Journal of Biomedical Science: IJBS*, *4*(2), 89-96.

Phaniendra, A., Jestadi, D. B., & Periyasamy, L. (2015). Free radicals: Properties, sources, targets, and their implication in various diseases. *Indian journal of clinical biochemistry*, *30*(1), 11-26.

Sargın, S. A., Akcicek, E., & Selvi, S. (2013). An ethnobotanical study of medicinal plants used by the local people of Alasehir (Manisa) in Turkiye. *J Ethnopharmacol*, *150*(3), 860-874.

Sarikurkcu, C., Kirkan, B., Ozer, M. S, Ceylan, O., Atilgan, N., Cengiz, M., & Tepe, B. (2018). Chemical characterization and biological activity of Onosma gigantea extracts. *Industrial Crops and Products ,115*, 323-329

Tepe, B., Sarikurkcu, C., Berk, S, Alim A, Akpulat, H. A. (2011). Chemical composition, radical scavenging and antimicrobial activity of the essential oils of Thymus boveii and Thymus hyemalis. *Records of Natural Products*, *5*(3), 208-220.

Toroglu, S., & Çenet, M. (2010). Tedavi amaclı kullanılan bazı bitkilerin kullanım alanları ve antimikrobiyal aktivitelerinin belirlenmesi için kullanılan metodlar. *KS Fen ve Muhendislik Dergisi*, *9*(2), 12-19.

Ulusoy, E., Kolaylı, S., & Sarıkaya, O. (2010). Antioxidant antimicrobial activity of different floral origin honeys from Turkiye. *Journal of Food Biochemistry*, *34*(1), 321-335.

Zazharskyi, V. V., Davydenko, P., Kulishenko, O., Borovik, I. V, & Brygadyrenko, V. V. (2019). Antimicrobial activity of 50 plant extracts. *Biosystems Diversity*, *27*(2), 163-169.

Zengin, G., Sarikurkcu, C., Gunes, E., Uysal, A., Ceylan, R., Uysal, S., Gungor, H., & Aktumsek, A. (2015). Two Gganoderma species: Profiling of phenolic compounds by HPLC-DAD, antioxidant, antimicrobial and inhibitory activities on key enzymes linked to diabetes mellitus, Alzheimer's disease and skin disorders. *Food & Function*, *6*(8), 2794-2802.

Zengin, G., Sarikurkcu, C., Uyar, P., Aktumsek, A., Uysal, S., Kocak, M. S., & Ceylan, R. (2015). Crepis foetida L. subsp. rhoeadifolia (Bieb.) Celak. as a source of multifunctional agents: Cytotoxic and phytochemical evaluation. *Journal of Functional Foods*, *17,* 698-708.

Zengin, G., Guler, G. O., Aktumsek, A., Ceylan, R., Nancy Picot, C. M, & Mahomoodally, M. F. (2015). Enzyme inhibitory properties, antioxidant activities, and phytochemical profile of three medicinal plants from Turkiye, *Advances in Pharmacological Sciences*, 1-8.

Author Information

Salih Muvakit
Gaziantep University
Gaziantep, Turkey

Mehmet Ozaslan
Gaziantep University
Gaziantep, Turkey
Contact e-mail: *ozaslanmd@gantep.edu.tr*

To cite this article:

Muvakit, S. & Ozaslan, M. (2023). Investigation of total phenolic, flavonoid content and antioxidant activity of *onobrychis megataphros* leaf extract. *The Eurasia Proceedings of Science, Technology, Engineering & Mathematics (EPSTEM), 25*, 42-49.

The Eurasia Proceedings of Science, Technology,
Engineering & Mathematics (EPSTEM)
ISSN: 2602-3199

The Eurasia Proceedings of Science, Technology, Engineering & Mathematics (EPSTEM), 2023

Volume 25, Pages 50-58

ICBAST 2023: International Conference on Basic Sciences and Technology

Approximate Analytic Solution for Fractional Differential Equations with a Generalized Fractional Derivative of Caputo-Type

Abedel-Karrem Alomari
Yarmouk University

Anwar Alsleeby
Yarmouk University

Abstract: This paper introduces the analytic series solution of the differential equation with fractional Caputo-type derivative including two parameters using the homotopy analysis method (HAM). The main properties of the fractional derivative with two parameters are illustrated. The standard HAM converges for a short domain, so we modify the method to overcome this issue by dividing the domain into finite subintervals and applying the method to each one. The initial conditions in each subinterval can be obtained from the previous one In this way, a continuous piecewise function that converges to the exact solution can be constructed. The effect of each fractional parameter on the solution behaviors is presented in figures and tables. Several examples are presented to verify the validity of the algorithm. A comparison with the exact solution in the case of integer derivative and with the Adaptive predictor corrected algorithm in the case of fractional one demonstrates the efficiency of the method.

Keywords: Fractional calculus, Homotopy analysis method, Riccati equation.

Introduction

Many different derivatives have been introduced, such as Hadamard, Grunwald Letnikov, Riesz, Caputo, and more (Kilbas et al., 2006; Samko et al., 1993). Based on the fractional integral, the fractional derivative is defined. One of these fractional integrals is the Riemann-Liouville fractional integral of order $\alpha > 0$, which is defined by

$$I_a^\alpha f(t) = \frac{1}{\Gamma(\alpha)} \int_a^t (t-s)^{\alpha-1} f(s) ds, \quad t > a, \tag{1}$$

This definition is widely studied. If we are based on this definition, the Riemann-Liouville fractional derivative and the Caputo-type fractional derivative of order $\alpha > 0$, are defined by

$$D_{a+}^\alpha (f(t)) = \frac{1}{\Gamma(m-\alpha)} \frac{d^m}{dt^m} \int_a^t (t-s)^{m-\alpha-1} f(s) ds \tag{2}$$

$$D_{a+}^\alpha (f(t)) = \frac{1}{\Gamma(m-\alpha)} \int_a^t (t-s)^{m-\alpha-1} f^{(m)}(s) ds \tag{3}$$

respectively, where $m-1 < \alpha \leq m$, and $m \in \aleph$. The Caputo fractional operator is widely used to model many physical problems in fractional calculus applications because it is suitable for initial value problems and has many characteristics similar to ordinary derivatives. For example, when $m-1 < \alpha \leq m$, the Caputo operator satisfies the rule

---

- Selection and peer-review under responsibility of the Organizing Committee of the Conference

$$I_{a+}^{\alpha}D_{a+}^{\alpha}(f(t)) = f(t) - \sum_{n=0}^{m-1}\frac{f^{(k)}(a)}{n!}(t-a)^n, \quad t > a. \tag{4}$$

Recently, (Odibat & Baleanu, 2020) introduced the generalized Caputo-type fractional derivative with properties similar to those of the Caputo derivative. This type of generalized derivative looks more like ordinary derivatives than other generalized derivatives. The generalized fractional derivative of a continuous function f is defined by

$$D_{a}^{\alpha,\rho}(f(t)) = \frac{\rho^{\alpha-m+1}}{\Gamma(m-\alpha)}\int_a^t s^{\rho-1}(t^\rho - s^\rho)^{m-\alpha-1}(s^{1-\rho}\frac{d}{ds})^m f(s)ds, \quad t > a, \tag{5}$$

this generalized order $\alpha > 0$, and $\rho > 0$, where $a \geq 0$ and $m-1 < \alpha \leq m$. Until now, there is no algorithm to solve fractional differential equations in the sense of a generalized fractional derivative of the Caputo-type by approximate analytic technique. Moreover, is the solution valid for a long time span? In this paper, we applied our result to the Riccati equation which is used in different areas of mathematics, such as in algebraic geometry the theory of conformal mapping, and physics. It also appears in many applications in engineering and science domains, such as robust stabilization, stochastic realization theory, network synthesis, optimal control, and financial mathematics. Recently, many researchers studied the Riccati differential equation of fractional order, such as (Cang et al., 2009) used HAM to solve non-linear Riccati differential equation with fractional order. The fractional Riccati equation with the generalized fractional derivative of Caputo-type definition can be written as:

$$D_a^{\alpha,\rho}y(t) = Ay(t) + By^2(t) + C,$$

subject to the initial condition $y(a) = c$. In the case of $\alpha = \rho = 1$, the fractional equation reduces to the classical Riccati differential equation.

Preliminaries

Recently, Almeida et al.[6] have introduced the Caputo–Katugampola derivative with two parameters defined by

$$D_{a+}^{\alpha,\rho}(f(t)) = \frac{\rho^{\alpha}}{\Gamma(1-\alpha)}\int_a^t (t^\rho - s^\rho)^{-\alpha}f'(s)ds, 0 < \alpha \leq 1, t > a \geq 0. \tag{6}$$

Later, (Odibat & Baleanu, 2020) extended the definition of two parameters, $m-1 < \alpha \leq m$ in arbitrary order α and $\rho > 0$. The generalized fractional derivative of a continuous function f is $D_a^{\alpha,\rho}(f(t))$ of order $\alpha > 0$ and $\rho > 0$ can be written as

$$D_{a}^{\alpha,\rho}(f(t)) = \frac{\rho^{\alpha-m+1}}{\Gamma(m-\alpha)}\int_a^t s^{\rho-1}(t^\rho - s^\rho)^{m-\alpha-1}(s^{1-\rho}\frac{d}{ds})^m f(s)ds, \quad t > a, \tag{7}$$

where $a \geq 0$ and $m-1 < \alpha \leq m$. We note that as $\rho = 1$ in (7), we have the standard Caputo fractional derivative in (3).

Definition 1 (Odibat & Baleanu, 2020) *The generalized fractional integral of the function* f, $I_{0+}^{\alpha,\rho}(f(t))$, *of order* $0 < \alpha$, *where* $\rho > 0$, *is defined by:*

$$I_{a+}^{\alpha,\rho}(f(t)) = \frac{\rho^{1-\alpha}}{\Gamma(\alpha)}\int_{a+}^t s^{\rho-1}(t^\rho - s^\rho)^{\alpha-1}f(s)ds. \tag{8}$$

The following property gives us the relation between generalized fractional integral and generalized Caputo-type fractional derivative(Odibat & Baleanu, 2020)] If $m-1 < \alpha \leq m$, $a \geqslant 0$, $\rho > 0$ and $f \in C^m[a,b]$, then for $a < t \leq b$,

$$I_{a+}^{\alpha,\rho}D_{a+}^{\alpha,\rho}(f(t)) = f(t) - \sum_{n=0}^{m-1}\frac{1}{\rho^n n!}(t^\rho - a^\rho)^n\left[\left(x^{1-\rho}\frac{d}{dx}\right)^n f(x)\right]|_{x=a}. \tag{9}$$

In the following, we present some propositions and basic properties of generalized fractional derivatives and integrals with two parameters, which we will need in the next chapter.

Proposition 1 *Let* $m-1<\alpha\leq m,\rho>0,$ *and* $n\in\mathbb{R}$ *then we have:*

$$I_{0+}^{\alpha,\rho}(t^n)=\frac{\rho^{-\alpha}t^{(\rho\alpha+n)}\Gamma(\frac{n}{\rho}+1)}{\Gamma(\alpha+1+\frac{n}{\rho})},\quad \Re(\rho)>0,\Re(n+\rho)>0,\Re(\alpha)>0. \tag{10}$$

proof: Let $n\in\mathbb{R}$, and $\alpha,\rho>0$ then we have

$$I_{0+}^{\alpha,\rho}(t^n)=\frac{\rho^{1-\alpha}}{\Gamma(\alpha)}\int_0^t s^{\rho-1}(t^\rho-s^\rho)^{\alpha-1}s^n ds, \tag{11}$$

$$=\frac{\rho^{1-\alpha}t^{\rho(\alpha-1)}}{\Gamma(\alpha)}\int_0^t s^{\rho-1+n}\left(1-\left(\frac{s}{t}\right)^\rho\right)^{\alpha-1}ds, \tag{12}$$

Set $u=(\frac{s}{t})^\rho$, so $s=u^{\frac{1}{\rho}}t$, and when $s=0,u=0$, when $s=t,u=1$, then Eq.(12) becomes

$$=\frac{\rho^{-\alpha}t^{(\rho\alpha+n)}}{\Gamma(\alpha)}\int_0^1 u^{\frac{u}{\rho}+1-1}(1-u)^{\alpha-1}du,$$

So, $I_{0+}^{\alpha,\rho}(t^n)=\frac{\rho^{-\alpha}t^{(\rho\alpha+n)}\Gamma(\frac{n}{\rho}+1)}{\Gamma(\alpha+1+\frac{n}{\rho})}$.

Remark1:

$$I_{0+}^{\alpha,\rho}(t)=\frac{\rho^{-1-\alpha}t^{(\rho\alpha+1)}\Gamma(\frac{1}{\rho})}{\Gamma(\alpha+1+\frac{1}{\rho})},\quad \Re(\rho)>0,\Re(\alpha)>0. \tag{13}$$

$$I_{0+}^{\alpha,\rho}(C)=\frac{C\rho^{-\alpha}t^{(\rho\alpha)}}{\alpha\Gamma(\alpha)},\quad \Re(\rho)>0,\Re(\alpha)>0,\quad \text{C is constant.} \tag{14}$$

If $m-1<\alpha\leq m$, $a\geqslant 0$, $\rho>0$, $C\in\mathbb{R}$ and $f,g\in C^m[a,b]$, then for $a<t\leq b$, we have:

$$I_{0+}^{\alpha,\rho}(Cf(t)+g(t))=CI_{0+}^{\alpha,\rho}(f(t))+I_{0+}^{\alpha,\rho}(g(t)).$$

Proposition 2 *Let* $0<\alpha\leq m,\rho>0,$ *and* $n\in\mathbb{R}$ *then we have:*

$$D_{0+}^{\alpha,\rho}(t^n)=\frac{\rho^{\alpha-m}t^{n-\alpha\rho}\Gamma(n+1)}{\Gamma(n-m+1)}\frac{\Gamma(\frac{n}{\rho}-m+1)}{\Gamma(\frac{n}{\rho}-\alpha+1)},\quad \Re(m)>\Re(\alpha). \tag{15}$$

Proof: Let $n\in\mathbb{R}$, and $\alpha,\rho>0$ then we have

$$D_{0+}^{\alpha,\rho}(t^n)=\frac{\rho^{\alpha-m+1}}{\Gamma(m-\alpha)}\int_0^t s^{\rho-1}(t^\rho-s^\rho)^{m-\alpha-1}\left(s^{1-\rho}\frac{d}{ds}\right)^m s^n ds, \tag{16}$$

$$=\frac{\rho^{\alpha-m+1}\Gamma(n+1)t^{\rho(m-\alpha-1)}}{\Gamma(m-\alpha)\Gamma(n-m+1)}\int_0^t s^{\rho-1-\rho m+n}\left(1-(\frac{s}{t})^\rho\right)^{m-\alpha-1}ds \tag{17}$$

Set $u=(\frac{s}{t})^\rho$, so $s=u^{\frac{1}{\rho}}t$, and when $s=0,u=0$, when $s=t,u=1$, then Eq.(17) becomes

$$D_{0+}^{\alpha,\rho}(t^n)=\frac{\rho^{\alpha-m}\Gamma(n+1)t^{n-\alpha\rho}}{\Gamma(m-\alpha)\Gamma(n-m+1)}\int_0^1 u^{\frac{n}{\rho}-m}(1-u)^{m-\alpha-1}du,\qquad \text{where}\quad \Re(n+\rho)>\Re(\rho\text{m}),$$

$$=\frac{\rho^{\alpha-m}\Gamma(n+1)t^{n-\alpha\rho}}{\Gamma(m-\alpha)\Gamma(n-m+1)}\beta\left(\frac{n}{\rho}-m+1,m-\alpha\right)$$

That is $D_{0+}^{\alpha,\rho}(t^n)=\frac{\rho^{\alpha-m}t^{n-\alpha\rho}\Gamma(n+1)}{\Gamma(n-m+1)}\frac{\Gamma(\frac{n}{\rho}-m+1)}{\Gamma(\frac{n}{\rho}-\alpha+1)}$.

Remark2:

$$D_{0+}^{\alpha,\rho}(t) = \frac{\rho^{\alpha-m}t^{1-\alpha\rho}\Gamma(1-m+\frac{1}{\rho})}{\Gamma(1-\alpha+\frac{1}{\rho})}, \quad \Re(\rho)+1 > \Re(\rho\mathrm{m}), \Re(m) > \Re(\alpha). \tag{18}$$

$$D_{0+}^{\alpha,\rho}(C) = 0, \quad \mathrm{C} \quad \text{is} \quad \text{constant}. \tag{19}$$

Proposition 3 *Let* $m-1 < \alpha \leq m$, $\rho > 0$, *and* $n \in \mathbb{R}$, *then we have:*

$$I_{a+}^{\alpha,\rho}(t^n) = \frac{\rho^{-\alpha}\Gamma(\frac{n}{\rho}+1)}{\Gamma(\frac{n}{\rho}+1+\alpha)}(t^{\alpha\rho+n} - a^{n+\alpha\rho}). \tag{20}$$

Proof: Let $n \in \mathbb{R}$, $a > 0$, and $\alpha, \rho > 0$. Then we have

$$I_{a+}^{\alpha,\rho}((t)^n) = \frac{\rho^{1-\alpha}}{\Gamma(\alpha)}\int_a^t s^{\rho-1+n}(t^\rho - s^\rho)^{\alpha-1}ds, \tag{21}$$

$$= \frac{\rho^{1-\alpha}t^{\rho(\alpha-1)}}{\Gamma(\alpha)}\int_a^t s^{\rho-1+n}\left(1-\left(\frac{s}{t}\right)^\rho\right)^{\alpha-1} ds, \tag{22}$$

set $u = (\frac{s}{t})^\rho$, so $s = u^{\frac{1}{\rho}}t$, and when $s = a$, $u = (\frac{a}{t})^\rho$, when $s = t$, $u = 1$, then Eq.(22) becomes

$$I_{0+}^{\alpha,\rho}(t^n) = \frac{\rho^{-\alpha}t^{(\rho\alpha+n)}}{\Gamma(\alpha)}\left(\int_{(\frac{a}{t})^\rho}^{0} u^{\frac{n}{\rho}}(1-u)^{\alpha-1}du + \int_0^1 u^{\frac{n}{\rho}}(1-u)^{\alpha-1}du\right),$$

Thus, $$I_{a+}^{\alpha,\rho}(t^n) = \frac{\rho^{-\alpha}\Gamma(\frac{n}{\rho}+1)}{\Gamma(\alpha+1+\frac{n}{\rho})}(t^{\rho\alpha+n} - a^{n+\alpha\rho}).$$

Remark4:

$$I_{a+}^{\alpha,\rho}(t) = \frac{\rho^{-1-\alpha}\Gamma(\frac{1}{\rho})}{\Gamma(\frac{1}{\rho}+1+\alpha)}(t^{\alpha\rho+1} - a^{1+\alpha\rho}). \tag{23}$$

$$I_{a+}^{\alpha,\rho}(C) = \frac{C\rho^{-\alpha}}{\alpha\Gamma(\alpha)}(t^{\alpha\rho} - a^{\alpha\rho}), \mathrm{C} \quad \text{is} \quad \text{constant}. \tag{24}$$

Proposition 4 *Let* $m-1 < \alpha \leq m$, $\rho > 0$, *and* $n \in \mathbb{R}$ *then we have:*

$$I_{a+}^{\alpha,\rho}((t^\rho - a^\rho)^n) = \frac{\rho^{-\alpha}(t^\rho-a^\rho)^{n+\alpha}\Gamma(n+1)}{\Gamma(\alpha+n+1)}. \tag{25}$$

Proof: $I_{a+}^{\alpha,\rho}((t^\rho - a^\rho)^n) = \frac{\rho^{1-\alpha}}{\Gamma(\alpha)}\int_a^t s^{\rho-1}(t^\rho - s^\rho)^{\alpha-1}(s^\rho - a^\rho)^n ds$

Set $z = s^\rho$, so $s = z^{\frac{1}{\rho}}$, and when $s = a$, $z = a^\rho$, when $s = t$, $z = t^\rho$, then

$$= \frac{\rho^{-\alpha}}{\Gamma(\alpha)}\int_{a^\rho}^{t^\rho} (t^\rho - z)^{\alpha-1}(z - a^\rho)^n dz$$

Next, we take $r = \frac{z-a^\rho}{t^\rho-a^\rho}$, so $z = a^\rho + r(t^\rho - a^\rho)$ and $\mathrm{d}r = \frac{\mathrm{dz}}{t^\rho-a^\rho}$, and when $z = a^\rho$, $r = 0$, when $z = t^\rho$, $r = 1$, then we get

$$= \frac{\rho^{-\alpha}}{\Gamma(\alpha)}(t^\rho - a^\rho)^{n+\alpha}\int_0^1 (1-r)^{\alpha-1}r^n dr,$$

That is $I_{a+}^{\alpha,\rho}((t^\rho - a^\rho)^n) = \frac{\rho^{-\alpha}(t^\rho-a^\rho)^{n+\alpha}\Gamma(n+1)}{\Gamma(\alpha+n+1)}$.

Proposition 5 (Odibat & Baleanu, 2020) *If* $m-1 < \alpha \leq m$, $n > m-1$ *and* $n \notin \aleph$, *then*

$$D_{a+}^{\alpha,\rho}(t^\rho - a^\rho)^n = \frac{\rho^\alpha (t^\rho - a^\rho)^{n-\alpha}\Gamma(n+1)}{\Gamma(n-\alpha+1)}. \qquad (26)$$

The Homotopy Analysis Method

In this work, we consider the following IVP

$$D_{0+}^{\alpha,\rho} y(t) = \mathcal{N}[y,t], \qquad (27)$$

where $\mathcal{N}$ is the nonlinear and $y(t)$ is an unknown function. The zeroth-order deformation equation can be defined as

$$(1-q)\mathcal{L}[\phi(t;q) - y_0(t)] + q\hbar(D_{0+}^{\alpha,\rho}[\phi(t;q)] - \mathcal{N}[\phi(t;q)]) = 0, \qquad (28)$$

where q is an embedding parameter belonging to $[0,1]$, $\hbar$ is the convergence control parameter, $\mathcal{L}$ is an auxiliary linear operator, $\mathcal{N}$ is the nonlinear operator and $y_0(t)$ is an initial guess of the exact solution $y(t)$. Now, we can expand $\phi(t;q)$ into a Taylor series with respect to q:

$$\phi(t;q) = y_0(t) + \sum_{j=1}^{\infty} y_j(t) q^j. \qquad (29)$$

When the embedding parameter q increases from 0 to 1; $\phi(t;0) = y_0(t)$, $\phi(t;1) = y(t)$, the solution $\phi(t;q)$ of the zeroth-order deformation (28) varies continuously from the initial guess $y_0(t)$ to the exact solution $y(t)$. If the auxiliary linear operator, the initial guess $y_0(t)$, and $\hbar$, are appropriately chosen, that (29) converges at $q = 1$, then we have the so-called homotopy-series solution

$$y(t) = y_0(t) + \sum_{j=1}^{\infty} y_j(t). \qquad (30)$$

By differentiating equation (28) i-time with respect to q and then putting $q = 0$, and finally dividing them by $i!$, we have the i-th order deformation equation:

$$\mathcal{L}[y_i(t) - \chi_i y_{i-1}(t)] = \hbar[D_{0+}^{\alpha,\rho} y_{i-1}(t) - \mathcal{R}_i(\vec{y}_{i-1}(t))], \qquad (31)$$

where $\mathcal{R}_i(\vec{y}_{i-1}(t)) = \frac{1}{i!}\frac{\partial^i[\mathcal{N}[\phi(t;q)]]}{\partial q^i}, \quad \chi_i = \begin{cases} 0, & i \le 1 \\ 1, & i > 1 \end{cases}$,

and $\vec{y}_{i-1}(t)$ is a vector $[y_o(t), \quad y_1(t), \quad y_2(t), \ldots\ldots, \quad y_{i-1}(t)]$. By taking $\mathcal{L}^{-1}$ for Eq (31), we get:

$$y_i(t) = \chi_i y_{i-1}(t) + \hbar\mathcal{L}^{-1}[D_{0+}^{\alpha,\rho} y_{i-1}(t) - \mathcal{R}_i(\vec{y}_{i-1}(t))].$$

where $\mathcal{L}^{-1}$ is the inverse of the linear operator. The solution can be expressed as:

$$y(t) = \sum_{j=0}^{M} y_j(t). \qquad (32)$$

Consider the fractional equation:

$$D_{0+}^{\alpha,\rho}(y(t)) = \mathcal{N}[y,t], \qquad (33)$$

subject to the initial condition $y(0) = c$, where $D_{a+}^{\alpha,\rho}$ is the generalized Caputo-type fractional derivative operator of parameters α and ρ. From now the value of m in $D_{a+}^{\alpha,\rho}$ is one. By assuming the linear operator $\mathcal{L} = D_{0+}^{\alpha,\rho}$, Eq.(31) becomes

$$D_{0+}^{\alpha,\rho}[y_i(t) - \chi_i y_{i-1}(t)] = \hbar[D_{0+}^{\alpha,\rho} y_{i-1}(t) - \mathcal{R}_i(\vec{y}_{i-1}(t))]. \qquad (34)$$

Now, apply $I_{0+}^{\alpha,\rho}$(10) on the right-hand and left-hand of Eq.(34), then we get

$$I_{0+}^{\alpha,\rho} D_{0+}^{\alpha,\rho}[y_i(t) - \chi_i y_{i-1}(t)] = \hbar[I_{0+}^{\alpha,\rho} D_{0+}^{\alpha,\rho} y_{i-1}(t) - I_{0+}^{\alpha,\rho}[\mathcal{R}_i(\vec{y}_{i-1}(t))]]. \qquad (35)$$

Next step, apply property (9) on the left-hand, and the first part on the right-hand side, take $0 < \alpha \leq 1$, then Eq.(35) becomes

$$y_i(t) = (\chi_i + \hbar)y_{i-1}(t) + y_i(0) - \chi_i y_{i-1}(0) - \hbar y_{i-1}(0) - \hbar I_{0+}^{\alpha,\rho}[\mathcal{R}_i(\vec{y}_{i-1}(t))]. \tag{36}$$

where the initial condition is $y_i(0) = \begin{cases} 0, & if \quad i = 1,2,3,.. \\ c, & if \quad i = 0. \end{cases}$

Multistage HAM

To express the solution by our proposed method, consider the generalized Caputo-type fractional IVP

$$D_{a+}^{\alpha,\rho}(y(t)) = f(t,y), \quad y(a) = c. \tag{37}$$

where $0 < \alpha \leq 1$ and $0 \leq t \leq T$. According to the i-th order of the deformation equation

$$D_{a+}^{\alpha,\rho}[y_i(t) - \chi_i y_{i-1}(t)] = \hbar[D_{a+}^{\alpha,\rho} y_{i-1}(t) - \mathcal{R}_i(\vec{y}_{i-1}(t))], \tag{38}$$

apply $I_{a+}^{\alpha,\rho}$(20) on Eq.(38) on the right-hand and left-hand sides:

$$I_{a+}^{\alpha,\rho} D_{a+}^{\alpha,\rho}[y_i(t) - \chi_i y_{i-1}(t)] = \hbar[I_{a+}^{\alpha,\rho} D_{a+}^{\alpha,\rho} y_{i-1}(t) - I_{a+}^{\alpha,\rho}\mathcal{R}_i(\vec{y}_{i-1}(t))],$$

then use the property (9), we have:

$$y_i(t) - \chi_i y_{i-1}(t) - y_i(a) + \chi_i y_{i-1}(a) = \hbar(y_{i-1}(t) - y_{i-1}(a)) - \hbar I_{a+}^{\alpha,\rho}(\mathcal{R}_i(\vec{y}_{i-1}(t))).$$

Thus, the i-th order of the approximate solution is given by:

$$y_i(t) = (\chi_i + \hbar)y_{i-1}(t) + y_i(a) - (\chi_i + \hbar)y_{i-1}(a) - \hbar I_{a+}^{\alpha,\rho}(\mathcal{R}_i(\vec{y}_{i-1}(t))). \tag{39}$$

where the initial condition is $y_i(a) = \begin{cases} 0, & if \quad i = 1,2,3,.. \\ c, & if \quad i = 0. \end{cases}$ We can simplify(39) to becomes

$$y_i(t) = (\chi_i + \hbar)y_{i-1}(t) - (1 - \chi_i)(\chi_i + \hbar)y_{i-1}(t) - \hbar I_{a+}^{\alpha,\rho}(\mathcal{R}_i(\vec{y}_{i-1}(t))), \tag{40}$$

So, the general solution of Eq.(37) using M-terms of the series is

$$Y(t) = \sum_{j=0}^{M} y_j(t). \tag{41}$$

To evaluate the solution $Y(t)$ given in (41) along $[a, T]$, we present our technique in the following steps:

1. Divide the interval $[a, T]$ into N equal sub-intervals as

$[t_0, t_1], [t_1, t_2], \ldots\ldots, [t_n, t_{n+1}] \ldots, [t_{N-1}, t_N]$, where $\begin{cases} t_0 = a, \\ t_n = n\Delta t, \\ \Delta t = \frac{T-a}{N}, \\ t_N = T, \end{cases}$ and Δt is the step size.

2. The solution along the sub-interval $[t_0, t_1]$ is given by a substitute $t_0 = a = 0$, and $y(0) = c$, and we label it as $Y_0(t)$.
3. To ensure the continuity of the solution we replace $c = Y_0(t_1)$, and $t_1 = a$, so that we have $Y_1(t)$.
4. Using the same manner the solution along the sub-interval $[t_n, t_{n+1}]$ has $t_n = a + n\Delta t$, and $c = Y_{n-1}(t_n)$, which is labeled by $Y_n(t)$. Thus, our continuous solution can be written as

$$\tilde{Y}(t) = \begin{cases} Y_0(t) & : \quad a \le t \le t_1 \\ Y_1(t) & : \quad t_1 \le t \le t_2 \\ Y_2(t) & : \quad t_2 \le t \le t_3 \\ \vdots & \\ Y_n(t) & : \quad t_n \le t \le t_{n+1} \\ \vdots & \\ Y_N(t) & : \quad t_{N-1} \le t \le t_N = T \end{cases}$$

where $Y_n(t), n = 0,1,2,\ldots,N$ is the continuous solution for (37) on the interval $[t_n, t_{n+1}]$, with I.C $y(t_n) = Y_{n-1}(t_n)$.

Numerical Results

Consider the following fractional Riccati equation

$$D_a^{\alpha,\rho} y(t) = 2y(t) - y^2(t) + 1, \tag{42}$$

$t > 0$, $0 < \alpha \le 1$, subject to the initial condition $y(a) = c$, where $D_a^{\alpha,\rho}$ is the generalized Caputo-type fractional derivative operator, of parameters α and ρ. The exact solution of the Riccati Eq.(45), when $\alpha = 1$ and $\rho = 1$, is

$$y(t) = 1 + \sqrt{2}\tanh[\sqrt{2}t + \tfrac{1}{2}\log(\tfrac{\sqrt{2}-1}{\sqrt{2}+1})]. \tag{43}$$

According to MHAM for some $T > 0$, the $i - th$ approximate solutions y_i is determined by the formula:

$$y_i(t) = (\chi_i + \hbar)y_{i-1}(t) + y_i(a) - (\chi_i + \hbar)y_{i-1}(a) - \hbar I_{a+}^{\alpha,\rho}(\mathcal{R}_i(\vec{y}_{i-1}(t))),$$

where $\quad \mathcal{R}_i(\vec{y}_{i-1}(t)) = 2y_{i-1} - \sum_{j=0}^{i-1} y_j y_{i-1-j} + (1 - \chi_i)$.

The initial condition is $y_i(a) = \begin{cases} 0, & if \quad i = 1,2,3,.. \\ c, & if \quad i = 0. \end{cases}$

For simplicity, let $\hbar = -1$. Using multistage HAM with uniform nodes, the first term of the series solution is:

$$y_1(t) = -\frac{\rho^{-\alpha} a^{\alpha\rho}}{\alpha\Gamma(\alpha)} + \frac{c^2 \rho^{-\alpha} a^{\alpha\rho}}{\alpha\Gamma(\alpha)} - \frac{2c\rho^{-\alpha} a^{\alpha\rho}}{\alpha\Gamma(\alpha)} - \frac{c^2 \rho^{-\alpha} t^{\alpha\rho}}{\alpha\Gamma(\alpha)} + \frac{2c\rho^{-\alpha} t^{\alpha\rho}}{\alpha\Gamma(\alpha)} + \frac{\rho^{-\alpha} t^{\alpha\rho}}{\alpha\Gamma(\alpha)}.$$

In the same way, we can find $y_i(t)$, for i=2,3,….The continuous solution of the Maclaurin series of (45), when $\alpha = 1$, $\rho = 1$, and $\Delta t = 0.1$, can be written as:

$$\tilde{Y}(t) =$$

$$\begin{cases} Y_0(t) = \frac{t^3}{3} + t^2 + t & : \quad 0 \le t \le 0.1 \\ Y_1(t) = 0.150869t^3 + 1.0299t^2 + 0.997987t + 0.0000844281 & : \quad 0.1 \le t \le 0.2 \\ Y_2(t) = -0.131482t^3 + 1.15935t^2 + 0.977604t + 0.00124216 & : \quad 0.2 \le t \le 0.3 \\ Y_3(t) = -0.491978t^3 + 1.43105t^2 + 0.90856t + 0.00723595 & : \quad 0.3 \le t \le 0.4 \\ \vdots & \\ Y_9(t) = -0.669366t^3 + 0.899396t^2 + 1.72969t - 0.270041 & : \quad 0.9 \le t \le 1 \end{cases}$$

In Table 1 we compare the approach with the adaptive P-C algorithm (Odibat & Baleanu, 2020) to fractional Riccati Eq.(42) when $\alpha = 1$, and $\rho = 1$ at $t = 1$, $t = 2$, and $t = 5$. It's clear from our data in Table1, that the numerical solutions obtained using our algorithm completely agreed with the exact solution (y_{Exact}) more than the adaptive P-C algorithm. we can observe when the step size Δt decreases our approximate values of $y(t)$ converge to the exact solutions. Table 2, presents numerical solutions obtained using our algorithm at $t = 2$, r, for different values of α and ρ. It is shown that the solution does not depend only on α but also on ρ. Figure 1 shows the exact solution with the approximate solutions of fractional Riccati Eq.(42) for $\alpha = \rho = 1$, and $\Delta t = 0.01$.

Table 1. Numerical solutions to fractional Riccati Eq.(45) when $\alpha = 1$ and $\rho = 1$.

	MHAM Algorithm			The Adptive P-C Algorithm		
Δt	t=1	t=2	t=5	t=1	t=2	t=5
1/10	1.68967243	2.35779846	2.41420179	1.68745117	2.35530727	2.41419835
1/40	1.68950123	2.35777211	2.41420167	1.68936339	2.35763805	2.41420152
1/160	1.68949843	2.35777166	2.41420167	1.68948986	2.35776357	2.41420166
1/640	1.68949839	2.35777165	2.41420167	1.68949786	2.35777115	2.41420167
y_Exact	1.68949839	2.35777165	2.41420167	1.68949839	2.35777165	2.41420167

Table 2. Numerical solutions to fractional Riccati Eq. (45) when $t = 2$.

	MHAM Algorithm			The Adptive P-C Algorithm		
Δt	α=1,ρ=0.9	α=0.95,ρ=0.75	α=0.9,ρ=1.2	α=1,ρ=0.9	α=0.95,ρ=0.75	α=0.9,ρ=1.2
1/10	2.36822637	2.32198326	2.22052899	2.36576348	2.34646084	2.26631061
1/40	2.36818244	2.32264980	2.21660104	2.36805246	2.34876916	2.26890814
1/160	2.36818165	2.32298363	2.21583356	2.36817385	2.34889710	2.26907235
1/640	2.36818164	2.32307541	2.21565525	2.36818116	2.34890540	2.26908393
1/1280	2.36818164	2.32309099	2.21562605	2.36818153	2.34890584	2.26908459

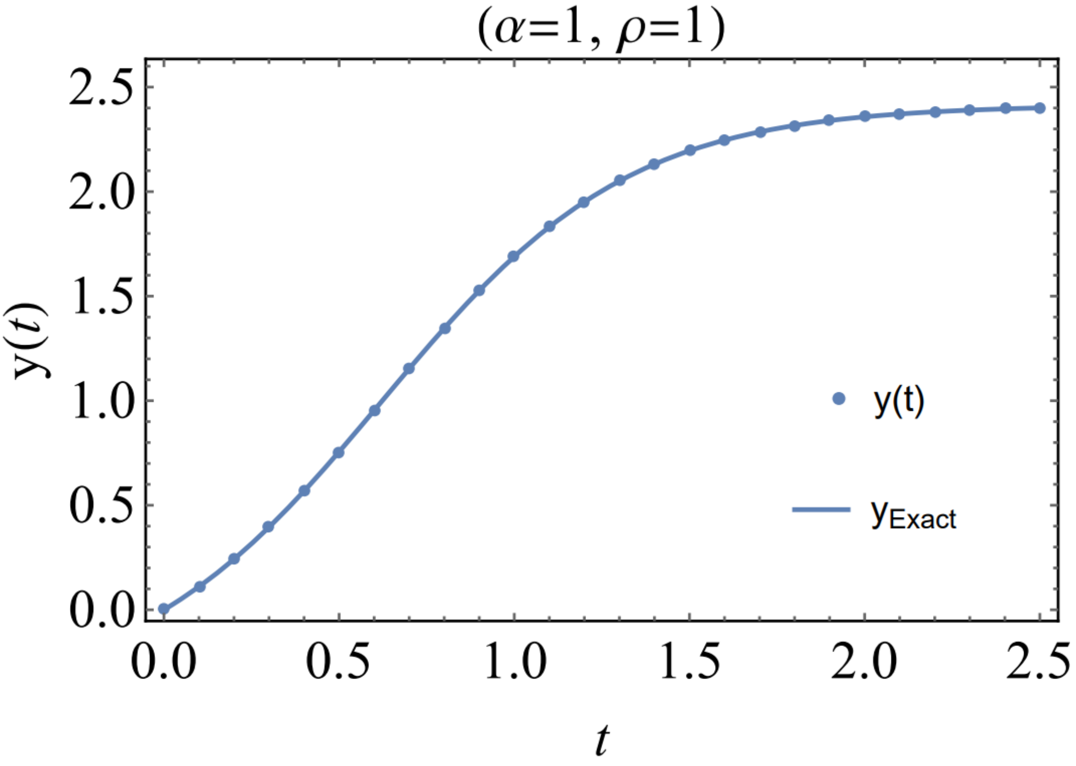

Figure 1. The approximation solutions and the Exact solution for (45), when $\Delta t = 0.01$, and $t \in [0,2.5]$.

Conclusion

This work successfully presented the analytic solution of the Riccati equation with a generalized Caputo fractional derivative in two parameters. A general framework for using the multistage homotopy analysis method for this kind of problem is constructed. Several properties of the fractional Caputo fractional derivative with two parameters are proved. The discussed example shows the efficiency of the new algorithm in terms of convergence and accuracy.

Scientific Ethics Declaration

The authors declare that the scientific ethical and legal responsibility of this article published in EPSTEM journal belongs to the authors.

Acknowledgements or Notes

* This article was presented as an oral presentation at the International Conference on Basic Sciences and Technology (www.icbast.net) held in Antalya/Turkey on November 16-19, 2023.

References

Almeida, R., Malinowska, A. B., & Odzijewicz, T. (2016). Fractional differential equations with dependence on the Caputo–Katugampola derivative. *Journal of Computational and Nonlinear Dynamics,11*(6), 061017

Cang, J., Tan, Y., Xu, H., & Liao, S. J. (2009). Series solutions of non-linear Riccati differential equations with fractional order. *Chaos, Solitons & Fractals, 40*(1), 1-9.

Kilbas, A. A., Srivastava, H. M., & Trujillo, J. J. (2006). *Theory and applications of fractional differential equations* (Volume 204). Elsevier.

Odibat, Z., & Baleanu, D. (2020). Numerical simulation of initial value problems with generalized Caputo-type fractional derivatives. *Applied Numerical Mathematics, 156,* 94-105.

Samko, S. G., Kilbas, A. A., & Marichev, O. I. (1993). *Fractional integrals and derivatives.* Yverdon-les-Bains, Switzerland.

Author Information

Abedel-Karrem Alomari
Yarmouk University
Irbid, Jordan
Contact e-mail: *abdomari2008@yahoo.com*

Anwar Alsleeby
Yarmouk University
Irbid, Jordan

To cite this article:

Alomari, A. K. & Alsleeby, A (2023). Approximate analytic solution for fractional differential equations with a generalized fractional derivative of caputo-type. *The Eurasia Proceedings of Science, Technology, Engineering & Mathematics (EPSTEM), 25,* 50-58.

The Eurasia Proceedings of Science, Technology,
Engineering & Mathematics (EPSTEM)
ISSN: 2602-3199

The Eurasia Proceedings of Science, Technology, Engineering & Mathematics (EPSTEM), 2023

Volume 25, Pages 59-66

ICBAST 2023: International Conference on Basic Sciences and Technology

Synthesis and Some Electrochemical Properties of Carbazole Derivative Monomers for Optoelectronic Device Design

Merve Yandimoglu
Eskisehir Osmangazi University

Kamuran Gorgun
Eskisehir Osmangazi University

Evrim Hur
Eskisehir Osmangazi University

Abstract: Low-cost instruments are used to achieve high sensitivity, accuracy and precision with electrochemical techniques, making them the most suitable analytical methods used to investigate the electrochemical properties of a new molecule. Among these techniques, cyclic voltammetry, which is widely employed, allows for the determination of electronic characteristics such as molecular energy levels and orbital structure, redox properties, sensor capabilities, surface activity, and more. The carbazole molecule can undergo derivatization from various positions, allowing for alterations in its electrical and optical properties. These compounds serve as heterocyclic building blocks that can be utilized as materials for organic sensitizers and semiconductors in optoelectronic devices. Due to the presence of a hydrogen atom in the nitrogen-hydrogen (N-H) bond within the carbazole structure, which can be replaced with different functional groups, carbazole is highly suitable for nitrogen-based derivatization studies. In this study, two different carbazole monomers (IIa and IIIa), which could be potential optoelectronic, were synthesized using the Ullman and Suzuki-Miyaura reaction and characterized using ^{1}H NMR, ^{13}C NMR, UV-Vis, and Flouresence spectroscopy techniques. The cyclic voltammetry experiments were performed using three different working electrodes (Au, Gc, Pt disk electrodes) for each compound. Since the optimum oxidation of the compounds was obtained from the voltammograms on the gold disk electrode, this electrode was used in the calculation of energy levels. HOMO and E_g values of the compounds were deduced from cyclic voltammetry experiments and the optical absorption bands, respectively.

Keywords: Organic optoelectronics, Suzuki-Miyaura reaction, Cyclic voltammetry, Band gap energy levels.

Introduction

Carbazole and its derivatives offer numerous advantages, such as excellent thermal and photochemical stability, solubility, easy modification, high quantum efficiency, electropolymerization capability, and strong intramolecular charge transfer (Zhu et al. 2015; Kandemir et al., 2018). Additionally, the carbazole structure can be readily functionalized at its 3-, 6-, or *N*-positions and covalently linked to other molecules (Justin Thomas et al., 2001).

These properties make these compounds valuable in various electroactive applications, including serving as light-emitting materials or hole-transporting materials in organic light-emitting diodes (OLEDs), organic sensitizers and semiconductors in optoelectronic devices, and sensors (Li et al., 2018; Liu et al., 2018; Battal et al., 2024; Karon & Lapkowski 2015).

- Selection and peer-review under responsibility of the Organizing Committee of the Conference

Cyclic voltammetry (CV) is considered one of the most precise methods for predicting energy band diagrams and characterizing the structures of compounds (Al-Ibrahim et al., 2005). The cyclic voltammetry technique, which has been successfully used to monitor the electrochemical behavior of a wide range of different compounds, stands out with advantages such as simplicity, sensitivity, speed, and low cost (Chooto, 2019). This technique allows for the measurement of oxidation potentials, which in turn enables the calculation of the HOMO (highest occupied molecular orbital) and LUMO (lowest unoccupied molecular orbital) values (Hwang & Chen, 2002). The first and most significant study on the electrochemical oxidation of carbazole was published by Ambrose and Nelson. According to their research, carbazole undergoes oxidation at approximately 1.2 V potential versus the Saturated Calomel Electrode (SCE) (Ambrose & Nelson, 1968).

In a previous study, the current-voltage characteristics of compound IIa photodiode at different illumination intensities were investigated. From the results obtained, it was determined that this diode absorbs light in the metal-semiconductor contact region (Gorgun et al. 2019a). In an another study, dye-sensitized solar cells were fabricated using IIIa compound as dye and ZnO and TiO_2 as photoelectrodes. The performances of the prepared cells were determined by current-voltage measurements. Remarkable results were obtained in the efficiency of compound IIIa cells prepared using Ruthenium sensitizer dye in TiO_2 photoelectrode (Gorgun et al., 2019b). In this study, electrochemical investigations of two different carbazole compounds, derived at the *N*-position, were carried out using cyclic voltammetry. HOMO energy levels were calculated from the obtained oxidation potentials, and E_g values were calculated from the absorption onset value. These data were used to determine the LUMO energy levels.

Method

Materials

All chemicals and solvents were obtained from Sigma-Aldrich. The organic solvents were purified by a standard procedure before using for reactions. The FT-IR spectra of the compounds were obtained with Bruker FT-IR Spectrometer (4000–400 cm^{-1}). ^{1}H NMR and ^{13}C NMR spectra were obtained on a JEOL ECZ500R UltrashieldTM 500 MHz and 125 MHz spectrometers. UV–Vis absorptions were obtained with SHIMADZU UV2450 UV-vis scanning spectrometer. Perkin-Elmer LS-55spectrophotometer was used to obtain the fluorescence spectra of the compounds. Cyclic voltammograms was performed with Gamry Reference 3000™ Potentiostat/Galvanostat/ZRA.

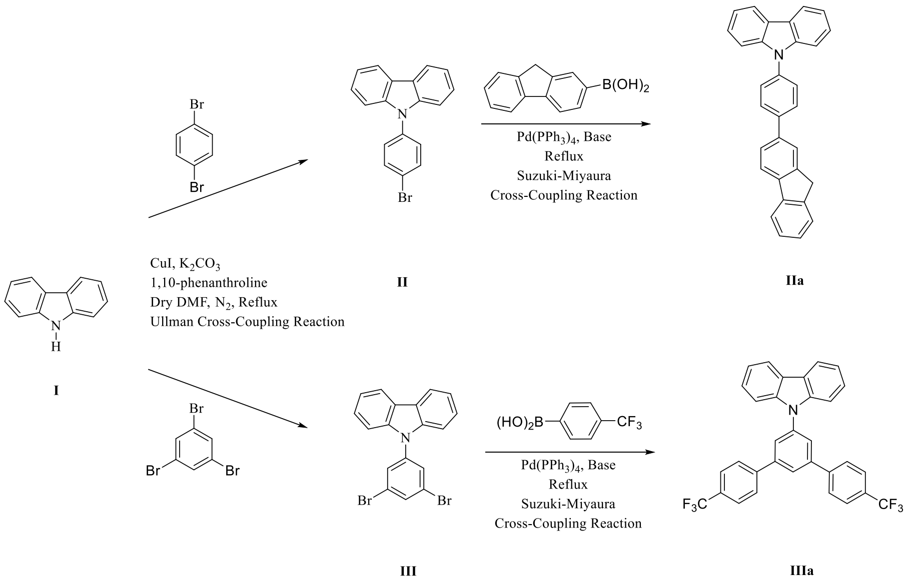

Figure 1. Synthetic route for the compounds IIa and IIIa.

Synthesis and Characterization of the Compounds

Synthesis of 9-(4-Bromophenyl)-9H-carbazole (II) (Görgün et al. 2019a).

To the solution of carbazole (I) (15.0 mmol) in 50 mL of dry *N,N*-dimethylformamide (DMF), 1,4-dibromobenzene (22.4 mmol), copper(I) iodide (1.5 mmol), 1,10-phenanthroline (0.75 mmol) and K_2CO_3 (30 mmol) were added and refluxed in N_2 atmosphere for 24 hours. Then the reaction mixture was cooled to room temperature and the solvent was removed in the evaporator. The residue was extracted in dichloromethane (DCM) and purified by column chromatography using n-hexane to obtain a white solid (compound II) (isolated yield 3.4 g, %71).

^{1}H NMR: (500 MHz, $CDCl_3$-d_1, δ): 7.20-7.37 (m, 6H), 7.44 (d, 2H, *J*=8.3 Hz), 7.69 (d, 2H, *J*=8.3 Hz), 8.07 (d, 2H, *J*=7.6 Hz).

Synthesis of 9-(3,5-Dibromophenyl)-9H-carbazole(III) (Görgün et al. 2019b).

Carbazole mixture (I) (30 mmol), 1,3,5-tribromobenzene (45 mmol), copper(I) iodide (3.0 mmol), 1,10-phenanthroline (3 mmol), K_2CO_3 (60 mmol), and 60 mL of dry DMF was refluxed under N_2 atmosphere for 24 h. Then the reaction mixture was cooled to room temperature before the solvent was removed under vacuum and the residue was extracted with DCM. The product were then obtained by column chromatography on silica gel with hexane as the eluent, to get white solid (compound III) (isolated yield 6.0 g, 50%).
^{1}H NMR: (500 MHz, $CDCl_3$-d_1, δ): 7.35 (t, 2H), 7.42-7.50 (m, 4H), 7.73 (s, 2H, *J*=8.3 Hz), 7.80 (s, 1H), 8.1 (d, 2H, *J*=7.5 Hz).

Synthesis of 9-(4-(9H-Fluoren-2-yl)phenyl)-9H-carbazole (IIa) (Görgün et al. 2019a).

9-(4-Bromophenyl)-9H-carbazole (II) (1 eg), fluorene-2-boronic acid (1.2 eg), K_2CO_3 (2M, 0.683 mL), 3 mol% $Pd(PPh_3)_4$ and tetrahydrofuran (THF) (25 ml) were mixed in a flask and this mixture was boiled under reflux at 70 °C for 24 hours. After the solvent was evaporated under vacuum, it was extracted with DCM (3x30 mL) and sodium sulfate. Then, after the solvent was evaporated under vacuum, the desired crude product was obtained by using column chromatography on silica gel and dichloromethane/n-hexane (1:5 v:v) technique, as a white solid (compound IIa) (isolated yield 0.182 g, 65%).

FT-IR (υ, cm^{-1}): 3040, 1603, 1522, 1482, 1450, 1404, 1231, 821, 737.
^{1}H NMR (500 MHz, $CDCl_3$-d_1, δ): 8.18 (2H, d, *J*=8.0 Hz), 7.94-7.80 (5H, m), 7.66 (3H, d, *J*=8.5 Hz), 7.60 (1H, d, *J*=7.0 Hz), 7.5 (2H, d, *J*=8.0 Hz), 7.45 (2H, d, *J*=9.0 Hz), 7.43 (1H, t, *J*=7.0 Hz), 7.31 (3H, t, *J*=7.5 Hz), 4.00 (2H, s, methylene).

Synthesis of 9-(4,4''-Bis(trifluoromethyl)-[1,1':3',1''-terphenyl]-5'-yl)-9H-carbazole (IIIa) (Görgün et al. 2019b).

9-(3,5-Dibromophenyl)-9H-carbazole (III) (1 eg), 4-trifluoromethylbenzene boronic acid (22 eg), K_2CO_3 (2M, 1,364 mL) was mixed with 3 mol% $Pd(PPh_3)_4$ and THF (25 ml) in a flask, and this mixture was refluxed at 70 °C for 24 hours. After the solvent was evaporated under vacuum, it was extracted with DCM (3x30 mL) and dried over sodium sulfate. Then, after the solvent was evaporated under vacuum, the desired crude product was obtained from petroleum ether by column chromatography on silica gel, as a white solid (compound IIIa) (isolated yield 0.23 g, 85%).

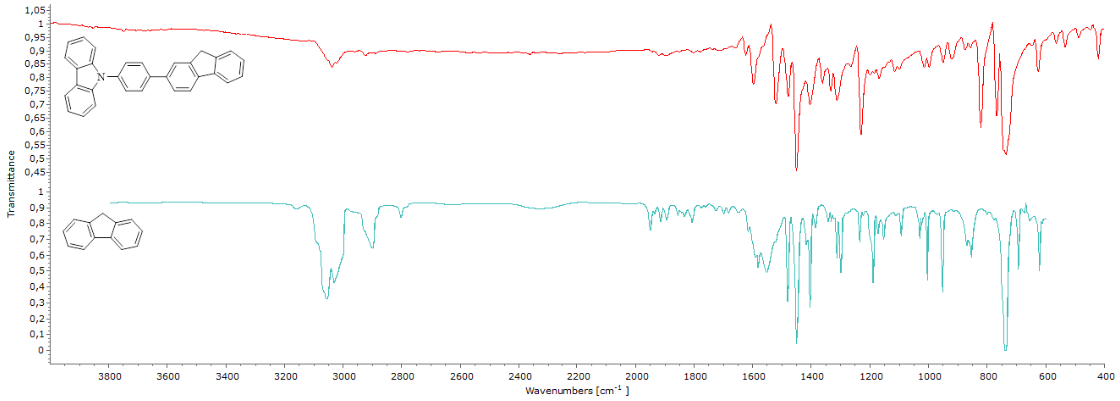

Figure 2. FT-IR spectrum of compound IIa.

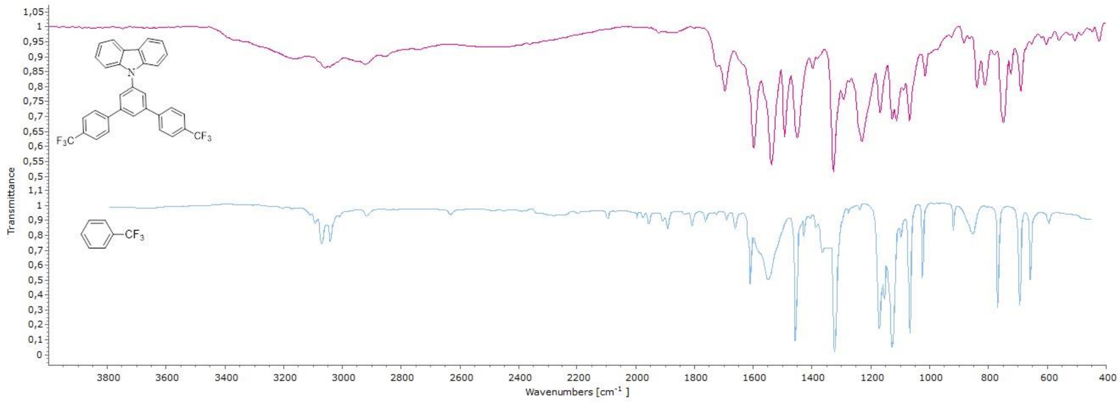

Figure 3. FT-IR spectrum of compound IIIa.

FT-IR (υ, cm^{-1}): 3064, 1698, 1600, 1539, 1453, 1329, 1231, 1170, 1130, 1112, 1069, 750, 691.
^{1}H NMR (500 MHz, $CDCl_3$-d_1, δ): 8.19 (2H, d, *J*=7.5 Hz), 7.9 (1H, s), 7.86 (2H, s), 7.82 (4H, d, *J*=9.0 Hz), 7.76 (4H, d, *J*=8.5 Hz), 7.52 (2H, d, *J*=7.5 Hz), 7.45 (2H, t, *J*=7.0 Hz, *J*=8.5 Hz), 7.33 (2H, t, *J*=6.5 Hz, *J*=8.5 Hz).
^{13}C NMR (125 MHz, $CDCl_3$-d_1, δ): 143.251, 142.454, 140.592, 139.181, 127.567, 126.146, 126.012, 125.983, 125.359, 125.081, 120.483, 120.310, 109.550, 29.497.

The IR spectra of compounds IIa and IIIa, as well as the spectra of the fluorene and (trifluoromethyl)benzene groups contained within these compounds, have been compared in Figures 2 and 3. The observed common signals support the accuracy of the structures of the synthesized compounds (NIST, 2023a; NIST, 2023b). The ^{1}H NMR spectra of compounds IIa and IIIa are presented in Figures 4 and 5, respectively.

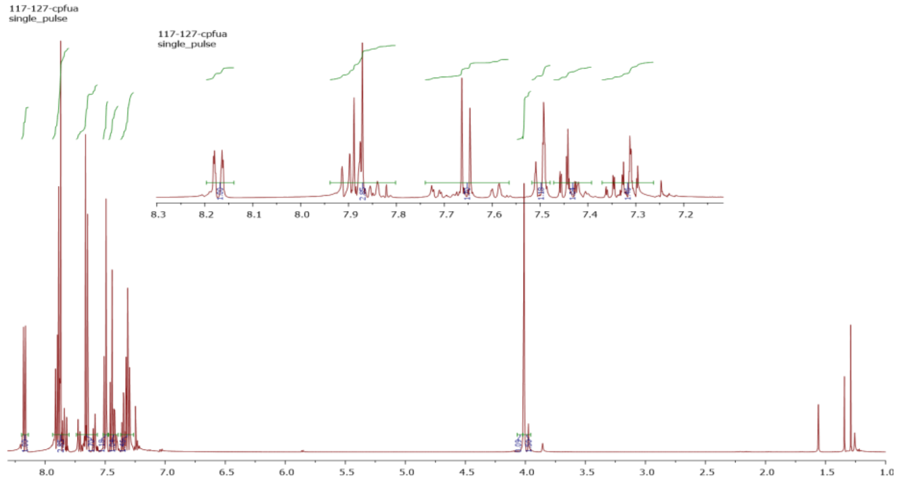

Figure 4. ^{1}H NMR spectrum of compound IIa.

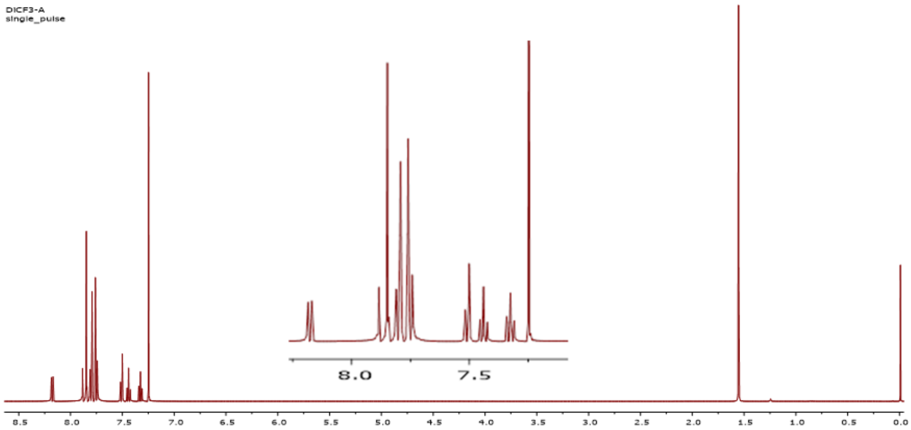

Figure 5. ^{1}H NMR spectrum of compound IIIa.

Optical Properties

The UV-GB absorption and fluorescence spectra of dilute solutions of compounds IIa and IIIa in various solvents (DCM, DMF, DMSO, n-hexane, THF and toluene) are shown in Figure 6. As shown in Figure 6a in dilute different solutions of compound IIa, π-π* transitions are observed in the 320 nm region. With an increase in solvent polarity, a general red shift (bathochromic effect) is typically observed. In addition, the fluorescence spectrum of compound IIa, a red shift is observed (Figure 6b). In the absorption spectrum of compound IIIa, the absorption maximum wavelengths of π-π* transitions show the red shift was observed with increasing polarity of solvents (Figure 6c). On the other hand, the fluorescence spectrum of compound IIIa has emission peaks in the range of 360-435 nm in all solutions. Two-shoulder emission peaks were observed at 415-435 nm in DCM. The effect of solvent polarity shows that red shift was observed with increasing polarity of solvents (Figure 6d).

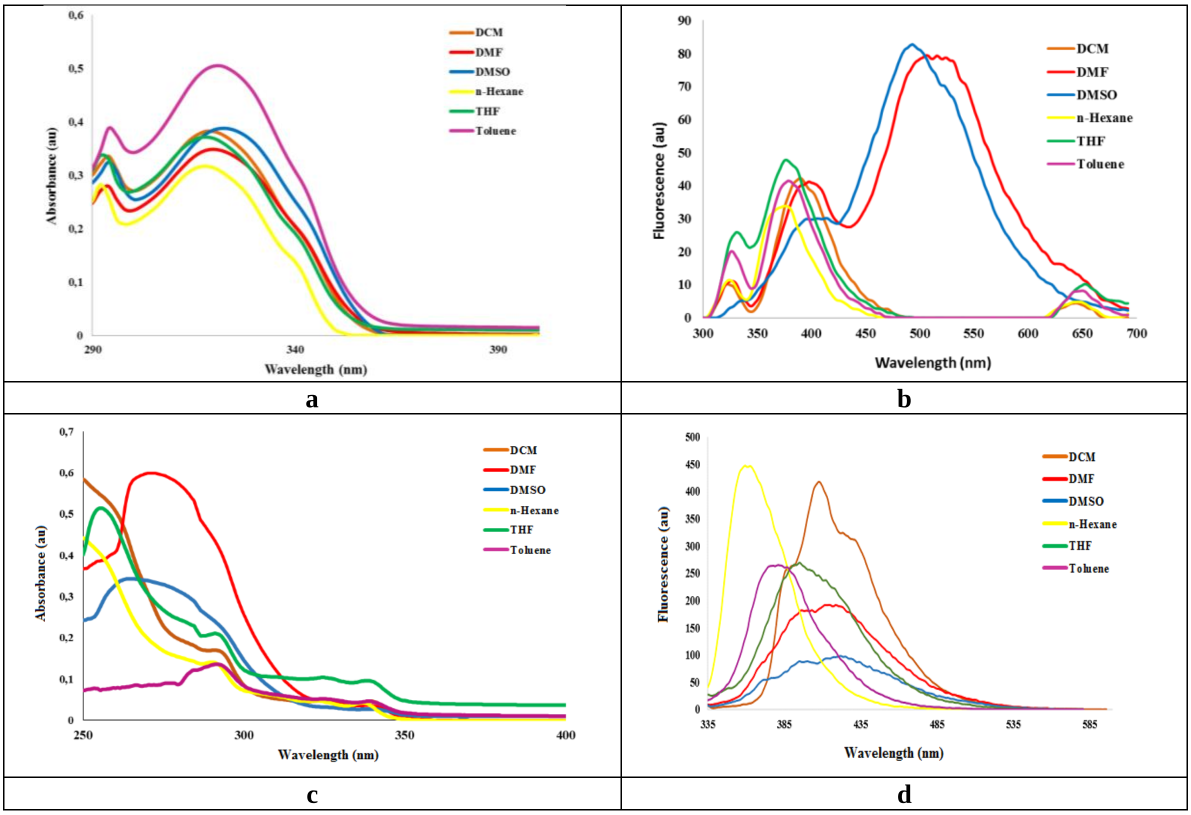

Figure 6. Absorption and emission spectra of compounds IIa and IIIa in different solvents. a) absorption spectrum of compound IIa (10^{-5} M), b) fluorescence spectrum of compound IIa (10^{-7} M), c) absorption spectrum of compound IIIa (10^{-5} M), d) fluorescence spectrum of compound IIIa (10^{-7} M).

Electrochemical Properties

In this study, a three-electrode type electrochemical cell with separate compartments for the reference electrode, counter electrode, and working electrode was employed. A silver wire (pseudo Ag/Ag^+) was used as the reference electrode, and a platinum wire was used as the counter electrode. Three different electrodes with a 3.0 mm diameter (Au, Gc, and Pt disk electrodes) were used as the working electrode. A solution containing 0.1 M tetrabutylammonium hexafluorophosphate (NBu_4PF_6) in DCM was used as the supporting electrolyte. The ferrocene-ferrocenium redox couple (Fc/Fc^+) was used as the internal reference.

Table 1. Electrochemical and optical data for the compounds.

	E_{onset}^{ox} [a] (V)	HOMO[b] (eV)	LUMO[c] (eV)	λ_{onset} [d] (nm)	Eg_{opt} [e] (V)
I	0.998	-5.58	-2.46	397	3.12
II	1.191	-5.71	-2.52	389	3.19
IIa	1.327	-5.65	-2.18	357	3.47
III	1.310	-5.81	-2.22	345	3.59
IIIa	1.333	-5.75	-2.19	348	3.56

[a]Determined from cyclic voltammetry experiments vs. Fc/Fc^{+} in dichloromethane on gold working electrode (Au).
[b]Calculated based on HOMO= - [E_{onset}^{ox} - $E_{1/2,\ Fc,Fc+}$ + 4.8] eV (Sathiyan et al., 2016).
[c]Obtained from LUMO = HOMO + E_{gopt} (Yang et al., 2018).
[d]Calculated from the cross point of absorption onset line and corrected base line.
[e]Estimated from the onset wavelength of the optical absorption bands.

The electrochemical investigation of the compounds was conducted separately for each working electrode in a cyclic potential sweeping mode within the potential range of -0.2 to 1.6 V (vs. pseudo Ag/Ag^{+} reference electrode) at a scan rate of 50 mV/s. The voltammograms were recorded using a 2x10^{-3} M solution of the molecules in DCM. The obtained cyclic voltammetry (CV) voltamograms are presented in Figure 7. Calculations were made based on the voltamogram values obtained for each electrode, and the best results were achieved using the Au disk electrode. The data obtained with the Au disk electrode are summarized in Table 1.

The onset oxidation potential was observed in the range of 0.998, 1.191, 1.327, 1.310, and 1.333 V and the HOMO energy levels were calculated based on these onset oxidation values, resulting in values of -5.58, -5.71, -5.65, -5.81, and -5.75 eV, additionally, the calculated LUMO energy levels were -2.46, -2.52, -2.18, -2.22, and -2.19 eV for compounds I, II, IIa, III, and IIIa, respectively. LUMO energy levels of the molecules were calculated based on the onset oxidation wavelengths of the optical absorption bands (Figure 8).

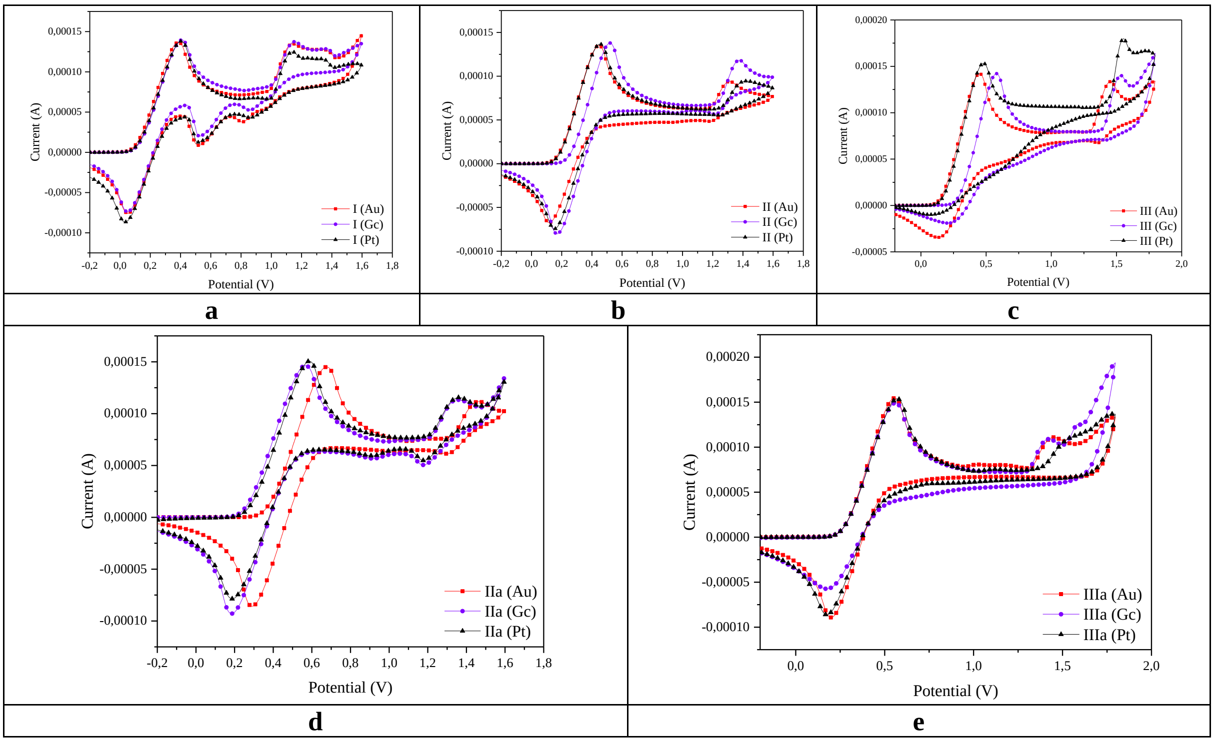

a **b** **c**

d **e**

Figure 7. Cyclic voltammograms of all the synthesized compounds in dichloromethane at room temperature; Au/Gc/Pt disk as working electrode; scan rate ν = 50 mV/s, 0.1 M Bu_4NPF_6 in DCM.

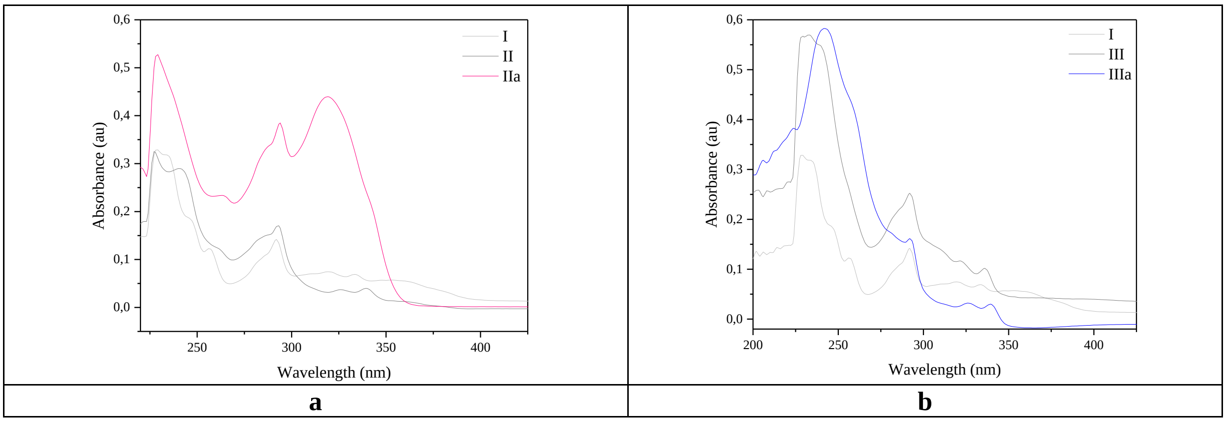

a **b**

Figure 8. Absorbance spectra of all the compounds in dichloromethane at room temperature.

The increase in the LUMO energy levels of the molecules is thought to be associated with an increase in delocalization within the π-conjugation system of the molecules (Shen et al., 2011). In a study conducted by Agarwal and colleagues, it was reported that the HOMO energy levels of the carbazole-derived molecules they synthesized varied between -5.67 and -6.02 eV depending on the electron-withdrawing or electron-donating groups attached to the aryl group and also these molecules could be used as materials for solar cells (Agarwal et al. 2011). Based on this, it can be suggested that the carbazole-derived molecules synthesized in our study may be suitable for use in solar cells.

Conclusion

In this study, two different carbazole monomers (IIa and IIIa), previously synthesized in our group in our earlier studies (Gorgun et al., 2019a; Gorgun et al., 2019b), were synthesized and characterized using the Ullman and Suzuki-Miyaura reactions. After the characterization studies were completed, cyclic voltammetry experiments were conducted using three different working electrodes (Au, Gc, Pt disk electrodes) for the synthesized compounds (IIa and IIIa). Since the best oxidation of the compounds was achieved on the gold disk electrode, this electrode was utilized in the calculation of energy levels. The HOMO and E_g values of the compounds were determined using cyclic voltammetry experiments and optical absorption bands, respectively. As a result of the electrochemical and optical studies, the found energy values matched the values given in the literature (Agarwal et al., 2011), suggesting that these synthesized materials could be used in solar cell.

Scientific Ethics Declaration

The authors declare that the scientific ethical and legal responsibility of this article published in EPSTEM journal belongs to the authors.

Acknowledgements or Notes

* This article was presented as an oral presentation at the International Conference on Basic Sciences and Technology (www.icbast.net) held in Antalya/Turkey on November 16-19, 2023.
* This work was supported by Eskisehir Osmangazi University Commission of Research Project under Grant no. 2016-1321.
* We would like to thank Betul Derince for all her contributions.

References

Agarwal, N., Nayak, P. K., Ali, F., Patankar, M. P., Narasimhan, K. L., & Periasamy, N. (2011). Tuning of HOMO levels of carbazole derivatives: New molecules for blue OLED. *Synthetic Metals, 161*(5-6), 466-473.

Al-Ibrahim, M., Roth, H. K., Schroedner, M., Konkin, A., Zhokhavets, U., Gobsch, G., & Sensfuss, S. (2005). The influence of the optoelectronic properties of poly (3-alkylthiophenes) on the device parameters in flexible polymer solar cells. *Organic Electronics, 6*(2), 65-77.

Ambrose, J. F., & Nelson, R. F. (1968). Anodic oxidation pathways of carbazoles: I. carbazole and N-substituted derivatives. *Journal of the Electrochemical Society, 115*(11), 1159.

Battal, A., Kassa, S. B., Gultekin, N. A., Tavasli, M., & Onganer, Y. (2024). A reaction-based carbazole-dicyanovinyl conjugated colorimetric and ratiometric fluorescent probe for selective detection of cyanide ions. *Spectrochimica Acta Part A: Molecular and Biomolecular Spectroscopy, 304*, 123350.

Chooto, P. (2019). *Cyclic voltammetry and its applications. Voltammetry*. IntechOpen, 1.

Gorgun, K., Caglar, M., Yandımoglu, M., & Sakarya, H. C. (2019). Eco-friendly carbazole-based molecules synthesis and their photodiode properties. Proceedings from: *6th International Materials Science and Nanotechology for Next Generation Conference*. Nigde, Turkey. Retrieved from http://msng2019.fytronix.com

Gorgun, K., Caglar, M., Yandımoglu, M., & Sakarya, H. C. (2019b). Synthesis of carbazole derived molecules with D-π-A structure and dye-sensitive solar cell applications. Proceedings from: *6th International Materials Science and Nanotechology for Next Generation Conference.* Nigde, Turkey Retrieved from http://msng2019.fytronix.com

Hwang, S. W., & Chen, Y. (2002). Photoluminescent and electrochemical properties of novel poly (aryl ether) s with isolated hole-transporting carbazole and electron-transporting 1, 3, 4-oxadiazole fluorophores. *Macromolecules, 35*(14), 5438-5443.

Justin Thomas, K. R., Lin, J. T., Tao, Y. T., & Ko, C. W. (2001). Light-emitting carbazole derivatives: potential electroluminescent materials. *Journal of the American Chemical Society, 123*(38), 9404-9411.

Kandemir, H., Kocak, A., Tumay, S. O., Çoşut, B., Zorlu, Y., & Sengul, I. F. (2018). Experimental and theoretical studies of carbazole-based Schiff base as a fluorescent Fe^{3+} probe. *Turkish Journal of Chemistry, 42*(2), 221-236.

Karon, K., & Lapkowski, M. (2015). Carbazole electrochemistry: A short review. *Journal of Solid State Electrochemistry, 19*, 2601-2610.

Li, M., Wang, Z., Liang, M., Liu, L., Wang, X., Sun, Z., & Xue, S. (2018). Low-cost carbazole-based hole-transporting materials for perovskite solar cells: influence of S, N-heterocycle. *The Journal of Physical Chemistry C, 122*(42), 24014-24024.

Liu, Y., Li, C., Ren, Z., Yan, S., & Bryce, M. R. (2018). All-organic thermally activated delayed fluorescence materials for organic light-emitting diodes. *Nature Reviews Materials,3*(4), 1-20.

NIST. (2023a). *Fluorene*. National Institute of Standards and Technology. Retrieved from https://webbook.nist.gov/cgi/cbook.cgi

NIST. (2023b). *Benzene, (trifluoromethyl)-*. National Institute of Standards and Technology. Retrieved from https://webbook.nist.gov/cgi/cbook.cgi?

Sathiyan, G., Thangamuthu, R., & Sakthivel, P. (2016). Synthesis of carbazole-based copolymers containing carbazole-thiazolo [5, 4-d] thiazole groups with different dopants and their fluorescence and electrical conductivity applications. *RSC Advances*, *6*(73), 69196-69205.

Shen, P., Tang, Y., Jiang, S., Chen, H., Zheng, X., Wang, X., & Tan, S. (2011). Efficient triphenylamine-based dyes featuring dual-role carbazole, fluorene and spirobifluorene moieties. *Organic Electronics, 12*(1), 125-135.

Yang, T., Xu, H., Wang, K., Tao, P., Wang, F., Zhao, B., & Xu, B. (2018). Bipolar host materials based on diphenylphosphine oxide and carbazole derivatives with high triplet energy: Synthesis, characterization and photoelectronic performance in PhOLEDs. *Dyes and Pigments, 153,* 67-73.

Zhu, W., Yang, L., Fang, M., Wu, Z., Zhang, Q., Yin, F., & Li, C. (2015). New carbazole-based Schiff base: Colorimetric chemosensor for Fe^{3+} and fluorescent turn-on chemosensor for Fe^{3+} and Cr^{3+}. *Journal of Luminescence, 158,* 38-43.

Author Information

Merve Yandimoglu
Eskisehir Osmangazi University
Eskisehir, Turkey
Contact e-mail: *mervesag26@gmail.com*

Kamuran Gorgun
Eskisehir Osmangazi University
Eskisehir, Turkey

Evrim Hur
Eskisehir Osmangazi University
Eskisehir, Turkey

To cite this article:

Yandimoglu, M., Gorgun, K., & Hur, E. (2023). Synthesis and some electrochemical properties of carbazole derivative monomers for optoelectronic device design. *The Eurasia Proceedings of Science, Technology, Engineering & Mathematics (EPSTEM), 25,* 59-66.

The Eurasia Proceedings of Science, Technology,
Engineering & Mathematics (EPSTEM)
ISSN: 2602-3199

The Eurasia Proceedings of Science, Technology, Engineering & Mathematics (EPSTEM), 2023

Volume 25, Pages 67-75

ICBAST 2023: International Conference on Basic Sciences and Technology

Some Fixed Point Results of $(\alpha,\beta,\varphi,\delta)$-Contractions in Extended Cone *b*-Metric Spaces

Zamir Selko
University of Elbasan “Aleksandër Xhuvani”

Eriola Sila
University of Tirana

Abstract This paper investigates the existence and uniqueness of fixed points for a class of generalized contractive mappings defined on extended cone metric spaces. Subsequently, we define and explore ($\alpha, \beta, \varphi, \delta$)-contractions, a generalization of traditional contractions that allows for a more nuanced understanding of the contraction behavior in extended cone metric spaces. The extended metric space was defined for the first time in 2017, by Kamran et al. (2017). They replaced the constant in the triangle inequality of the metric with a two-variable function and explored various fixed point theorems. In 2022, Das and Bag[4] introduced extended cone metric spaces by incorporating a three-variable map into the third condition of the cone metric. Afterwards, Selko and Sila introduced the concept of extended quasi cone b-metric spaces and demonstrated the Banach contraction within this framework. In 2018, Alqahtani. (2018) and colleagues established several fixed point results for a pair of orbital cyclic functions in an extended metric space. In this paper we prove some fixed point theorems for (α,β)-orbital-cyclic functions in extended cone metric spaces by using the continuous map φ and a nonnegative constant δ.

Keywords: (α,β)-orbital-cyclic functions, Fixed point, Extended cone metric space, Cone metric space

Introduction and Preliminaries

Cone metric spaces are a generalization of traditional metric spaces that allow for more flexible notions of distance and convergence. In a cone metric space, the usual notion of distance is replaced by a cone metric, which measures the distance between points in a way that is not constrained by the triangle inequality as in traditional metric spaces. Cone metric spaces are used in various mathematical contexts, including functional analysis and topology. These spaces are used in various fields, including mathematics, computer science, and engineering, to model situations where distances between points are not well-defined or are subject to certain uncertainties. Cone metric spaces are a way to extend the concept of a metric space to a more flexible and versatile setting. Let us start with the cone definition.

Definition 1.1 Das and Bag (2022). Let P be a nonempty subset of E, where E is an ordered Banach space. The set P is called a *cone* if and only if:

(i) P is closed, nonempty and $P \neq \{\theta\}$,
(ii) $a,b \in \mathbb{R}$; $a,b \geq 0$, $x,y \in P$ implies $ax+by \in P$,
(iii) $x \in P$ and $-x \in P$ implies $x=\theta$.

- Selection and peer-review under responsibility of the Organizing Committee of the Conference

The cone *P* is called *normal* if there is a positive real number *K* such that, for all x, y in *P* we have:

$$\theta \circ \; x \circ \; y \Rightarrow \|x\| \leq K \|y\| \tag{1}$$

or, equivalently, for three given sequences with terms from P, the sandwich rule holds i.e.

$$x_n \circ \; y_n \circ \; z_n \text{ and } \lim_{n\to\infty} x_n = \lim_{n\to\infty} z_n = c \text{ implies that } \lim_{n\to\infty} y_n = c \tag{2}$$

The positive number *K* is called *the normality constant* of P.

The cone *P* is called *regular* if every increased sequence which is bounded from above is convergent. That is, if $\{x_n\}_{n=1}^{\infty}$ is a sequence such $x_1 \leq x_2 \leq \cdots \leq b$ for some $b \in E,$ then there is a $x \in E,$ such that $\lim_{n\to\infty} \|x_n - x\| = 0.$ Equivalently, the cone *P* is called *regular* if every decreasing sequence, which is bounded from below is convergent. Regular cones are normal and there exist normal cones which are not regular.

In a cone $P \subset E,$ a partial ordering relation $\circ$ with respect to the cone *P* is defined as follows:

$$x \circ_P \; y \text{ iff } -x \in P \text{ for all } x, y \in P. \tag{3}$$

We also write $x \prec y$ if, $x \circ \; y$ and $x \neq y,$ while for every $x, y \in P, x \circ_P \; y$ if f $y - x \in Int(P).$ In the following, always *P* is a cone in the ordered Banach space *E*.

Definition 1.2 Das and Bag (2022). Let *P* be a cone and *X* a non-empty set. The function $d : X \times X \to P$ is called a *cone metric* if it satisfies the following conditions:

$(c1)$ $d(x, y) \succ \theta$ for all $x, y \in X,$ and $d(x, y) = \theta$ iff $x = y,$
$(c2)$ $d(x, y) = d(y, x)$ for all $x, y \in X,$
$(c3)$ $d(x, z) \circ \; d(x, y) + d(y, z)$ for all $x, y, z \in X.$

Then *d* is called *cone* metric on *X* and the pair (X, d) is called a *cone* metric space. Czerwik and Bakhtin introduced the concept of *b*-metric space and generalized the Banach contraction principle in such spaces.

Definition 1.3 Czerwik (1993). Let be *X* a nonempty set and $s \geq 1$ be a given real number. A function $d : X \times X \to \square^{+}$ is called a *b*-metric if, for all $x, y, z \in X$ it satisfies the conditions:

$(b1)$ $d(x, y) = 0$ iff $x = y,$
$(b2)$ $d(x, y) = d(y, x),$
$(b3)$ $d(x, z) \leq s\left[d(x, y) + d(y, z)\right].$

The pair (X, d) is called *b*-metric space with parameter *s*.
According to this definition, the cone *b*-metric notion will be defined as follows:

Definition1.4 Czerwik (1993). Let be *X* a nonempty set and $s \geq 1$ be a given real number. Suppose the mapping $d : X \times X \to E$ satisfies the conditions:

(i) $d(x, y) \succ \theta$ for all $x, y \in X$ and $d(x, y) = \theta$ iff $x = y,$
(ii) $d(x, y) = d(y, x)$ for all $x, y \in X,$
(iii) $d(x, z) \circ \; s\left[d(x, y) + d(y, z)\right]$ for all $x, y, z \in X.$

Then *d* is called a cone *b*-metric on *X* and the pair (X, d) is called a cone *b*-metric space.

As a development of the b-metric spaces, Kamran et al. [2] in 2017, introduced the notion of extended *b*-metric spaces taking instead of the coefficient *s,* a two-variable function θ.

Definition 1.5 Das and Bag (2022). Let X be a nonempty set and $\theta : X \times X \to [1, +\infty)$. A function $d_\theta : X \times X \to [0, +\infty)$ is an *extended cone metric,* if for all $x, y, z \in X$ it satisfies:

$(d_\theta 1)$ $d_\theta(x,y) = 0$ iff $x = y$;
$(d_\theta 2)$ $d_\theta(x,y) = d_\theta(y,x)$, for all $x, y \in X$;
$(d_\theta 3)$ $d_\theta(x,z) \le \theta(x,z)\left[d_\theta(x,y) + d_\theta(y,z)\right]$ for all $x, y, z \in X$.
The pair $\left(X, d_\theta\right)$ is called an *extended cone metric space.*

Remark 1.6 Das and Bag (2022). If $\theta : X \times X \to [1, +\infty)$, where $\theta(x,y) = s$, for $x, y \in X$, where $s \in [1, +\infty)$ is a constant, then we obtain the *b*-metric space definition, and when *s*=1 we obtain the cone metric space definition.

Example 1.7 Czerwik (1993). Let $X = \{1,\ 2,\ 3,\ \ldots\}$. Define $\theta : X \times X \to [1, +\infty)$ and $d_\theta : X \times X \to \mathbb{R}^+$ as:

$$\theta(x,y) = \begin{cases} |x-y| & \text{for } x \ne y \\ 1 & \text{for } x = y \end{cases} \quad \text{and} \quad d_\theta(x,y) = (x-y)^4$$

The pair (X, d_θ) is an extended *b*-metric space.

In 2022, Das and Bag extended the function θ from $X \times X$ to $X \times X \times X$ obtaining this

Definition 1.8 Das and Bag (2022). Let be X a nonempty set and $\theta : X \times X \times X \to [1 + \infty)$. Let $d_\theta : X \times X \to \mathbb{R}^+$ be a function which satisfies the following conditions:

$(d_\theta 1)$ $d_\theta(x,y) \ge 0$ for all x, y and $d_\theta(x,y) = 0$ iff $x = y$,
$(d_\theta 2)$ $d_\theta(x,y) = d_\theta(y,x)$ for all x, y in X,
$(d_\theta 3)$ $d_\theta\left(x,y\right) \le \theta(x,y,z)\left[d_\theta(x,z) + d_\theta(z,y)\right]$.

The function d_θ is called *extended cone metric* on X and the pair (X, d_θ) is called *extended cone metric space.*

Example 1.9 Let $X = \{2,\ 4,\ 6\}$ and $\theta : X \times X \to [1, +\infty)$ defined by $\theta(x,y) = 1 + 2x + 3y$. Let be the cone $P = \{(a,b) \in \mathbb{R}^2 : a, b \ge 0\}$. Define the function d_θ by :

$d_\theta(2,4) = d_\theta(4,2) = (10,10)$
$d_\theta(2,6) = d_\theta(6,2) = (20,20)$
$d_\theta(4,6) = d_\theta(6,4) = (30,30)$
$d_\theta(2,2) = d_\theta(4,4) = d_\theta(6,6) = (0,0) = \theta$

It is evident by the definition of d_θ that the first and second conditions of extended cone metric space are fulfilled. Let now check the third condition:

$$d_\theta(x,z) \le \theta(x,z)\left[d_\theta(x,y) + d_\theta(y,z)\right] \text{ for all } x, y, z \in X \text{ or,}$$
$$\theta(x,z)\left[d_\theta(x,y) + d_\theta(y,z)\right] - d_\theta(x,z) \ge \theta$$

$\theta(2,6)\left[d_\theta(2,4) + d_\theta(4,6)\right] - d_\theta(2,6) = 23\left[(10,10) + (30,30)\right] - (20,20) = (900,900) \in P$
$\theta(2,4)\left[d_\theta(2,6) + d_\theta(6,4)\right] - d_\theta(2,4) = 17\left[(20,20) + (30,30)\right] - (10,10) = (840,840) \in P$
$\theta(4,6)\left[d_\theta(4,2) + d_\theta(2,6)\right] - d_\theta(4,6) = 27\left[(10,10) + (20,20)\right] - (30,30) = (780,780) \in P$

Then (X, d_θ) is an extended *cone* metric space.
Some basic concepts, like convergence, Cauchy sequence, continuity and completeness in cone metric spaces are defined as follows.

Definition 1.10 Kamran et al. (2017). Consider a sequence $\{x_n\}$ in a cone metric space (X, d) and P be a normal cone in E with normal constant M. Then

1. $\{x_n\}$ converges to x if for every $c \in E$ with $c \succcurlyeq \theta$, $\exists N \in \mathbb{N}$ such that for all $n \geq N$, $d(x_n, x) \preccurlyeq c$. Denoted by $\lim_{n\to\infty} x_n = x$ or $x_n \xrightarrow[n\to\infty]{} x$.
2. $\{x_n\}$ is said to be Cauchy in X if for every $c \in E$ with $c \succcurlyeq \theta$, $\exists N \in \mathbb{N}$ such that for all $n, m \geq N \Rightarrow d(x_n, x_m) \preccurlyeq c$.
3. The mapping $T : X \to X$ is said to be continuous at a point $x \in X$ if for every sequence $\{ x_n \}$ converging to x it follows that $\lim_{n\to\infty} Tx_n = T \lim_{n\to\infty} x_n = Tx$.
4. (X, d) is said to be a complete cone metric space if every Cauchy sequence in X is convergent in X.

2 (S,T)-Orbital-Cyclic Admissible Pair

Popescu in his paper in 2014 introduced the concept of α-orbital admissible functions as follows:

Definition 2.1 Popescu (2014). Let $T : X \to X$ and $\alpha : X \times X \to [0,\infty)$. We say that T is an α –orbital admissible if for all $x, y \in X$, we have

$$\alpha(x,Tx) \geq 1 \quad \Rightarrow \quad \alpha(Tx,T^2x) \geq 1 \tag{4}$$

Definition 2.2. Khamsi, (2010).A set X is regular with respect to mapping α: $X \times X \to [0, \infty)$ if, whenever $\{x_n\}$ is a sequence in X such that $\alpha(x_n, x_{n+1}) \geq 1$ and $\alpha(x_{n+1}, x_n) \geq 1$ for all n and $x_n \to x \in X$ as $n \to \infty$, then there exists a subsequence $\{x_{n(k)}\}$ of $\{x_n\}$ such that $\alpha(x_{n(k)}, x) \geq 1$ and $\alpha(x, x_{n(k)}) \geq 1$ for all n.
Alqahtani et al. (2018) introduced the concept of (α, β)-orbital-cyclic admissible pair and proved some fixed point results for a couple of orbital cyclic functions in extended b-metric spaces.

Definition 2.3 Alqahtani et al. (2018). Let S, T are two self-mappings on a complete extended cone metric space (X, d_θ). Suppose that there are two functions $\alpha, \beta : X \times X \to [0,\infty)$ such that for any $x \in X$,

$$\begin{aligned} &\alpha(x,Tx) \geq 1 \quad \Rightarrow \quad \beta(Tx,STx) \geq 1 \quad \text{and} \\ &\beta(x,Sx) \geq 1 \quad \Rightarrow \quad \alpha(Sx,TSx) \geq 1 \end{aligned} \tag{5}$$

Then the pair (S, T) is called (α, β)*-orbital -cyclic admissible* pair.

Main Result

Below, we give this key-lemma which is essential for our main results.

Lemma 2.4 *Let (X, d_θ) be an extended cone metric space and let P be a normal cone with normality constant K. If there exists $q \in [0,1)$ such that the sequence $\{x_n\}$ for an arbitrary $x_0 \in X$ satisfies*

$$\lim_{n,m\to\infty} \theta(x_n, x_m, x_{n+1}) < \frac{1}{q} \text{ and also}$$
$$\theta \prec d_\theta(x_n, x_{n+1}) \circ \; q d_\theta(x_{n-1}, x_n) \text{ for any } n \in \mathbb{N}, \tag{6}$$

then the sequence $\{x_n\}$ is Cauchy in X.

Proof. Using the inequality (6) recursively it follows that

$$\theta \circ\ d_\theta(x_n, x_{n+1}) \circ\ q^n d_\theta(x_1, x_0) \tag{7}$$

Taking the limits in both sides for *n* to infinity and using the fact that $q < 1$, it follows that

$$\lim_{n\to\infty} d_\theta(x_n, x_{n+1}) = 0. \tag{8}$$

From $(d_\theta 3)$ property of extended cone metric and the triangular inequality we can write as follows

$$\begin{aligned} d_\theta(x_{n+p}, x_n) &\circ\ \theta\left(x_{n+p}, x_{n+p-1}, x_n\right)\cdot\left(d_\theta(x_{n+p}, x_{n+p-1}) + d_\theta(x_{n+p-1}, x_n)\right) \\ &\circ\ \theta\left(x_{n+p}, x_{n+p-1}, x_n\right)\cdot\theta\left(x_{n+p-1}, x_{n+p-2}, x_n\right)\cdot\left(d_\theta(x_{n+p-1}, x_{n+p-2}) + d_\theta(x_{n+p-2}, x_n)\right) \\ &+\theta\left(x_{n+p}, x_{n+p-1}, x_n\right)\cdot d_\theta(x_{n+p}, x_{n+p-1}) \\ &\circ\ \theta\left(x_{n+p}, x_{n+p-1}, x_n\right)\cdot\theta\left(x_{n+p-1}, x_{n+p-2}, x_n\right)\cdots\theta\left(x_{n+2}, x_{n+1}, x_n\right)\cdot q^n\cdot d_\theta(x_1, x_0) \\ &+\cdots+\theta\left(x_{n+p}, x_{n+p-1}, x_n\right)\cdot q^{n+p-1}\cdot d_\theta(x_1, x_0) \end{aligned} \tag{9}$$

Taking the norm for both sides of the final inequality, it follows that:

$$\left\|d_\theta(x_{n+p}, x_n)\right\| \le K\left[\theta\left(x_{n+p}, x_{n+p-1}, x_n\right)\cdot\theta\left(x_{n+p-1}, x_{n+p-2}, x_n\right)+\cdots+\theta\left(x_{n+2}, x_{n+1}, x_n\right)\cdot q^{n+p-1}\right]\left\|d_\theta(x_1, x_0)\right\| \tag{10}$$

Remember that *K* is the normality constant of the cone *P*.

Consequently,

$$\left\|d_\theta(x_{n+p}, x_n)\right\| \le K\cdot\left(S_{n+p} - S_n\right)\cdot\left\|d_\theta(x_1, x_0)\right\| \tag{11}$$

where S_n are the partial sums of the convergent series $\sum_{i=1}^{\infty} q^p\cdot\prod_{i=2}^{p}\theta(x_{n+i}, x_{n+i-1}, x_n)$.

Then,

$$\lim_{n,p\to\infty}\left\|d_\theta(x_{n+p}, x_n)\right\| = 0$$

which implies that the sequence $\{x_n\}$ is Cauchy.

Theorem 2.5. *Let T, S be two self-mappings on a complete extended cone metric space* (X, d_θ) *such that the pair (T, S) is* (α,β)*-orbital-cyclic admissible. Suppose that there is a constant* $\delta > 0$ *and a continuous comparison function* $\varphi : X \to E$ *such that* $\lim_{n\to\infty}\left\|\varphi^n(t)\right\| = 0$ *and*

(i) *for each* $x_0 \in X$, $\lim_{n,m\to\infty}\theta(x_n, x_m, x_{n+1}) < \frac{1-k}{k}$, *where* $x_{2n} = Sx_{2n-1}$ *and* $x_{2n+1} = Tx_{2n}$ *for each* $n \in \square$,

(ii) *there exists* $x_0 \in X$ *such that* $\alpha(x_0, Tx_0) \ge 1$,

(iii) *S and T are continuous and satisfies the following inequality*

$$\begin{aligned} &\alpha(x,Tx)\beta(y,Sy)d_\theta(Tx,Sy) \circ\ \varphi\left(\max\left\{d_\theta(x,Tx),\, d_\theta(y,Sy)\right\}\right) \\ &+\delta\min\left\{d_\theta(x,Tx), d_\theta(y,Sy), d_\theta(Tx,y), d_\theta(x,Sy)\right\}. \end{aligned} \tag{12}$$

Then the pair of mappings (T,S) *has a common fixed point u, that is* $Tu=u=Su$.

Proof. By assumption (ii) there exists $x_0\in X$ such that $\alpha(x_0,Tx_0)\geq 1$. Let be $x_1=Tx_0$ and $x_2=Sx_1$. Continuing in this way inductively, we construct the sequence $\{x_n\}$ where

$$x_{2n}=Sx_{2n-1}\quad\text{and}\quad x_{2n+1}=Tx_{2n}\quad \forall n\in\mathbb{N} \tag{13}$$

We have $\alpha(x_0,Tx_0)=\alpha(x_0,x_1)\geq 1$ and since (*S*, *T*) is an (α,β) -orbital-cyclic admissible pair, it follows that

$$\alpha(x_0,x_1)\geq 1 \;\Rightarrow\; \beta(x_0,STx_0)=\beta(x_1,x_2)\geq 1$$

and

$$\beta(x_1,x_2)\geq 1 \;\Rightarrow\; \alpha(Sx_1,TSx_1)=\alpha(x_2,x_3)\geq 1$$

Applying again (5),

$$\alpha(x_2,x_3)\geq 1 \;\Rightarrow\; \beta(Tx_2,STx_2)=\beta(x_3,x_4)\geq 1$$

and

$$\beta(x_3,x_4)\geq 1 \;\Rightarrow\; \alpha(Sx_3,TSx_3)=\alpha(x_4,x_5)\geq 1.$$

Recursively, we obtain

$$\alpha(x_{2n},x_{2n+1})\geq 1 \quad \text{for all } n\in\mathbb{N} \tag{14}$$

and

$$\beta(x_{2n+1},x_{2n+2})\geq 1 \quad \text{for all } n\in\mathbb{N} \tag{15}$$

We can continue the proof assuming that $x_n\neq x_{n+1}$ for all $n\in\mathbb{N}$. This assumption doesn't loss the generality of the proof. Indeed, if there exists any $n_0\in\mathbb{N}$ such that $x_{n_0}=x_{n_0+1}$, the common fixed point of mappings *S*, *T* is $u=x_{n_0}$. To see that $u=x_{n_0}$ is the requested point, we study the following two cases.

(i) If $n_0=2k$, we have $x_{2k}=x_{2k+1}=Tx_{2k}$. Thus, x_{2k} is a fixed point of *T*. To show that x_{2k+1} is also a fixed point of *S* we must prove that $x_{2k+1}=Sx_{2k+1}$ or, equivalently $Tx_{2k}=Sx_{2k+1}$.

Suppose on the contrary, that $d_\theta(x_{2k+1},Sx_{2k+1})\succ\theta$. Replacing $x=x_{2k}$ and $y=x_{2k+1}$ in (12) and using (14), (15) we obtain:

$$\begin{aligned}\theta &\prec d_\theta(x_{2k+1},x_{2k+2})=d_\theta(Tx_{2k},Sx_{2k+1})\\ &\circ\; \alpha(x_{2k},Tx_{2k})\beta(x_{2k+1},Sx_{2k+1})d_\theta(Tx_{2k},Sx_{2k+1})\\ &\circ\; \varphi\big(\max\{d_\theta(x_{2k},Tx_{2k}),d_\theta(x_{2k+1},Sx_{2k+1}),\}\big)+\delta\min\{d_\theta(x_{2k},x_{2k+1}),d_\theta(x_{2k},Tx_{2k}),d_\theta(x_{2k+1},Tx_{2k+1})\}\end{aligned}$$

By replacing $d_\theta(x_{2k},Tx_{2k})=\theta$, $d_\theta(x_{2k},x_{2k+1})=\theta$ and using the fact that $\varphi(t)<t$ we obtain

$$\theta\prec d_\theta(x_{2k+1},x_{2k+2})\circ\; \varphi(d_\theta(x_{2k+1},x_{2k+2}))\prec d_\theta(x_{2k+1},x_{2k+2}) \tag{16}$$

which is a contradiction. Thus, $d_\theta(x_{2k+1},Sx_{2k+1})=\theta$ or $d_\theta(Tx_{2k},Sx_{2k+1})=0$ and $x_{2k}=x_{2k+1}=Tx_{2k}=Sx_{2k+1}$ which implies that $u=x_{2k}=x_{2k+1}$ is a common fixed point of *T* and *S*.
(ii) If $n_0=2k+1$ we can proceed analogously obtaining the same result.
From now on, we suppose that $x_n\neq x_{n+1}$ for all $n\in\mathbb{N}$.
Now, we shall prove that $\{x_n\}$ is a Cauchy sequence. For this, it is enough to prove that our sequence fulfills the requirements of Lemma 2.4.

$$\begin{aligned}\theta &\prec d_\theta(x_{2n+1},x_{2n+2})\leq\alpha(x_{2n,},Tx_{2n})\beta(x_{2n+1},Sx_{2n+1})d_\theta(Tx_{2n},Sx_{2n+1})\\ &\circ\; \varphi\Big(\max\big\{d_\theta(x_{2n,}Tx_{2n}),d_\theta(x_{2n+1},Sx_{2n+1})\big\}\Big)\\ &+\delta\min\big\{d_\theta(x_{2n,}Tx_{2n}),d_\theta(x_{2n+1},Sx_{2n+1}),d_\theta(Tx_{2n},x_{2n+1}),d_\theta(x_{2n},Sx_{2n+1})\big\}\end{aligned} \tag{17}$$

Since $d_\theta(Tx_{2n}, x_{2n+1}) = d_\theta(x_{2n+1}, x_{2n+1}) = \theta,$ it follows that

$$\min\left\{d_\theta(x_{2n,}Tx_{2n}), d_\theta(x_{2n+1}, Sx_{2n+1}), d_\theta(Tx_{2n}, x_{2n+1}), d_\theta(x_{2n}, Sx_{2n+1})\right\} = \theta$$

Therefore, the inequality (17) will be write more simply

$$\begin{aligned} \theta \prec_\theta\ (x_{2n+1}, x_{2n+2}) \circ\ & \alpha(x_{2n,}Tx_{2n})\beta(x_{2n+1}, Sx_{2n+1})d_\theta(Tx_{2n}, Sx_{2n+1}) \\ \circ\ & \varphi\left(\max\left\{d_\theta(x_{2n,}Tx_{2n}), d_\theta(x_{2n+1}, Sx_{2n+1})\right\}\right) \end{aligned} \tag{18}$$

Further, using the property of maximal element of a set and the monotony of $\varphi,$ we have

$$\begin{aligned} d_\theta(x_{2n+1}, x_{2n+2}) \circ\ & \varphi\left(\max\left\{d_\theta(x_{2n,}Tx_{2n}),\ d_\theta(x_{2n+1}, Sx_{2n+1})\right\}\right) \\ &= \varphi\left(\max\left\{d_\theta(x_{2n,}x_{2n+1}),\ d_\theta(x_{2n+1}, x_{2n+2})\right\}\right) \end{aligned} \tag{19}$$

If $\max\left\{d_\theta(x_{2n,}x_{2n+1}),\ d_\theta(x_{2n+1}, x_{2n+2})\right\} = d_\theta(x_{2n+1}, x_{2n+2})$ then from the inequality $\varphi(t) < t$ it follows that

$$d_\theta(x_{2n+1}, x_{2n+2}) \prec d_\theta(x_{2n+1}, x_{2n+2})$$

which is contradiction. As a consequence, we have

$$\max\left\{d_\theta(x_{2n,}x_{2n+1}),\ d_\theta(x_{2n+1}, x_{2n+2})\right\} = d_\theta(x_{2n}, x_{2n+1}).$$

Therefore, from (19)

$$d_\theta(x_{2n+1}, x_{2n+2}) < \varphi\left(d_\theta(x_{2n,}x_{2n+1})\right) \tag{20}$$

From Lemma 2.4 and the first condition of our theorem, it follows that $\{x_n\}$ is a Cauchy sequence in X. Since (X, d_θ) is complete, there exists $u \in X$ such that

$$\lim_{n\to\infty} x_n = u. \tag{21}$$

From (21) it is clear that as subsequences of $\{x_n\}$, we have that $\{x_{2n}\}$ and $\{x_{2n+1}\}$ converges at the point $u \in X$

$$\lim_{n\to\infty} x_{2n} = \lim_{x\to\infty} x_{2n+1} = u. \tag{22}$$

By using the continuity of S and T we obtain

$$u = \lim_{n\to\infty} x_{n+1} = \lim_{n\to\infty} Tx_n = T \lim_{n\to\infty} x_n = Tu$$

and

$$u = \lim_{n\to\infty} x_{n+1} = \lim_{n\to\infty} Sx_n = S \lim_{n\to\infty} x_n = Su.$$

Thus, the point u is a common fixed point for the pair of mappings (S, T).
Now, before we prove the uniqueness of u, we accept that for all x, y common fixed point of mappings S and T (denoted $x, y \in CT(S, T)$) we have

$$\alpha(x, Tx) \geq 1 \text{ and } \beta(y, Sy) \geq 1. \tag{23}$$

Suppose on the contrary that v is another fixed point of the mapping T where $u \neq v.$ Therefore, $u = Tu = Su$ and $v = Tv = Sv.$ From (23) we derive that

$$\alpha(u,Tu)\geq 1 \text{ and } \beta(v,Sv)\geq 1. \tag{24}$$

Using the inequality (12), for T we have

$$\begin{aligned}&\alpha(u,Tu)\beta(v,Sv)d_\theta(Tu,Sv)\circ\ \varphi\left(\max\left\{d_\theta(u,Tu),\, d_\theta(v,Sv)\right\}\right)\\ &+\delta\min\left\{d_\theta(u,Tu), d_\theta(v,Sv), d_\theta(Tu,v), d_\theta(v,Su)\right\}.\end{aligned}$$

Since $u,v\in CT(S,T)$), from the last inequality, we get that

$$\begin{aligned}d_\theta(Tu,Sv)\circ\ &\varphi\left(\max\left\{\theta,\theta\right\}\right)+\delta\min\left\{\theta,\theta,d_\theta(Tu,v),d_\theta(v,Su)\right\}\\ &=\varphi(\theta)+\delta\cdot\theta\\ &=\theta.\end{aligned}$$

Finally, the inequality $d_\theta(Tu,Sv)=d_\theta(u,v)\leq\theta$ is possible only when $d_\theta(u,v)=\theta$ or $u=v$ which is a contradiction. Thus, u is unique fixed point of T.

2.1 (α,β) -Orbital-Cyclic Admissible Mappings

Definition 2.1.1 Alqahtani et al. (2018). Let X be a nonempty set, $T:X\to X$ $\alpha,\beta:X\times X\to[0,\infty)$. We say that T is an (α,β) -orbital-cyclic admissible mapping if

$$\begin{aligned}&\alpha(x,Tx)\geq 1 \text{ implies } \beta(Tx,T^2x)\geq 1 \qquad \text{and}\\ &\beta(x,Tx)\geq 1 \text{ implies } \alpha(Tx,T^2x)\geq 1\end{aligned} \tag{25}$$

Corollary 2.1.2 *Let T be a self-mapping on a complete extended cone metric space* (X,d_θ) *such that the mapping T forms an* (α,β) *-orbital-cyclic admissible mapping. Suppose that there is a constant* $\delta>0$ *and a continuous comparison function* $\varphi:X\to E$ *such that* $\lim\limits_{n\to\infty}\left\|\varphi^n(t)\right\|=0$ *and*

(i) *for each* $x_0\in X$, $\lim_{n,m\to\infty}\theta(x_n,x_m,x_{n+1})<\dfrac{1-k}{k}$, *where* $x_{2n}=Sx_{2n-1}$ *and* $x_{2n+1}=Tx_{2n}$ *for each* $n\in\Box$,

(ii) *there exists* $x_0\in X$ *such that* $\alpha(x_0,Tx_0)\geq 1$,

(iii) *T is continuous and satisfies this inequality*

$$\begin{aligned}&\alpha(x,Tx)\beta(y,Ty)d_\theta(Tx,Ty)\leq\varphi\left(\max\left\{d_\theta(x,Tx),\, d_\theta(y,Ty)\right\}\right)\\ &+\delta\min\left\{d_\theta(x,Tx), d_\theta(y,Ty), d_\theta(Tx,y), d_\theta(x,Ty)\right\}\end{aligned} \tag{26}$$

then T has a fixed point $u=Tu$.

Proof. If we replace $S=T$ in the Theorem 2.5 the result is evident.

Corollary 2.1.3 *Let T be a self-mapping on a complete extended cone metric space* (X,d_θ) *such that the mapping T forms an* (α,β) *-orbital-cyclic admissible mapping. Suppose that there is a constant* $\delta>0$ *and a continuous comparison function* $\varphi:X\to E$ *such that* $\lim\limits_{n\to\infty}\left\|\varphi^n(t)\right\|=0$ *and*

(i) *for each* $x_0\in X$, $\lim_{n,m\to\infty}\theta(x_n,x_m,x_{n+1})<\dfrac{1-k}{k}$, *where* $x_{2n}=Sx_{2n-1}$ *and* $x_{2n+1}=Tx_{2n}$ *for each* $n\in\Box$,

(ii) *there exists* $x_0\in X$ *such that* $\alpha(x_0,Tx_0)\geq 1$,

(iii) *T is continuous and satisfies this inequality*

$$\begin{aligned}&\alpha(x,Tx)\alpha(y,Ty)d_\theta(Tx,Ty)\le\varphi\left(\max\left\{d_\theta(x,Tx),\ d_\theta(y,Ty)\right\}\right)\\&+\delta\min\left\{d_\theta(x,Tx),d_\theta(y,Ty),d_\theta(Tx,y),d_\theta(x,Ty)\right\}\end{aligned}\tag{27}$$

then T has a fixed point $u = Tu$.
Proof: By taking $\beta(x,y)=\alpha(x,y)$ in Corollary 2.1.2, the proof is done.

Scientific Ethics Declaration

The authors declare that the scientific ethical and legal responsibility of this article published in EPSTEM journal belongs to the authors.

Acknowledgements or Notes

* This article was presented as an oral presentation at the International Conference on Basic Sciences and Technology (www.icbast.net) held in Antalya/Turkey on November 16-19, 2023.

References

Alqahtani, B., Fulga, A. & Karapınar, E. (2018). Common fixed point results on an extended b-metric space. *Journal of Inequalities and Applications, 158.*

Czerwik, S. (1993). Contraction mappings in b-metric spaces." *Acta Mathematica et Informatica Universitatis Ostraviensis, 1*(1), 5-11. Retrieved from http://eudml.org/doc/23748.

Das, A., & Bag, T. (2022). Some fixed point theorems in extended cone -metric spaces. *Communications in Mathematics and Applications*, *13*(2), 647–659.

Kamran, T., Samreen, M., & Ain, O.U. (2017). A generalization of *b*-metric space and some fixed point theorems. *Mathematics, 5*(2), 19.

Khamsi, M. (2010). Remarks on cone metric spaces and fixed point theorems of contractive mappings. *Fixed Point Theory Applications*, (1).

Popescu, O. (2014). Some new fixed point theorems for α-Geraghty contraction type maps in metric spaces. *Fixed Point Theory and Applications*,190.

Author Information

Zamir Selko	**Eriola Sila**
University of Elbasan “Aleksandër Xhuvani” Elbasan, Albania Contact e-mail: zamir.selko@uniel.edu.al	University of Tirana, Tirana, Albania

To cite this article:

Selko, Z. & Sila, E. (2023). Some fixed point results of $(\alpha,\beta,\varphi,\delta)$ -contractions in extended cone *b*-metric spaces. *The Eurasia Proceedings of Science, Technology, Engineering & Mathematics (EPSTEM), 25,* 67-75.

The Eurasia Proceedings of Science, Technology,
Engineering & Mathematics (EPSTEM)
ISSN: 2602-3199

The Eurasia Proceedings of Science, Technology, Engineering & Mathematics (EPSTEM), 2023

Volume 25, Pages 76-96

ICBAST 2023: International Conference on Basic Sciences and Technology

Soft G*β-Separation Axioms in Soft Topological Spaces

Raja Mohammad Latif
Prince Mohammad Bin Fahd University

Abstract: Soft set theory is a newly emerging tool to deal with uncertain problems and has been studied by researchers in theory and practice. The concept of soft topological space is a very recently developed area having many research scopes. Soft sets have been studied in proximity spaces, multicriteria decision-making problems, medical problems, mobile cloud computing networks, defense learning system, approximate reasoning etc. In 2020 Punitha Tharani and H. Sujitha introduced a new class of soft generalized star β-closed $\left(S_{ft}g*\beta-\text{closed}\right)$ sets and $S_{ft}g*\beta-$open sets in soft topological spaces. They investigated some basic properties of $S_{ft}g*\beta-$closed sets and $S_{ft}g*\beta-$open sets. They also studied the relationship between this type of closed sets and other existing closed sets in soft topological spaces. The aim of this paper is to introduce some soft separation axioms called $S_{ft}g*\beta-R_0$ space, $S_{ft}g*\beta-R_1$ space, $S_{ft}g*\beta-T_0$ space, $S_{ft}g*\beta-T_1$ space, $S_{ft}g*\beta-T_2$ space, $S_{ft}g*\beta-$regular space and $S_{ft}g*\beta-$normal space in soft topological spaces. We investigate several properties and characterizations of this spaces in soft topological spaces.

Keywords: $S_{ft}-$Top$-$Space, $S_{ft}g*\beta-R_i$ space, $S_{ft}g*\beta-T_i$ space, $S_{ft}g*\beta-$normal space

1. Introduction

During recent years, soft set theory emerged as a best mathematical tool to deal with uncertainties, imprecision and vagueness. Many engineering, medical science, economics, environment problems have various uncertainties, and the soft set theory came up with the reasonable solutions to these problems. A soft set is a collection of approximate descriptions of objects. Some researchers have presented a systematic survey of the literature and the developments of Topological Spaces in soft set theory. They have also provided some applications of soft set theory in software engineering, innovation, medical diagnosis, data analysis, decision making etc. All these tools require the specification of some parameter to start with. The theory of soft sets gives a vital mathematical tool for handling uncertainties and vague concepts. Recently several researchers introduced the notion of soft topology and established that every soft topology induces a collection of topologies called the parametrized family of topologies induced by the soft topology. They discussed soft set-theoretical operations and gave an application of soft set theory to a decision-making problems. Several mathematicians published papers on applications of soft sets and soft topology. Soft sets and soft topology have applications in data mining, image processing, decision-making problems, spatial modeling, and neural patterns. Research works on soft set theory and its applications in various fields are progressing rapidly. Decision-making and topology have a long joint tradition since the modern statement of the classical Weierstrass extreme value theorem. It combines two topological concepts called continuity of a real-valued function and compactness of the domain (both with respect to a given topology). They represent a necessary and sufficient condition to guarantee the existence of the maximum and minimum values of the function. The success of Mathematical Problems in Engineering technique was amplified by its adoption in fields like engineering sciences, computer sciences, and mathematical economics. This matter can be adopted on the version of soft setting by replacing the classical notions (compactness, function, and real numbers) by their soft counterparts (soft compactness, soft function, and soft real numbers). Some practical experiments in the civil engineering require classification of the

---

- Selection and peer-review under responsibility of the Organizing Committee of the Conference

materials according to their characteristics (attribute set or parameter set E) which can be expressed using the concept of soft sets. We study the separation of them with respect to the group of soft sets which are constructed from the practical experiments. In this group of soft sets, we add the absolute and null soft sets to initiate a soft weak structure. The researchers in the communication engineering endeavor to select the best protocol to solve the noisy problems in wireless networks. They evaluate the performance of these protocols according to the proposed scenarios. The researchers in Soft Theory may plan with some engineers to propose some protocols using the appropriate soft structure to select the optimal protocol to solve the interference problems in wireless networks. The main objective of this paper is to introduce some soft separation axioms called $S_{ft}g^*\beta-R_0$ space, $S_{ft}g^*\beta-R_1$ space, $S_{ft}g^*\beta-T_0$ space, $S_{ft}g^*\beta-T_1$ space, $S_{ft}g^*\beta-T_2$ space, $S_{ft}g^*\beta-\text{regular}$ space and $S_{ft}g^*\beta-\text{normal}$ space in soft topological spaces. We investigate several properties and characterizations of these new notions in soft topological spaces.

2. Preliminaries

Definition 2.1. Let X be an initial universe set and E be a collection of all possible parameters with respect to X, where parameters are the characteristics or properties of objects in X Let $P(X)$ denote the power set of X, and let A be a non-empty subset of E. A pair (F, A) is called a soft set over X, where F is a mapping given by $F: A \to P(X)$. In other words, a soft set over X is a parameterized family of subsets of the universe X. For $e \in A$, $F(e)$ may be considered as the set $e-$approximate elements of the soft set (F, A). Clearly, a soft set is not a set. For two soft sets (F, A) and (G, B) over the common universe X, we say that (F, A) is a soft subset of (G, B) if (i) $A \subseteq B$ and (ii) for all $e \in A$, $F(e)$ and $G(e)$ are identical approximations. We write $(F, A) \subseteq (G, B)$. (G, B) is said to be a soft superset of (F, A), if (F, A) is a soft subset of (G, B). Two soft sets (F, A) and (G, B) over a common universe X are said to be soft equal if (F, A) is a soft subset of (G, B) and (G, B) is a soft subset of (F, A).

Definition 2.2. The union of two soft sets of (F, A) and (G, B) over the common universe X is soft set $(H, C) = (F, A) \cup (G, B)$, where $C = A \cup B$, and $H(e) = F(e)$ if $e \in A - B$, $H(e) = G(e)$ if $e \in B - A$ and $H(e) = F(e) \cup G(e)$ if $e \in A \cap B$.

Definition 2.3. The Intersection (H, C) of two soft sets (F, A) and (G, B) over a common universe X denoted $(F, A) \cap (G, B)$ is defined as $C = A \cap B$ and $H(e) = F(e) \cap G(e)$ for all $e \in C$.

Definition 2.4. For a soft set (F, A) over the universe U, the relative complement of (F, A) is denoted by $(F, A)^C$ and is defined by $(F, A)^C = (F^C, A)$, where $F^C: A \to P(X)$ is a mapping defined by $F^C(e) = X - F(e)$ for all $e \in A$.

Definition 2.5. A soft set (F, E) over X is said to be (i) A null soft set, denoted by $\tilde{\phi}$, if $\forall$ $e \in E$, $F(e) = \phi$. (ii) An absolute soft set, denoted by $\tilde{X}$, if $\forall$ $e \in E$, $F(e) = X$.

Definition 2.6. Let $\tilde{\tau}$ be the collection of soft sets over X. Then $\tilde{\tau}$ is said to be a soft Topology on X if

(i) $\tilde{\phi}$, $\tilde{X}$ belong to $\tilde{\tau}$

(ii) The union of any number of soft sets in $\tilde{\tau}$ belongs to $\tilde{\tau}$

(iii) The intersection of any two soft sets belongs to $\tilde{\tau}$.

The triplet $(\tilde{X},\tilde{\tau},E)$ is called a soft topological space over X. The complement of a soft open set is called soft closed set over X.

Definition 2.7. Let $(\tilde{X},\tilde{\tau},E)$ be a soft topological space over X and (F,E) be a soft set over X. Then

(i) Soft interior of a soft set (F,E) denoted by $S_{ft}Int(F,E)$ is defined as the union of all soft open sets over X contained in (F,E).

(ii) Soft closure of a soft set (F,E) denoted by $S_{ft}Cl(F,E)$ is defined as the intersection of all soft closed super sets over X containing (F,E).

Definition 2.8. A $S_{ft}-$subset (F,E) of a $S_{ft}-Top-Space$ $(\tilde{X},\tilde{\tau},E)$ is called a $S_{ft}\alpha-open$ set if $(F,E)\subseteq S_{ft}Int\left[S_{ft}Cl\left(S_{ft}Int(F,E)\right)\right]$ and a $S_{ft}\alpha-closed$ set if $S_{ft}Cl\left[S_{ft}Int\left(S_{ft}Cl(F,E)\right)\right]\subseteq(F,E)$. The complement of a $S_{ft}\alpha-closed$ set is called $S_{ft}\alpha-open$ set.

Definition 2.9. A $S_{ft}-$subset (F,E) of a $S_{ft}-Top-Space$ $(\tilde{X},\tilde{\tau},E)$ is called a $S_{ft}\beta-open$ set if $(F,E)\subseteq S_{ft}Cl\left[S_{ft}Int\left(S_{ft}Cl(F,E)\right)\right]$ and $S_{ft}\beta-closed$ set if $S_{ft}Int\left[S_{ft}Cl\left(S_{ft}Int(F,E)\right)\right]\subseteq(F,E)$. The complement of a $S_{ft}\beta-closed$ set is called $S_{ft}\beta-open$ set.

Definition 2.10. A $S_{ft}-$subset (F,E) of a $S_{ft}-Top-Space$ $(\tilde{X},\tilde{\tau},E)$ is called a $S_{ft}g-closed$ set if $S_{ft}Cl(F,E)\subseteq(U,E)$ whenever $(F,E)\subseteq(U,E)$ and (U,E) is $S_{ft}-open$ in $(\tilde{X},\tilde{\tau},E)$. The complement of a $S_{ft}g-closed$ set is called a $S_{ft}g-open$ set.

Definition 2.11. A $S_{ft}-$subset (F,E) of a $S_{ft}-Top-Space$ $(\tilde{X},\tilde{\tau},E)$ is called a soft generalized β closed $(S_{ft}g\beta-closed)$ set if $S_{ft}\beta-Cl(F,E)\subseteq(U,E)$ whenever $(F,E)\subseteq(U,E)$ and (U,E) is $S_{ft}-open$ in $(\tilde{X},\tilde{\tau},E)$. The complement of a $S_{ft}g\beta-closed$ set is called a $S_{ft}g\beta-open$ set.

Definition 2.12. A $S_{ft}-$subset (F,E) of a $S_{ft}-Top-Space$ $(\tilde{X},\tilde{\tau},E)$ is called a $S_{ft}S_{emi}-open$ set if $(F,E)\subseteq S_{ft}Cl\left[S_{ft}Int(F,E)\right]$ and $S_{ft}S_{emi}-closed$ if $S_{ft}Int\left[S_{ft}Cl(F,E)\right]\subseteq(F,E)$. The complement of a $S_{ft}S_{emi}-closed$ set is called a $S_{ft}S_{emi}-open$ set.

Definition 2.13. A $S_{ft}-$subset (F,E) of a $S_{ft}-Top-Space$ $(\tilde{X},\tilde{\tau},E)$ is called a $S_{ft}g*-closed$ set if $S_{ft}Cl(F,E)\subseteq(U,E)$ whenever $(F,E)\subseteq(U,E)$ and (U,E) is $S_{ft}g-open$ set in X. The complement of a $S_{ft}g*-closed$ set is called a $S_{ft}g*-open$ set.

Definition 2.14. A $S_{ft}-$subset (F,E) of a $S_{ft}-Top-Space$ $(\tilde{X},\tilde{\tau},E)$ is called a soft generalized star β closed $(\text{briefly } S_{ft}g*\beta-closed)$ set if $S_{ft}\beta Cl(F,E)\subseteq(U,E)$, whenever $(F,E)\subseteq(U,E)$ and (U,E) is $S_{ft}g*-open$ in $(\tilde{X},\tilde{\tau},E)$. The complement of a $S_{ft}g*\beta-closed$ set is called a $S_{ft}g*\beta-open$ set. The family of all $S_{ft}g*\beta$-open (respectively $S_{ft}g*\beta$-closed) in $(\tilde{X},\tilde{\tau},E)$ is denoted by $S_{ft}g*\beta\text{-}O(\tilde{X},\tilde{\tau},E)=S_{ft}g*\beta\text{-}O(\tilde{X})$ (respectively $S_{ft}g*\beta\text{-}C(\tilde{X},\tilde{\tau},E)=S_{ft}g*\beta\text{-}C(\tilde{X})$).

Definition 2.15. Let $(\tilde{X},\tilde{\tau},E)$ be a S_{ft}-Top-Space over X and (F,A) be a soft set over X. Then

(i) $S_{ft}g*\beta$-interior of a soft set (F,A) denoted by $S_{ft}g*\beta\text{-}Int(F,A)$ is defined as the union of all soft $S_{ft}g*\beta$-open sets over X contained in (F,A).

(ii) $S_{ft}g*\beta$-closure of a soft set (F,A) denoted by $S_{ft}g*\beta\text{-}Cl(F,A)$ is defined as the intersection of all $S_{ft}g*\beta$-closed sets over X containing (F,A).

Theorem 2.16. (i) Every S_{ft}-closed set in a soft topological space is $S_{ft}g*\beta$-closed set.

(ii) Every S_{ft}-open set in a S_{ft}-Top-Space is $S_{ft}g*\beta$-open set.

Theorem 2.16. Let (F,A) and (G,B) be two S_{ft}-subsets of a S_{ft}-Top-Space $(\tilde{X},\tilde{\tau},E)$ Then the following statements are true.

(i) (F,A) is $S_{ft}g*\beta$-open if and only if $S_{ft}g*\beta\text{-}Int(F,A)=(F,A)$.

(ii) $S_{ft}g*\beta\text{-}Int(F,A)$ is $S_{ft}g*\beta$-open.

(iii) (F,A) is $S_{ft}g*\beta$-closed if and only if $S_{ft}g*\beta\text{-}Cl(F,A)=(F,A)$.

(iv) $S_{ft}g*\beta\text{-}Cl(F,A)$ is $S_{ft}g*\beta$-closed.

(v) $S_{ft}g*\beta\text{-}Cl[(X,E)-(F,A)]=(X,E)-[S_{ft}g*\beta\text{-}Int(F,A)]$.

(vi) $S_{ft}g*\beta\text{-}Int[(X,E)-(F,A)]=(X,E)-[S_{ft}g*\beta\text{-}Cl(F,A)]$.

(vii) If (F,A) is $S_{ft}g*\beta$-open in $(\tilde{X},\tilde{\tau},E)$ and (G,B) is S_{ft}-open in $(\tilde{X},\tilde{\tau},E)$ then $(F,A)\cap(G,B)$ is $S_{ft}g*\beta$-open in $(\tilde{X},\tilde{\tau},E)$.

$(viii)$ A point $x_\alpha\in S_{ft}g*\beta\text{-}Cl(F,A)$ if and only if every $S_{ft}g*\beta$-open set in $(\tilde{X},\tilde{\tau},E)$ containing x intersects (F,A).

(ix) Finite intersection of $S_{ft}g*\beta$-closed sets in $(\tilde{X},\tilde{\tau},E)$ is $S_{ft}g*\beta$-closed in $(\tilde{X},\tilde{\tau},E)$.

(x) Finite union of $S_{ft}g*\beta$-open sets in $(\tilde{X},\tilde{\tau},E)$ is $S_{ft}g*\beta$-open in $(X,\tilde{\tau},E)$.

3. $S_{ft}g*\beta$-R_0 Space and $S_{ft}g*\beta$-R_1 Space

In this section we define two types of spaces called $S_{ft}g*\beta\text{-}R_i$ spaces for $i=0,1$.

Definition 3.1. A S_{ft}-Top-Space $(\tilde{X},\tilde{\tau},E)$ is called $S_{ft}g*\beta\text{-}R_0$ if for every $S_{ft}g*\beta$-open set (F,E), $S_{ft}g*\beta\text{-}Cl(\{x_\alpha\})\subseteq(F,E)$ for every $x_\alpha\in(F,E)$.

Definition 3.2. Let $(\tilde{X},\tilde{\tau},E)$ be a S_{ft}-Top-Space and $(F,E)\subseteq\tilde{X}$, Then $S_{ft}g*\beta$-Kernel of (F,E) is defined to be the intersection of all $S_{ft}g*\beta$-open sets containing (F,E) and denoted by $S_{ft}g*\beta\text{-}Ker(F,E)$ that is $S_{ft}g*\beta\text{-}Ker(F,E)=\cap\{(G,E)\in S_{ft}g*\beta\text{-}O(X):(F,E)\subseteq(G,E)\}$.

Lemma 3.3. Let $\left(\tilde{X},\tilde{\tau},E\right)$ be a S_{ft}-Top-Space and $x_\alpha \in \tilde{X}$. Then $y_\beta \in S_{ft}g*\beta\text{-}Ker\left(\left\{x_\alpha\right\}\right)$ if and only if $x_\alpha \in S_{ft}g*\beta\text{-}Cl\left(\left\{y_\beta\right\}\right)$.

Proof. Suppose that $x_\alpha \notin S_{ft}g*\beta\text{-}Ker\left(F,E\right)$. Then there exists a $S_{ft}g*\beta$-open set $\left(F,E\right)$ containing x_α such that $y_\beta \notin \left(F,E\right)$. Therefore, we have $x_\alpha \notin S_{ft}g*\beta\text{-}Cl\left(\left\{y_\beta\right\}\right)$. The proof of converse can be done similarly.

Theorem 3.4. Let $\left(\tilde{X},\tilde{\tau},E\right)$ be a S_{ft}-Top-Space. Then the following statements are equivalent:

(1). $\left(X,\tau,E\right)$ is $S_{ft}g*\beta\text{-}R_{\mathbf{0}}$.

(2). For any $\left(K,E\right) \in S_{ft}g*\beta\text{-}C\left(X\right)$ and $x_\alpha \notin \left(K,E\right)$ there exists $\left(F,E\right) \in S_{ft}g*\beta\text{-}O\left(X\right)$ such that $\left(K,E\right) \subseteq \left(F,E\right)$ and $x_\alpha \notin \left(F,E\right)$.

(3). For any $\left(K,E\right) \in S_{ft}g*\beta\text{-}C\left(X\right)$ and $x_\alpha \in \left(K,E\right)$ implies that $\left(K,E\right) \cap S_{ft}g*\beta\text{-}Cl\left(\left\{x_\alpha\right\}\right) = \tilde{\phi}$.

(4). For any two distinct soft points $x_\alpha, y_\beta \in \tilde{X}$ either $S_{ft}g*\beta\text{-}Cl\left(\left\{x_\alpha\right\}\right) = S_{ft}g*\beta\text{-}Cl\left(\left\{y_\beta\right\}\right) = \tilde{\phi}$ or $\left[S_{ft}g*\beta\text{-}Cl\left(\left\{x_\alpha\right\}\right)\right] \cap \left[S_{ft}g*\beta\text{-}Cl\left(\left\{y_\beta\right\}\right)\right] = \tilde{\phi}$.

Proof $(1)\Rightarrow(2)$: Let $\left(K,E\right) \in S_{ft}g*\beta\text{-}C\left(\tilde{X}\right)$ and $x_\alpha \notin \left(K,E\right)$. Then by (1) $S_{ft}g*\beta\text{-}Cl\left(\left\{x_\alpha\right\}\right) \subseteq \tilde{X} - \left(K,E\right)$. Let $\left(F,E\right) = \tilde{X} - \left(K,E\right)$. Then $\left(F,E\right) \in S_{ft}g*\beta\text{-}O\left(\tilde{X}\right)$, $\left(K,E\right) \subseteq \left(F,E\right)$ and $x_\alpha \notin \left(F,E\right)$.

$(2)\Rightarrow(3)$: Let $\left(K,E\right) \in S_{ft}g*\beta\text{-}C\left(\tilde{X}\right)$ and $x_\alpha \notin \left(K,E\right)$. Then there exists $\left(F,E\right) \in S_{ft}g*\beta\text{-}O\left(\tilde{X}\right)$ such that $\left(K,E\right) \subseteq \left(F,E\right)$ and $x_\alpha \notin \left(F,E\right)$. Since $\left(K,E\right) \subseteq \left(F,E\right)$, so by (2) $\left(F,E\right) \cap S_{ft}g*\beta\text{-}Cl\left(\left\{x_\alpha\right\}\right) = \tilde{\phi}$. This implies that $\left(K,E\right) \cap S_{ft}g*\beta\text{-}Cl\left(\left\{x_\alpha\right\}\right) = \tilde{\phi}$.

$(3)\Rightarrow(4)$: Let x_α and y_β be two distinct soft points of $\tilde{X}$. Suppose that $S_{ft}g*\beta\text{-}Cl\left(\left\{x_\alpha\right\}\right) \neq S_{ft}g*\beta\text{-}Cl\left(\left\{y_\beta\right\}\right)$. Then there exists a soft point z_γ such that $z_\gamma \in S_{ft}g*\beta\text{-}Cl\left(\left\{x_\alpha\right\}\right)$ and $z_\gamma \notin S_{ft}g*\beta\text{-}Cl\left(\left\{y_\beta\right\}\right)$ or $z_\gamma \in S_{ft}g*\beta\text{-}Cl\left(\left\{y_\beta\right\}\right)$ such that $z_\gamma \notin S_{ft}g*\beta\text{-}Cl\left(\left\{x_\alpha\right\}\right)$ and there exists $\left(F,E\right) \in S_{ft}g*\beta\text{-}O\left(\tilde{X}\right)$ such that $y_\beta \notin \left(F,E\right)$ and $z_\gamma \in \left(F,E\right)$, hence $x_\alpha \in \left(F,E\right)$, therefore, we have $x_\gamma \notin S_{ft}g*\beta\text{-}Cl\left(\left\{y_\beta\right\}\right)$ by (3) we obtain $\left[S_{ft}g*\beta\text{-}Cl\left(\left\{x_\alpha\right\}\right)\right] \cap \left[S_{ft}g*\beta\text{-}Cl\left(\left\{y_\beta\right\}\right)\right] = \tilde{\phi}$.

$(4)\Rightarrow(1)$: Let $\left(F,E\right) \in S_{ft}g*\beta\text{-}O\left(\tilde{X}\right)$ and $x_\alpha \in \left(F,E\right)$, for each $y_\beta \notin \left(F,E\right)$. Then $x_\alpha \neq y_\beta$ and $x_\alpha \notin S_{ft}g*\beta\text{-}Cl\left(\left\{y_\beta\right\}\right)$, this shows that $S_{ft}g*\beta\text{-}Cl\left(\left\{x_\alpha\right\}\right) \neq S_{ft}g*\beta\text{-}Cl\left(\left\{y_\beta\right\}\right)$, then by (4) $\left[S_{ft}g*\beta\text{-}Cl\left(\left\{x_\alpha\right\}\right)\right] \cap \left[S_{ft}g*\beta\text{-}Cl\left(\left\{y_\beta\right\}\right)\right] = \tilde{\phi}$, for each $y_\beta \in \tilde{X} - \left(F,E\right)$. On the other hand, since $\left(F,E\right) \in S_{ft}g*\beta\text{-}O\left(\tilde{X}\right)$ and $y_\beta \in \tilde{X} - \left(F,E\right)$, we have $S_{ft}g*\beta\text{-}Cl\left(\left\{y_\beta\right\}\right) \subseteq \tilde{X} - \left(F,E\right)$. Hence $\tilde{X} - \left(F,E\right) = \bigcup\left\{S_{ft}g*\beta\text{-}Cl\left(\left\{y_\beta\right\}\right) : y_\beta \in \tilde{X} - \left(F,E\right)\right\}$. Therefore, we obtain that $\left[\tilde{X} - \left(F,E\right)\right] \cap S_{ft}g*\beta\text{-}Cl\left(\left\{x_\alpha\right\}\right) = \tilde{\phi}$ and $S_{ft}g*\beta\text{-}Cl\left(\left\{x_\alpha\right\}\right) \subseteq \left(F,E\right)$. This shows that $\left(\tilde{X},\tilde{\tau},E\right)$ is $S_{ft}g*\beta\text{-}R_{\mathbf{0}}$.

Theorem 3.5. A S_{ft}-Top-Space $(\tilde{X},\tilde{\tau},E)$ is a $S_{ft}g^*\beta\text{-}R_0$ space if and only if for any $x_\alpha, y_\beta \in \tilde{X}$, $S_{ft}g^*\beta\text{-}Cl(\{x_\alpha\}) \neq S_{ft}g^*\beta\text{-}Cl(\{y_\beta\}) \Rightarrow [S_{ft}g^*\beta\text{-}Cl(\{x_\alpha\})] \cap [S_{ft}g^*\beta\text{-}Cl(\{y_\beta\})] = \tilde{\phi}$.

Proof. This is an immediate consequence of Theorem 3.4.

Theorem 3.6. Let x_α and y_β be any distinct soft points in a S_{ft}-Top-Space $(\tilde{X},\tilde{\tau},E)$. Then $S_{ft}g^*\beta\text{-}Ker(\{x_\alpha\}) \neq S_{ft}g^*\beta\text{-}Ker(\{y_\beta\})$ if and only if $S_{ft}g^*\beta\text{-}Cl(\{x_\alpha\}) \neq S_{ft}g^*\beta\text{-}Cl(\{y_\beta\})$.

Proof. <u>Necessity</u>. Suppose that $S_{ft}g^*\beta\text{-}Ker(\{x_\alpha\}) \neq S_{ft}g^*\beta\text{-}Ker(\{y_\beta\})$. Then there exists a soft point $z_\gamma \in X$ such that $z_\gamma \in S_{ft}g^*\beta\text{-}Ker(\{x_\alpha\})$ and $z_\gamma \notin S_{ft}g^*\beta\text{-}Ker(\{y_\beta\})$. Since $z_\gamma \in S_{ft}g^*\beta\text{-}Ker(\{x_\alpha\})$. So $\{x_\alpha\} \cap [S_{ft}g^*\beta\text{-}Cl(\{z_\gamma\})] \neq \tilde{\phi}$. This implies that $x_\alpha \in S_{ft}g^*\beta\text{-}Cl(\{z_\gamma\})$ and since $z_\gamma \notin S_{ft}g^*\beta\text{-}Ker(\{y_\beta\})$. We have $\{y_\beta\} \cap [S_{ft}g^*\beta\text{-}Cl(\{z_\gamma\})] = \tilde{\phi}$. Since $x_\alpha \in S_{ft}g^*\beta\text{-}Cl(\{z_\gamma\})$, so $S_{ft}g^*\beta\text{-}Cl(\{x_\alpha\}) \subseteq S_{ft}g^*\beta\text{-}Cl(\{z_\gamma\})$ and hence $\{y_\beta\} \cap S_{ft}g^*\beta\text{-}Cl(\{x_\alpha\}) = \tilde{\phi}$. Therefore, $S_{ft}g^*\beta\text{-}Cl(\{x_\alpha\}) \neq S_{ft}g^*\beta\text{-}Cl(\{y_\beta\})$.

<u>Sufficiency.</u> Suppose that $S_{ft}g^*\beta\text{-}Cl(\{x_\alpha\}) \neq S_{ft}g^*\beta\text{-}Cl(\{y_\beta\})$. Then there exists a soft point z_γ in $\tilde{X}$ such that $z_\gamma \in S_{ft}g^*\beta\text{-}Cl(\{x_\gamma\})$ and $z_\gamma \notin S_{ft}g^*\beta\text{-}Cl(\{y_\beta\})$. Thus there exists a $S_{ft}g^*\beta$*-open* set (F,E) containing z_γ (and hence x_α) but not y_β, that is $y_\beta \notin S_{ft}g^*\beta\text{-}Ker(\{x_\alpha\})$. Therefore, $S_{ft}g^*\beta\text{-}Ker(\{x_\alpha\}) \neq S_{ft}g^*\beta\text{-}Ker(\{y_\beta\})$.

Theorem 3.7. A S_{ft}-Top-Space $(\tilde{X},\tilde{\tau},E)$ is a $S_{ft}g^*\beta\text{-}R_0$ space if and only if for any two distinct soft points $x_\alpha, y_\beta \in \tilde{X}$, $S_{ft}g^*\beta\text{-}Ker(\{x_\alpha\}) \neq S_{ft}g^*\beta\text{-}Ker(\{y_\beta\})$ implies $[S_{ft}g^*\beta\text{-}Ker(\{x_\alpha\})] \cap [S_{ft}g^*\beta\text{-}Ker(\{y_\beta\})] = \tilde{\phi}$.

Proof. Necessity. Suppose that $(\tilde{X},\tilde{\tau},E)$ is $S_{ft}g^*\beta\text{-}R_0$. Then by Theorem 3.6, for any distinct soft points x_α and y_β in $\tilde{X}$, if $S_{ft}g^*\beta\text{-}Ker(\{x_\alpha\}) \neq S_{ft}g^*\beta\text{-}Ker(\{y_\beta\})$, then $S_{ft}g^*\beta\text{-}Cl(\{x_\alpha\}) \neq S_{ft}g^*\beta\text{-}Cl(\{y_\beta\})$. Assume that $S_{ft}g^*\beta\text{-}Ker(\{x_\alpha\}) \cap S_{ft}g^*\beta\text{-}Ker(\{y_\beta\})$. Since $x_\alpha \in S_{ft}g^*\beta\text{-}Ker(\{x_\alpha\})$, and by Theorem 3.4 it follows that $x_\alpha \in S_{ft}g^*\beta\text{-}Cl(\{z_\alpha\})$. Since $x_\alpha \in S_{ft}g^*\beta\text{-}Cl(\{x_\alpha\})$, by Theorem 3.4 it follows that $S_{ft}g^*\beta\text{-}Cl(\{x_\alpha\}) = S_{ft}g^*\beta\text{-}Cl(\{z_\gamma\})$. Similarly we have $S_{ft}g^*\beta\text{-}Cl(\{x_\alpha\}) = S_{ft}g^*\beta\text{-}Cl(\{z_\gamma\}) = S_{ft}g^*\beta\text{-}Cl(\{y_\beta\})$, which is contradiction. Thus, $[S_{ft}g^*\beta\text{-}Ker(\{x_\alpha\})] \cap [S_{ft}g^*\beta\text{-}Ker(\{y_\beta\})] = \tilde{\phi}$.

Sufficiency. Let $(\tilde{X},\tilde{\tau},E)$ be a S_{ft}-Top-Space such that for any distinct soft points x_α and y_β in $\tilde{X}$, $[S_{ft}g^*\beta\text{-}Ker(\{x_\alpha\})] \neq [S_{ft}g^*\beta\text{-}Ker(\{y_\beta\})]$ implies that $[S_{ft}g^*\beta\text{-}Ker(\{x_\alpha\})] \cap [S_{ft}g^*\beta\text{-}Ker(\{y_\beta\})] = \tilde{\phi}$. If $[S_{ft}g^*\beta\text{-}Cl(\{x_\alpha\})] \neq [S_{ft}g^*\beta\text{-}Cl(\{y_\beta\})]$, hence by Theorem 3.6, $\left[S_{ft}g*\beta\text{-}Ker(\{x_\alpha\})\right]\neq\left[SS_{ft}g*\beta\text{-}Ker(\{y_\beta\})\right]$. Therefore, $\left[S_{ft}g*\beta\text{-}Ker(\{x_\alpha\})\right]\cap\left[S_{ft}g*\beta\text{-}Ker(\{y_\beta\})\right]=\tilde{\phi}$. Which implies that $\left[S_{ft}g*\beta\text{-}Cl(\{x_\alpha\})\right]\cap\left[S_{ft}g*\beta\text{-}Cl(\{y_\beta\})\right]=\tilde{\phi}$, because $z_\gamma\in S_{ft}g*\beta\text{-}Cl(\{x_\alpha\})$ implies that $x_\alpha\in S_{ft}g*\beta\text{-}Ker(\{z_\gamma\})$. Therefore, $\left[S_{ft}g*\beta\text{-}Ker(\{x_\alpha\})\right]\cap\left[S_{ft}g*\beta\text{-}Ker(\{y_\beta\})\right]\neq\tilde{\phi}$. By hypothesis we have, $\left[S_{ft}g*\beta\text{-}Ker(\{x_\alpha\})\right]=\left[S_{ft}g*\beta\text{-}Ker(\{z_\gamma\})\right]$, then $z_\gamma\in\left[S_{ft}g*\beta\text{-}Cl(\{x_\alpha\})\right]\cap\left[S_{ft}g*\beta\text{-}Cl(\{y_\beta\})\right]$ implies that $S_{ft}g*\beta\text{-}Ker(\{x_\alpha\})=S_{ft}g*\beta\text{-}Ker(\{z_\gamma\})=S_{ft}g*\beta\text{-}Ker(\{y_\beta\})$, this is a contradiction. Therefore, $\left[S_{ft}g*\beta\text{-}Cl(\{x_\alpha\})\right]\cap\left[S_{ft}g*\beta\text{-}Cl(\{y_\beta\})\right]=\tilde{\phi}$. Hence by Theorem 3.4, (X,τ,E) is $S_{ft}g*\beta\text{-}R_0$.

Theorem 3.8. Let $(\tilde{X},\tilde{\tau},E)$ be a S_{ft}-Top-Space. Then the following statements are equivalent:

(1). $(\tilde{X},\tilde{\tau},E)$ is $S_{ft}g*\beta\text{-}R_0$.

(2). For any non-empty soft sets (F,E) and $(G,E)\in S_{ft}g*\beta\text{-}O(\tilde{X})$ such that $(F,E)\cap(G,E)\neq\tilde{\phi}$, there exists $(K,E)\in S_{ft}g*\beta\text{-}C(\tilde{X})$ such that $(K,E)\cap(F,E)\neq\tilde{\phi}$ and $(K,E)\subseteq(G,E)$.

(3). For any $(G,E)\in S_{ft}g*\beta\text{-}O(\tilde{X})$, $(G,E)=\bigcup\{(K,E)\in S_{ft}g*\beta\text{-}C(\tilde{X}):(K,E)\subseteq(G,E)\}$

(4). For any $(K,E)\in S_{ft}g*\beta\text{-}C(\tilde{X})$, $(K,E)=\bigcap\{(G,E)\in S_{ft}g*\beta\text{-}O(\tilde{X}):(K,E)\subseteq(G,E)\}$

(5). For any $x_\alpha\in\tilde{X}$, $S_{ft}g*\beta\text{-}Cl(\{x_\alpha\})\subseteq S_{ft}g*\beta\text{-}Ker(\{x_\alpha\})$.

Proof. $(1)\Rightarrow(2)$: Let (F,E) be a non-empty soft subset of $\tilde{X}$ and $(G,E)\in S_{ft}g*\beta\text{-}O(\tilde{X})$ such that $(F,E)\cap(G,E)\neq\tilde{\phi}$. Let $x_\alpha\in(F,E)\cap(G,E)$. Since $x_\alpha\in(G,E)\in S_{ft}g*\beta\text{-}O(\tilde{X})$, so by (1), we have $S_{ft}g*\beta\text{-}Cl(\{x_\alpha\})\subseteq(G,E)$. set $(K,E)=S_{ft}g*\beta\text{-}Cl(\{x_\alpha\})$ then $(K,E)\in SS_{ft}g*\beta\text{-}C(\tilde{X})$ such that $(K,E)\subseteq(G,E)$ and $(F,E)\cap(K,E)\neq\tilde{\phi}$.

$(2)\Rightarrow(3)$: Let $(G,E)\in S_{ft}g*\beta\text{-}O(\tilde{X})$. Then $\bigcup\{(K,E)\in S_{ft}g*\beta\text{-}C(X):(K,E)\subseteq(G,E)\}\subseteq(G,E)$. Now let x_α be any soft point of (G,E). By (2) there exists $(K,E)\in S_{ft}g*\beta\text{-}C(\tilde{X})$, such that $x_\alpha\in(K,E)$ and $(K,E)\subseteq(G,E)$. So $x_\alpha\in(K,E)\subseteq\bigcup\{(K,E)\in S_{ft}g*\beta\text{-}C(\tilde{X}):(K,E)\subseteq(G,E)\}$. Thus, $(G,E)=\bigcup\{(K,E)\in S_{ft}g*\beta\text{-}C(\tilde{X}):(K,E)\subseteq(G,E)\}$.

$(3)\Rightarrow(4)$: Obvious.

$(4)\Rightarrow(5)$: Let x_α be any soft point of $\tilde{X}$ and $y_\beta\notin S_{ft}g*\beta\text{-}Ker(\{x_\alpha\})$. So there exists $(H,E)\in S_{ft}g*\beta\text{-}O(\tilde{X})$ such that $x_\alpha\in(H,E)$ and $y_\beta\notin(H,E)$. Hence $\left[S_{ft}g*\beta\text{-}Cl(\{y_\beta\})\right]\cap(H,E)=\tilde{\phi}$. By (4), we have $\left[\bigcap\{\ (G,E)\in S_{ft}g*\beta\text{-}O(\tilde{X}):\right.$

$S_{ft}g*\beta-Cl(\{y_\beta\})\subseteq(G,E)\}\big]\cap(H,E)=\tilde{\phi}$, Where $(G,E)\in S_{ft}g*\beta-O(\tilde{X})$ such that $x_\alpha\notin(G,E)$ and $S_{ft}g*\beta-Cl(\{y_\beta\})\subseteq(G,E)$. Therefore $S_{ft}g*\beta-Cl(\{x_\alpha\})\cap(G,E)=\tilde{\phi}$ and hence $y_\beta\notin S_{ft}g*\beta-Cl(\{x_\alpha\})$. Consequently, we obtain $S_{ft}g*\beta-Cl(\{x_\alpha\})\subseteq S_{ft}g*\beta-Ker(\{x_\alpha\})$.

$(5)\Rightarrow(1)$: Let $(G,E)\in S_{ft}g*\beta-O(\tilde{X})$ and $x_\alpha\in(G,E)$, let $y_\beta\in S_{ft}g*\beta-Ker(\{x_\alpha\})$. Then $x_\alpha\in S_{ft}g*\beta-Cl(\{y_\beta\})$ and $y_\beta\in(G,E)$. This implies that $S_{ft}g*\beta-Ker(\{x_\alpha\})\subseteq(G,E)$. Therefore, we get $S_{ft}g*\beta-Cl(\{x_\alpha\})\subseteq S_{ft}g*\beta-Ker(\{x_\alpha\})\subseteq(G,E)$. This shows that $(\tilde{X},\tilde{\tau},E)$ is $S_{ft}g*\beta-R_{\mathbf{0}}$.

Theorem 3.9. Let $(\tilde{X},\tilde{\tau},E)$ be a $S_{ft}-Top-Space$. Then the following statements are equivalent:

(1). $(\tilde{X},\tilde{\tau},E)$ is a $S_{ft}g*\beta-R_{\mathbf{0}}$ space.

(2). $S_{ft}g*\beta-Cl(\{x_\alpha\})=S_{ft}g*\beta-Ker(\{x_\alpha\})$, for all $x_\alpha\in\tilde{X}$.

Proof $(1)\Rightarrow(2)$: Suppose that $(\tilde{X},\tilde{\tau},E)$ is a $S_{ft}g*\beta-R_{\mathbf{0}}$ space. By Theorem 3.8 $S_{ft}g*\beta-Cl(\{x_\alpha\})\subseteq S_{ft}g*\beta-Ker(\{x_\alpha\})$, for all $x_\alpha\in\tilde{X}$. Let $y_\beta\in S_{ft}g*\beta-Ker(\{x_\alpha\})$. Then $x_\alpha\in S_{ft}g*\beta-Cl(\{y_\beta\})$, and by Theorem 3.4 $S_{ft}g*\beta-Cl(\{x_\alpha\})=S_{ft}g*\beta-Cl(\{y_\beta\})$. Therefore $y_\beta\in S_{ft}g*\beta-Cl(\{x_\alpha\})$ and hence $S_{ft}g*\beta-Ker(\{x_\alpha\})\subseteq S_{ft}g*\beta-Cl(\{x_\alpha\})$, This shows that $S_{ft}g*\beta-Cl(\{x_\alpha\})=S_{ft}g*\beta-Ker(\{x_\alpha\})$, for all $x_\alpha\in\tilde{X}$.

$(2)\Rightarrow(1)$: Follows from Theorem 3.8.

Theorem 3.10. Let $(\tilde{X},\tilde{\tau},E)$ be a $S_{ft}-Top-Space$. Then the following statements are equivalent:

(1). $(\tilde{X},\tilde{\tau},E)$ is a $S_{ft}g*\beta-R_{\mathbf{0}}$ space.

(2). $x_\alpha\in S_{ft}g*\beta-Cl(\{y_\beta\})$ if and only if $y_\beta\in S_{ft}g*\beta-Cl(\{x_\alpha\})$ for any two distinct soft points $x_\alpha,y_\beta\in\tilde{X}$.

Proof. $(1)\Rightarrow(2)$: Assume that $(\tilde{X},\tilde{\tau},E)$ is a $S_{ft}g*\beta-R_{\mathbf{0}}$ space. Let $x_\alpha\in S_{ft}g*\beta-Cl(\{y_\beta\})$ and (H,E) be any $S_{ft}g*\beta-open$ set containing y_β. By (1) $S_{ft}g*\beta-Cl(\{y_\beta\})\subseteq(H,E)$, hence $x_\alpha\in(H,E)$. Therefore, every $S_{ft}g*\beta-open$ set containing y_β contains x_α, so $y_\beta\in S_{ft}g*\beta-Cl(\{x_\alpha\})$.

$(2)\Rightarrow(1)$: Let (G,E) be any $S_{ft}g*\beta-open$ set containing x_α, if $y_\beta\notin(G,E)$, then $x_\alpha\notin S_{ft}g*\beta-Cl(\{y_\beta\})$ and by (2), we have $y_\beta\notin S_{ft}g*\beta-Cl(\{x_\alpha\})$. This implies that $S_{ft}g*\beta-Cl(\{x_\alpha\})\subseteq(G,E)$, hence $(\tilde{X},\tilde{\tau},E)$ is a $S_{ft}g*\beta-R_{\mathbf{0}}$ space.

Theorem 3.11. A $S_{ft}-Top-Space$ $(\tilde{X},\tilde{\tau},E)$ is a $S_{ft}g*\beta-R_{\mathbf{0}}$ space if and only if $S_{ft}g*\beta-Ker(\{x_\alpha\})\neq S_{ft}g*\beta-Ker(\{y_\beta\})$, for all $x_\alpha\neq y_\beta$.

Proof. Follows from Theorem 3.9 and Theorem 3.10.

Lemma 3.12. Let $(\tilde{X},\tilde{\tau},E)$ be a $S_{ft}-\text{Top}-\text{Space}$ and $(F,E)\subseteq\tilde{X}$.
Then $S_{ft}g*\beta-\text{Ker}(F,E)=\{x_\alpha\in\tilde{X}:S_{ft}g*\beta-\text{Cl}(\{x_\alpha\})\cap(F,E)\neq\tilde{\phi}\}$.

Proof. Let $x_\alpha\in S_{ft}g*\beta-\text{Ker}(F,E)$ and suppose $[S_{ft}g*\beta-\text{Cl}(\{x_\alpha\})]\cap(F,E)=\tilde{\phi}$. Hence $x_\alpha\notin\tilde{X}-[S_{ft}g*\beta-\text{Cl}(\{x_\alpha\})]$ which is a $S_{ft}g*\beta$-open set containing (F,E) and this is impossible, since $x_\alpha\in S_{ft}g*\beta-\text{Ker}(F,E)$, hence $S_{ft}g*\beta-\text{Cl}(\{x_\alpha\})\cap(F,E)\neq\tilde{\phi}$. Again let $x_\alpha\in\tilde{X}$ such that $[S_{ft}g*\beta-\text{Cl}(\{x_\alpha\})]\cap(F,E)\neq\tilde{\phi}$ and suppose that $x_\alpha\notin S_{ft}g*\beta-\text{Ker}(F,E)$. Then there exists a $S_{ft}g*\beta$*-open* set (G,E), such that $x_\alpha\notin(G,E)$ and $(F,E)\subseteq(G,E)$. Let $y_\beta\in[S_{ft}g*\beta-\text{Cl}(\{x_\alpha\})]\cap(F,E)$. Hence (G,E) is a $S_{ft}g*\beta$*-open* neighborhood of y_β which does not contain x_α. This contradicts that $x_\alpha\in S_{ft}g*\beta-\text{Ker}(F,E)$ so the claim.

Theorem 3.13. Let $(\tilde{X},\tilde{\tau},E)$ be a $S_{ft}-\text{Top}-\text{Space}$. Then the following statements are equivalent:

(1). $(\tilde{X},\tilde{\tau},E)$ is a $S_{ft}g*\beta-R_0$ space.

(2). If (K,E) is $S_{ft}g*\beta$*-closed*, then $(K,E)=S_{ft}g*\beta-\text{Ker}(K,E)$.

(3). If (K,E) is $S_{ft}g*\beta$*-closed*, and $x_\alpha\in(K,E)$, then $S_{ft}g*\beta-\text{Ker}(\{x_\alpha\})\subseteq(K,E)$.

(4). If $x_\alpha\in\tilde{X}$, then $S_{ft}g*\beta-\text{Ker}(\{x_\alpha\})\subseteq S_{ft}g*\beta-\text{Cl}(\{x_\alpha\})$.

Proof. $(1)\Rightarrow(2)$. Let (K,E) be a $S_{ft}g*\beta$-closed set and $x_\alpha\notin(K,E)$. Thus $\tilde{X}-(K,E)$ is $S_{ft}g*\beta$-open set containing x_α. Since $\tilde{X}$ is a $S_{ft}g*\beta-R_0$ space, so $S_{ft}g*\beta-\text{Cl}(\{x_\alpha\})\subseteq\tilde{X}-(K,E)$, thus $[S_{ft}g*\beta-\text{Cl}(\{x_\alpha\})]\cap(K,E)=\tilde{\phi}$, by Lemma 3.12 $x_\alpha\notin S_{ft}g*\beta-\text{Ker}(K,E)$. Therefore $S_{ft}g*\beta-\text{Ker}(\{x_\alpha\})\subseteq(K,E)$, hence $(K,E)=S_{ft}g*\beta-\text{Ker}((K,E))$.

$(2)\Rightarrow(3)$. In general, $(F,E)\subseteq(G,E)$ implies that $S_{ft}g*\beta-\text{Ker}((F,E))\subseteq S_{ft}g*\beta-\text{Ker}((G,E))$. Therefore, it follows from (2) that $S_{ft}g*\beta-\text{Ker}(\{x_\alpha\})\subseteq S_{ft}g*\beta-\text{Ker}((K,E))=(K,E)$.

$(3)\Rightarrow(4)$. Since $x_\alpha\in S_{ft}g*\beta-\text{Cl}(\{x_\alpha\})$ and $S_{ft}g*\beta-\text{Cl}(\{x_\alpha\})$ is $S_{ft}g*\beta$-closed, so by (3), we obtain $S_{ft}g*\beta-\text{Ker}(\{x_\alpha\})\subseteq S_{ft}g*\beta-\text{Cl}(\{x_\alpha\})$.

$(4)\Rightarrow(1)$. Let $x_\alpha\in S_{ft}g*\beta-\text{Cl}(\{y_\beta\})$, then by Theorem 3.3 $y_\beta\in S_{ft}g*\beta-\text{Ker}(\{x_\alpha\})$. $x_\alpha\in S_{ft}g*\beta-\text{Cl}(\{x_\alpha\})$ and $S_{ft}g*\beta-\text{Cl}(\{x_\alpha\})$ is $S_{ft}g*\beta$-closed. So by (4) we obtain $y_\beta\in S_{ft}g*\beta-\text{Ker}(\{x_\alpha\})\subseteq S_{ft}g*\beta-\text{Cl}(\{x_\alpha\})$. Therefore $x_\alpha\in S_{ft}g*\beta-\text{Cl}(\{y_\beta\})$ implies that $y_\beta\in S_{ft}g*\beta-\text{Cl}(\{x_\alpha\})$, on the same way, if $y_\beta\in S_{ft}g*\beta-\text{Cl}(\{x_\alpha\})$, we get $x_\alpha\in S_{ft}g*\beta-\text{Cl}(\{y_\beta\})$, so by Theorem 3.10 $(\tilde{X},\tilde{\tau},E)$ is a $S_{ft}g*\beta-R_0$ space.

Definition 3.14. A soft filter base $\Im$ is called $S_{ft}g*\beta$*-convergent* to a point x_α in $\tilde{X}$, if for any $S_{ft}g*\beta$*-open* set (H,E) of $\tilde{X}$ containing x_α there exists (G,E) in $\Im$ such that $(G,E)\subseteq(H,E)$.

Lemma 3.15. Let $(\tilde{X},\tilde{\tau},E)$ be a S_{ft}-Top-Space and let x_α and y_β be any two soft points in $\tilde{X}$ such that every net $\{x_{\alpha_i} : i \in \Lambda\}$ in $\tilde{X}$ $S_{ft}g^*\beta$*-converging* to y_β $S_{ft}g^*\beta$*-converges* to x_α. Then $x_\alpha \in S_{ft}g^*\beta\text{-}Cl(\{y_\beta\})$.

Proof. Suppose that $x_\alpha = y_\beta$ for each $i \in \Lambda$. Then $\{x_{\alpha_i} : i \in \Lambda\}$ is a net in $S_{ft}g^*\beta\text{-}Cl(\{y_\beta\})$. By the fact that $\{x_{\alpha_i} : i \in \Lambda\}$ $S_{ft}g^*\beta$*-converges* to y_β, then $\{x_{\alpha_i} : i \in \Lambda\}$ $S_{ft}g^*\beta$*-converges* to x_α and this means that $x_\alpha \in S_{ft}g^*\beta\text{-}Cl(\{y_\beta\})$.

Theorem 3.16. Let $(\tilde{X},\tilde{\tau},E)$ be a S_{ft}-Top-Space. Then the following statements are equivalent:

(1). $(\tilde{X},\tilde{\tau},E)$ is $S_{ft}g^*\beta\text{-}R_0$.

(2). If $x_\alpha, y_\beta \in \tilde{X}$, then $y_\beta \in S_{ft}g^*\beta\text{-}Cl(\{x_\alpha\})$ if and only if every net in $\tilde{X}$ $S_{ft}g^*\beta$*-converging* to y_β $S_{ft}g^*\beta$*-converges* to x_α.

Proof $(1)\Rightarrow(2)$. Let x_α, $y_\beta \in \tilde{X}$ such that $y_\beta \in S_{ft}g^*\beta\text{-}Cl(\{x_\alpha\})$. Let $\{x_{\alpha_i} : i \in \Lambda\}$ be a net in $\tilde{X}$ such that $\{x_{\alpha_i} : i \in \Lambda\}$ $S_{ft}g^*\beta$*-converges* to y_β. Since $y_\beta \in S_{ft}g^*\beta\text{-}Cl(\{x_\alpha\})$, by Theorem 3.5 we have $S_{ft}g^*\beta\text{-}Cl(\{x_\alpha\}) = S_{ft}g^*\beta\text{-}Cl(\{y_\beta\})$. Therefore $x_\alpha \in S_{ft}g^*\beta\text{-}Cl(\{y_\alpha\})$, This means that $\{x_{\alpha_i} : i \in \Lambda\}$ $S_{ft}g^*\beta$*-converges* to x_α.

Conversely, let x_α, $y_\beta \in \tilde{X}$ such that every net in $\tilde{X}$ $S_{ft}g^*\beta$*-converging* to y_β $S_{ft}g^*\beta$*-converges* to x_α. Then $x_\alpha \in S_{ft}g^*\beta\text{-}Cl(\{y_\beta\})$ by Lemma 3.12. By Theorem 3.6, we have $S_{ft}g^*\beta\text{-}Cl(\{x_\alpha\}) = S_{ft}g^*\beta\text{-}Cl(\{y_\beta\})$. Therefore $y_\beta \in S_{ft}g^*\beta\text{-}Cl(\{x_\alpha\})$.

$(2)\Rightarrow(1)$. Assume that x_α and y_β are any two distinct soft points of $\tilde{X}$ such that $S_{ft}g^*\beta\text{-}Cl(\{x_\alpha\}) \cap S_{ft}g^*\beta\text{-}Cl(\{y_\beta\}) \neq \tilde{\phi}$. Let $z_\gamma \in S_{ft}g^*\beta\text{-}Cl(\{x_\alpha\}) \cap S_{ft}g^*\beta\text{-}Cl(\{y_\beta\})$. So there exists a net $\{x_{\alpha_i} : i \in \Lambda\}$ in $S_{ft}g^*\beta\text{-}Cl(\{x_\alpha\})$ such that $\{x_{\alpha_i} : i \in \Lambda\}$ $S_{ft}g^*\beta$*-converges* to z_γ. Since $z_\gamma \in S_{ft}g^*\beta\text{-}Cl(\{y_\beta\})$ then $\{x_{\alpha_i} : i \in \Lambda\}$ $S_{ft}g^*\beta$*-converges* to y_β. It follows that $y_\beta \in S_{ft}g^*\beta\text{-}Cl(\{x_\alpha\})$. By the similarity we obtain $x_\alpha \in S_{ft}g^*\beta\text{-}Cl(\{y_\beta\})$. Therefore $S_{ft}g^*\beta\text{-}Cl(\{x_\alpha\}) = S_{ft}g^*\beta\text{-}Cl(\{y_\beta\})$ and by Theorem 3.6 $(\tilde{X},\tilde{\tau},E)$ is a $S_{ft}g^*\beta\text{-}R_0$ space.

Definition 3.17. A S_{ft}-Top-Space $(\tilde{X},\tilde{\tau},E)$ is called $S_{ft}g^*\beta\text{-}R_1$ if for any two distinct soft points $x_\alpha, y_\beta \in \tilde{X}$ with $S_{ft}g^*\beta\text{-}Cl(\{x_\alpha\}) \neq S_{ft}g^*\beta\text{-}Cl(\{y_\beta\})$ there exist disjoint $S_{ft}g^*\beta$-open sets (F,E) and (G,E) such that $S_{ft}g^*\beta\text{-}Cl(\{x_\alpha\}) \subseteq (F,E)$ and $S_{ft}g^*\beta\text{-}Cl(\{y_\beta\}) \subseteq (G,E)$.

Theorem 3.18. Suppose that a S_{ft}-Top-Space $(\tilde{X},\tilde{\tau},E)$ is $S_{ft}g^*\beta\text{-}R_1$, then it is a $S_{ft}g^*\beta\text{-}R_0$ space.

Proof. Suppose that $(\tilde{X},\tilde{\tau},E)$ is $S_{ft}g^*\beta\text{-}R_1$. Let (H,E) be any $S_{ft}g^*\beta$*-open* set containing a soft point x_α. Then for each $y_\beta \in \tilde{X} - (H,E)$, $S_{ft}g^*\beta\text{-}Cl(\{x_\alpha\}) \neq S_{ft}g^*\beta\text{-}Cl(\{y_\beta\})$. Since $(\tilde{X},\tilde{\tau},E)$ is

$S_{ft}g*\beta - R_1$, there exist disjoint $S_{ft}g*\beta$ -open sets (K,E) and (G,E) such that $S_{ft}g*\beta - Cl(\{\mathbf{x}_\alpha\}) \subseteq (K,E)$ and $S_{ft}g*\beta - Cl(\{y_\beta\}) \subseteq (G,E)$. Let $(F,E) = \cup\{(G,E) : y_\beta \in \tilde{X} - (H,E)\}$, then $\tilde{X} - (H,E) \subseteq (F,E)$, $x_\alpha \notin (F,E)$ and (F,E) is a $S_{ft}S_{emi}{}^{\#}g\alpha - open$ set. Therefore, $S_{ft}g*\beta - Cl(\{\mathbf{x}_\alpha\}) \subseteq \tilde{X} - (F,E) \subseteq (H,E)$. Hence (X,τ,E) is $S_{ft}g*\beta - R_0$.

Theorem 3.19. A space $\tilde{X}$ is $S_{ft}g*\beta - R_0$ if and only if for every $S_{ft}g*\beta - closed$ set (K,E) and $x_\alpha \notin (K,E)$, there exists a $S_{ft}g*\beta - open$ open set (G,E) such that $x_\alpha \notin (G,E)$ and $(K,E) \subseteq (G,E)$.

Proof. Let $\tilde{X}$ be $S_{ft}g*\beta - R_0$ space and (K,E) be $S_{ft}g*\beta - closed$ subset of $\tilde{X}$ not containing $x_\alpha \in \tilde{X}$. Then $\tilde{X} - (K,E)$ is $S_{ft}g*\beta - open$ set containing x_α. Since $\tilde{X}$ is $S_{ft}g*\beta - R_0$ space implies that $S_{ft}g*\beta - Cl(\{x_\alpha\}) \subseteq \tilde{X} - (K,E)$ and then $(K,E) \subseteq \tilde{X} - [S_{ft}g*\beta - Cl(\{x_\alpha\})]$. Now let $(G,E) = \tilde{X} - [S_{ft}g*\beta - Cl(\{x_\alpha\})]$, then (G,E) is $S_{ft}g*\beta - open$ set not containing x_α and $(K,E) \subseteq (G,E)$.

Conversely: Let $x_\alpha \in (G,E)$ where (G,E) is $S_{ft}g*\beta - open$ set in $\tilde{X}$. Then $\tilde{X} - (G,E)$ is $S_{ft}g*\beta - closed$ set and $x_\alpha \notin \tilde{X} - (G,E)$, by hypothesis there exists a $S_{ft}g*\beta - open$ set (H,E) such that $x_\alpha \notin (H,E)$ and $\tilde{X} - (G,E) \subseteq (H,E)$. Now $\tilde{X} - (H,E) \subseteq (G,E)$ and $x_\alpha \in \tilde{X} - (H,E)$, but $\tilde{X} - (H,E)$ is $S_{ft}g*\beta - closed$ set, then $S_{ft}g*\beta - Cl(\{x_\alpha\}) \subseteq \tilde{X} - (H,E) \subseteq (G,E)$. This implies that $\tilde{X}$ is a $S_{ft}g*\beta - R_0$ space.

4. $S_{ft}g*\beta - T_i$ Spaces for $(i = 0,1,2)$

In this section, we define $S_{ft}g*\beta - T_i$ spaces for $(i = 0,1,2)$ by using $S_{ft}g*\beta$ -open and separating the S_{ft} -Top -Space. Several relations between these S_{ft} -Spaces and other types of soft separation axioms are investigated.

Definition 4.1. A S_{ft} -Top -Space $(\tilde{X},\tilde{\tau},E)$ is said to be $S_{ft}g*\beta - T_0$ if for each pair of distinct soft points $x_\alpha, y_\beta \in \tilde{X}$, there exist $S_{ft}g*\beta$ -open sets (F,E) and (G,E) such that $x_\alpha \in (F,E)$ and $y_\beta \notin (F,E)$ or $y_\beta \in (G,E)$ and $x_\alpha \notin (G,E)$.

Definition 4.2. A S_{ft} -Top -Space $(\tilde{X},\tilde{\tau},E)$ is said to be $S_{ft}g*\beta - T_1$ if for each pair of distinct soft points $x_\alpha, y_\beta \in \tilde{X}$, there exist $S_{ft}g*\beta$ -open sets (F,E) and (G,E) such that $x_\alpha \in (F,E)$ but $y_\beta \notin (F,E)$ and $y_\beta \in (G,E)$ but $x_\alpha \notin (G,E)$.

Definition 4.3. A S_{ft}-Top-Space $(\tilde{X},\tilde{\tau},E)$ is said to be $S_{ft}g*\beta-T_2$ if for each pair of distinct soft points $x_\alpha, y_\beta \in \tilde{X}$, there exist two disjoint $S_{ft}g*\beta$-open sets (F,E) and (G,E) containing x_α and y_β, respectively.

Proposition 4.4. A S_{ft}-Top-Space $(\tilde{X},\tilde{\tau},E)$ is $S_{ft}g*\beta-T_0$ if and only if $S_{ft}g*\beta$-closure of any two soft points is distinct.

Proof. Let $(\tilde{X},\tilde{\tau},E)$ be a $S_{ft}g*\beta-T_0$ space and $x_\alpha, y_\beta \in \tilde{X}$ with $x_\alpha \neq y_\beta$. Then, there exists a $S_{ft}g*\beta$-open set (F,E) containing one of the soft points, say x_α, but not the other. Then, $\tilde{X}-(F,E)$ is a $S_{ft}g*\beta$-closed set which does not contain x_α but contains y_β. Since, $S_{ft}g*\beta\text{-}Cl(\{y_\beta\})$ is the smallest $S_{ft}g*\beta$-*closed* set containing y_β, $S_{ft}g*\beta\text{-}Cl(\{y_\beta\}) \subseteq \tilde{X}-(F,E)$ and therefore $x_\alpha \notin S_{ft}g*\beta\text{-}Cl(\{y_\beta\})$. Consequently, $S_{ft}g*\beta\text{-}Cl(\{x_\alpha\}) \neq S_{ft}g*\beta\text{-}Cl(\{y_\beta\})$.

Conversely, suppose that $x_\alpha, y_\beta \in \tilde{X}$ is such that $x_\alpha \neq y_\beta$ and $S_{ft}g*\beta\text{-}Cl(\{x_\alpha\}) \neq S_{ft}g*\beta\text{-}Cl(\{y_\beta\})$. Let z_γ be a soft point in $\tilde{X}$ such that $z_\gamma \in S_{ft}g*\beta\text{-}Cl(\{x_\alpha\})$, but $z_\gamma \notin S_{ft}g*\beta\text{-}Cl(\{y_\beta\})$. We claim that $x_\alpha \in S_{ft}g*\beta\text{-}Cl(\{y_\beta\})$. For, if $x_\beta \notin S_{ft}g*\beta\text{-}Cl(\{y_\beta\})$, then $S_{ft}g*\beta\text{-}Cl(\{x_\alpha\}) \subseteq S_{ft}g*\beta\text{-}Cl(\{y_\beta\})$. This contradicts the fact that $z_\gamma \notin S_{ft}g*\beta\text{-}Cl(\{y_\beta\})$. Consequently, x_α belongs to the $S_{ft}g*\beta$-open set $(G,E) = \tilde{X} - \left[S_{ft}g*\beta\text{-}Cl(\{y_\beta\})\right]$. Then (G,E) is the complement of $S_{ft}g*\beta$-closed set. Thus (G,E) is a $S_{ft}g*\beta$-open set which contains x_α but not y_β. Hence, $(\tilde{X},\tilde{\tau},E)$ is $S_{ft}g*\beta-T_0$ space.

Proposition 4.5. If $(\tilde{X},\tilde{\tau},E)$ is $S_{ft}g*\beta-T_0$, space, then $\left[S_{ft}g*\beta\text{-}Cl(\{x_\alpha\})\right] \cap \left[S_{ft}g*\beta\text{-}Cl(\{y_\beta\})\right] = \tilde{\phi}$, for each pair of distinct soft points $x_\alpha, y_\beta \in \tilde{X}$.

Proof. Let $(\tilde{X},\tilde{\tau},E)$ be a $S_{ft}g*\beta-T_0$ space and $x_\alpha, y_\beta \in \tilde{X}$ such that $x_\alpha \neq y_\beta$. Then, there exists a $S_{ft}g*\beta$-open set (F,E) containing x_α or y_β, which implies that $x_\alpha \in (F,E)$ and $y_\beta \notin (F,E)$, then $y_\beta \in \tilde{X}-(F,E)$ and $\tilde{X}-(F,E)$ is $S_{ft}g*\beta$-closed. Now $S_{ft}g*\beta\text{-}Int(\{y_\beta\}) \subseteq S_{ft}g*\beta\text{-}Cl\left[S_{ft}g*\beta\text{-}Int(\{y_\beta\})\right] \subseteq \tilde{X}-(F,E)$, which implies that $(F,E) \cap S_{ft}g*\beta\text{-}Cl\left[S_{ft}g*\beta\text{-}Int(\{y_\beta\})\right] = \tilde{\phi}$, then $(F,E) \subseteq \tilde{X} - S_{ft}g*\beta\text{-}Cl\left[S_{ft}g*\beta\text{-}Int(\{y_\beta\})\right]$. Since $x_\alpha \in (F,E) \subseteq \tilde{X} - S_{ft}g*\beta\text{-}Cl\left[S_{ft}g*\beta\text{-}Int(\{y_\beta\})\right]$, then $S_{ft}g*\beta\text{-}Cl(\{x_\alpha\}) \subseteq \tilde{X} - S_{ft}g*\beta\text{-}Cl\left[S_{ft}g*\beta\text{-}Int(\{y_\beta\})\right]$, which implies that $S_{ft}g*\beta\text{-}Cl\left[S_{ft}g*\beta\text{-}Int(\{x_\alpha\})\right] \subseteq S_{ft}g*\beta\text{-}Cl(\{x_\alpha\}) \subseteq \tilde{X} - S_{ft}g*\beta\text{-}Cl\left[S_{ft}g*\beta\text{-}Int(\{y_\beta\})\right]$.

Thereore, $S_{ft}g*\beta\text{-}Cl(\{x_\alpha\}) \cap S_{ft}g*\beta\text{-}Cl(\{y_\beta\}) = \tilde{\phi}$.

Theorem 4.6. A $S_{ft}-\mathrm{Top}-\mathrm{Space}$ $(\tilde{\mathrm{X}},\tilde{\tau},\mathrm{E})$ is a $S_{ft}g*\beta-\mathrm{T}_1$ space if and only if for each $x_\alpha \in \tilde{X}$, every soft singleton $\{x_\alpha\}$ is a $S_{ft}g*\beta-\mathrm{closed}$ set.

Proof. Necessity. Suppose that $(\tilde{\mathrm{X}},\tilde{\tau},\mathrm{E})$ is $S_{ft}g*\beta-\mathrm{T}_1$ space and $x_\alpha \in \tilde{X}$. We have to prove that the soft singleton $\{x_\alpha\}$ is a $S_{ft}g*\beta-\mathrm{closed}$ set. Since $(\tilde{\mathrm{X}},\tilde{\tau},\mathrm{E})$ is a $S_{ft}g*\beta-\mathrm{T}_1$ space, for each soft point $y_\beta \in \tilde{X}-\{x_\alpha\}$ we can find a $S_{ft}g*\beta-\mathrm{open}$ set (F,E) of y_β such that $x_\alpha \notin (F,E)$. The union of all these $S_{ft}g*\beta-\mathrm{open}$ sets is a $S_{ft}g*\beta-\mathrm{open}$ set and it is the complement of $\{x_\alpha\}$ in $\tilde{X}$. Hence $\{x_\alpha\}$ is a $S_{ft}g*\beta-\mathrm{closed}$ set.

Sufficiency. Suppose that $x_\alpha \in \tilde{X}$, every soft singleton $\{x_\alpha\}$ is a $S_{ft}g*\beta-\mathrm{closed}$ set in $(\tilde{\mathrm{X}},\tilde{\tau},\mathrm{E})$. We have to prove that $(\tilde{\mathrm{X}},\tilde{\tau},\mathrm{E})$ is a $S_{ft}g*\beta-\mathrm{T}_1$ space. Let $x_\alpha, y_\beta \in \tilde{X}$ and $x_\alpha \neq y_\beta$ such that $\{x_\alpha\}$ and $\{y_\beta\}$ are $S_{ft}g*\beta-\mathrm{closed}$ and hence $\tilde{X}-\{x_\alpha\}$ and $\tilde{X}-\{y_\beta\}$ are $S_{ft}g*\beta-\mathrm{open}$ sets. Therefore, $y_\beta \in \tilde{X}-\{x_\alpha\}$ but $x_\alpha \notin \tilde{X}-\{x_\alpha\}$ and $x_\alpha \in \tilde{X}-\{y_\beta\}$ but $y_\beta \notin \tilde{X}-\{y_\beta\}$. Thus $(\mathrm{X},\tau,\mathrm{E})$ is a $S_{ft}g*\beta-\mathrm{T}_1$ space.

Theorem 4.7. Let $(\tilde{\mathrm{X}},\tilde{\tau},\mathrm{E})$ be a $S_{ft}-\mathrm{Top}-\mathrm{Space}$. Then following statements are equivalent:

(i) $(\tilde{\mathrm{X}},\tilde{\tau},\mathrm{E})$ is a $S_{ft}g*\beta-\mathrm{T}_1$ space.

(ii) Each $S_{ft}-\mathrm{subset}$ of $\tilde{X}$ is the soft intersection of all $S_{ft}g*\beta-\mathrm{open}$ sets containing it.

(iii) The soft intersection of all $S_{ft}g*\beta-\mathrm{open}$ sets containing the soft point $x_\alpha \in \tilde{X}$ is $\{x_\alpha\}$.

Proof. $(\mathrm{i})\Rightarrow(\mathrm{ii})$. Let $(\tilde{\mathrm{X}},\tilde{\tau},\mathrm{E})$ be a $S_{ft}g*\beta-\mathrm{T}_1$ space and (F,E) be a $S_{ft}-\mathrm{subset}$ of $\tilde{X}$. Then for each $y_\beta \in \tilde{X}-(F,E)$ there exists a $S_{ft}-\mathrm{set}$ $\tilde{X}-\{y_\beta\}$ such that $(F,E)\subseteq \tilde{X}-\{y_\beta\}$. By Theorem 4.6, the soft set $\tilde{X}-\{y_\beta\}$ is $S_{ft}g*\beta-\mathrm{open}$ set for every y_β. This implies that $(F,E)=\bigcap\left\{\tilde{X}-\{y_\beta\} : y_\beta \in \tilde{X}-(F,E)\right\}$. So the soft intersection of all $S_{ft}g*\beta-\mathrm{open}$ sets containing (F,E) is (F,E) itself.

$(\mathrm{ii})\Rightarrow(\mathrm{iii})$. Let $x_\alpha \in \tilde{X}$. Then $\{x_\alpha\}$ is a soft subset of $\tilde{X}$. By (ii), the soft intersection of all $S_{ft}g*\beta-\mathrm{open}$ sets containing $\{x_\alpha\}$ is $\{x_\alpha\}$ itself.

$(\mathrm{iii})\Rightarrow(\mathrm{i})$. Let $x_\alpha, y_\beta \in \tilde{X}$ such that $x_\alpha \neq y_\beta$. By (iii), the soft intersection of all $S_{ft}g*\beta-\mathrm{open}$ sets containing x_α and y_β are $\{x_\alpha\}$ and $\{y_\beta\}$ respectively. Then there exist $S_{ft}g*\beta-\mathrm{open}$ sets (F,E) and (G,E) such that $x_\alpha \in (F,E)$ and $y_\beta \notin (F,E)$ and $x_\alpha \notin (G,E)$ and $y_\beta \in (G,E)$. Therefore, $(\mathrm{X},\tau,\mathrm{E})$ is a a $S_{ft}g*\beta-\mathrm{T}_1$ space.

Theorem 4.8. Let $(\tilde{\mathrm{X}},\tilde{\tau},\mathrm{E})$ be a $S_{ft}g*\beta-\mathrm{T}_2$ space. Then the following statements are equivalent:

(i) $(\tilde{\mathrm{X}},\tilde{\tau},\mathrm{E})$ is a $S_{ft}g*\beta-\mathrm{T}_2$ space.

(ii) If $x_\alpha \in \tilde{X}$, then for each $y_\beta \neq x_\alpha$, there exists a $S_{ft}g*\beta-\mathrm{open}$ set (F,A) containing x_α such that

$y_\beta \notin S_{ft}g*\beta-Cl(F,A)$.

(iii) $\{x_\alpha\} = \bigcap\{S_{ft}g*\beta-Cl(F,A) : x_\alpha \in (F,A)$ and (F,A) is $S_{ft}g*\beta-$open set in $\tilde{X}\}$ for every $x_\alpha \in \tilde{X}$.

Proof. $(i) \Rightarrow (ii)$. Let $(\tilde{X},\tilde{\tau},E)$ be a $S_{ft}g*\beta-T_2$ space and x_α, y_β are any two distinct soft points of $\tilde{X}$. Then there exist disjoint $S_{ft}g*\beta-$open sets (F,A) and (G,B) such that $x_\alpha \in (F,A)$, $y_\beta \in (G,B)$, Then $(G,B)^C$ is a $S_{ft}g*\beta-$closed set such that $(F,A) \subseteq (G,B)^C$. By the definition of $S_{ft}g*\beta-$closure, $y_\beta \notin S_{ft}g*\beta-Cl(F,A)$, since $S_{ft}g*\beta-Cl(F,A)$ is the smallest $S_{ft}g*\beta-$closed set containing (F,A).

$(ii) \Rightarrow (iii)$. Suppose that $x_\alpha \in \tilde{X}$. By hypothesis, for any soft point $y_\beta(\neq x_\alpha) \in \tilde{X}$, there exists a $S_{ft}g*\beta-$open set (F,A) containing x_α such that $y_\beta \notin S_{ft}g*\beta-Cl(F,A)$. Therefore $y_\beta \notin \bigcap\{S_{ft}g*\beta-Cl(F,A) : x_\alpha \in (F,A) \in S_{ft}g*\beta-O(\tilde{X})\}$. Thus consequently, we obtain $\{x_\alpha\} = \bigcap\{S_{ft}g*\beta-Cl(F,A) : x_\alpha \in (F,A) \in S_{ft}g*\beta-O(\tilde{X})\}$.

$(iii) \Rightarrow (i)$. Suppose that x_α and y_β are any two distinct soft points in $\tilde{X}$. By hypothesis, there exists a $S_{ft}g*\beta-$open set (F,A) containing x_α such that $y_\beta \notin S_{ft}g*\beta-Cl(F,A)$. Let $(G,B) = \tilde{X} - S_{ft}g*\beta-Cl(F,A)$, then $y_\beta \in (G,B)$, $x_\alpha \in (F,A)$ and $(F,A) \cap (G,B) = \tilde{\phi}$. Therefore, (X,τ,E) is a $S_{ft}g*\beta-T_2$ space.

Proposition 4.9. Every $S_{ft}S_{emi}{}^{\#}g\alpha-T_1$ *space* $(\tilde{X},\tilde{\tau},E)$ is $S_{ft}g*\beta-R_0$.

Proof. Obvious.

Theorem 4.10. Let $(\tilde{X},\tilde{\tau},E)$ be a $S_{ft}-$Top$-$Space. Then the following implications are true:
(X,τ,E) is $S_{ft}g*\beta-T_2$ space $\Rightarrow$ (X,τ,E) is $S_{ft}g*\beta-T_1$ space $\Rightarrow$ (X,τ,E) is $S_{ft}g*\beta-T_0$ space.

Proof. $\underline{S_{ft}g*\beta-T_2 \text{ space} \Rightarrow S_{ft}g*\beta-T_1 \text{ space}}$: Let (X,τ,E) be a $S_{ft}g*\beta-T_2$ space. Then, for every $x_\alpha, y_\beta \in \tilde{X}$ and $y_\beta \neq x_\alpha$, there exist $S_{ft}g*\beta-$open sets (F,A) and (G,B) of x_α and y_β such that $(F,A) \cap (G,B) = \tilde{\phi}$. $x_\alpha \in (F,A) \Rightarrow x_\alpha \notin (G,B)$ as $(F,A) \cap (G,B) = \tilde{\phi}$. Similarly, $y_\beta \in (G,B)$. This implies $y_\beta \notin (F,A)$. Hence, $x_\alpha \in (F,A)$ but $y_\beta \notin (F,A)$ and $y_\beta \in (G,B)$ but $x_\alpha \notin (G,B)$. Therefore, $(\tilde{X},\tilde{\tau},E)$ is a $S_{ft}g*\beta-T_1$ space.

$\underline{S_{ft}g*\beta-T_1 \text{ space} \Rightarrow S_{ft}g*\beta-T_0 \text{ space}}$: Let (X,τ,E) be a $S_{ft}g*\beta-T_1$ space. Then for every $x_\alpha, y_\beta \in \tilde{X}$ with $x_\alpha \neq y_\beta$, there exist $S_{ft}g*\beta-$open sets (F,A) and (G,B) such that $x_\alpha \in (F,A)$ but $y_\beta \notin (F,A)$ and $y_\beta \in (G,B)$ but $x_\alpha \notin (G,B)$. Therefore, $(\tilde{X},\tilde{\tau},E)$ is a $S_{ft}g*\beta-T_0$ space.

Proposition 4.11. A $S_{ft}-$Top$-$Space $(\tilde{X},\tilde{\tau},E)$ is $S_{ft}g*\beta-T_1$ if and only if $\tilde{X}$ is both $S_{ft}g*\beta-T_0$ and $S_{ft}g*\beta-R_0$.

Proof. Necessity. Let $\tilde{X}$ be $S_{ft}g*\beta-T_1$, then by Proposition 3.19, $\tilde{X}$ is $S_{ft}g*\beta-R_0$ and since every $S_{ft}g*\beta-T_1$ is $S_{ft}g*\beta-T_0$ that completes the proof.

Sufficiency. Assume that $\tilde{X}$ is both $S_{ft}g*\beta-T_0$ and $S_{ft}g*\beta-R_0$. Let $x_\alpha, y_\beta \in \tilde{X}$ be any pair of distinct soft points, since $\tilde{X}$ is $S_{ft}g*\beta-T_0$, there exists a $S_{ft}g*\beta-open$ set (H,E) such that $x_\alpha \in (H,E)$ and $y_\beta \notin (H,E)$ or there exists a $S_{ft}g*\beta-open$ set (G,E) such that $y_\beta \in (G,E)$ and $x_\alpha \notin (G,E)$. Suppose that $x_\alpha \in (H,E)$ and $y_\beta \notin (H,E)$. Since $\tilde{X}$ is $S_{ft}g*\beta-R_0$, then $S_{ft}g*\beta-Cl\{x_\alpha\} \subseteq (H,E)$. As $y_\beta \notin (H,E)$ implies $y_\beta \notin S_{ft}g*\beta-Cl\{x_\alpha\}$. Hence $y_\beta \in (G,E) = \tilde{X} - [S_{ft}g*\beta-Cl\{x_\alpha\}]$ and it is clear that $x_\alpha \notin (G,E)$, this implies that there exist $S_{ft}g*\beta-open$ sets (G,E) and (H,E) containing x_α and y_β respectively such that $x_\alpha \notin (G,E)$ and $y_\beta \notin (H,E)$. Therefore $(\tilde{X},\tilde{\tau},E)$ is a $S_{ft}g*\beta-T_1$ space.

Theorem 4.12. A space $\tilde{X}$ is $S_{ft}g*\beta-T_2$ if and only if it is $S_{ft}g*\beta-R_1$ and $S_{ft}g*\beta-T_0$.

Proof. Let $\tilde{X}$ be $S_{ft}g*\beta-T_2$. Then from Theorem 4.10, $\tilde{X}$ is $S_{ft}g*\beta-T_0$ and to show $\tilde{X}$ is $S_{ft}g*\beta-R_1$ space, let $x_\alpha, y_\beta \in \tilde{X}$ such that $S_{ft}g*\beta-Cl\{x_\alpha\} \neq S_{ft}g*\beta-Cl\{y_\beta\}$ and since $\tilde{X}$ is $S_{ft}g*\beta-T_1$ space so by Theorem 4.6, every singleton set in $\tilde{X}$ is $S_{ft}g*\beta-closed$, this means $S_{ft}g*\beta-Cl(\{x_\alpha\}) = \{x_\alpha\}$ and $S_{ft}g*\beta-Cl(\{y_\beta\}) = \{y_\beta\}$ implies that $\{x_\alpha\} \neq \{y_\beta\}$ and since $\tilde{X}$ is $S_{ft}g*\beta-T_2$ space so there exist two disjoint $S_{ft}g*\beta-open$ sets (G,E) and (H,E) such that $x_\alpha \in (G,E)$ and $y_\beta \in (H,E)$ implies that $S_{ft}g*\beta-Cl(\{x_\alpha\}) \subseteq (G,E)$ and $S_{ft}g*\beta-Cl(\{y_\beta\}) \subseteq (H,E)$. Thus $\tilde{X}$ is a $S_{ft}g*\beta-R_1$ space.

Conversely, let $\tilde{X}$ be $S_{ft}g*\beta-R_1$ and $S_{ft}g*\beta-T_0$ space and $x_\alpha, y_\beta \in \tilde{X}$ such that $x_\alpha \neq y_\beta$. Now since $\tilde{X}$ is $S_{ft}g*\beta-T_0$ so by Definition 4.1 there exists a $S_{ft}g*\beta-open$ set (G,E) such that $x_\alpha \in (G,E)$ and $y_\beta \notin (G,E)$ or $y_\beta \in (G,E)$ and $x_\alpha \notin (G,E)$, take $x_\alpha \in (G,E)$ and $y_\beta \notin (G,E)$ implies that $(G,E) \cap \{y_\beta\} = \tilde{\phi}$, and then $S_{ft}g*\beta-Cl(\{y_\beta\})$. This implies that $S_{ft}g*\beta-Cl(\{x_\alpha\}) \neq S_{ft}g*\beta-Cl(\{y_\beta\})$ and since $\tilde{X}$ is $S_{ft}g*\beta-R_1$ so there exist two disjoint $S_{ft}g*\beta-open$ sets (G,E) and (H,E) such that $S_{ft}g*\beta-Cl(\{x_\alpha\}) \subseteq (G,E)$ and $S_{ft}g*\beta-Cl(\{y_\beta\}) \subseteq (H,E)$ implies that $x_\alpha \in (G,E)$ and $y_\beta \in (H,E)$. Thus $\tilde{X}$ is $S_{ft}g*\beta-T_2$.

Theorem 4.13. Let $(\tilde{X},\tilde{\tau},E)$ be a $S_{ft}g*\beta-T_2$ space. If for any $x_\alpha, y_\beta \in \tilde{X}$ such that $x_\alpha \neq y_\beta$, then there exist $S_{ft}g*\beta-$closed sets (F_1,E) and (F_2,E) such that $x_\alpha \in (F_1,E)$, $y_\beta \notin (F_1,E)$ and $x_\alpha \notin (F_2,E)$, $y_\beta \in (F_2,E)$, and $(F_1,E) \cup (F_2,E) = \tilde{X}$.

Proof. Since $(\tilde{X},\tilde{\tau},E)$ is a $S_{ft}g*\beta-T_2$ space and $x_\alpha, y_\beta \in \tilde{X}$ such that $x_\alpha \neq y_\beta$, there exist $S_{ft}g*\beta-$open sets (G_1,E) and (G_2,E) such that $x_\alpha \in (G_1,E)$ and $y_\beta \in (G_2,E)$ and $(G_1,E) \cap (G_2,E) = \tilde{\phi}$. Clearly $(G_1,E) \subseteq (G_2,E)^C$ and $(G_2,E) \subseteq (G_1,E)^C$. Hence $x_\alpha \in (G_2,E)^C$. Put

$(G_2,E)^C = (F_1,E)$. This gives $x_\alpha \in (F_1,E)$ and $y_\beta \notin (F_1,E)$. Also $y_\beta \in (G_1,E)^C$. Put $(G_1,E)^C = (F_2,E)$. Therefore $x_\alpha \in (F_1,E)$ and $y_\beta \in (F_2,E)$. Moreover $(F_1,E) \cup (F_2,E) = (G_2,E)^C \cup (G_1,E)^C = \tilde{X}$.

5. $S_{ft}g*\beta$ –Regular, $S_{ft}g*\beta$ –Normal Spaces and $S_{ft}g*\beta$ –T_i Spaces for $(i = 3,4)$

In this section, we redefine $S_{ft}g*\beta$ –regular spaces, $S_{ft}g*\beta$ –normal spaces and $S_{ft}g*\beta$ –T_i spaces for $(i = 3,4)$. We investigate properties as well as characterizations of these spaces in soft topological spaces.

Definition 5.1. Let $(\tilde{X},\tilde{\tau},E)$ be a S_{ft} –Top –Space. Let (F,A) be a $S_{ft}g*\beta$ –closed set and $x_\alpha \in \tilde{X}$ such that $x_\alpha \notin (F,A)$. If there exist $S_{ft}g*\beta$ –open sets (G,B) and (H,C) such that $x_\alpha \in (G,B)$, $(F,A) \subseteq (H,C)$ and $(G,B) \cap (H,C) = \tilde{\phi}$, then $(\tilde{X},\tilde{\tau},E)$ is called a $S_{ft}g*\beta$ –regular space.

Theorem 5.2. Let $(\tilde{X},\tilde{\tau},E)$ be a S_{ft} –Top –Space. Then the following statements are equivalent:

(i) $(\tilde{X},\tilde{\tau},E)$ is a $S_{ft}g*\beta$ –regular space.

(ii) For any $S_{ft}g*\beta$ –open set (F,A) in $(\tilde{X},\tilde{\tau},E)$ and $x_\alpha \in (F,A)$, there is a $S_{ft}g*\beta$ –open set (G,B) containing x_α such that $x_\alpha \in S_{ft}g*\beta\text{–}Cl(G,B) \subseteq (F,A)$.

(iii) Each soft point in $(\tilde{X},\tilde{\tau},E)$ has a $S_{ft}g*\beta$ –neighbourhood base consisting of $S_{ft}g*\beta$ –closed sets.

Proof. $(i) \Rightarrow (ii)$. Let (F,A) be a $S_{ft}g*\beta$ –open set in $(\tilde{X},\tilde{\tau},E)$ and $x_\alpha \in (F,A)$. Then $(F,A)^C$ is a $S_{ft}g*\beta$ –closed set such that $x_\alpha \notin (F,A)^C$. By the $S_{ft}g*\beta$ –regularity of $(\tilde{X},\tilde{\tau},E)$, there are $S_{ft}g*\beta$ –open sets (G,B), (H,C) such that $x_\alpha \in (H,B)$, $(F,A)^C \subseteq (H,C)$ and $(G,B) \cap (H,C) = \tilde{\phi}$. Clearly $(H,C)^C$ is a $S_{ft}g*\beta$ –closed set contained in (F,A). Thus $(G,B) \subseteq (H,C)^C \subseteq (F,A)$. This gives $S_{ft}g*\beta\text{–}Cl(G,B) \subseteq (H,C)^C \subseteq (F,A)$. Consequently, $x_\alpha \in (G,B) \subseteq S_{ft}g*\beta\text{–}Cl(G,B) \subseteq (F,A)$.

$(ii) \Rightarrow (iii)$. Let $x_\alpha \in \tilde{X}$ and $S_{ft}g*\beta$ –open set (F,A) in $(\tilde{X},\tilde{\tau},E)$ such that $x_\alpha \in (F,A)$. Then there is a is a $S_{ft}g*\beta$ –open set (G,B) containing x_α such that $x_\alpha \in S_{ft}g*\beta\text{–}Cl(G,B) \subseteq (F,A)$. Thus for each $x_\alpha \in \tilde{X}$, the sets $S_{ft}g*\beta\text{–}Cl(G,B)$ form a $S_{ft}g*\beta$ –neighbourhood base consisting of $S_{ft}g*\beta$ –closed sets of $(\tilde{X},\tilde{\tau},E)$.

$(iii) \Rightarrow (i)$. Let (F,A) be a $S_{ft}g*\beta$ –closed set such that $x_\alpha \notin (F,A)$. Then $(F,A)^C$ is a $S_{ft}g*\beta$ –open neighborhood of x_α. By (iii), there is a $S_{ft}g*\beta$ –closed set (G,B) which contains x_α and is a $S_{ft}g*\beta$ –neighbourhood of x_α with $(G,B) \subseteq (F,A)^C$. Then $x_\alpha \notin (G,B)^C$, $(F,A) \subseteq (G,B)^C = (H,C)$ and $(G,B) \cap (H,C) = \tilde{\phi}$. Therefore $(\tilde{X},\tilde{\tau},E)$ is $S_{ft}g*\beta$ –regular space.

Theorem 5.3. Prove that $S_{ft}-\text{Top}-\text{Space}\ (\tilde{X},\tilde{\tau},E)$ is $S_{ft}g*\beta-\text{regular}$ if and only if for each $x_\alpha \in \tilde{X}$ and a $S_{ft}g*\beta-\text{closed}$ set (F,A) in $(\tilde{X},\tilde{\tau},E)$ such that $x_\alpha \notin (F,A)$, there exist $S_{ft}g*\beta-\text{open}$ sets (G,B), (H,C) in $(\tilde{X},\tilde{\tau},E)$ such that $x_\alpha \in (G,B)$ and $(F,A) \subseteq (H,C)$ and $S_{ft}g*\beta-\text{Cl}(G,B) \cap S_{ft}g*\beta-\text{Cl}(H,C) = \tilde{\phi}$.

Proof. For each $x_\alpha \in \tilde{X}$ and a $S_{ft}g*\beta-\text{closed}$ set (F,A) such that $x_\alpha \notin (F,A)$, by Theorem 5.2 (ii), there is a $S_{ft}g*\beta-\text{open}$ set (G,B) such that $x_\alpha \in (G,B)$, $S_{ft}g*\beta-\text{Cl}(G,B) \subseteq (F,A)^C$. Again by Theorem 5.2 (ii), there is a $S_{ft}g*\beta-\text{open}$ set (H,C) containing x_α such that $S_{ft}g*\beta-\text{Cl}(H,C) \subseteq (G,B)$. Let $(M,K) = \left[S_{ft}g*\beta-\textit{open}(G,B)\right]^C$. Then $S_{ft}g*\beta-\text{Cl}(H,C) \subseteq (G,B) \subseteq S_{ft}g*\beta-\text{Cl}(G,B) \subseteq (F,A)^C$ implies $(F,A) \subseteq \left[S_{ft}S_{emi}{}^{\#}g\alpha-\text{Cl}(G,B)\right]^C = (M,K)$ or $(F,A) \subseteq (M,K)$. Also

$$S_{ft}g*\beta-\text{Cl}(H,C) \cap S_{ft}g*\beta-\text{Cl}(M,K) =$$

$$S_{ft}g*\beta-\text{Cl}(H,C) \cap S_{ft}g*\beta-\text{Cl}\left[\left(\left(S_{ft}g*\beta-\text{Cl}(G,B)\right)\right)^C\right] \subseteq (G,B) \cap S_{ft}g*\beta-\text{Cl}\left[\left(S_{ft}g*\beta-\text{Cl}(G,B)\right)^C\right] \subseteq$$

$$S_{ft}g*\beta-\text{Cl}\left[(G,B) \cap \left(S_{ft}g*\beta-\text{Cl}(G,B)\right)^C\right] = S_{ft}g*\beta-\text{Cl}(\tilde{\phi}) = \tilde{\phi}.$$

Thus (H,C) and (M,K) are the required $S_{ft}g*\beta-\text{open}$ sets in $(\tilde{X},\tilde{\tau},E)$.
This proves the necessity. The sufficiency is immediate.

Definition 5.4. Let $(\tilde{X},\tilde{\tau},E)$ be a $S_{ft}-\text{Top}-\text{Space}$. Then $(\tilde{X},\tilde{\tau},E)$ is said to be a $S_{ft}g*\beta-T_3$ space, if it is a $S_{ft}g*\beta-\text{regular}$ and a $S_{ft}g*\beta-T_1$ space.

Definition 5.5. Let $(\tilde{X},\tilde{\tau},E)$ be a $S_{ft}-\text{Top}-\text{Space}$, (F,A) and (G,B) be $S_{ft}g*\beta-\text{closed}$ sets such that $(F,A) \cap (G,B) = \tilde{\phi}$. If there exist $S_{ft}g*\beta-\text{open}$ sets (H,C) and (M,K) such that $(F,A) \subseteq (H,C)$, $(G,B) \subseteq (M,K)$ and $(H,C) \cap (M,K) = \tilde{\phi}$, then (X,τ,E) is called a $S_{ft}g*\beta-\text{normal}$ space.

Definition 5.6. Let $(\tilde{X},\tilde{\tau},E)$ be a $S_{ft}-\text{Top}-\text{Space}$. Then $(\tilde{X},\tilde{\tau},E)$ is said to be a $S_{ft}g*\beta-T_4$ space, if it is a $S_{ft}S_{emi}{}^{\#}g\alpha-\text{normal}$ space and a $S_{ft}g*\beta-T_1$ space.

Theorem 5.7. A $S_{ft}-\text{Top}-\text{Space}\ (\tilde{X},\tilde{\tau},E)$ is $S_{ft}g*\beta-\text{normal}$ if and only if for any $S_{ft}g*\beta-\text{closed}$ set (F,A) and a $S_{ft}g*\beta-\text{open}$ set (G,B) such that $(F,A) \subseteq (G,B)$, there exists at least one $S_{ft}g*\beta-\text{open}$ set (H,C) containing (F,A) such that $(F,A) \subseteq (H,C) \subseteq S_{ft}g*\beta-\text{Cl}(H,C) \subseteq (G,B)$.

Proof. Suppose that $(\tilde{X},\tilde{\tau},E)$ is a $S_{ft}g*\beta-\text{normal}$ space and (F,A) is any $S_{ft}g*\beta-\text{closed}$ subset of $(\tilde{X},\tilde{\tau},E)$ and (G,B) be a $S_{ft}g*\beta-\text{open}$ set such that $(F,A) \subseteq (G,B)$. Then $(G,B)^C$ is $S_{ft}g*\beta-\text{closed}$ and $(F,A) \cap (G,B)^C = \tilde{\phi}$. So by hypothesis, there are $S_{ft}g*\beta-\text{open}$ sets (H,C) and (M,K) such that $(F,A) \subseteq (H,C)$, $(G,B)^C \subseteq (M,K)$ and $(H,C) \cap (M,K) = \tilde{\phi}$. Since $(H,C) \cap (M,K) = \tilde{\phi}$,

$(H,C)\subseteq(M,K)^C$. But $(M,K)^C$ is $S_{ft}g*\beta$-closed, so that $(F,A)\subseteq(H,C)\subseteq S_{ft}g*\beta\text{-}Cl(H,C)\subseteq(M,K)^C\subseteq(G,B)$. Hence $(F,A)\subseteq(H,C)\subseteq S_{ft}g*\beta\text{-}Cl(H,C)\subseteq(G,B)$.

Conversely, suppose that for every $S_{ft}g*\beta$-closed (F,A) and a $S_{ft}g*\beta$-open set (G,B) such that $(F,A)\subseteq(G,B)$, there is a $S_{ft}g*\beta$-open set (H,C) such that $(F,A)\subseteq(H,C)\subseteq S_{ft}g*\beta\text{-}Cl(H,C)\subseteq(G,B)$. Let (J,L) and (M,K) be any two disjoint $S_{ft}g*\beta$-closed sets. Then $(J,L)\subseteq(M,K)^C$, where $(M,K)^C$ is $S_{ft}g*\beta$-open set. Hence there is a $S_{ft}g*\beta$-open set (H,C) such that $(J,L)\subseteq(H,C)\subseteq S_{ft}g*\beta\text{-}Cl(H,C)\subseteq(M,K)^C$. But then $(M,K)\subseteq\left[S_{ft}g*\beta\text{-}Cl(H,C)\right]^C$ and $(H,C)\cap\left[S_{ft}g*\beta\text{-}Cl(H,C)\right]^C=\tilde{\phi}$. Hence $(J,L)\subseteq(H,C)$, $(M,K)\subseteq\left[S_{ft}g*\beta\text{-}Cl(H,C)\right]^C$ with $(H,C)\cap\left[S_{ft}g*\beta\text{-}Cl(H,C)\right]^C=\tilde{\phi}$. Hence $(\tilde{X},\tilde{\tau},E)$ is a $S_{ft}g*\beta$-normal space.

Theorem 5.8. Prove that a $S_{ft}g*\beta$-closed subspace $(\tilde{Y},\tilde{\tau}_Y,E)$ of a $S_{ft}g*\beta$-normal space $(\tilde{X},\tilde{\tau},E)$ is $S_{ft}g*\beta$-normal.

Proof. Let $(\tilde{Y},\tilde{\tau}_Y,E)$ be a $S_{ft}g*\beta$-closed subspace of a $S_{ft}g*\beta$-normal space $(\tilde{X},\tilde{\tau},E)$. Let (F,A) and (G,B) be a disjoint pair of $S_{ft}g*\beta$-closed subsets of $(\tilde{Y},\tilde{\tau}_Y,E)$. Since $(\tilde{Y},\tilde{\tau}_Y,E)$ is a $S_{ft}g*\beta$-closed subspace of $(\tilde{Y},\tilde{\tau}_Y,E)$. The intersection of two $S_{ft}g*\beta$-closed subsets of $(\tilde{X},\tilde{\tau},E)$ is $S_{ft}g*\beta$-closed. Therefore (F,A) and (G,B) are disjoint $S_{ft}g*\beta$-closed subsets of $(\tilde{Y},\tilde{\tau}_Y,E)$. By hypothesis, $(\tilde{X},\tilde{\tau},E)$ is a $S_{ft}g*\beta$-normal space. There exist (J,L) and (M,K) $S_{ft}g*\beta$-open subsets of $(\tilde{X},\tilde{\tau},E)$ such that $(F,A)\subseteq(J,L)$, $(G,B)\subseteq(M,K)$ and $(J,L)\cap(M,K)=\tilde{\phi}$. Let $(P,Q)=(J,L)\cap\tilde{Y}$ and $(S,T)=(M,K)\cap\tilde{Y}$. Then (P,Q) and (S,T) are $S_{ft}g*\beta$-open subsets of $(\tilde{Y},\tilde{\tau}_Y,E)$ such that $(F,A)\subseteq(P,Q)$, $(G,B)\subseteq(S,T)$ and $(P,Q)\cap(S,T)=\tilde{\phi}$. Thus $(\tilde{Y},\tilde{\tau}_Y,E)$ is a $S_{ft}g*\beta$-normal space.

Theorem 5.9. Let $f:(\tilde{X},\tilde{\tau},E)\to(\tilde{Y},\tilde{\sigma},E)$ be a surjective function which is both $S_{ft}g*\beta$-irresolute and $S_{ft}g*\beta$-open where $(\tilde{X},\tilde{\tau},E)$ and $(\tilde{Y},\tilde{\sigma},E)$ are S_{ft}-Top-Spaces. If $(\tilde{X},\tilde{\tau},E)$ is $S_{ft}g*\beta$-normal, then $(\tilde{Y},\tilde{\sigma},E)$ is also $S_{ft}g*\beta$-normal.

Proof. Let (F,A) and (G,B) be a disjoint pair of $S_{ft}g*\beta$-closed subsets of $(\tilde{Y},\tilde{\sigma},E)$. As f is $S_{ft}g*\beta$-irresolute $f^{-1}(F,A)$ and $f^{-1}(G,B)$ are disjoint $S_{ft}S_{emi}{}^{\#}g\alpha$-closed subsets of $(\tilde{X},\tilde{\tau},E)$. This implies there exist disjoint $S_{ft}g*\beta$-open sets (J,L) and (M,K) such that $f^{-1}(F,A)\subseteq(J,L)$ and $f^{-1}(G,B)\subseteq(M,K)$, since $S_{ft}g*\beta$-normal. Then $(F,A)\subseteq f(J,L)$ and $(G,B)\subseteq f(M,K)$. This implies $f(J,L)$ and $f(M,K)$ are disjoint $S_{ft}g*\beta$-open sets of $(\tilde{Y},\tilde{\sigma},E)$ containing (F,A) and (G,B) respectively. Condequently we conclude that $(\tilde{Y},\tilde{\sigma},E)$ is also $S_{ft}g*\beta$-normal.

Theorem 5.10. $S_{ft}g*\beta\text{-}T_4\Rightarrow S_{ft}g*\beta\text{-}T_3\Rightarrow S_{ft}g*\beta\text{-}T_2$.

Proof. $\underline{S_{ft}g*\beta-T_4 \Rightarrow S_{ft}g*\beta-T_3}$**:** Let $(\tilde{X},\tilde{\tau},E)$ be a $S_{ft}g*\beta-T_4$ space. Let x_α and (F,A) be a pair of soft points and $S_{ft}g*\beta-$closed subsets of $(\tilde{X},\tilde{\tau},E)$ such that $x_\alpha \notin (F,A)$. Then $S_{ft}g*\beta-Cl(\{x_\alpha\})$ is the $S_{ft}g*\beta-$closed set containing x_α. As $S_{ft}g*\beta-T_4$ space is $S_{ft}g*\beta-T_1$ space and hence every point in $(\tilde{X},\tilde{\tau},E)$ is $S_{ft}g*\beta-$closed. Hence $S_{ft}g*\beta-Cl(\{x_\alpha\})$ and (F,A) are disjoint $S_{ft}g*\beta-$closed sets of $(\tilde{X},\tilde{\tau},E)$. Then by the definition of $S_{ft}g*\beta-$normal there exist two disjoint $S_{ft}g*\beta-$open sets (J,L) and (M,K) such that $x_\alpha \in (J,L)$ and $(F,A) \subseteq (M,K)$. Therefore $(\tilde{X},\tilde{\tau},E)$ is a $S_{ft}g*\beta-T_3$ space.

$\underline{S_{ft}g*\beta-T_3 \Rightarrow S_{ft}g*\beta-T_2}$: Let $(\tilde{X},\tilde{\tau},E)$ be a $S_{ft}g*\beta-T_3$ space. Let x_α and y_β be two distinct soft points of $(\tilde{X},\tilde{\tau},E)$. Then by the definition of $S_{ft}g*\beta-T_1$ space $\{x_\alpha\}$ is a $S_{ft}g*\beta-$closed set. Hence, we have a soft point and a $S_{ft}g*\beta-$closed set such that $y_\beta \notin S_{ft}g*\beta-Cl(\{x_\alpha\})$. Hence there exist disjoint $S_{ft}g*\beta-$open sets (J,L) and (M,K) such that $x_\alpha \in (J,L)$ and $y_\beta \in (M,K)$. Consequently $(\tilde{X},\tilde{\tau},E)$ is a $S_{ft}g*\beta-T_2$ space.

Conclusion

Soft set theory is very important during the study towards possible applications in classical and nonclassical logic. In recent years many researchers worked on the findings of structures of soft sets theory initiated by Molodtsov and applied to many problems having uncertainties. It is worth mentioning that soft topological spaces based on soft set theory which is a collection of information granules is the mathematical formulation of approximate reasoning about information systems. In the last two decades the soft set theory, new definitions, examples, new classes of soft sets, and properties for mappings between different classes of soft sets are introduced and studied. After then, the theory of soft topological spaces is investigated. These soft separation axioms would be useful for the development of the theory of soft topology to solve the complicated problems containing uncertainties in economics, engineering, medical, environment and in general man-machine systems of various types. These findings are the addition for strengthening the toolbox of soft topology. Soft separation axioms are among the most widespread and important concepts in soft topology because they are utilized to classify the objects of study and to construct different families of soft topological spaces. We have introduced some soft separation axioms called $S_{ft}g*\beta-R_0$ space, $S_{ft}g*\beta-R_1$ space, $S_{ft}g*\beta-T_0$ space, $S_{ft}g*\beta-T_1$ space, $S_{ft}g*\beta-T_2$ space, $S_{ft}g*\beta-$regular space and $S_{ft}g*\beta-$normal space in soft topological spaces. We have investigated their properties and characterizations in soft topological spaces. In the future I plan to study $S_{ft}g*\beta-$compact space, $S_{ft}g*\beta-$Lindelof space, countably $S_{ft}g*\beta-$compact space, $S_{ft}g*\beta-$connected spaces as well as $S_{ft}g*\beta-$continuous function, $S_{ft}g*\beta-$open function, $S_{ft}g*\beta-$closed function and $S_{ft}g*\beta-$irresolute function in soft topological spaces. We hope that the concepts initiated herein will be beneficial for researchers and scholars to promote and progress the study of soft topology and decision-making problems with applications in many fields soon.

Scientific Ethics Declaration

The author declares that the scientific ethical and legal responsibility of this article published in EPSTEM journal belongs to the author.

Acknowledgment

* This article was presented as an oral presentation at the International Conference on Basic Sciences and Technology (www.icbast.net) held in Antalya/Turkey on November 16-19, 2023.

* The author is highly and greatly indebted to Prince Mohammad bin Fahd University Al Khobar Saudi Arabia, for providing all necessary research facilities during the preparation of this research paper.

References

Abd El-Latif, A. M., & Rodyna, Hosny, A. (2016). On soft separation axioms via fuzzy α-open soft sets. *Information Science Letters, 5*(1), 1 – 9.

Alias & Khalaf, B. (2022). "Soft separation axioms and functions with soft closed graphs". *Proyecciones Journal of Mathematics, 11*(1), 177 – 195

Akdag, M., & Ozkan, A. (2014). On soft preopen sets and soft pre separation Axioms. *Gazi University Journal of Science, 27*(4), 1077 – 1083.

Akdag ,M., & Ozkan, A. (2014). On soft α-separation axioms. *Journal of Advanced Studies in Topology, 5*(4), 16 – 24.

Al-Shami, T. M., & Abo-Tabi, E.S.A. (2022). Soft α-separation axioms and α-fixed soft points, *AIMS Mathematics, 6*(6), 5675 – 5694.

Al-Shami, T. M., Ameen, Z. A., Azzam, A. A. & El-Shafei, M. E. (2022). Soft separation axioms via soft topological operators, *AIMS Mathematics, 7*(8), 15107 – 15119.

Al-Shami, T. M. (2021). On soft separation axioms and their applications on decision-making problem, mathematical problems in engineering. Retrieved from https://www.hindawi.com/journals/mpe/2021/8876978/

Askandar, S. W. (2016). On i – separation axioms. *International Journal of Scientific and Engineering Research, 7*(5), 367 – 373.

El-Sheikh, S. A., Rodyna, A., Hosny, A. M., & Abd El-Latif, A. M. (2015). Characterizations of b-soft separation axioms in soft topological spaces. *Information Sciences Letters, 4*(3), 125 – 133.

El-Shafei, M. E., Abo-Elhamayel M., & Al-Shami, T. M. (2018). Partial soft separation axioms and soft compact spaces. *Filomat, 32*(13), 4755 – 4771.

El-Shafei, M. E., & Al-Shami, T. M. (2020). Applications of partial belong and total non-belong relations on soft separation axioms and decision-making problem. *Journal of Computational and Applied Mathematics, 39,* 138.

Feng, F., Li, C., Davaz, B., & Ali, M. I.(2010). Soft sets combined with fuzzy sets and rough sets: a tentative approach. *Soft Computing, 14*(99), 899–911.

Gocur, O., & Kopuzlu, A. (2015). On soft separation axioms. *Annals of Fuzzy Mathematics and Informatics, 9*(5), 817 – 822.

Hussain, S., & Ahmad, B. (2015). Soft separation axioms in soft topological spaces. *Hacettepe Journal of Mathematics and Statistics, 44*(3), 559 – 568.

Kalavathi, A., & Sai Sundara Krishnan, G. (2016). Soft g*closed and soft g*open sets in soft topological spaces. *Journal of Interdisciplinary Mathematics, 19*(1), 65 – 82.

Kokilovani, V., & Vivek Prabu, M. (2013). Semi #generalized α closed sets and Semi #generalized α-homeomorphism in topological spaces, Proceedings of *National Conference on Recent Advances in Mathematical Analysis and Applications – NCRAMAA*, 153 – 161.

Kokilovani, V., & Vivek Prabu, M. (2015). Applications of Semi #generalized α-closed sets in topological spaces. *International Journal of Mathematics and Applications, 3*(3), 57-63.

Kokilovani, V., Sindu, D., & Vivek Prabu, M. (2014). Soft #generalized α-closed sets in soft topological spaces. *International Journal of Advanced and Innovative Research, 3*(10), 265 – 271.

Karuppayal, V. R., & Malarvizhi, M. (2014). Soft generalized #α-Closed Sets in Soft Topological Spaces. *International Journal of Advanced and Innovative Research, 3*(10), 298 – 305.

Khalaf, A. B., & Ahmed, N. K.. (2022). Soft pre separation axioms and functions with soft pre closed graph. *General Letters in Mathematics (GLM), 12*(2), 75-84. Retrieved from www.refaad.com

Khattak, A. M., Khan, G. A., Ishfaq, M., & Jamal, F. (2017). Characterization of soft α-separation axioms and soft β-separation axioms in soft single point spaces and in soft ordinary spaces. *Journal of New Theory, 19*, 63 – 81.

Kiruthika, M. (2022). Separation axioms on soft topology. *Advances and Applications in Mathematical Sciences, 21*(6), 3469 – 3477.

Molodtsov, D. (1999). Soft set theory-first results. *Computers & and Mathematics with Applications, 37*(4-5), 19-31.

Punitha Tharani, A., & Sujitha, H. (2020). The concept of g*β-closed sets in topological spaces, *International Journal of Mathematical Archive, 11*(4), 14 – 23.

Punitha Tharani, A., & Sujitha, H. (2020). Soft g*β closed Sets in Soft Topological Spaces. *Journal of Mechanics of Continua and Mathematical Sciences, 15*(8), 188 – 195.

Sabih W. Askandar & Amir, Mohammed, A. (2020). I-soft separation axioms in soft topological spaces. *Tikrit Journal of Pure Science, 25* (6), 130 – 138.

Singh, A., & Noorie, N. S. (2017). Remarks on soft axioms. *Annals of Fuzzy Mathematics and Informatics, 11*(5), 503 – 513.

Tantawy, O., El-Sheikh, S. A., & Hamde, S. (2016). Separation axioms on soft topological spaces. *Annals of Fuzzy Mathematics and Informatics, 14*(4), 511 - 525.

Terepeta, M. (2019). On separating axioms and similarity of soft topological spaces. *Soft Computing, 23*(3), 1049 – 1057.

Xuechong, G. (2021). *Comparison of two types of separation axioms in soft topological spaces*. Jiangsu Normal University.

Author Information

Raja Mohammad Latif
Prince Mohammad Bin Fahd University,
Al Khobar, Kingdom of Saudi Arabia.
Contact e- mail: *rlatif@pmu.edu.sa,*

To cite this article:

Latif, R. M. (2023). Soft G*β-separation axioms in soft topological spaces. *The Eurasia Proceedings of Science, Technology, Engineering & Mathematics (EPSTEM), 25,* 76-96.

The Eurasia Proceedings of Science, Technology, Engineering & Mathematics (EPSTEM), 2023

Volume 25, Pages 97-102

ICBAST 2023: International Conference on Basic Sciences and Technology

On Fixed Point Results for Nonlinear Contractions in Fuzzy Cone Metric Space

Dritan Gerbeti
University of Shkodra

Eriola Sila
University of Tirana

Sidite Duraj
University of Shkodra

Abstract: The study of Fixed Point Theory in various metric space has been on focus of scientific development for many authors. It has been advanced either by generalizing the contractive inequality or by extending the conditions of metric. Fuzzy metric space has been defined as space in which the distance between elements is not an exact number in difference with metric space. Fixed point Theory is an important framework point of view in fuzzy metric spaces. Many studies have been showed the existence and uniqueness of a fixed point for different type of contractions in these spaces. Nonlinear contractions and their generalizations have been under investigations in several metric spaces. The aim of this paper is the study of fixed points for generalized nonlinear contractions in fuzzy metric space. Our results guarantee the existence and uniqueness of a fixed point for these contractions and extend some known theorems in metric space to fuzzy metric space. As an application of main theorem an example is taken.

Keywords: Fixed point, Fuzzy cone metric space, Generalized nonlinear contraction, Auxiliary function

1. Introduction

The Fuzzy metric space was introduced by Kramosil and Michalek (1975) as an approach of probabilistic space in Fuzzy sets Theory studied by Zadeh (1965). In 1994, George and Veeramani defined GV Fuzzy metric space by replacing the last condition of Fuzzy metric with a stronger one. The concept of cone metric space was introduced by Huang and Zhang (2007) by generalizing metric using a subset of an ordered Banach space.

In 2015, Öner et al. generalized GV Fuzzy metric space to Fuzzy cone metric space. They studied the topology of this space, its metrizability (Oner et al., 2016) and showed some fixed-point results in them (Oner et al., 2016). There are many authors, who have given their contribution in studying Fixed point theory on Fuzzy cone metric spaces. (Rehman & Li, 2017; Chen et al., 2020) .In this paper, we establish and prove some fixed point results on fuzzy cone metric space related to generalized nonlinear contractions.

2. Preliminaries

Firstly, we begin with some main concepts on Fuzzy metric.

- Selection and peer-review under responsibility of the Organizing Committee of the Conference

Definition 2.1 Schweizer and Sklar (1960) A continuous t-norm is called an operation $*: [0,1] \times [0,1] \rightarrow [0,1]$ that satisfies the following conditions:

1. $*$ is associative, commutative and continuous;
2. For each $u_{0,}, u_1, v_0, v_1 \; \in [0,1] u_0 \leq u_1 and \; v_0 \leq v_1$ it yields $1 * u_0 = v_0,\; u_0 * v_0 \leq u_1 * v_1$

Examples (Schweizer and Sklar 1960)

The operations defined as below:

$*: [0,1] \times [0,1] \rightarrow [0,1]$

1. $U * V = UV$ (t-norm product)
2. $U * V = max\{\mathrm{U} + \mathrm{V}, -1, 0\}$ → Lukasiericz t-norm)

are continuous t-norms.

Definition 2.2 (Kramosil & Michalek ,1975) Let X be an arbitrary set, $*$ is a continuous t-norm, M is a Fuzzy set on $X^2 \times (0, \infty)$. The 3 – tuple (X, M, $*$) is called a Fuzzy metric space if it completes the conditions below:

$(FM_1)\; For\; each\; x, y \in X,\; t \in (0, \infty)\; M(x, y, t) > 0;$
$(FM_2)\; For\; each\; x, y \in X^2 \times (0, \infty), M(x, y, t) = M(y, x, t);$
(FM_3) $M(x, y, t) \; * M(y, z, s) \leq M(x, z, t + s)$ for each $x, y \in X^2$ and $t, s \in (0, \infty)$;
(FM_4) $M(x, y, \cdot): (0, \infty) \rightarrow [0,1]$ is left continuous.

In 1994, George and Veeramani generalized the concept of Fuzzy metric space to GV Fuzzy metric space as follows.

Definition 2.3 Let X be an arbitrary set, , $*$ is a continuous t-norm, M is a Fuzzy set on $X^2 \times (0, \infty)$.
Is a continuous t-norm, and M a Fuzzy set on $X^2 \times [0, \infty)$.

$(X, M, *)$ is called GV-fuzzy metric space if it satisfies the following conditions:
(GVFM$_1$) For each $(x, y, t) \in X^2 \times [0, \infty), M(x, y, t) > 0;$
(GVFM$_2$) For each $(x, y, t) \in X^2 \times [0, \infty),\; M(x, y, t) = 1$ iff $x = y$;
(GVFM$_3$) For each $(x, y, t) \in X^2 \times [0, \infty),\; M(x, y\,, t) = M(y, x, t)$;
(GVFM$_4$) For each $(x, y, t, s) \in X^2 \times [0, \infty) \times [0, \infty),\; M(x, y\,, t + s) \geq M(x, y, t) * M(x, y, s)$.
(GVFM$_5$) For each $(x, y) \in X^2$ the function $M(x, y, \cdot): (0, \infty) \rightarrow \; [0,1]$ is continuous.

Below, there is given the concept of cone.

Let E be a real Banach space.

Definition 2.4 (Huang & Zhang, 2007) The subset $P \subseteq E$ that satisfies the following conditions:

1. P is closed, P≠ Φ and P≠ {0};
2. For each $\alpha, \beta \in [0, \infty)$ and x, y$\in P, then\; \alpha x + \beta y \in P$;
3. For each x$\in P, if\; (-x) \in P\; then\; x = 0$.

Is called a cone.
In the cone P a partial ordering "≤" is defined as below: For every $x, y \in P\; x \leq y$ iff $x - y \in int\; P$.

Suppose that $int\; P \neq \Phi$.

Definition 2.5 (Öner et al., 2015)

Let $P \subseteq E$ be a cone with nonempty interior, X be an arbitrary set, $*$ a continuous t-norm and M a fuzzy set on $X \times X \times int\; P$. The 3-tuple $(X, M, *)$ is called a Fuzzy cone metric space if it satisfies the following conditions:

(FCM$_1$): For each $(x, y) \; \in X \times X\,,\; t \in int\; P\,,\; M(x, y, t) > 0$ and $M(x, y, t) = 1$ iff $x = y$;

(FCM$_2$): For each $(x, y, t) \in X \times X \times int\ P$, $M(x, y, t) = M(y, x, t)$;
(FCM$_3$): For each $x, y, z \in X$ and $t, s \in Int\ P$, $M(x, y, t) * M(y, z, x) \leq M(x, z, t + s)$;
(FCM$_4$): $M(x, y, \cdot)$: $int\ P \to [0, 1]$is continuous.

Below, there are given the definition of convergent sequences, Cauchy sequences (Öner et al. 2015) in a Fuzzy cone metric space.

Let $(X, M, *)$ be a Fuzzy cone metric space and $(xn)\ n \in N$ a sequence in X and $x \in X$.
The sequence $(x_n)_{n\in N}$ is called convergent to x if for each $r \in (0, 1)$ there exist a natural number $n_0 \in N$, such that for every natural number $n > n_0$, $M(x_n, x, t) > 1 - r$ for $t > 0$.
The sequence $(x_n)_{n\in N}$ is called Cauchy if for each $r \in (0, 1)$, there exist $n_0 \in N$ that for each $n, m > n_0$, $M(x_n, x_m, t) > 1 - r$.
A Fuzzy cone metric space is called complete if every Cauchy sequence is convergent on it.

Definition 2.6 (Alam et al., 2022)

Let $\varphi: [0, \infty) \to [0, \infty)\ and\ \psi: [0, \infty) \to [0, \infty)$ such that $\varphi(0) = 0$

1. $\varphi\ is\ right\ continuous$;
2. $\varphi\ is\ monoton\ increasing$;
3. $\psi(t)>0$, $t>0$
4. $\lim_{t\to r} inf\ \psi(t) > 0, for\ every\ r > 0$.

The function $T: X \to X$ that satisfies the inequality

$$\varphi(d(Tx, Ty) \leq \varphi(d(x, y)) - \psi(d(x, y))$$

is called generalized nonlinear contraction in metric space (X, d).

Initiating from above we extend this concept to fuzzy metric spaces
The function $T: X \to X$ that satisfies the inequality:

$$\varphi\left(\frac{1}{M(Tx, Ty, t)} - 1\right) \leq \varphi\left(\frac{1}{M(x, y, t)} - 1\right) - \psi\left(\frac{1}{M(x, y, t)} - 1\right)$$

For every $x, y \in X$ is called generalized nonlinear contraction on Fuzzy cone metric space $(X, M, *)$

3. Main Results

In this section, we prove some fixed point results related to generalized nonlinear contractions on Fuzzy cone metric space.

Theorem 3.1 Let$(X, M, *)$ be a complete Fuzzy metric space and $T: X \to X$ a continuous generalized nonlinear contraction. Then it has a unique fixed point on X.

Proof. Let x_0 be an arbitrary element of X and $\{x_n\}_{n\in N}$ is the iterative sequence constructed as follows:
$x_1 = Tx_0, x_2 = Tx_1, \dots, x_n = Tx_{n-1}, \dots$.

If there exist any $x_k \in X$ such that $x_k = x_{k+1}$, then $Tx_k = x_k$ and x_k is the fixed point of function T.

Suppose that for each $n \in N, x_{n+1} \neq x_n$, and see

$$\varphi\left(\frac{1}{M(x_{n+1}, x_n, t)} - 1\right) \leq \varphi\left(\frac{1}{M(x_n, x_{n-1}, t)} - 1\right) - \psi\left(\frac{1}{M(x_n, x_{n-1}, t)} - 1\right) \leq \varphi\left(\frac{1}{M(x_n, x_{n-1}, t)} - 1\right).$$

As a result, we have that $\frac{1}{M(x_{n+1}, x_n, t)} - 1 \leq \frac{1}{M(x_n, x_{n-1}, t)} - 1$, for each $n \in N$, and the sequence $\left\{\frac{1}{M(x_n, x_{n-1}, t)} - 1\right\}_{n\in N}$ is monotone decreasing.

This sequence is bounded from below by zero $\frac{1}{M(x_n,x_{n-1},t)} - 1 > 0$.

As a consequence, it is convergent to a point $m \geq 0$

$$\lim_{n\to\infty}\left(\frac{1}{M(x_n, x_{n-1}, t)} - 1\right) = m \geq 0$$

Let us prove that $m = 0$.

Suppose that $m > 0$. Since φ is continuous we have $\lim_{n\to\infty} sup\ \varphi\left(\frac{1}{M(x_n,x_{n-1},t)} - 1\right) = \varphi(m)$
Using the following inequality

$$\lim_{n\to\infty}\varphi\left(\frac{1}{M(x_{n+1}, x_n, t)} - 1\right) \leq \varphi\left(\frac{1}{M(x_n, x_{n-1}, t)} - 1\right) - \psi\left(\frac{1}{M(x_n, x_{n-1}, t)} - 1\right)$$

we take

$$\lim_{n\to\infty} sup\ \varphi\left(\frac{1}{M(x_{n+1}, x_n, t)} - 1\right) \leq \lim_{n\to\infty} sup\ \varphi\left(\frac{1}{M(x_n, x_{n-1}, t)} - 1\right) + \lim_{n\to\infty} sup\ -\psi\left(\frac{1}{M(x_n, x_{n-1}, t)} - 1\right) =$$

$= \lim_{n\to\infty} sup\ \varphi\left(\frac{1}{M(x_n,x_{n-1},t)} - 1\right) - \lim_{n\to\infty} inf\ \psi\left(\frac{1}{M(x_n,x_{n-1},t)} - 1\right)$.

Consequently, the following relationship holds:

$\varphi(m) \leq \varphi(m) - \psi(\mathrm{m})$ and $\psi(\mathrm{m}) \leq 0$ which means that $m = 0$

As a results, $\lim_{n\to\infty}\frac{1}{M(x_{n+1},x_n,t)} - 1 = 0$

The next step is to show that the sequence $\{x_n\}_{n\in N}$ is Cauchy.
Suppose that the sequence $\{x_n\}_{n\in N}$ is not Cauchy.
As a result there exist $r_0 > 0$ and the sequence $\{x_{nk}\}_{k\in N}, \{x_{nl}\}_{l\in N}$ such that $m_k > m_l$ and $M(x_{nk}, x_{nl}, t) < 1 - r_0 \leq M(x_{nk}, x_{nl-1}, t)$ or $\frac{1}{M(x_n,x_{n-1},t)} - 1 > \frac{1}{1-r_0} - 1 = \frac{r_0}{1-r_0} \geq \frac{1}{M(x_{nk,}x_{nl},t)} - 1$.

From the inequality

$$\varphi\left(\frac{1}{M(x_{nk}, x_{nl}, t)} - 1\right) \leq \varphi\left(\frac{1}{M(x_{nk-1}, x_{nl-1}, t)} - 1\right) - \psi\left(\frac{1}{M(x_{nk-1}, x_{nl-1}, t)} - 1\right)$$

and using $\lim_{n\to\infty} sup\ \varphi\left(\frac{1}{M(x_{nk,}x_{nl},t)} - 1\right) = \varphi\left(\frac{r_0}{1-r_0}\right)$,

we have

$$\varphi\left(\frac{r_0}{1 - r_0}\right) \leq \varphi\left(\frac{r_0}{1 - r_0}\right) - \lim_{n\to\infty} inf\ \psi\left(\frac{1}{M(x_{nk-1}, x_{nl-1}, t)} - 1\right)$$

Which yields $\lim_{n\to\infty} inf\ \psi\left(\frac{1}{M(x_{nk-1},x_{nl-1},t)} - 1\right) \leq 0$,which is contradiction.

Consequently, the sequence $\{x_n\}_{n\in N}$is Cauchy.

Since $(X, M,*)$ is complete, it yields that the sequence $\{x_n\}_{n\in N}$ converges to a point x^*, so $\lim_{n\to\infty} x_{n+1} = x^*$
Since T, is continuous, we have

$$\lim_{n\to\infty} x_{n+1} = \lim_{n\to\infty} Tx_n = Tx^*.$$

From the uniqueness of the limit, we have $Tx^* = x^*$.
As a result, x^* is a fixed point of function T.

The next step is to prove the uniqueness of fixed point x^* of T.
Suppose that there exist, another fixed point $y^* \in X$, $x^* \neq y^*$such that $Ty^* = y^*$
From the inequality

$$\varphi\left(\frac{1}{M(Tx^*, Ty^*, t)} - 1\right) \leq \varphi\left(\frac{1}{M(x^*, y^*, t)} - 1\right) - \psi\left(\frac{1}{M(x^*, y^*, t)} - 1\right)$$

we have that

$$\varphi\left(\frac{1}{M(x^*,y^*,t)} - 1\right) \leq \varphi\left(\frac{1}{M(x^*,y^*,t)} - 1\right) - \psi\left(\frac{1}{M(x^*,y^*,t)} - 1\right).$$

As a result, $\psi\left(\frac{1}{M(x^*,y^*,t)} - 1\right) \leq 0$ which is a contradiction, consequently $x^* = y^*$.

Corollary 3.2 Let $(X, M,*)$ be a complete Fuzzy cone metric space and T is a nonlinear contraction that satisfies the inequality

$$\frac{1}{M(Tx, Ty, t)} - 1 \leq \frac{1}{M(x, y, t)} - 1 - \psi\left(\frac{1}{M(x, y, t)} - 1\right)$$

Then the function T has a unique fixed point x^* in X.

Proof. Taking $\varphi(t) = t$ in the inequality

$$\varphi\left(\frac{1}{M(Tx, Ty, t)} - 1\right) \leq \varphi\left(\frac{1}{M(x, y, t)} - 1\right) - \psi\left(\frac{1}{M(x, y, t)} - 1\right)$$

We are in condition of Theorem 3.1. As a result, the function T has a unique fixed point.

Corollary 3.3 Let $(X, M,*)$ be a complete Fuzzy metric space and $T: X \to X$ a function that satisfies the Banach inequality

$$\frac{1}{M(Tx, Ty, t)} - 1 \leq k\left(\frac{1}{M(x, y, t)} - 1\right)$$

for $0 < k < 1$. Then the function T has a unique fixed point.

Proof. By replacing $\psi(t) = (1 - k)t$ in inequality of Corollary 3.2, the result is clear.

Example 3.4

Let $X = (0, \infty)$, $*$ be a continuous t-norm, and $M: X^2 \times (0, \infty) \to [0,1]$, $M(x, y) = \begin{cases} 1, & x = y \\ \frac{min(x,y)}{max(x,y)} s(t) , & x \neq y \end{cases}$ where $s(t) = \begin{cases} t, & t \leq 1 \\ 1, & t > 1 \end{cases}$. Taking the cone $P =]0, \infty[$ with $int\ P \neq 0$, $(X, M,*)$ is a complete Fuzzy cone metric space.
Choosing $\varphi(t) = \frac{t}{2}$, $\psi(t) = \frac{2}{5}t$, $Tx = \frac{1}{10}x + \frac{1}{10}$, we see that

$$\varphi\left(\frac{1}{M(Tx,Ty,t)} - 1\right) \leq \varphi\left(\frac{1}{M(x,y,t)} - 1\right) - \psi\left(\frac{1}{M(x,y,t)} - 1\right).$$

Consequently, we are in conditions of Theorem 3.1, and the function T has a unique fixed point $x = \frac{1}{9}$

Conclusions

In this paper, there are studied the existence and uniqueness of a fixed point for generalized nonlinear contractions in Fuzzy cone metric spaces. Our results are the extensions of Jachemsky (1997) and Sutfa and Choudhury (2008) on Fuzzy cone metric spaces.

Scientific Ethics Declaration

The authors declare that the scientific ethical and legal responsibility of this article published in EPSTEM journal belongs to the authors.

Acknowledgements or Notes

* This article was presented as an oral presentation at the International Conference on Basic Sciences and Technology (www.icbast.net) held in Antalya/Turkey on November 16-19, 2023.

References

Alam, A., Sk, F., & Khan, H. Q. (2022) Discussion on generalized nonlinear contractions. U.*P.B. Sci. Bull. Series A, 84*(2), 23-34.

Chen, GX., Jabeen, S., Rehman, S.U., Kanwal, A., Abbas, F., Ullah, H., & Khalil, A. M. (2020). Coupled fixed point analysis in fuzzy cone metric spaces with an application to nonlinear integral equations. *Advances in Difference Equations, 671*. https://doi.org/10.1186/s13662-020-03132-8

Dutta, P. N., & Choudhury, B. S. (2008). A generalization of contraction principle in metric spaces, *Fixed Point Theory Applications*, *2008*(1), 1-8.

George, A., & Veeramani, P. (1994). On some results in fuzzy metric spaces. *Fuzzy Sets and Systems, 64*(3), 395-399.

Huang, L.G., & Zhang, X. (2007). Cone metric spaces and fixed point theorems of contractive mappings. *Journal of Mathematical Analysis and Applications, 332*(2), 1468-1476.

Jachymski, J. (2011) Equivalent conditions for generalized contractions on (ordered) metric spaces. *Nonlinear Analysis, 74*(3), 768-774.

Kramosil, I. & Michalek, J. (1975). Fuzzy metric and statistical metric spaces. *Kybernetika, 11*(5), 326-334.

Zadeh, L. A. (1965). Fuzzy Sets. *Information and Control, 8*(3), 338-353.

Oner, T. Kandemire, M. B., & Tanay, B. (2015) Fuzzy cone metric spaces. *Journal of Nonlinear Sciences and Applications, 8*(5), 610–616.

Oner, T. (2016). On the metrizability of fuzzy cone metric spaces. *International Journal of Management and Applied Science, 2*(5), 133–135.

Oner, T. (2016). On some results in fuzzy cone metric spaces. *International Journal of Advanced Computational Engineering and Networking, 4*(5), 37– 39.

Rehman, S.U., & Li, H. X. (2017). Fixed point theorems in fuzzy cone metric spaces. *Journal of Nonlinear Sciences and Applications.JNSA, 10*(11), 5763–5769.

Schweizer, B. & Sklar, A. (1960) Statistical metric spaces. *Pacific Journal of Math., 10*(1), 313-334.

Author Information

Dritan Gerbeti
University of Shkodra
Shkoder, Albania
Contact e-mail: *tangerbeti@gmail.com*

Eriola Sila
University of Tirana
Tirana, Albania

Sidite Duraj
University of Shkodra
Shkoder, Albania

To cite this article:

Gerbeti, D., Sila, E., & Duraj, S. (2023). On fixed point results for nonlinear contractions in fuzzy cone metric space. *The Eurasia Proceedings of Science, Technology, Engineering & Mathematics (EPSTEM), 25,* 97-102.

The Eurasia Proceedings of Science, Technology,
Engineering & Mathematics (EPSTEM)
ISSN: 2602-3199

The Eurasia Proceedings of Science, Technology, Engineering & Mathematics (EPSTEM), 2023

Volume 25, Pages 103-111

ICBAST 2023: International Conference on Basic Sciences and Technology

DFT Study of a Series of Nicotinic Acid Benzylidenehydrazide Derivatives: Structure, Stability and Reactivity

Noura Kichou
Mouloud Mammeri University of Tizi-Ouzou (UMMTO)

Nabila Guechtouli
Mouloud Mammeri University of Tizi-Ouzou (UMMTO)

Manel Taferguennit
University of Sciences and Technology Houari Boumediene

Zakia Hank
University of Sciences and Technology Houari Boumediene

Abstract: Hydrazones especially nicotinic acid benzylidenehydrazide derivatives constitute an important class of compounds that has received much interest in recent years, due to their diverse biological characteristics, such as antimicrobial, anticonvulsant, analgesic, anti-inflammatory, antiplatelet, antituberculous and antitumor activities. These compounds have donor sites such as N and O which have non-bonding doublets which allow them to coordinate with metal ions. For this purpose, ten hydrazones structures were optimized in the DFT method, using the B3LYP functional, with the basis 6-31G** for all atoms, in the gas phase using the Gaussian 09 program. The structural, energetic (energies, EHOMO-LUMO gaps), electronic (dipolar moments, atomic charges) parameters were determined. A study of the stability of the ligands was carried out based on the relative energies to study the chemical reactivity of the optimized structures, we calculated the global reactivity parameters (ionization potential, electronic affinity, electronic chemical potential, absolute hardness, overall softness and overall electrophilicity). The results obtained show that All the systems considered are stabilized by two types of electronic effect. Either; an inductive attractor effect, with a coexistence of mesomeric effects. Analysis of chemical hardness values indicates that the most stable isomers found are the hardest, with larger HOMO/LUMO gaps, and therefore less reactive. As a result, charge transfer will be predominant. The most nucleophilic systems are also determined based on the calculation of the eletrophicity and nucleophilicity indices.

Keywords: Hydrazones, DFT, Reactivity, Stability.

Introduction

Hydrazones were the subject of many interesting studies due to their important applications in much synthetic areas especially in indicators-chemistry. Hydrazones are being used extensively in detection and quantitative determination of several metals, for the preparation of compounds having diverse structures, analytical chemistry for the identification and isolation of carbonyl compounds (Mıtu, 2012). A number of nicotinic acid benzylidenehydrazide derivatives have been synthesized from isoniazid and were found to have potentiated activities against various bacterial and fungal strains (Maccari, 2005) including hydrazones with benzohydrazide and menthone (Al-Khattaf, 2021), Furthermore, metal complexes of isonicotinic hydrazones including, copper, zinc, manganese, nickel showed enhanced activities against microbes, tumor and free radicals (Jabeen, 2018).

- Selection and peer-review under responsibility of the Organizing Committee of the Conference

Nowadays many inorganic chemists have been made citing the successes of different density functional theory (DFT) methods compared to the experimental methods, in computing the molecular structure and reactivity of synthesized compounds, which are very important in order to disclose the relationship between the structure and chemical properties with their biological activity. These compounds coordinate at the metallic ions by oxygen amide (O=C) and the azomethine nitrogen (Ashma,2022). Quantum chemical calculations have been performed in order to compare the structural parameters to that of theoretical data.

Method

Computational Method and Quantum Mechanical Analysis

Full geometry optimization have been made with density functional theory (DFT) using Kohn–Sham's Density Functional Theory subjected to the gradient-corrected hybrid density functional B3LYP. This functional is a is the combinaison of Becke's three parameters hybrid method and the Lee-Yang-Parr correlation functional (B3LYP) (Lee, 1988), and 6-31G (d,p) for all others atoms (H, N, C, O) (Pearson, 1985) in gas phase, as implemented by Gaussian 09 program (Fresch, 2009), without any constraint of symmetry, followed by a calculation of the normal modes of vibration, to make sure that the stationary points were minima. Our complexes are all minima in their potential energy surface. Indeed, the analysis of the frequencies of the normal modes of vibration gives no imaginary frequency. We used the GaussView program to draw the optimized geometries and to visualize the the normal modes vibrations (Fresch, 2009).

We have determined the structure, the electronic parameters, the energies and the gaps E_{HOMO}/E_{LUMO}. Natural bond orbitals (NBO) atomic charges were also reported. The theoretical results obtained are compared with the available experimental data.

In order to study the chemical reactivity of the ligand and its optimized complexes, we calculated the following parameters of several global reactivity descriptors by means of DFT, such as: the ionization potential (I), the electron affinity (A), electronic chemical potential (μ), the absolute hardness (η), the global softness (S) and the global electrophilicity (ω) (Gazquez, 2008). The electronic chemical potential(μ) is defined by Parr and Pearson (Parr, 1983):

$$\mu = -\frac{1}{2}(I + A) = -\chi \qquad (1)$$

Were χ is the electronegativity given by Mulliken.
The global hardness is defined by (Parr, 1991):

$$\eta = \frac{1}{2}(I - A) \qquad (2)$$

The global softness *S* is obtained from:

$$S = \frac{1}{2\eta} \qquad (3)$$

The global electrophilicity (ω) measures the affinity of compounds given by Parr (Parr, 1999) is calculated by:

$$\omega = \frac{\mu^2}{2\eta} \qquad (4)$$

The nucleophilicity index equal to the negative of the ionization potential:

$$Nu = -I \qquad (5)$$

A high value of the nucleophilicity index Nu characterizes a good nucleophile, while a low value indicates a good electrophile.

Results and Discussion

Geometry

Figure 1 shows the optimized structures of a series of nicotinic acid benzylidene hydrazide derivatives (A-J) and all geometric parameters are depicted in Tables 1,2 and 3.

The tables 1,2 and 3 show that in all ligands studied, the 1C-6N and 3C-11C distances are shorter than their 11C-13N and 15C-17N counterparts, respectively, confirming their double bond character. The lengths of the CO double bond are between 1.21 and 1.26 Å. these values are in agreement with the average value for a CO double bond. We notice the absence of the CO single bond. Indeed, there has been an electronic delocalization in the system considered. The analysis of dihedral angles confirms the flatness of the molecules.

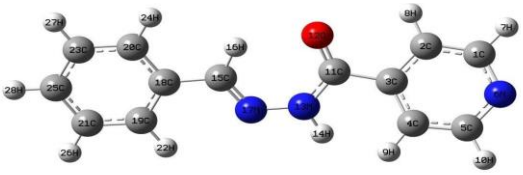

A

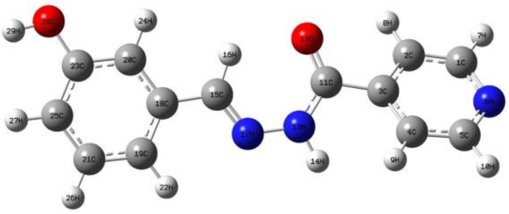

B

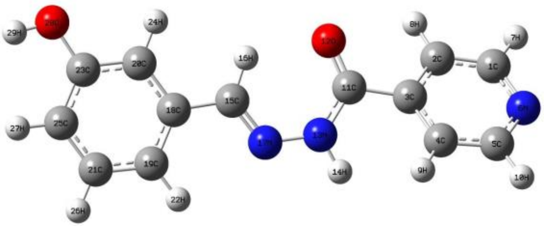

C

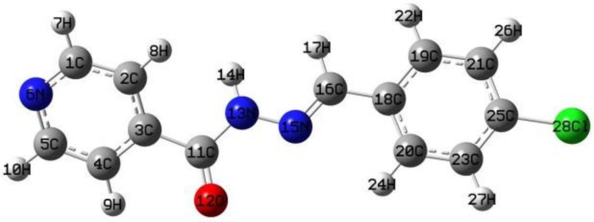

D

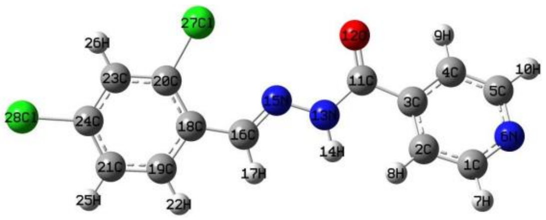

E

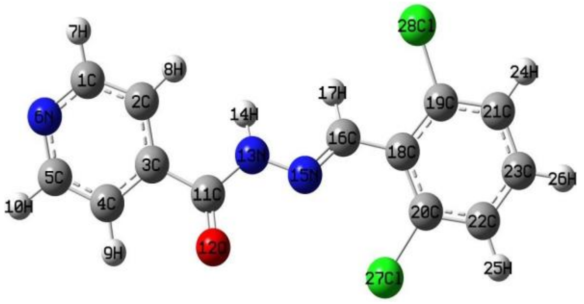

F

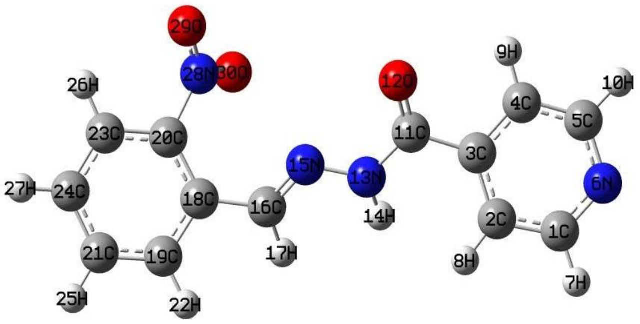

G

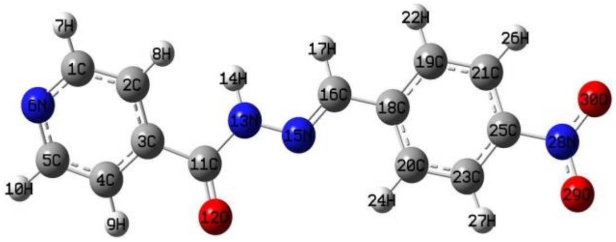

H

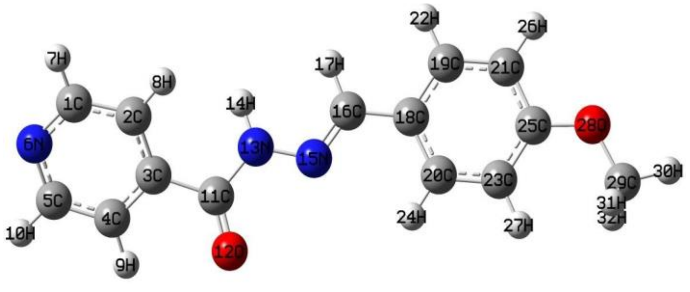

I

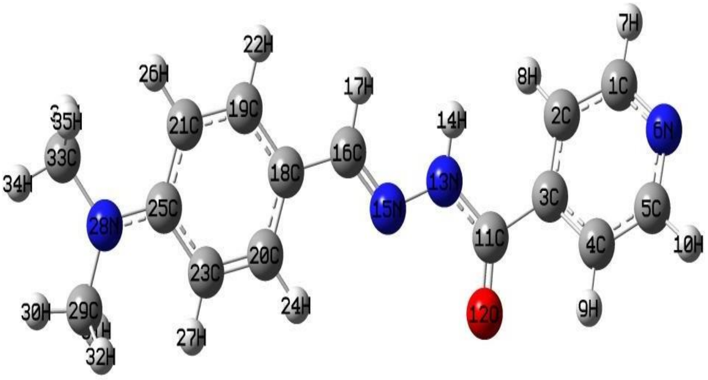

J

Figure 1. The optimized structures of the optimized structures A-J

Table1. Structural parameters (angles) at DFT/B3LYP.

	A	B	C	D	E	F	G	H	I	J
H8C2C3	119.6	119.6	121.8	121.9	121.8	121.8	121.9	121.8	121.7	121.7
C1C2C3	118.7	118.7	118.7	118.7	118.9	118.6	118.6	118.8	118.7	118.7
C2C3C11	117.6	117.6	124.5	124.1	124.2	124.4	124.5	124.1	124.5	124.6
C3C11O12	121.4	121.3	122.0	122.1	121.9	122.2	122.3	122.2	122.0	121.8
N13C11O12	124.2	114.3	123.8	123.6	121.9	123.6	123.5	122.9	123.8	124.1
C11N13H14	117.7	124.2	119.2	119.3	119.5	119.3	119.3	119.6	119.2	119.2
N13N17C15	120.6	119.5	116.8	117.1	120.6	116.3	120.5	118.5	120.8	121.0
N17C15C18	119.7	117.7	116.4	116.6	114.6	123.3	121.3	120.9	122.2	121.1
C18C20H24	119.3	121.2	118.7	119.1	119.9	115.5	118.5	118.6	118.7	118.7
N17C15H16	122.5	111.0	121.3	121.4	120.5	121.0	122.1	121.8	121.3	121.1
C19C21H26	119.7	118.8	120.2	120.7	118.9	119.6	119.7	121.8	121.4	118.8

Table 2. Structural parameters (dihedral angles) at DFT/B3LYP

	A	**B**	**C**	**D**	**E**
C1C2C3C4	1.3	1.3	-0.9	-0.7	-1.0
C1C2C3C11	179.7	179.7	-179.1	-178.8	-179.1
N6C1C2C3	-0.7	-0.7	-0.1	-0.2	-0.0
C5N6C1C2	0.3	0.3	-0.8	-0.8	-0.7
C2C3C11O12	-24.7	-25.0	-27.1	-29.7	-25.5
C2C3C11N13	154.4	154.1	153.5	150.7	155.6
O12C11N13H14	171.7	171.6	169.3	170.2	170.7

Table 3. Optimized structural parameters at DFT

	A	B	C	D	E	F	G	H	I	J
20C=23C	1.394	1.397	1.384	1.390	1.396	1.394	1.391	1.390	1.390	1.383
3C-11C	1.507	1.376	1.507	1.506	1.499	1.506	1.505	1.497	1.507	1.508
15C=17N	1.290	1.289	/	/	/	1.283	1.281	1.295	1.285	1.286
11C-13N	1.376	1.376	1.383	1.385	1.391	1.389	1.391	1.394	1.382	1.380
11C=12O	1.226	1.226	1.218	1.219	1.240	1.215	1.214	1.240	1.218	1.219
1C=6N	1.340	1.340	1.337	1.338	1.350	1.337	1.337	1.350	1.337	1.337
13N-14H	1.008	1.008	1.017	1.017	1.017	1.017	1.017	1.017	1.017	1.017
17N=15C	1.290	1.289	/	/	/	/	/	/	/	/
17N=13N	1.373	1.373	/	/	/	/	/	/	/	/
16C=15N	/	/	1.285	1.284	1.294	1.283	1.286	1.281	1.295	1.285
15N=13N	/	/	1.361	1.358	1.369	1.354	1.363	1.352	1.366	1.361

Energetic Properties

The calculated dipole moment, HOMO, LUMO and gap energy are listed in Table 4

The two isomers B and C are very close in energy. The isomer F is more stable than the isomer E (difference 167.3 Kcal/mole) and the H structure of H is less stable than the G structure . structure of H is less stable than G structure (difference 184.5 Kcal/mole). Compound G is the most polar. Indeed, it has the largest dipole moment (7.20 D), because the polarity of the two carbon-nitrogen bonds adds up.

Table 4. Eenergetic properties of the compounds A-G at DFT.

Compound	Energy (u a)	Related energy kcal/mole	HOMO/LUMO (eV)	Dipole Moment (D)
A	-741.47718727	/	2,721	1.94
B	-816.69699792	0	2,811	3.17
C	-816.69649090	0,31814757	4,048	5.95
D	-1201.09804047	/	2,309	4.16
E	-1660.38218807	167,3192664	2,248	5.47
F	-1660.64882886	0	2,318	4.34
G	-945.95768193	0	2,763	7.20
H	-945.66365691	184,5036278	2,463	6.44
I	-856.00166548	/	2,572	4.18
J	-875.45149019	/	2,185	6.95

Mulliken Charges

The Mulliken charges calculated are listed in Table 5, We notice that oxygen atoms are more negatively charged than nitrogen atoms. Which confirms that they are more reactive with respect to nitrogen. In isomers B and C, the oxygen atoms of the OH group are richer in electrons, which explains the pronounced inductive attracting effect of the oxygen atom. In the E and F isomers, we note that the carbon atoms which are closer to those of chlorine are more negatively charged, compared to those of the D isomer. Indeed, the negative partial charges carried by the carbon atoms close are more important if the two chlorine atoms are involved.

Table 5. Mulliken charges calculated by DFT/B3LYP

	A	**B**	**C**	**D**	**E**	**F**	**G**	**H**	**I**	**J**
1C	0.090	0.091	0.092	0.584	-0.006	-0.093	0.091	0.093	-0.005	0.092
2C	-0.100	-0.101	-0.133	0.405	-0.124	-0.132	-0.133	-0.132	-0.124	-0.133
3C	0.050	0.051	0.054	0.089	-0.025	-0.053	0.054	0.053	0.026	0.054
4C	-0.131	-0.132	-0.102	0.824	-0.112	-0.101	-0.102	-0.100	-0.111	-0.102
5C	0.091	0.092	0.089	0.443	-0.005	-0.090	0.088	0.090	-0.005	0.089
6N	-0.420	-0.421	-0.422	-0.130	-0.353	-0.421	-0.424	-0.420	-0.351	-0.423
7H	0.107	0.108	0.103	0.150	0.152	0.106	0.102	0.105	0.155	0.103
8H	0.123	0.124	0.090	0.052	0.137	0.093	0.089	0.089	0.138	0.090
9H	0.095	0.096	0.125	0.182	0.181	0.126	0.123	0.129	0.182	0.124
10H	0.107	0.106	0.107	0.149	0.157	0.109	0.105	0.110	0.159	0.107
18C	0.089	0.087	0.091	-0.301	0.156	0.156	0.095	0.132	0.111	0.091
19C	-0.096	-0.102	-0.134	-0.533	-0.174	-0.153	-0.143	-0.141	-0.182	-0.131
20C	-0.126	-0.143	-0.111	0.246	-0.283	-0.137	-0.123	0.199	-0.149	-0.119
12O	-0.509	-0.507	-0.475	-0.397	-0.399	-0.463	-0.481	-0.457	-0.401	-0.477
28O	/	-0.578	-0.549	/	/	/	/	/	/	-0.514
29O	/	/	/	/	/	/	/	-0.369	-0.288	/
30O	/	/	/	/	/	/	/	-0.377	-0.514	/

Frontier Molecular Orbital (FMO)

All the HOMO/LUMO energy gaps obtained for the ligands studied are small, which confirms their good reactivity. The CO fragment mainly contributes to the HOMO, this indicates how electron delocalization can involve the entire system. Although there is some residual pπ contribution from the atoms at its left and right sides. Indeed, this molecular orbital involved has a π character which extends over the molecule. While the LUMO of all systems is located practically on all the atoms constituting the molecules, with an almost homogeneous distribution.

Table 6. FMO for the studied structures.

Molecules	HOMO	LUMO
A	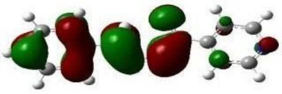	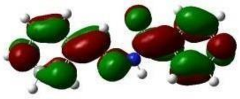
B	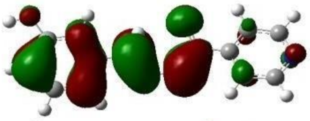	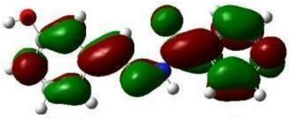
C	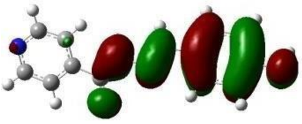	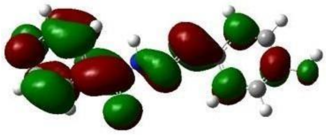
D	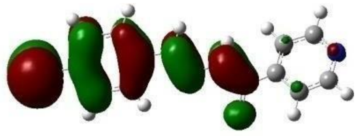	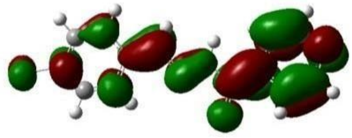
E	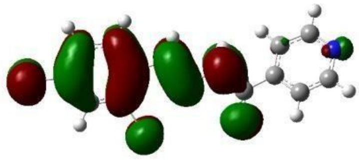	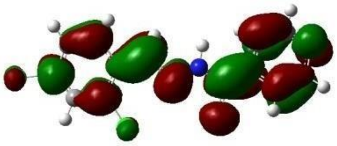
F	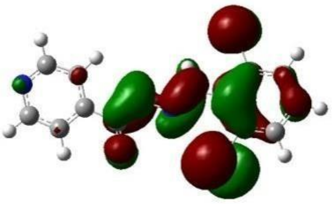	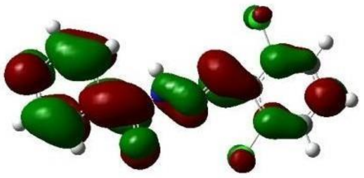
G	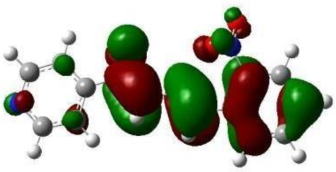	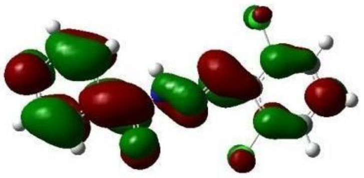
H	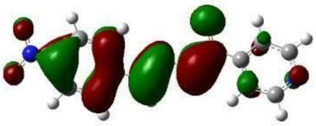	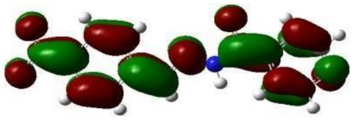
I	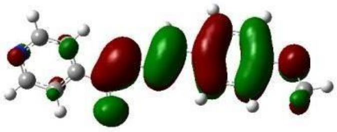	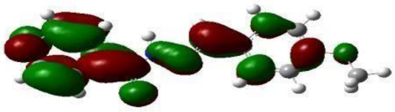
J	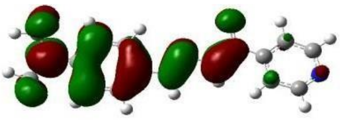	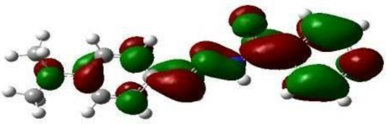

Reactivity

The parameters μ, η, S, ω and Nu were calculated using the equations 1-5. The results are summarized in the Table 7. Analysis of chemical hardness values indicates that the most stable isomers found are the hardest, with larger HOMO/LUMO gaps, and therefore less reactive. Note that the isomer J is the softest. Therefore, the charge transfer will be predominant. The values of μ and ω indicate that compounds F and G are more electrophilic than the others. While system J is the least electrophilic and the most nucleophilic according to the values of Nu.

Table 7. The parametersμ,η, S, ω and Nu of the studied structures

	EH	**EL**	**I**	**A**	μ	η	**S**	ω
A	-6,1587	-1,9038	6,1587	1,9038	-2,1274	2,1274	0,2350	4,8142
B	-5,9804	-1,8837	5,9804	1,8837	-2,0483	2,0483	0,2441	4,2972
C	-5,8087	-1,7604	5,8087	1,7604	-2,0241	2,0241	0,2470	4,1466
D	-6,5695	-2,4031	6,5695	2,4031	-2,0831	2,0831	0,2400	4,5202
E	-6,6392	-2,3327	6,6392	2,3327	-2,1532	2,1532	0,2322	4,9918
F	-6,5206	-2,0897	6,5206	2,0897	-2,2154	2,2154	0,2256	5,4368
G	-6,6754	-2,3615	6,6754	2,3615	-2,1569	2,1569	0,2318	5,01743
H	-6,9692	-3,1988	6,9692	3,1988	-1,8852	1,8852	0,2652	3,3502
I	-5,7293	-1,7425	5,7293	1,7425	-1,9934	1,9934	0,2508	3,9605
J	-5,1236	-1,5672	5,1236	1,5672	-1,7781	1,7781	0,2811	2,8112

Conclusion

The reactivity of a molecule is linked to its structure and electronic properties. The reactivity indices indicate that all the ligands studied have good chemical reactivity, which will allow their complexation. Quantum chemistry has made it possible to characterize and better understand the electronic properties of these molecules. A chemical group can exert effects of different natures on the distribution of the electronic density of a molecule. There are different types of electronic effects coexistence of both inductive and mesomeric effects. , in the case of isomers containing a single group, the distances are influenced, and the most stable geometry is the one which most allows delocalization under the control of the mesomeric effect.

In the case of a single grouping, the inductive effect prevails by favoring the structure with free rotation. The reactivity of a molecule is linked to its structure and electronic properties. The reactivity indices indicate that all the ligands studied have good chemical reactivity, which will allow their complexation.

Scientific Ethics Declaration

The authors declare that the scientific ethical and legal responsibility of this article published in EPSTEM journal belongs to the authors.

Acknowledgements or Notes

* This article was presented as a poster presentation at the International Conference on Basic Sciences and Technology (www.icbast.net) held in Antalya/Turkey on November 16-19, 2023.

References

Al-Khattaf, F.S, Mani, A, Hatamleh, A. A., & Akbar, I. (2021). Antimicrobial and cytotoxic activities of isoniazid connected menthone derivatives and their investigation of clinical pathogens causing infectious disease. *Journal of Infection and Public Health, 14*(4), 533–542.

Ashma, A., Subramani, A., Tamilarasan, R., & Karnan, M. (2022). Synthesis of new nicotinic acid hydrazid metal complexes: Potential anti-cancer drug, supramolecular architecture, antibacterial studies and catalytic properties. *Journal of Molecular Structure, 1250*(6).

Azquez, J. L. (2008). Perspectives on the density functional theory of chemical reactivity. *Journal of the Mexican Chem. Soc., 52(1),* 3.

Fresch, A., Nielson, A. B., & Holder, A. J. (2009). *Gaussview user manual*. Gaussian.Inc., Pittsburgh.

Jabeen, M., Mehmood, K., Ain Khan, M., Aslam, N., Zafar, A.M., Noreen, S., Aslam, S., & Ghafoor. A. (2018). Microwave and conventional synthesis of Co (II), Cu (II) and Ni (II) metal complexes of some acid hydrazones with their spectral characterization and biological evaluation. *Pak. J. Pharm. Sciences, 31*(3), 1003- 1011.

Mitu, L., & Ravichandran, S. (2012). Transition metal complexes of isonicotinoyl- -hydrazone-4-diphenylaminobenzaldehyde: Synthesis, characterization and antimicrobial studies. *E-Journal of Chemistry, 9*(1), 365-372.

Parr, R. G., Szentpaly, L., & Liu, S. (1999). Electrophilicity index. *Journal of the American Chemical Society, 121*, 1922-1924.

Pearson, R. G. (1985). Absolute electronegativity and absolute hardness of Lewis acids and bases. *Journal of American Chemical Society, 107*(24), 6801-6806.

Author Information

Noura Kichou
University Mouloud Mammeri of Tizi-Ouzou
Tizi-Ouzou, Algeria
Contact e-mail: *noura.kichou@ummto.dz*

Nabila Guechtouli
University Mouloud Mammeri of Tizi-Ouzou
Tizi-Ouzou, Algeria

Manel Taferghennit
University of Sciences and Technology Houari Boumediene
Algiers, Algeria.

Zakia Hank
University of Sciences and Technology Houari Boumediene
Algiers, Algeria.

To cite this article:

Kichou, N., Guechtouli, N., Taferghennit, M., & Hank, Z. (2023). DFT study of a series of nicotinic acid benzylidenehydrazide derivatives: Structure, stability and reactivity. *The Eurasia Proceedings of Science, Technology, Engineering & Mathematics (EPSTEM), 25,* 103-111.

The Eurasia Proceedings of Science, Technology, Engineering & Mathematics (EPSTEM), 2023

Volume 25, Pages 112-119

ICBAST 2023: International Conference on Basic Sciences and Technology

Chemical Composition and Biological Potential of Different Extracts of Two Medicinal Plants from Northern Algeria

Fernane Farida
Mouloud Mammeri's University

Aitissad Hakima
Mouloud Mammeri's University

Chaouchi Ouardia
Mouloud Mammeri's University

Sehaki Chabha
Mouloud Mammeri's University

Daoudi Nacira
Mouloud Mammeri's University

Houali Karim
Mouloud Mammeri's University

Abstract: This work aime to study the chemical composition and the main biological properties contained in the extracts of *Lavandula stoechas* and *Pistacia lentiscus* collected in northern Algeria. *Lavandula stoechas* and *Pistacia lentiscus* are two medicinal plants belonging to the botanical family Labiatae and Anacardeacea respectively. They are grow wild in the northen Algeria and widely used in traditional Algerian medicine. The GC/MS analysis of the essential oils of *Lavandula stoechas* extracted by hydrodistillation showed that the latter are of fenchone chemotype whatever the period and the site of harvest. LC/MS analysis of tannin powders extracted by maceration of the leaves in a hydroalcoholic solvent reveals that they mainly contain rosmarinic acid. Essential oils extracted from the leaves of *Pistacia lentiscus* showed a large variability in terpenoid. The antioxidant activity of the different essential oils varied according to the harvesting period and the altitude. The highest antiradical effects were observed with the FRAP test. An another side the *Pistacia lentiscus* extracts showed to have an α-glucosidase inhibition effect that was more or less impactful according to the plant's living environment (mountain or littoral) and the considered organ (leaves, stem barks or fruits).

Keywords: *Lavandula stoechas*, *Pistacia lentiscus*, Essential oils, Antioxidant activity, α-glucosidase inhibition

Introduction

Remedies made from natural substances and plants have been widely used for the management of variable diseases due to their safety and reduced side effects.Today, doctors, health organizations and pharmaceutical laboratories recognize the value and effectiveness of treatments based on medicinal and aromatic plants. They admit that the place of these plants is increasingly important in modern pharmaceutical production. Furthermore, nearly 25% of drugs currently used in modern medicine are derived from medicinal plants (Kifle, 2021). Northern Algeria is characterized by a diverse plant cover and the genera Lavandula and Pistacia are the most

---

important medicinal and aromatic plants in this region. *Lavandula stoechas* from the *Lamiaceae* family has been used for centuries, in the form of essential oils or dried flowers, for numerous cosmetic and therapeutic applications. Traditionally, this plant is used as a carminative, antispasmodic, unclogging, stimulating, expectorant and against skin problems (Matos et al., 2009). *Pistacia lentiscus* (lentisk) is a plant species of the Anacardiaceae family. Lentisk has been used in traditional medicine for the treatment of several diseases, such as gastrointestinal diseases, eczema, throat infections (Dragovi´c et al.,2020; Ljubuncic et al., 2005), diabetes for its hypoglycemic effect (Jamila et al., 2014) tooth ache and respiratory disorders (Abdeldjelil, et al.,2014).

Previously, the chemical profile and antibacterial properties of essential oils of *Lavandula stoechas* and *Pistacia lentiscus* have mainly been examined (Alejandro et al., 2015; Boudieb et al., 2019). However, work on other significant biological activities of essential oils and hydroalcoholic extracts of these two Algerian medicinal plants is limited. This present work was developed to explore the chemical composition of the essential oils of *Lavandula stoechas* and *Pistacia lentiscus* and to study the effect of the harvest season on the variation of their chemotypes as well as on their antioxidant power. The other objective of this study is the characterization of the phytochemical profiles of leaves, stem bark and mastic fruits of lentiscus harvested at two different altitudes (mountain and coastal) with regard to their antidiabetic potential. This is carried out using a metabolomics approach based on the link between phytochemical profiling (evaluated by ultra-high performance liquid chromatography coupled with UHPLC-ESI-HRMS mass spectrometry) and the α-glucosidase assay.

Materials and Methods

Chemicals

The main chemicals used for the measurements of α-glucosidase inhibition were α-glucosidase from Bacillus stearothermophilus (G3651-250 UN, 84 units/mg, 86% protein), p-nitrophenyl α-D-glucopyranoside (N1377,≥99.0%) and acarbose (PHR1253-Pharmaceutical Secondary Standard; Certified Reference Material). The analytical standards for the UHPLC-ESI-HRMS analysis were (−)-epigallocatechin (EGC)(≥90%, 08108-supeclo), myricitrin (≥99.0%, 91255, Sigma-Aldrich, Saint Quentin Fallavier, France),apigenin 7-glucoside (≥97.0%, 44692, Supelco) and tiliroside (≥95.0%, PHL89809-phyproof®Reference Substance). These analytical-grade chemicals used were purchased from Supelco and Sigma-Aldrich, Saint Quentin Fallavier, France.

Plant Collection

The samples of aerial parts (leaves, stems, tops and fruits) of *Lavandula stoechas* and *Pistacia lentiscus* were collected separately (Figure 1).For this study, we selected two geographical sites in the Tizi-Ouzou region: the mountain and the littoral. For *Lavandulas stoechas* two sites are considered SiteL1 (254m in altitude) and Site L2 (750m in altitude). For *Pistacia lentiscus* two another sites are considered mountain (876m in altitude) and littoral (13m in altitude). According to the period and altitude of the harvest, eight groups of essential oils were obtained for *Pistacia lentiscus*: winter mountain, spring mountain, summer mountain, autumn mountain, winter littoral, spring littoral, summer littoral, and autumn littoral.

Figure 1. Aerial part of *Lavandula stoechas* (a) and *Pistacia lentiscus* (b)

Extraction of Essential Oils

All samples were cleaned of debris and air dried in the dark for 7 days at a temperature of 25–30°C. The essential oils (EOs) were extracted by hydrodistillation process using a Clevenger-type apparatus. Then they were stored in opaque glass bottles at 4 °C until further use.

Extraction of Tannins and Flavonoids from *Lavandula Stoechas*

The tannins and flavonoids are extracted from *Lavandula stoechas* leaves and stems by hydroalcoholic extraction with methanol and water mixture. After filtation of mixture the solvants were evaporated and extract obtained.

GC-MS Analysis of Essential Oils

The chemical analysis of the EOs was carried out by gas chromatography mass spectrometry (GC-MS) using a Trace GC-Ultra instrument coupled to a DSQ-II (singlequadrupole) mass spectrometer supplied by Thermo Fisher Scientific. The chromatographic separation was conducted on a 30 m × 0.25 mm × 0.25 µm TR-5 MS capillary column (5% phenyl and 95% polysiloxane from Thermo-France). One microliter of sample was injected in the splitless mode at 200 °C. The oven temperature was set at 50°C for three minutes; then, it was programmed to increase from 50 to 270°C at a rate of 5/min and then to increase to 330°C at a rate of 10/min. Helium was used as carrier gas (flow rate 1 mL/min). The transfer line was heated to 280°C. Ionization in the electron impact mode was conducted at 220°C with an energy of 70 eV. A full-scan detection for masses (m/z) between 35 and 350 UMA was performed at a rate of 3000 UMA/sec. Each sample of essential oil was diluted 1000 times in hexane containing pentadecane (1/4000 v/v) as the internal standard.

The identification of oil components was assigned by comparison of their retention times and retention indices (RIs). Experimental RIs were calculated as the relative retention times of compounds compared with those of (C10–C40) n-alkanes. Moreover, identification was confirmed by comparing the mass spectra of each molecule with (i) those available in the NIST 05 library of the GC/MS data system and with(ii) the mass spectra published (Adams R.P,2007). The relative quantification of each compound within a sample was based on the peak relative (%) surface measured with the total ion current (TIC) after normalization of the surface area to the internal standard.

Antioxidant Activity of Lentisk Essential Oils

The antioxidant activity of lentisk EOs was assessed using three techniques: the DPPH radical-scavenging test, the ferric reducing antioxidant power (FRAP) assay, and the ABTS radical-cation reduction test. All measurements were spectrophotometry determined and expressed in Trolox equivalent antioxidant capacity (TEAC). Trolox is the hydrophilic equivalent of vitamin E and it was used as the standard for all three tests. All measurements were performed in triplicate and the results are expressed as Trolox equivalent (i.e., mg of Trolox equivalent/g of essential oil; mg TE/g EO) for all tests (i.e., DPPH, FRAP, and ABTS). Vitamin C (ascorbic acid) was tested as the control for the three tests. The results are expressed as mg Trolox equivalent/g of vitaminC.

α-Glucosidase-Inhibitory Activity of Lentisk Extract

The samples of each lentisk organ (stems, leaves and fruits) were dried and then ground using the ball mill.Each extract was obtained by maceration of 200 mg of powder in 1.5 ml of methanol at 70°C for 30 min in an Eppendorf ThermoMixer. The mixture was centrifuged at 1100 G for 5 min. The recovered supernatant was evaporated under a stream of nitrogen. The dry crude extract recovered after evaporation of the methanol was dissolved in a mixture [water (750 µl)/cyclohexane (750 µl)]. After centrifugation, the aqueous phase was collected and lyophilized. The lyophilized aqueous extract was stored at −20°C for LC-MS analysis and evaluation of α-glucosidase activity.The measurement of the effect of lentisk extract on the catalytic activity of α-glucosidase was performed according to the method of (Bachhawat J.A et al. 2011), with a slight modification.

In a 96-well plate, a reaction mixture containing 50 µL of phosphate buffer (50 mM, pH = 6.8), 10µL of α-glucosidase (1 U/mL) and 20 µL of varying concentrations of extract (0, 2, 4, 6, 8 and 10 µg/mL) was preincubated at 37 °C for 15 min. Then, 20 µL of p-nitrophenyl α-D-glucopyranoside (PNPG) (1 mM) was added as a substrate, and the mixture was incubated again at 37 °C for 20 min. The reaction was stopped by adding 50 µL of sodium carbonate (0.1 M). The yellow color produced was read at 405 nm using a plate reader. Acarbose at various concentrations (0.2–1 mg/mL) was included as a positive control. A negative control without extracts was assayed in parallel. The experiment was performed three times for each sample. The UHPLC-ESI-HRMS injected standards were also tested for their effect on α-glucosidase inhibition. The results are expressed as percentages of inhibition, which were calculated according to the following formula :

$$\mathbf{Inhibition}\ (\%) = \frac{\left(\mathbf{A}_{\mathbf{negatif\ control}} - \mathbf{A}_{\mathbf{sample}}\right)}{\mathbf{A}_{\mathbf{negatif\ control}}} \times \mathbf{100}\%$$

where $A_{\text{negatif control}}$ corresponds to the absorbance of the control mixture (mixture with the buffer instead of the inhibitor), and A_{sample} represents the absorbance of the samples containing an inhibitor (extracts or acarbose). The α-glucosidase inhibitions of the standards injected for the UHPLC-ESI-HRMS analysis were also tested.

Results and Discussion

Chemical Composition of *Lavandula Stoechas* Essential Oil

The results obtained are summarized in Table 1. These results show that the samples of *Lavandula stoechas* are of the fenchone chemotype which is the majority compound (72 to 77%) of the EO, followed by camphor and cineol. Our results agree with those obtained by Angioni et al. (2006) and Tuttolomondo et al. (2015) for the essential oil of *Lavandula stoechas* collected in Sardaigne and Sicile respectively. On the other hand, our results show that the content of the essential oil in main compounds is influenced essentially by the harvest region but not by the part of the plant used (leaves or flowering tops).

Table 1. Content (in %) of the main compounds of essential oil extracted from leaves of *Lavandula stoechas* harvested on the two sites

Components	Site L1(%)	Site L2(%)
Cineol	02.34	04.19
Fenchone	**77.19**	**72.85**
Camphor	09.34	11.62
Borneol	00.99	01.14
Borneolacetat	03.49	03.13
Mertenylacetat	02.71	03.20
Cubedol	00.71	00.95

Tannin and Flavonoids Yields of *Lavandula Stoechas* Leaves and Tops

The results shown in Table 2 reveal that the highest contents of tannins and flavonoids were obtained with the leaves of *Lavandula stoechas* harvested at the end of May in the Site L1. We recorded a content of 5.7% and 5.8% respectively for flavonoids and tannins.

Table 2. Yield of flavonoids and tannins extracted from leaves and tops of *Lavandula stoechas*

Components	%Site L1	%Site L2
Flavonoids/Leaves	2.96	**5.80**
Tannins/Leaves	3.96	**5.70**
Flavonoids/Tops	1.06	1.60
Tannins/Tops	1.06	3.34

Multivariate Analysis of All the Components Detected in the EOs of *Pistacia Lentiscus*

In order to show differentiation of the chemical compositions between the different EOs, a principal component analysis (PCA) was carried out on the 47 major compounds annotated above (Figure 1). The two axes of the

PCA show 78.6% of the variation. The score plot (Figure 2A) on Axis 1 separates the samples of the two groups according to the sampling site. In each group, the samples for seasons are separated based on Axis 2 of the PCA. Winter and autumn appear mainly separated by Component 2. The mountain group occupies a larger space than the littoral one (i.e., distances between the four seasons were higher for the mountain EOs). This indicates that the variations in the compositions according to the harvesting season were higher at the mountain than at the coastal site. The loading plot (Figure 2B) shows that the most discriminating compounds were the “major” compounds, which appeared at least once at a level greater than 5%.

According to the score and loading plots, the compositions of the EOs analyzed could be subdivided into five sub-chemotypes: Groups 1, 2, 3, 4, and 5. A difference in altitude is usually accompanied by changes in a range of environmental conditions such as temperature, water precipitation, wind exposure, sunlight intensity, UV radiation, and air humidity (Edreva. A et al. 2008). Climatic conditions at (relatively) high altitudes are mainly lower average temperatures, increased thermal amplitude between day and night, and higher light intensity. Such environmental conditions cause plants to change their morphology, physiology, and productivity in order to protect themselves and adapt to such stressful conditions (Edreva. A et al. 2008). In order to evaluate a potential link between our EOs’ profiles and their antioxidant properties, further studies were performed with a primary focus on antioxidant activity measurements.

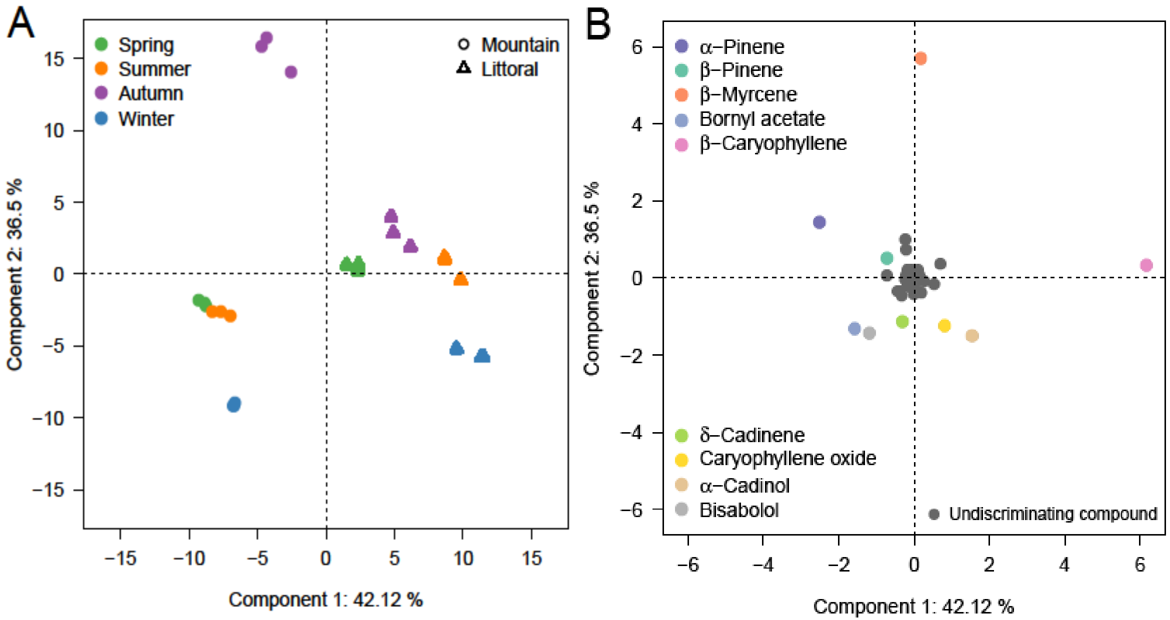

Figure2. PCA analysis performed on all the compounds from the essential oils of Pistacia lentiscus leaf samples collected at the two altitude sites (△ for littoral versus ◯ for mountain) and in 4 consecutive seasons: (A) score plot of PC1 versus PC2 scores; (B) loading plot of PC1- and PC2-contributing EO compounds (the most discriminating compounds are represented in color).

According to the score and loading plots, the compositions of the EOs analyzed could be subdivided into five sub-chemotypes: Groups 1, 2, 3, 4, and 5. A difference in altitude is usually accompanied by changes in a range of environmental conditions such as temperature, water precipitation, wind exposure, sunlight intensity, UV radiation, and air humidity (Edreva et al., 2008). Climatic conditions at (relatively) high altitudes are mainly lower average temperatures, increased thermal amplitude between day and night, and higher light intensity. Such environmental conditions cause plants to change their morphology, physiology, and productivity in order to protect themselves and adapt to such stressful conditions (Edreva et al., 2008). In order to evaluate a potential link between our EOs’ profiles and their antioxidant properties, further studies were performed with a primary focus on antioxidant activity measurements.

Antioxidant Activity of EOs of *Pistacia Lentiscus*

The antioxidant activities (AOx) of the different essential oils, assessed by the ferric reducing power (FRAP), free radical scavenging activity (DPPH), and the ABTS radical cation reduction tests are presented in Table 3.

Table 3. Evaluation of the antioxidant activities of Pistacia lentiscus essential oils using FRAP, ABTS, and DPPH tests

Essential oil samples		FRAP (mg TE/gEO)	ABTS (mg TE/g EO)	DPPH (mgTE/g EO)
Mountain	Winter	11.3 ± 0.1	0.28 ± 0.01	0.12 ± 0.0
	Spring	9.6 ± 0.3	0.32 ± 0	0.44 ± 0.01
	Summer	22.3 ± 0.2	0.09 ± 0.01	0.08 ± 0.01
	Autumn	14.3 ± 0.1	0.24 ± 0.01	0.11 ± 0.0
Littoral	Winter	6.4 ± 0.9	0.09 ± 0	0.06 ± 0.0
	Spring	6.6 ± 1.1	0.23 ± 0.01	0.06 ± 0.0
	Summer	15.7 ± 0.5	0.30 ± 0.01	0.08 ± 0.0
	Autumn	14.8 ± 0.4	0.13 ± 0.01	0.06 ± 0.0
Altitude*Season interaction		***	***	***
Vitamin C(mg TE/g vit C)		1083 ± 144	894 ± 88	1348 ± 192

α-Glucosidase Inhibitory Activity

The pairwise comparison through Kruskal-Wallis test adjusted with Bonferroni allowed to study the significance of the variation of this inhibition according to the organ and also the location. The results of this statistical test are shown by the letters (groups, a, b and ab) in Figure 3. Depending on the part of the plant used, effect is significant between stem barks and fruits, and between leaves and fruits.

We also tested acarbose (positive control), a drug (α-glucosidase inhibitor) used for the treatment of type 2 diabetes. The inhibition of acarbose on α-glucosidase is about 100%. Comparing the effect of these extracts with acarbose we can say that the inhibitory effects of acarbose and stem bark extracts on α-glucosidase are comparable

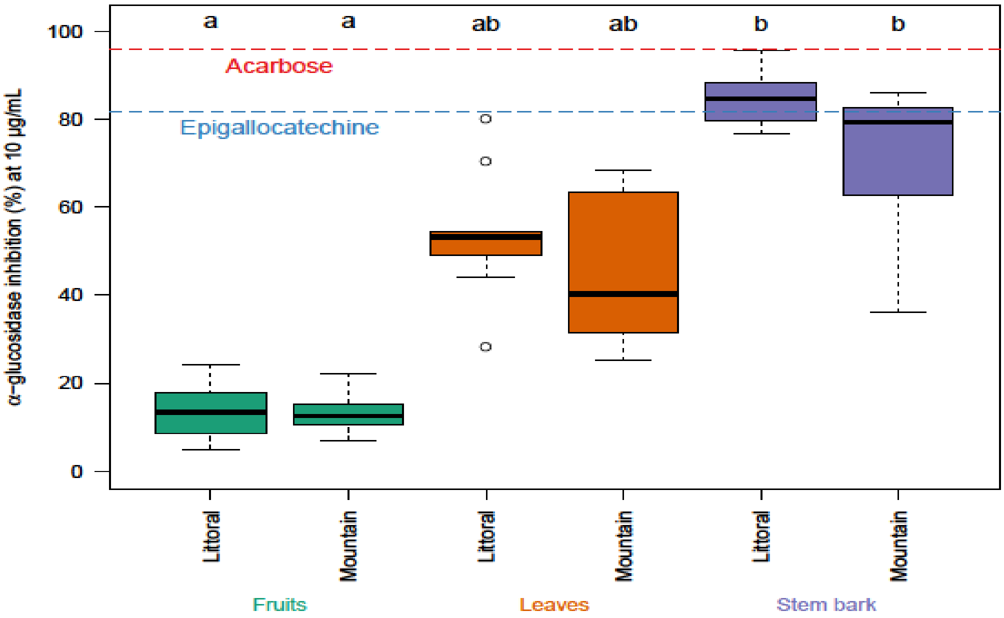

Figure 3. Boxplot showing the inhibitory effect of leaves, stems barks and fruits of lentisk from mountain and littoral on α-glucosidase.

Conclusion

Essential oils of *Lavandula stoechas* are essentially of fenchone chemotype. Essential oils from the leaves of *Pistacia lentiscus* contain mainly 47 compounds. EOs from coastal site were characterized by high amounts of β-caryophyllene. Those from the mountain site were seasonally variable. The chemical class of monoterpene hydrocarbons was higher in the mountains.

The results of this work revealed that the stem bark and leaves from *Pistacia lentiscus* harvested from different areas of Algeria presented a significant activity of α-glucosidase inhibition. The stem barks harvested at the littoral had the highest inhibitory activity toward α-glucosidase. This activity was comparable to that of acarbose. The results collected in this present work show that the species *Lavandula stoechas* and *Pistacia lentiscus* are rich in bioactive molecules with therapeutic interest. This explains their strong use in traditional Algerian medicine.

Recommendations

The goals of the nutrition labeling are to reduce consumer confusion about food labels, help consumers make healthy food choices, and provide an incentive for firms to improve the nutritional quality of food. Nutrition information on food labels should be more understandable to consumers. If necessary, training on reading nutrition labels and evaluating nutrition labels should be provided. The limitation of this study was obtaining the nutrient label of the packaged foods. In this study, only 1000 foods were examined. To obtain more meaningful results, more commercially packaged foods should be studied. In addition, the lack of a previous study on this topic shows the originality of the study, but since there is no source to discuss the results in the discussion section, the study is discussed with its own data.

Scientific Ethics Declaration

The authors declare that the scientific ethical and legal responsibility of this article published in EPSTEM journal belongs to the authors.

Acknowledgements or Notes

* This article was presented as an poster presentation at the International Conference on Basic Sciences and Technology (www.icbast.net) held in Antalya/Turkey on November 16-19, 2023.

References

Abdeldjelil, M.C., Bensegueni, A., Messaï, A., Agabou, A., & Benazzouz, H. (2014). Medicinal use of *Pistacia lentiscus* fixed oil in Constantine province, north-east Algeria. *J. Nat. Prod. Plant Resour., 4(1),* 48–51.

Adams, R.P. (2007) *Identification of essential oil components by gas chromatography/Mass Spectrometry*, (4th ed., p.811). Carol Stream, IL, USA: Allured Publishing.

Alejandro, C., Vanessa, O.R., Ramiro, M.G., Virginia, T., & Jose, T. (2015) *Lavandula stoechas* essential oil from Spain: Aromatic profile determined by gas chromatography–mass spectrometry, antioxidant and lipoxygenase inhibitory bioactivities. *Industrial Crop and Products. 73*,16–27

Angioni, A., Barra, A., Coroneo, V., Dessi, A., & Cabras, P. (2006). Chemical composition, seasonal variability, and antifungal activity of lavandula stoechas L. ssp. stoechas essential oils from stem/leaves and flowers. *Journal of Agricultural Food and Chemistry* , *54*(12),4364-4370.

Bachhawat, J.A., Shihabudeen, M.S., & Thirumurugan, K. (2011) Screening of fifteen Indian ayurvedic plants for alpha-glucosidase inhibitory activity and enzyme kinetics. *International Journal of Pharmacy and Pharmaceutical Sciences, 3,* 267-74.

Boudieb, K., Ait Slimane, A. K ., & Amellal-Chibane, H. (2019) Traditional uses, phytochemical study and morphological characterization of *Pistacia lentiscus L.* fruits from three areas of northern Algeria. *Journal of Applied Biosciences 135,* 13788 – 13797.

Dragovi´c, S., Dragovi´c-Uzelac, V., Pedisi´c, S., Coši´c, Z., Friš ̌ci´c, M., Garofuli´c, I.E., & Zori´c, Z. (2020) The mastic tree (*Pistacia lentiscus L.*) leaves as source of BACs: Effect of growing location, phenological stage and extraction solvent on phenolic content. *Food Technology and Biotechnology, 58,* 303.

Edreva, A., Velikova, V., Tsonev, T., Dagnon, S., Gurel, A., Aktas, L., & Gesheva, E. (2008) Stress-protective role of secondary metabolites: Diversity of functions and mechanisms. *General and Applied Plant Physiology, 34*(1-2), 67–78.

Jamila, F., & Mostafa, E. (2014) Ethnobotanical survey of medicinal plants used by people in Oriental Morocco to manage various ailments. *Journal of Ethnopharmacology, 154,* 76–87.

Kifle, Z. D. (2021). Prevalence and correlates of complementary and alternative medicine use among diabetic patients in a resource-limited setting. *Metabolism Open, 10.*

Ljubuncic, P., Song, H., Cogan, U., Azaizeh, H., & Bomzon, A. (2005) The effects of aqueous extracts prepared from the leaves of *Pistacia lentiscus* in experimental liver disease. *Journal of Ethnopharmacology, 100*, 198–204.

Matos, F., Miguel, M. G., & Duarte, J. (2009). Antioxidant capacity of the essential oils from Lavandula luisieri, L stoechas subsp. lusitanica, L stoechas subsp. lusitanica x L iuisieri and L viridis grown in Algarve (Portugal). *Journal of Essential Oil Research* , *21*(4) 327-336.

Tuttolomondo, T., Dugo, G., Ruberto, G., Leto, C., Napoli, E.M., & Potortì, A.G. (2015) Agronomical evaluation of Sicilian biotypes of Lavandula stoechas L. spp. stoechas and analysis of the essential oils. *Journal of Essential Oil Research, 27*(2), 115 - 124

Author Information

Fernane Farida
Mouloud Mammeri's University
Tizi Ouzou, Algeria
Contact e-mail: *farida.fernane@ummto.dz*

Aitissad Hakima
Mouloud Mammeri's University
Tizi Ouzou, Algeria

Chaouchi Ouardia
Mouloud Mammeri's University
Tizi Ouzou, Algeria

Sehaki Chabha
Mouloud Mammeri's University
Tizi Ouzou, Algeria

Daoudi Nacira
Mouloud Mammeri's University
Tizi Ouzou, Algeria

Houali Karim
Mouloud Mammeri's University
Tizi Ouzou, Algeria

To cite this article:

Fernane, F., Aitissad, H., Chaouchi,O., Sehaki, C., Daoudi, N., & Houali, K (2023). Chemical composition and biological potential of different extracts of two medicinal plants from northern Algeria. *The Eurasia Proceedings of Science, Technology, Engineering & Mathematics (EPSTEM), 25,* 112-119.

The Eurasia Proceedings of Science, Technology, Engineering & Mathematics (EPSTEM)
ISSN: 2602-3199

The Eurasia Proceedings of Science, Technology, Engineering & Mathematics (EPSTEM), 2023

Volume 25, Pages 120-133

ICBAST 2023: International Conference on Basic Sciences and Technology

Electrochemical Polymerization of a Novel Thiophene-Derived Monomer and Its Use as Support Material for Methanol Oxidation

Sadaf Adhami
Eskisehir Osmangazi University

Yagmur Dumlu
Eskisehir Osmangazi University

Deniz Hur
Eskisehir Technical University

Gokhan Kilic
Eskisehir Osmangazi University

Evrim Hur
Eskisehir Osmangazi University

Abstract: This research, conductive polymer supported modified electrode system which was prepared for usage in direct methanol fuel cells. To test the behavior of these electrode system for methanol oxidation, cyclic voltammetry (CV), chronoamperometry (CHR) and electrochemical impedance spectroscopy (EIS) methods were used as electrochemical methods. As the working electrode, pencil graphite electrode (PGE) was preferred because of its porous structure, good ion conductivity, practicality in application and ease of preparation and obtaining. Thiophene derivative 4,4')-2,2'-(diazen-1,2 diylbis(4,1 phenylene))bis(4 (thiophene-2-ylmethylene) oxazol-5(4H)-one), (DiAzBiPhBiTyOx) monomer was prepared and electrochemically polymerized by CV method in 0.01M TBAP and 0.05 $HClO_4$ containing ACN solution on the surfaces of PGE. The spectroscopic characterization of the synthesized monomer was performed by NMR spectroscopy. Optimum polymerization conditions of monomer was determined according to scanning rate, potential range and acid density. The obtained modified electrode system (PGE/PDiAzBiPhBiTyOx) was doped with chloroplatinic acid hexahydrat-Pt2Cl6.6H2O (Pt) at different densities and the optimum catalyst density was determined as 3.25mM (PGE/3.25mMPt@PDiAzBiPhBiTyOx). The methanol oxidation performances of conductive polymer film, platinum and conductive polymer supported platinum catalyst systems were investigated separately. While the methanol oxidation responses of the conductive polymer film and platinum are almost similar, the methanol oxidation response of the platinum doped conductive polymer film catalyst system is higher. The modified electrode characterization was performed by CV, CHR and EIS methods. Furtheremore obtained modified electrode systems were characterized by FESEM/EDS, XRD to confirm the structures and morphologies. Also, the theoretical values such as electrochemical surface area (ECSA) and specific capacitance (Cs) were calculated in aqueous acidic solution with and without methanol. Cs values of the PGE/3.25mMPt@PDiAzBiPhBiTyOx electrode in aqueous acidic solution with and without methanol were 3.861 and 3x10-4Fg^{-1} respectively. Also, the electrochemical surface area values of the same electrode in aqueous acidic solution with and without methanol were 196.437 and 21.150m2g^{-1} respectively.

Keywords: Methanol oxidation, Platinum, Conductive polymer, Polythiophene, Fuel cell

Introduction

- Selection and peer-review under responsibility of the Organizing Committee of the Conference

Highly efficient, renewable and environmentally friendly alternative energy sources are the focus of today's world and are still in the research and development process. Fuel cells are one of the systems worth investigating as an alternative energy source. Direct methanol fuel cells (DMFCs), a type of fuel cell, represent a promising energy source for a portable and clean environment that can be easily applied in modern life (Kamarudin et al., 2009; Andújar & Segura, 2009; Verma, 2000). Since they emit a low amount of pollutant, can be operated at a low working temperature and having high energy-conversion efficiency. Energy is generated by the exchange of ions at the interface of the active material coated on the working electrode surface and the electrolyte in fuel cells. Extensive application of DMFCs requires electrode materials based on dispersed electrocatalytic noble metals (mainly platinum or Pt-based alloys) on a conductive, stable, high surface area substrate (Spătaru et al., 2011; Zainoodin et al., 2010). Carbon-based materials with high conductivity and surface area such as activated carbon, carbon nanofibers, carbon nanotubes and graphene are widely used for DMFCs (Moussa et al., 2016). PGE was chosen as the carbon-based material for this research due to its porous structure, high ion conductivity, practicality in application, ease of preparation and low cost (Kilic et al., 2017; Arslan et al., 2019, Hur et al., 2013). On the otherhand the porous structure and high surface area of many conducting polymers have been led to their use as supporting materials in the development of new electrocatalytic materials. Conducting polymers have a single-electrone polaron state and are mechanically stable and they exhibit a low ohmic resistance across the electrode (Arico et al., 2000; Surampudi et al., 2003; Breiter, 1967; Lee et al., 2004; Raghuveer & Manthiram, 2005; Weidlich et al., 2005; Kitani et al., 2001; Liu et al., 2007; Kost et al., 1988; Rajesh et al., 2003). Electrode modification target with conducting polymers allows an easy flow of current during the electrochemical oxidation of methanol, increasing electrode conductivity, selectivity and reduce the poisoning of the electrode with intermediates. Methanol can be oxidized to carbon dioxide (CO_2) via a carbon monoxide (CO) or carboxylate ($HCOO^-$) reactive intermediates and the formation of strongly adsorbed linearly bonded CO leads to the self-poisoning of Pt electrocatalysts (Baldauf & Preidel, 1999). The biggest factors limiting the widespread use of fuel cells are; the high cost of the metallic catalysts used and the CO gas released during the reaction poisons the catalyst (Chen et al., 2003; Zhu et al., 2001; Herrero et al., 1995; Wu et al., 2004). Due to the relative high electric conductivity of some polymers, it is possible to transfer electrons through polymer chains, between the electrode and dispersed metal particles, where the electrocatalytic reaction occurs. Electrochemical deposition is adviced as an efficient method for the preparation of metal particles. Because of this, the conducting polymer used in this work was electrodeposited on PGE with CV (Domínguez-Domínguez et al., 2008).

In this work, 4,4')-2,2'-(diazen-1,2 diylbis(4,1-phenylene))bis(4 (thiophene-2-ylmethylene) oxazol-5(4H)-one) (DiAzBiPhBiTyOx), a new thiophene (Th) derivative, was chemically synthesized by our group. The advantage of this newly synthesized Th derivative monomer over Th in the electrochemical polymerization process is it's lower potential oxidation. This new polymer has been proposed as an alternative catalyst support material for use as a DMFC anode. Because of PDiAzBiPhBiTyOx is suitable medium for dispersing $H_2PtCl_6.6H_2O$ (Pt), Pt was elctrodeposited on the PGE/PDiAzBiPhBiTyOx modified electrode surface. In order to increase the catalytic effect of Pt with the supporting conductive polymer and to be more economical, it was investigated to decrease the amount of Pt catalyst. In order to eliminate self-poisoning of Pt by the effect of (CO) formed as an intermediate, which limits the common use of DMFCs, it is aimed to investigate the effect of PDiAzBiPhBiTyOx. This mechanism has shown at Figure 1.

$$\text{Pt} + \text{CH}_3\text{OH} \longrightarrow \text{Pt-(CH}_3\text{OH)}_{ad} \tag{1}$$

$$\text{Pt-(CH}_3\text{OH)}_{ad} + \text{Pt} \longrightarrow \text{Pt-(CH}_2\text{OH)}_{ad} + \text{Pt-H}_{ad} \tag{2}$$

$$\text{Pt-(CH}_2\text{OH)}_{ad} + \text{Pt} \longrightarrow \text{Pt-(CHOH)}_{ad} + \text{Pt-H}_{ad} \tag{3}$$

$$\text{Pt-(CHOH)}_{ad} + \text{Pt} \longrightarrow \text{Pt-(COH)}_{ad} + \text{Pt-H}_{ad} \tag{4}$$

$$\text{Pt-(COH)}_{ad} + \text{Pt} \longrightarrow \text{Pt(CO)}_{ad} + \text{Pt-H}_{ad} \tag{5}$$

$$\text{Pt-H}_{ad} \longrightarrow \text{H}^+ + \text{Pt} + \text{e}^- \tag{6}$$

$$2\text{Pt} + \text{H}_2\text{O} \longrightarrow \text{Pt(OH)}_{ad} + \text{Pt-H}_{ad} \tag{7}$$

$$\text{Pt-(CO)}_{ad} + \text{Pt-(OH)}_{ad} \longrightarrow \text{CO}_2 + \text{H}^+ + 2\ \text{Pt} \tag{8}$$

The oveall reaction is :

$$\text{CH}_3\text{OH} + \text{H}_2\text{O} \longrightarrow \text{CO}_2 + 6\text{H}^+ + 6\text{e}^- \tag{9}$$

Figure 1. Pt-catalyzed methanol oxidation mechanism

Method

Materials

All the chemicals and the solvents used for this experiment were of analytical purity and used without further purification. NMR spectra was recorded on Bruker NMR equipment in deuterated chloroform ($CDCl_3$) with tetramethylsilane (TMS) as the internal standard for ^{1}H (500MHz). Electrochemical measurements including CV, EIS and CHR methods were performed in a conventional three electrode system. PGE, platinum sheet and silver (Ag) wire (for unaques solutions experiments) and Ag/AgCl (for aques solution experiments) were used as working, counter and reference electrodes, respectively. Pencil graphide electrode (PGE) used for preparation of the working electrode. 2cm of 0,50mm of PGE (0,48cm^2) were used in tests. Before use, PGE washed in an ultrasonic bath (with distilled pure acetone, pure ethanol and acetonitrile respectively at room temperature, for 2 minutes each). Electrochemical measurements were performed on potentiostat-galvanostat system (Gamry 3000 potentiostat/galvanostat/ZRA) and were analyzed by software (Gamry CMS-300 (version 5.50b) framework/analysis). All electrochemical measurments were repeated three times. All experiments were performed at room temperature.

The structural and morphological characterization of conducting polymer and Pt doped conducting polymer were done by X-ray diffraction (XRD) and by field emission-scanning electron micrograph (FE-SEM/EDS). The devices used for FESEM and XRD are Hitachi Regulus 8230 FE-SEM and RIGAKU brand SmartLab model X-ray Diffractometer equipped with Cu target respectively.

Synthesis of Monomer

Synthesis of DiAzBiPhBiTyOx monomer was conducted according to our previous procedure and summarized in Figure 2 (Arslan et al., 2019)

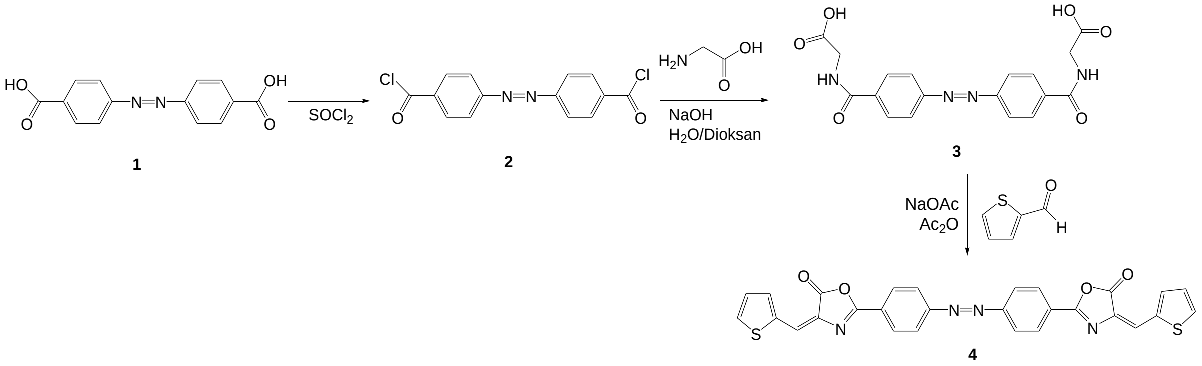

Figure 2. Chemical synthesis of DiAzBiPhBiTyOx monomer

Synthesis of (4,4')-2,2'-(diazen-1,2-diylbis(4,1-phenylene))bis(4-thiophen-2 ylmethylene)oxazole-5(4H)-on), DiAzBiPhBiTyOx, 4

4-[2-(4-carboxyphenyl)diazen-1-yl]benzoic acid, 1 (1 eq. mol) was refluxed in thionyl chloride ($SOCl_2$, excess) in the presence of a catalytic amount (1.2 drops) of DMF under nitrogen atmosphere for 5 hours. At the end of the reaction, excess $SOCl_2$ was evaporated under vacuum distillation. Thus, the carboxy functions were chlorinated to obtain 4-[2-(4-carboxyphenyl)diazen-1yl]benzoyl chloride, 2 in 95% yield and used in the next reaction without any purification. Glycine (2 eq. mol) and NaOH (4 eq mol) were dissolved in 40 mL of water. To this mixture, a solution of 4-[2-(4-carboxyphenyl)diazen-1-yl]benzoyl chloride, 2, (1 eq. mol) in dioxane (80mL) was added dropwise. The reaction mixture was stirred at room temperature for 2 hours. At the end of the reaction time, the dioxane was evaporated under vacuum. The remaining reaction mixture was diluted with water and extracted with ethyl acetate (EtOAc) (3x30mL). 10% HCl (aqueous) solution was added to the collected water phase until pH=2. This solution was extracted with EtOAc again and the amide compound formed was taken to the organic phase. The organic phase was dried with Na_2SO_4 and filtered. The filtrate was evaporated in vacuo to remove EtOAc and diglycinamide, 3, was obtained in, 72% yield. Oxazolone rings were formed by boiling diglycinamide, 3 (1 eq. mol) in acetic anhydride (10mL) under reflux for 2 hours with thiophene-2-carbaldehyde (2 eq. mol) and sodium acetate (NaOAc, 2 eq. mol). The reaction mixture was evaporated under vacuum and ethanol (10mL) was added to the obtained residue, and it was kept in the refrigerator at 5^{o}C overnight. The product, DiAzBiPhBiTyOx, 4, was obtained in 67% yield as a dark red precipitate.

^{1}H NMR (500 MHz, $CDCl_3$, TMS) δ ppm: 9.58 (d, J= 1.67 Hz, 1H), 8.60 (dd, J= 2.06, 8.30 Hz, 1H), 8.49 (s, 1H), 8.47 (s, 1H), 7.86-7.85 (m, 2H), 7.75 (d, J= 3.33 Hz, 1H), 7.72 (d, J= 3.62 Hz, 1H), 7.69 (s, 1H), 7.65 (s, 1H), 7.25 (d, J= 3.85 Hz, 1H), 7.24 (d, J= 3.82 Hz, 1H) ppm.

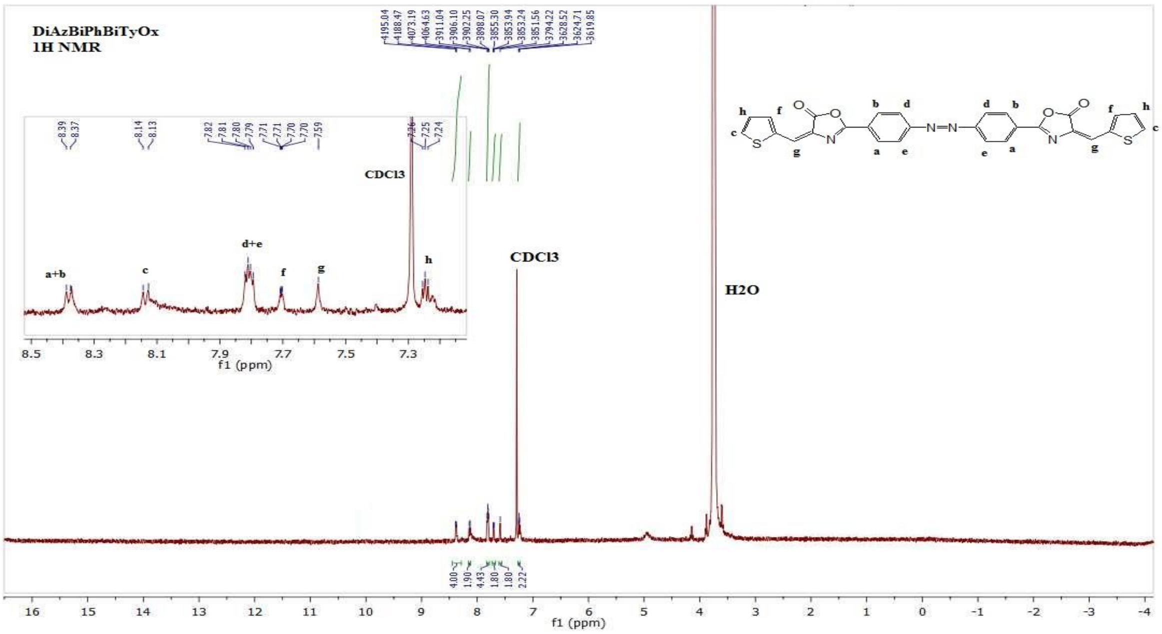

Figure 3. ^{1}H NMR spectrum of DiAzBiPhBiTyOx

Preparation of the Catalyst Support Material

The catalyst support material was formed by electrochemical deposition of PDiAzBiPhBiTyOx on PGE in ACN solution which contains 1.00 x 10^{-4}M DiAzBiPhBiTyOx, 0.10M TBAP and 0.05M $HClO_4$ using CV method. Electropolymerization was performed in the potential range of +0.20 to +2.00 V at a scan rate of 30 mVs^{-1} for 40 cycles. After electropolymerization, the modified electrode (PGE/PDiAzBiPhBiTyOX) was rinsed with ACN and air dried after the electrochemical polymerization.

Platinum Electrodeposition onto Support Material

The electrodeposition of platinum onto the PGE/PDiAzBiPhBiTyOx electrode was carried out in a conventional electrochemical cell consisting of 3 electrode at room temperature. An aqueous solution containing 0.5 M H_2SO_4 (Sigma-Aldrich) and 5mM $H_2PtCl_6.6H_2O$ (Sigma-Aldrich) was used as the electrodeposition solution. Electrodeposition was applied in the potential range of -0.10 to +0.80 V at a scan rate of 50 mVs^{-1} for 50 cycles.

Methanol Oxidation Analysis

The electrochemical properties of the prepared Pt-supported electrode (PGE/3.25mMPt@PDiAzBiPhBiTyOx) was tested form methanol oxidation, which was measured in a 0.5 M CH_3OH + 0.5 M H_2SO_4 solution by cyclic voltammetry, over a potential range of -0.30, +1.00 V with a scan rate of 50 mVs^{-1}, CHR was taken at 0.50 V potential for 300 seconds and EIS was taken between 10^{-2} and 10^{4} frequency range.

Results and Discussion

Electrochemical preparation and characterization of PGE/PDiAzBiPhBiTyOx

PGE/PDiAzBiPhBiTyOx was prepared by forming PDiAzBiPhBiTyOx on PGE using CV technique. The optimization measurement were utilized to determine the effect of potential range, scan rate and acid concentration on the preparation of the electrodes. Firstly, PDiAzBiPhBiTyOx films were formed on PGE carrying out different potential ranges at 50mVs^{-1} for 10 cycles. Single cycle voltammograms of the electrodes were recorded in ACN solution which contains 0.1M TBAP in the potential range where polymerization was done at 50mVs^{-1}. The highest anodic peak current was obtained for the potential range between +0.20 and +2.10V (Figure 4a). Different scan rates were applied to determine the optimum scan rate. Thus, films were formed in the ACN solution which contains 0.10M TBAP+ 1.00 × 10^{-4}M on PGE in the potential range between +0.20 and +2.10V for 10 cycles. The highest current was obtained for 30mVs^{-1} from single cycle voltammograms (Figure 4b). In order to examine the effect of acid concentration on PDiAzBiPhBiTyOx formation, measurements were conducted by changing the $HClO_4$ concentration and taking 40 cycles at 30 mV in the potential range of +0.20 to +2.10V. Single cycle voltammograms of the electrodes were recorded under the same conditions. The highest current was obtained for 0.03M acid from single cycle voltammograms (Figure 4c). According to optimization measurements, optimum conditions for PGE/PDiAzBiPhBiTyOx electrode were found using CV in the potential range between +0.20 and +2.10V for 40 cycles at 30mVs^{-1} in ACN which contains 1.00 × 10^{-4}M monomer, 0.10 M TBAP and 0.03M $HClO_4$.

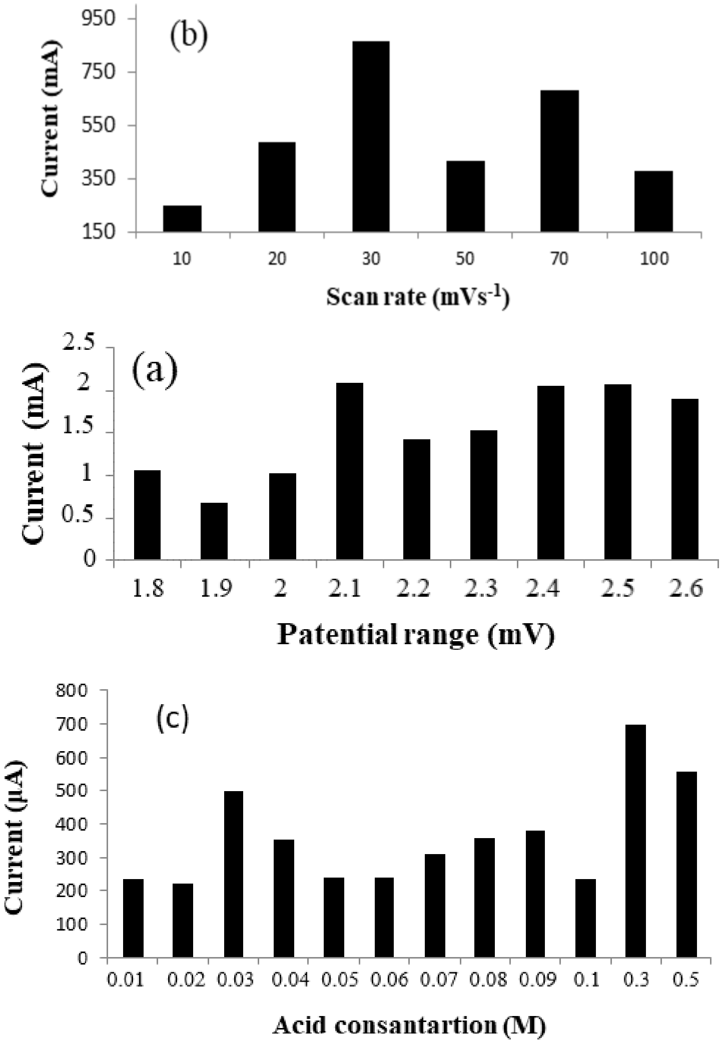

Figure 4. The effect of (a) potential range, (b) scan rate and (c) acid consantration on the formation of PDiAzBiPhBiTyOx on PGE at a scan rate of 30mV s^{-1} in ACN which contains 1.00 × 10^{-4}M monomer, 0.10 M TBAP

DiAzBiPhBiTyOx monomer was polymerized on the PGE electrode under optimum conditions determined by the CV method (in the potential range of +0.20V to +2.10V, scan rate of 30mVs^{-1} for 40 cycles). The multi-cycle voltammogram of the electropolymerization and the voltammograms of the first and last cycles are given in Figure 5 respectively.

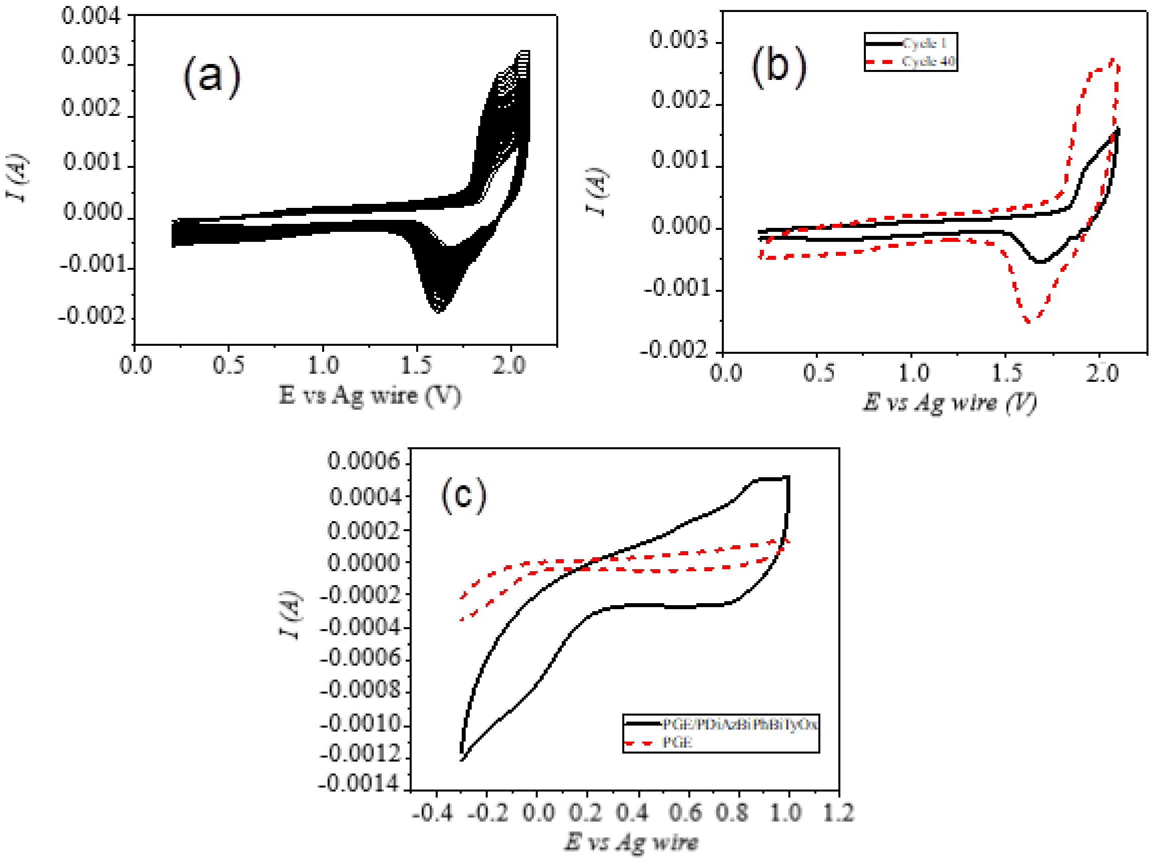

Figure 5. Cyclic voltammograms of PDiAzBiPhBiTyOx polymer film (a) 40 cycles, (b) first and last cycle (c) electrochemical characterization of PGE and PGE/PDiAzBiPhBiTyOx at a scan rate of 50mVs^{-1} in monomer free solution

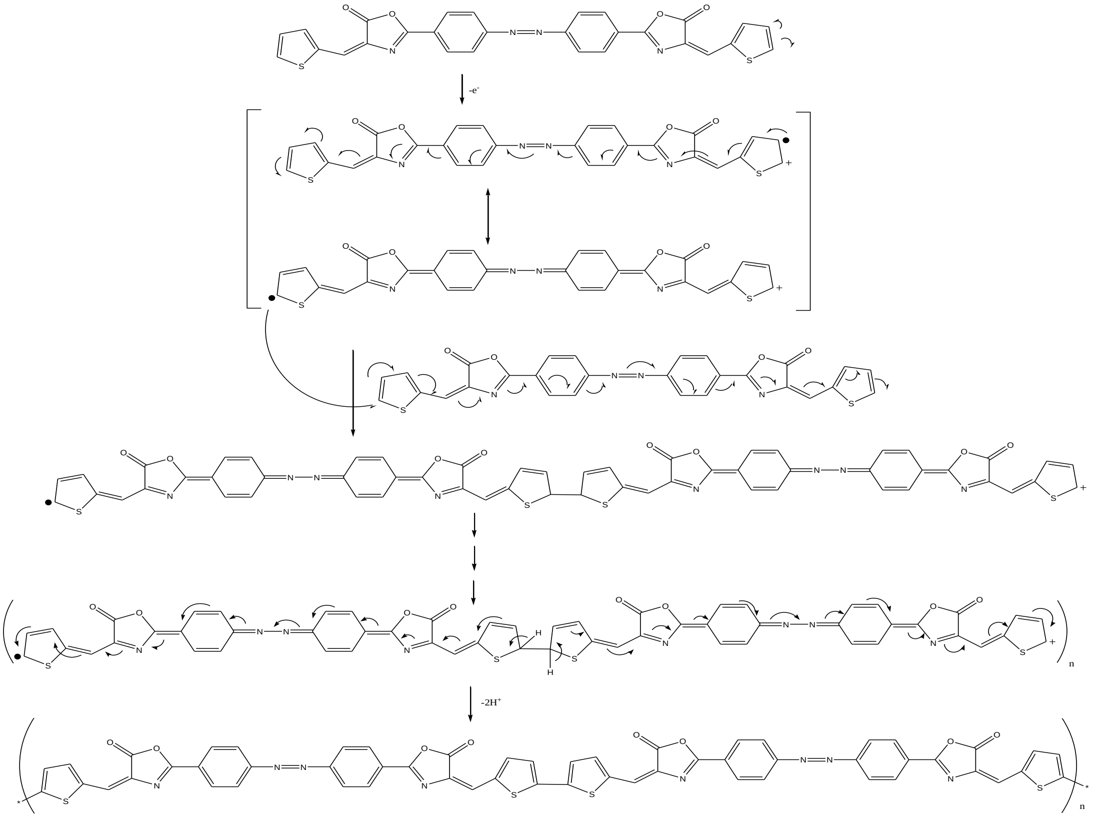

Figure 6. Proposed polymerization mechanism of DiAzBiPhBiTyOx

During polymerization process of DiAzBiPhBiTyOx monomer on PGE by CV method, recorded first cycle was belong to oxidation of monomer. The oxidation peak of the monomer (forward peak) was around +1.80V (+915µA) and the reduction peak (backward peak) was observed around +1.60V (-533µA) in the first cycle. In the last cycle, forward and backward peaks can be seen around +1.95V (at +2.560 mA) and +1.62V (-1.514mA) potentials, respectively. As the number of loops increases, the oxidation peak current increases significantly, indicated that the modified PGE electrode has a higher capacitance. This shows that the amount of monomer decreases in the solution medium, therefore, while the transferred ions decrease, polymer is formed on the electrode surface. In addition, the increase in current with the number of cycles proves that the modified electrode has higher capacitance than the PGE electrode (Fu et al., 2012; Lai et al., 2011; Montilla et al., 2011;Data et al., 2014). The polymer mass was determined as 0.24mg/cm^2 by a precision balance after keeping under reduced pressure. Proposed polymerization mechanism of DiAzBiPhBiTyOx is given in Figure 6.

Electrochemical characterization of PGE and PGE/PDiAzBiPhBiTyOx electrodes were investigated in the potential range of -0.30 V to +1.00 V at 50 mVs^{-1} scan rate, in 10 ml of ACN solution containing 0.10 M TBAP and 0.05 M $HClO_4$ by CV method (Figure 5.c). According to voltammograms, it is seen that the PGE/PDiAzBiPhBiTyOx has higher current value than the PGE electrode. As a result, it can be said that the PGE/PDiAzBiPhBiTyOx electrode has a higher surface area than the PGE electrode, therefore it has higher electrical conductivity and specific capacitance values (Li et al., 2010; Chen et al., 2006).

Platinum Electrodeposition and Electrochemical Characterization of PGE/ PDiAzBiPhBiTyOx

The optimum amount of catalyst (Pt) to be used with the polymer support for methanol oxidation was determined. The PGE/PDiAzBiPhBiTyOx electrode surface was doped with Pt in the potential range of -0.10 V to +0.80 V for 25 cycles at 50 mVs^{-1} in 10 ml distilled water containing 0.50 M H_2SO_4 and 3mM $H_2PtCl_6.6H_2O$ as 3.25, 3.50 and 3.75 mM. Obtained electrodes described as PGE/3mMPt@PDiAzBiPhBiTyOx, PGE/3.25mMPt@PDiAzBiPhBiTyOx,PGE/3.50mMPt@PDiAzBiPhBiTyOx,PGE/3.75mMPt@PDiAzBiPhBiTyOx, respectively. Single-cycle voltammograms of the electrodes were taken in 10 ml distilled water containing 0.50 M H_2SO_4 and 0.50 M CH_3OH at the scan rate of 50 mVs^{-1}. The optimum catalyst density was determined by electrochemical characterization of modified electrodes doped with platinum at different densities using the CV method. The obtained results are given as CV voltammograms and, current value graphic in Figure 7a and 7b, respectively.

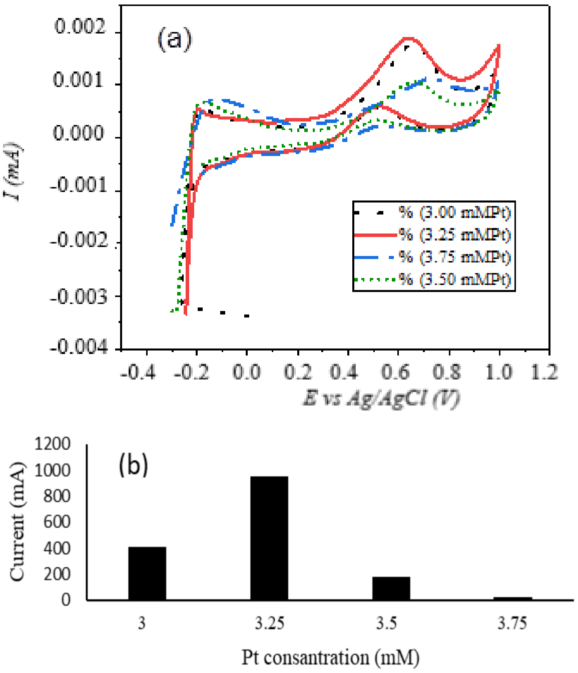

Figure 7. (a) The cyclic voltammograms of Pt density effect, (b) graph of current values versus pt density on PGE/Pt@PDiAzBiPhBiTyOx

In addition, the electrochemical active surface area (ECSA) values of the modified electrodes were calculated using the data obtained from the integration of single-cycle voltammograms in 10ml distilled water containing

0.50M H_2SO_4 and 0.50M CH_3OH. Atomic adsorption of hydrogen which obtained from voltammograms was used to estimate the surface area of the catalysts. It can be said that the presence of cathodic and anodic peaks in the potential range of -0.15V and 0.20V is due to H-adsorption and H-desorption in acidic medium. The ECSA value of the polymer supported catalyst can be calculated using the Q_h charge value from H desorption (Liu et al., 2016). ECSA values was calculated by the following equation;

$$ECSA = \frac{QH}{m.c} \qquad \text{(Eq. (1))}$$

Where; Q_H is the charge of hydrogen desorption (mCcm^{-2}), *m* is the weight of deposited catalyst on the electrode (mgcm^{-2}) and *c* is the charge required to oxidize a single layer of hydrogen on the polymer supported catalyst, respectively. The calculated ECSA values for each modified electrode are given at Table 1.

Table 1. Calculated ECSA values for each modified electrode

Modified Electrode System	ECSA value calculated for the PGE modified electrode (m^2/g)
PGE/3mMPt@PDiAzBiPhBiTyOx	89.571
PGE/3.25mMPt@PDiAzBiPhBiTyOx	196.437
PGE/3.50mMPt@PDiAzBiPhBiTyOx	5.126
PGE/3.75mMPt@PDiAzBiPhBiTyOx	140.300

It can be seen that the ECSA value of the PGE/3.25mMPt@PDiazBiPhBiTyOx electrode is quite high when compared to the available literature (Liu et al., 2016; Karim & Yahya, 2018; Tian et al., 2017). The modified electrode systems in which Pt is used as a catalyst form methanol oxidation and the ECSA values compiled from the literatüre are given in Table 2.

Table 2. Comparison of ECSA values of modified electrode systems using Pt as a catalyst in the oxidation of methanol according to available literature

Electrode/ Catalyst System	ECSA (m^2/g)	Reference
Pt/C	38.900	(Liu et al., 2016)
Pt/rGO	8.700	(Liu et al., 2016)
Pt/GO	64.480	(Karim & Yahya, 2018)
Pt/CNT	33.680	(Karim & Yahya, 2018)
PtAu/rGO	13.120	(Karim & Yahya, 2018)
PtFe/rGO	18.000	(Karim & Yahya, 2018)
P/CNT@TiCoN	55.900	(Karim & Yahya, 2018)
Pt/CNTs@TiN	50.500	(Karim & Yahya, 2018)
Pt/G	45.800	(Tian et al., 2017)

The optimum catalyst amount was determined as 3.25 mM as can be seen from Figure 7a, b and Table 1. According to this results, the methanol oxidation response of the PGE/3.25mMPt@PDiAzBiPhBiTyOx modified electrode was investigated by CV, CHR and EIS methods. The current and resistance values obtanined from these methods in aqueous solution with and without methanol are given in Table 3 comparatively.

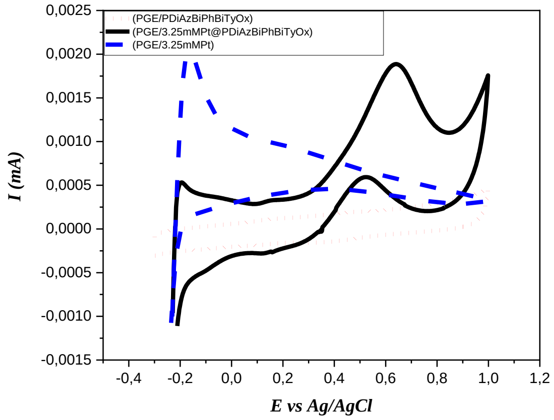

Figure 8. Cyclic voltammograms of PGE/3.25mMPt@PDiAzBiPhBiTyOx, PGE/PDiAzBiPhBiTyOx and PGE/3.25mMPt in methanol containing 0.5M H_2SO_4 aqueous solution at scan rate 50mVs^{-1}

The methanol oxidation performance of the PGE/3.25mMPt@PDiAzBiPhBiTyOx electrode was compared with single cycle voltammograms of PGE/PDiAzBiPhBiTyOx and PGE/3.25mMPt in 0.50 M H_2SO_4 solution with and without methanol. As can be seen from Figure 8, the CO_2 peak belonging to the methanol oxidation of the PGE/3.25mMPt@PDiAzBiPhBiTyOx electrode has the highest current value. The CO_2 peak, which is expected to be observed in the 0.60 - 0.80V potential range, is not evident in the single-cycle voltammograms of the PGE/PDiAzBiPhBiTyOx and PGE/3.25mMPt electrodes.

The methanol oxidation response of the PGE/3.25mMPt@PDiAzBiPhBiTyOx electrode was investigated in with and without methanol containing 0.50 M H_2SO_4 aqueous solutions. According to the CV method, it was observed that the CO2 peak current increased in the methanol solution. Maximum peak currents were obtained at with and without methanol 0.50 M H_2SO_4 aqueous solutions as 350 µA and 955.2 µA, respectively (Figure 9a).

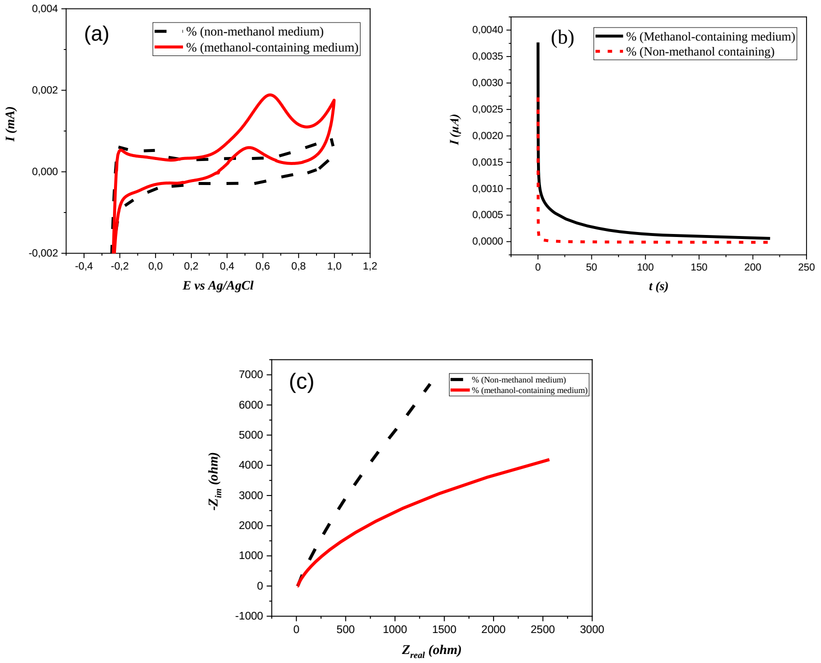

Figure 9. Graphical comparison of methanol oxidation behavior of PGE/3.25mMPt@DiAzBiPhBiTyOx electrode in aqueous solution with and without methanol using by a) CV, b) CHR, c) EIS methods

The methanol oxidation performance of PGE/3.25mMPt@DiAzBiPhBiTyOx conductive polymer supported catalyst system was investigated by chronoamperometry method in aqueous solution with and without methanol. According to the obtained results, for PGE/3.25mMPt@DiAzBiPhBiTyOx system the current value was recorded at 56.15µA in methanol-free medium, while it was recorded 148.90µA in methanol-containing medium (Figure 9b) The sharp current decrease was seen in chronoamperograms, can be explained by the formation of intermediate products such as CO etc. Stabilization of PGE/3.25mMPt@PDiAzBiPhBiTyOx modified electrode at higher current in methanol containing aqueos medium shows that it has the higher tolerance limit against CO poisoning (Xing, 2010; Prabakar, 2016).

The methanol oxidation performance of the PGE/3.25mMPt@DiAzBiPhBiTyOx conductive polymer supported catalyst system was investigated by EIS method. Nyquist plot of phase angle-log Freq and log Z-log Freq obtained in aqueous solution containing 0.05M H_2SO_4, 0.50M CH_3OH for 1 hour exposure time for PGE/3.25mMPTDiAzBiPHBiTyOx electrode and corresponding Bode plots are given in Figure 9c. R values calculated from Bode plots were obtained in in aqueous solution with and without methanol as 3.223kohm and 6.758kohm, respectively.

Resistance is an important performance indicator in energy storage devices, and it can be said that the performance of the low resistance device is higher (Morali & Erol, 2020). The resistance value obtained from Nyquist curves of the PGE/3.25mMPTDiAzBiPHBiTyOx electrode in aqueous methanol solution show that, because of methanol oxidation performance of this electrode, its use in methanol fuel cells is promising.

Table 3**.** Comparison of methanol oxidation behavior of PGE/3.25mMPt@DiAzBiPhBiTyOx electrode in aqueous solution with and without methanol using CV, CHR, EIS methods.

Method/Parameter/Unit	0.05 M H_2SO_4 PGE/3.25mMPt@PDiAzBiPhBiTyOx
CV/ I/ μA	350
CHR/ I/ μA	67.890
EIS/ R/ Ω	49.510
	0.05 M H_2SO_4 + 0.50 M CH_3OH
CV/ I/ μA	955.200
CHR/ I/ μA	58.260
EIS/ R/ Ω	$1x10^{-6}$

In addition, the theoretical specific capacitance (C_s) value was calculated from the Nyquist plot obtained from 0.50M H_2SO_4 aqueous solution containing 0.50M CH_3OH (aqueous solution with methanol) of the modified electrode (Eq. (2)). The inverse of the slope, obtained from the Z_{im} plot drawn against the $1/(2\pi f)$ value, calculated from the frequency value which was obtained from this curve gives the capacitance value (Xing et al., 2010). Methanol fuel cells can transfer energy as much as the power they store while being charged in the discharge process. Accordingly, as the Cs value of the modified electrode system, which is related to the energy storage capacity, increases, the energy storage capacity of the methanol fuel cell will also increase (Snook et al. 2011; Li et al., 2010).

$$C_s = -\frac{1}{2\pi f Zim.m} \qquad \text{(Eq. (2))}$$

The calculated theoretical Cs values of the PGE/3.25mMPt@PDiAzBiPhBiTyOx electrode in aqueous medium with and without methanol are 3.8613 and $3x10^{-4}Fg^{-1}$ respectively. Therefore, the higher specific capacitance of the modified electrode in aqueous solution with methanol is an advantage for energy storage systems. The Cs value of the PGE electrode calculated in the aqueous solution with methanol is higher than in the methanol-free one, shows it’s properity for use in methanol fuel cells.

Morphological and Structural Characterization of Pt Doped PGE/ PDiAzBiPhBiTyOx

The methanol oxidation performance of the modified electrode was not change in direct proportion to the amount of catalyst doped on the catalyst support layer according to the results obtained by the electrochemical measurements (CV, CHR and EIS). This can be related to the fact that the maximum amount of catalyst that catalyst support can take, is limited. This suggestion supported by FESEM/EDS analyses.

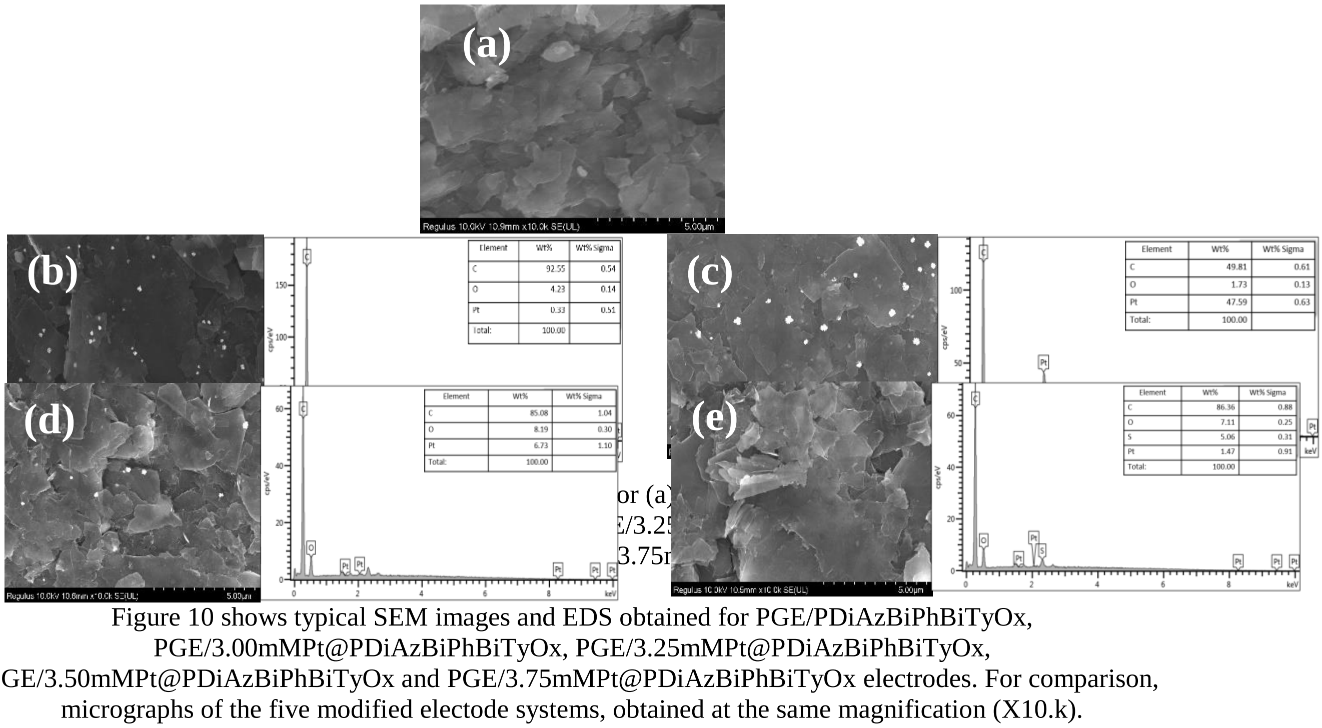

(b)

Element	Wt%	Wt% Sigma
C	92.55	0.54
O	4.23	0.14
Pt	0.33	0.51
Total:	100.00	

(c)

Element	Wt%	Wt% Sigma
C	49.81	0.61
O	1.73	0.13
Pt	47.59	0.63
Total:	100.00	

(d)

Element	Wt%	Wt% Sigma
C	85.08	1.04
O	8.19	0.30
Pt	6.73	1.10
Total:	100.00	

(e)

Element	Wt%	Wt% Sigma
C	86.36	0.88
O	7.11	0.25
S	5.06	0.31
Pt	1.47	0.91
Total:	100.00	

Figure 10 shows typical SEM images and EDS obtained for PGE/PDiAzBiPhBiTyOx, PGE/3.00mMPt@PDiAzBiPhBiTyOx, PGE/3.25mMPt@PDiAzBiPhBiTyOx, PGE/3.50mMPt@PDiAzBiPhBiTyOx and PGE/3.75mMPt@PDiAzBiPhBiTyOx electrodes. For comparison, micrographs of the five modified electode systems, obtained at the same magnification (X10.k).

Figure 10(a) shows conductive polymer coated PGE. A porous surface morphology is desirable for electrodes used for fuel cell applications, as the porous structure morphology provides easy access for Pt ions to be used as catalysts to enter the electrode/electrolyte interface.

Figure 10 (b, c, d and e) shows SEM/EDS images of different Pt doped electrodes that named as PGE/3.00mMPt@PDiAzBiPhBiTyOx, PGE/3.25mMPt@PDiAzBiPhBiTyOx, PGE/3.50mMPt@PDiAzBiPhBiTyOx, PGE/3.75mMPt@PDiAzBiPhBiTyOx, respectively. As can be seen from the figures, it is clear that PGE/PDiAzBiPhBiTyOx is doped on its surface. It is seen that the concentration of Pt particles on the surface is the highest on the surface of PGE/3.25mMPt@PDiAzBiPhBiTyOx, while the least on the surface of the PGE/3.75mMPt@PDiAzBiPhBiTyOx electrode.

Element contents for Pt catalyst of all modified electrode systems were determined by EDS detection. The EDS results show that different amounts of Pt are doped on the surface of the PGE/PDiAzBiPhBiTyOx electrodes. Pt metal loadings were 0.33, 47.59, 6.73 and 1.47 wt.% in PGE/3.00mMPt@PDiAzBiPhBiTyOx, PGE/3.25mMPt@PDiAzBiPhBiTyOx, PGE/3.50mMPt@PDiAzBiPhBiTyOx, PGE/3.75mMPt@PDiAzBiPhBiTyOx respectively.

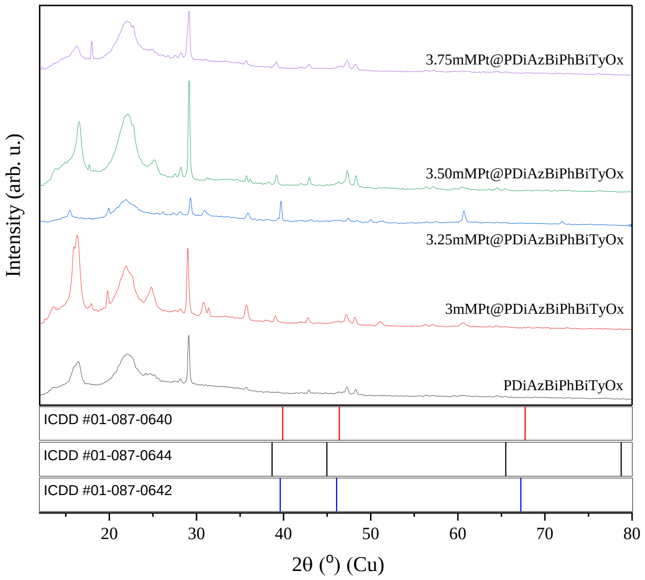

Figure 11. XRD patterns of PGE/PDiAzBiPhBiTyOx and Pt doped PGE/PDiAzBiPhBiTyOx XRD patterns in the range of 2θ=10-80° and characteristic Pt patterns (ICDD # 01-087-0640, ICDD # 01-087-0644, ICDD # 01 087-0642) to determine the presence of Pt within the structure of PDiAzBiPhBiTyOx and Pt@PDiAzBiPhBiTyOx are given in Figure 11.

As it can be seen from the Figure 11, two broad bands observed around 12° and 22° in the 2θ=10-40° region. XRD patterns are known to belong to the PDiAzBiPhBiTyOx polymer and these regions are known to correspond to different structures belonging to C (ICDD # 00-050-0926) and S (ICDD # 00-042-1278) and in addition, the sharp and intense peak around 29° is known to correspond to N (ICDD # 96-901-477).

In XRD pattern of PDiAzBiPhBiTyOx, the absence of a distinct diffraction peak around 2θ=39°, which was observed in other samples, indicated the presence of Pt in Pt@PDiAzBiPhBiTyOx samples. These peaks in the XRD patterns correspond to Pt that has crystalline parameters belonging to cubic crystal system (a=b=c=3.911Å) in cubic Fm-3m space group.

According to three different reference patterns, cubic Pt has diffraction peaks within the range of 38.5-40°, 45-46.5°, 65.5-67.5° and also at 78.6°. However, among the peaks seen in the patterns of Pt@PDiAzBiPhBiTyOx samples, the peak in the 2θ=39° de (111) orientation is observed as the dominant peak, the diffraction peak belonging 2θ=39° (200) is barely present. In reference patterns belonging to cubic Pt, 65° (220) and 78° (311) peaks that are known to have low intensity could not be encountered (Arbizzani et al., 2008). The most distinct and intense diffraction peak (111) at 2θ=39° was observed in the pattern belonging to PGE/3.25mMPt@PDiAzBiPhBiTyOx sample.

Conclusion

PDiAzBiPhBiTyOx, a new thiophene-based conductive polymer, was prepared and investigated for the first time in this study as a catalyst support material for Pt catalyst to be used directly in methanol fuel cells. Methanol oxidation performance of modified electrode (PGE/PDiAzBiPhBiTyOx) was tested by using CV, CHR and EIS methods. In addition, theoretical calculations were done using the values obtained from these methods. ECSA and C_s values were obtained as a result of theoretical calculations. PDiAzBiPhBiTyOx monomer, which is the Th derivative synthesized for this study, is oxidized at a lower potential than Th and can be polymerized more easily. The fact that the calculated ECSA values for PDiAzBiPhBiTyOx, which is used as a catalyst support for Pt, are higher than that of PTh and Pt in the literature, indicates that catalytic activity of is PDiAzBiPhBiTyOx also high. Moreover, the new modified electrode system proposed in this study was also effective in elimination of CO poisoning. Another novelty of this study in terms of literature is that C_s value, which is related to the energy storage capacity of the modified electrode systems, was calculated for the first time in this study according to EIS analysis results. This approach can be considered as a new proposal to the literature for future researches on methanol fuel cells. Electrochemical characterization methods show that the electrode with the best methanol oxidation performance is the 3.25mM Pt doped modified electrode system. The structural and surface analysis results of these electrodes with FESEM/EDS and XRD also show that the optimum amount of Pt added to the catalyst support is 3.25mM.

Scientific Ethics Declaration

The authors declares that the scientific ethical and legal responsibility of this article published in EPSTEM Journal belongs to the authors.

Acknowledgements or Notes

* This article was presented as an oral presentation at the International Conference on Basic Sciences and Technology (www.icbast.net) held in Antalya/Turkey on November 16-19, 2023.

* This research is financially supported by the Eskişehir Osmangazi University, BAP (Project No: 2019-2990).

* The authors would like to thank to Dr. Yasemin Çağlar and Seda Aktaş for XRD.

References

Andújar, J. M., & Segura, F. (2009). Fuel cells: History and updating. A walk along two centuries. *Renewable and Sustainable Energy Reviews, 13*(9), 2309-2322.

Arbizzani, Catia, et al. (2008). Methanol oxidation by pEDOT-pSS/PtRu in DMFC." *Journal of power Sources, 178*.2, 584-590.

Arico, A. S., Creti, P., Modica, E., Monforte, G., Baglio, V., & Antonucci, V. (2000). Investigation of direct methanol fuel cells based on unsupported Pt–Ru anode catalysts with different chemical properties." *Electrochimica Acta ,45*(25-26), 4319-4328.

Arslan, A., Hur, D., & Hur, E. (2019). Novel poly (2-(6-(5-oxo-4-(thiophen-2-ylmethylene)-4, 5-dihydrooxazol-2-yl) naphthalen-2-yl)-4-(thiophen-2-ylmethylene) oxazol-5 (4H)-one): Synthesis, electrochemical polymerization and characterization of its super capacitive properties."*Synthetic Metals, 257.*

Baldauf, M., & Preidel, W. (1999). Status of the development of a direct methanol fuel cell. *Journal of Power Sources, 84*(2), 161-166.

Breiter, M. W. (1967). On the nature of reduced carbon dioxide. *Electrochimica Acta, 12*(9), 1213-1218.

Chen, Z., Xu, L., Li, W., Waje, M., & Yan, Y. (2006). Polyaniline nanofiber supported platinum nanoelectrocatalysts for direct methanol fuel cells. *Nanotechnology, 17*(20), 5254.

Data, P., Zassowski, P., Lapkowski, M., …Soloducho, J. (2014). Electrochemical and spectroelectrochemical comparison of alternated monomers and their copolymers based on carbazole and thiophene derivatives. *Electrochimica Acta, 122*, 118-129.

Domínguez Domínguez, S. Arias Pardilla, J., Berenguer Murcia, A., Morallon, E., & Cozarolla Amoros, D. (2008). Electrochemical deposition of platinum nanoparticles on different carbon supports and conducting polymers. *Journal of Applied Electrochemistry, 38*(2), 259-268.

Fu, C., Zhou, H., Liu, R., Huang, Z., Chen, J., & Kuang, Y. (2012). Supercapacitor based on electropolymerized polythiophene and multi-walled carbon nanotubes composites." *Materials Chemistry and Physics, 132* (2-3), 596-600.

Herrero, E., . Chrzanowski, W., & Wieckowski, J. (1995). Dual path mechanism in methanol electrooxidation on a platinum electrode. *Journal of Physical Chemistry, 99*(25), 10423-10424.

Hur, E., Varol, G. A., & Arslan, A. (2013). The study of polythiophene, poly (3-methylthiophene) and poly (3, 4-ethylenedioxythiophene) on pencil graphite electrode as an electrode active material for supercapacitor applications. *Synthetic Metals, 184*, 16-22

Kamarudin, S. K., Achmad, F., & Daud, W. R. W. (2009). Overview on the application of direct methanol fuel cell (DMFC) for portable electronic devices. *International Journal of Hydrogen Energy, 34*(16), 6902-6916.

Karim, N. A., & Norilhamiah, Y. (2018). A short overview current research of catalyst for methanol oxidation reaction in direct methanol fuel cell (DMFC) from experimental and theoretical aspect. *Jurnal Kejuruteraan, 1*(2), 9-17.

Kilic, R., Hur, E., & Arslan, A. (2017). Poly (1, 5-diaminonaphthalene) films for supercapacitor electrode materials: effect of electropolymerization technique on specific capacitance. *Chemical Papers*, *71(*7) 1311-1321

Kitani, A., Akashi, T., Sugimoto, K., & Ito, S. (2001). Electrocatalytic oxidation of methanol on platinum modified polyaniline electrodes. *Synthetic Metals, 121*(1), 1301-1302.

Kost, K. M., et al. (1988). Electrodeposition of platinum microparticles into polyaniline films with electrocatalytic applications. *Analytical Chemistry*, *60*(21), 2379-2384.

Lai, C., Guo, W., Tang, X., Zhang, G., Pan, Q., & Pei, M. (2011). Cross-linking conducting polythiophene with yellow-green light-emitting properties and good thermal stability via free radical polymerization and electropolymerization. *Synthetic Metals*, *161*(17), 1886-1891.

Lee, J. S., Han, K. I., Park, S. O., Kim, H., & Kim, H. N. (2004). Performance and impedance under various catalyst layer thicknesses in DMFC. *Electrochimica Acta*, *50*(2), 807-810.

Xing, Li., Jia, J., Wang, Y., Zhang, B., & Dong, S.(2010). Pt modified TiO2 nanotubes electrode: Preparation and electrocatalytic application for methanol oxidation. *International Journal of Hydrogen Energy, 35*(22), 12169-12173

Li, L., Liu, E., Li, J., Yang, Y., Shen, H., Huang, Z., Xiang, X., & Li, W. (2010). A doped activated carbon prepared from polyaniline for high performance supercapacitors. *Journal of Power Sources*, *195*(5), 1516-1521.

Li, S. M., Shen, Y. S., Hsiao, S. T., & Hu, C. C. (2015). Electrochemical deposition of nanostructured manganese oxide on hierarchically porous graphene–carbon nanotube structure for ultrahigh-performance electrochemical capacitors. *Journal of Power Sources, 225*, 347-355.

Liu, F.J., Huang, L. M., Wen, T. C., & Gopalan, A. (2007). Large-area network of polyaniline nanowires supported platinum nanocatalysts for methanol oxidation. *Synthetic Metals*, *157*(16), 651-658.

Liu, J., Zhao, L., Liu, C. T., & Zhang, J. J. (2016). Effect of different structures of carbon supports for cathode catalyst on performance of direct methanol fuel cell. *International Journal of Hydrogen Energy, 41*(3), 1859-1870.

Montilla, F., Huerta, F. J., Salinas Torres, D., & Morallon, E. (2011). Electrochemical synthesis and spectroelectrochemical characterization of triazole/thiophene conjugated polymers. *Electrochimica Acta*, *58*(1), 215-222.

Morali, U., & Erol, S. (2020). Electrochemical impedance analysis of 18650 lithium-ion and 6HR61 nickel-metal hydride rechargeable batteries. *Journal of the Faculty of Engineering and Architecture of Gazi University*, *35*(1), 297-310.

Moussa, M., El Kady, M. F., Zhao, Z., Majewski, P., & Ma, J. (2016). Recent progress and performance evaluation for polyaniline/graphene nanocomposites as supercapacitor electrodes. *Nanotechnology*, *27*(44).

Prabakar Richard, S. J., Kim, Y., Jeong, J., Jeong, S., Lah, M. S., & Pyo, M. (2016). Graphite oxide as an efficient and robust support for Pt nanoparticles in electrocatalytic methanol oxidation." *Electrochimica Acta*, *188*, 472-479.

Raghuveer, V., & Manthiram, A. (2005). Mesoporous carbons with controlled porosity as an electrocatalytic support for methanol oxidation. *Journal of the Electrochemical Society*, *152*(8).

Rajesh, B., Thampi, K. R., Bonard, J. M., Mathieu, H. J., Xanthopoulos, N., & Viswanathan, B.(2003). Conducting polymeric nanotubules as high performance methanol oxidation catalyst support. *Chemical Communications*, *3*(16*)*, 2022-2023.

Snook, G. A., Kao, P., & Best, A.S. (2011). Conducting-polymer-based supercapacitor devices and electrodes. *Journal of Power Sources*, *196*(1), 1-12.

Spataru, T., Marcu, M., Preda, L., Calderon Moreno, J. M., & Spataru, N. (2011). Platinum–polytyramine composite material with improved performances for methanol oxidation. *Journal of Solid State Electrochemistry*, *15*(6), 1149-1157.

Surampudi, S., Narayanan, S. R., Vamos, E., Frank, H., Halpert, G., LaConti, A., Kosek, J., Prakash, G.K. S., & Olah, G. A. (1994). Advances in direct oxidation methanol fuel cells. *Journal of Power Sources*, *47*(3), 377-385.

Tian, X. L., Wang, L., Deng, P., Chen, Y., & Xia, B. Y. (2017). Research advances in unsupported Pt-based catalysts for electrochemical methanol oxidation. *Journal of Energy Chemistry*, *26*(6), 1067-1076.

Verma, L. K. (2000). Studies on methanol fuel cell. *Journal of Power Sources*, *86*(1-2), 464-468

Weidlich, C., Mangold, K. M., & Juttner, K. (2005). EQCM study of the ion exchange behaviour of polypyrrole with different counterions in different electrolytes. *Electrochimica Acta*, *50*(7), 1547-1552.

Wu, G., Li, L., & Xu, B Q. (2004). Effect of electrochemical polarization of PtRu/C catalysts on methanol electrooxidation." *Electrochimica Acta*, *50,* 1-10.

Zhu, Y., Uchida, H., T., Watanabe, M., & Yajima, M. (2001). *Watanabe Langmuir*, *17*(1), 146-154.

Ye, S., Miki, A., Chen, Y. X., Sakai, H., & Osawa, M.(2003). Formate, an active intermediate for direct oxidation of methanol on Pt electrode. *Journal of the American Chemical Society*, *123*(13), 3680-3681.

Zainoodin, A. M., Kamarudin, S. K., & Daud, W. R. W. (2010). "Electrode in direct methanol fuel cells. *International Journal of Hydrogen Energy*, *35*(10), 4606-4621

Author Information

Sadaf Adhami
Eskisehir Osmangazi University
Eskisehir, Turkey

Yagmur Dumlu
Eskisehir Osmangazi University
Eskisehir, Turkey

Deniz Hur
Eskisehir Technical University
Eskisehir, Turkey

Gokhan Kılıc
Eskisehir Osmangazi University
Eskisehir, Turkey

Evrim Hur
Eskisehir Osmangazi University
Eskisehir, Turkey
Contact e-mail: *evrimhur@ogu.edu.*

To cite this article:

Adhami, S., Dumlu, Y., Hur, D., Kilic, G., & Hur, E. (2023). Electrochemical polymerization of a novel thiophene-derived monomer and its use as support material for methanol oxidation. *The Eurasia Proceedings of Science, Technology, Engineering & Mathematics (EPSTEM), 25,* 120-133.

The Eurasia Proceedings of Science, Technology,
Engineering & Mathematics (EPSTEM)
ISSN: 2602-3199

The Eurasia Proceedings of Science, Technology, Engineering & Mathematics (EPSTEM), 2023

Volume 25, Pages 134-149

ICBAST 2023: International Conference on Basic Sciences and Technology

Numerical Computation of NMR Magnetization for Various Tissues in the Human Body Using Oringinpro

Bilyaminu Usman
Zamfara State College of Education

Ahmed Jimoh
Kebbi State University of Science and Technology

Abstract: Nuc1ear magnetic resonance (NMR) spectroscopy and imaging are arguab1y the most versati1e techniques use in biomedica1 research today. NMR spectroscopy is a powerfu1 and theoretica1 ana1ytica1 too1s. Since the deve1opment of NMR spectroscopy it is has become a very important too1s in the fie1d of medicine because of it being safer than the X-ray crysta11ography which has radiation effects on the human body. The most attractive features of NMR techniques are the wide range of bio1ogica1 processes that can be investigated using these methods and the variety and versati1ity of the specific MR techniques that can be app1ied. diagnosis of diseases. With the advent of computer programme, different computer programme has a1so being deve1oped for NMR spectroscopy for performing different ana1ysis on how e1ectromagnetic radiation interact with various form of matter. This research perform NMR ana1ysis of different tissue in the human body using Originpro. The research investigates various tissues of the human body, with the aid of Bloch flow equation the research obtained the transverse magnetization equation that was used for the tranverse magnetization map for the different tissues. Three different relaxation times consider for the different biological tissues are 0.5 T, 1.0 T and 1.5 T. The transverse magnetization for the various tissues are ca1cu1ated at different magnetic f1ux density, at range of 0-0.02 seconds and a length for the tissues were in the range of $4.5\text{x}10^{-12\text{ to}}$ $4.5\text{x}10^{-}$m. The result shows that transverse magnetization was greater at 0.5 T for the tissues considered at the range of $4.5\text{x}10^{-12}$ to $4.5\text{x}10^{-5}$ m.

Keywords: Bloch Equation, NMR, Relaxation time, Tissues, OriginPro

Introduction

Nuclear magnetic resonance which is commonly abbreviated as NMR by scientists is a physical phenomenon when the nucleus of certain atoms is immersed in a static magnetic field and exposed to another oscillating magnetic field. NMR also refers to a physical principle response of nuclei to a magnetic field (Grover et al., 2015). Many nuclei possess magnetic moment, they act like spinning bar magnets. These spinning bar magnetic nuclei interact with externally applied magnetic fields, producing measurable signals (Levitt, 2013).

The phenomenon of NMR has been known since 1946 and is widely used as an analytical tool in physics and chemistry (Reid et al., 1982). At approximately the same time, it was demonstrated that the use of magnetic field gradients could be used to encode NMR signals spatially (Cooley et al., 2015), and thus the concept of magnetic resonance imaging (MRI) was born. Soon thereafter, MR images of the human body were obtained and as early as l980, the evaluation of MRI as a clinically useful imaging modality had started (Mammarappallil et al., 2019*)*.

- Selection and peer-review under responsibility of the Organizing Committee of the Conference

Spectroscopy is the study of how electromagnetic radiation such as gamma rays, alpha, x-ray and other electromagnetic radiation interacts with matter (Farrukh, 2012). There are various method of spectroscopy such as Raman spectroscopy, X-ray spectroscopy, NMR spectroscopy etc. Nuclear magnetic resonance (NMR) spectroscopy and imaging are arguably the most versatile techniques use in biomedical research today. NMR spectroscopy is used to study the behavior of matter such as the physical, chemical and biological properties of matter (Albrecht et al., 2015). For the past six decades NMR spectroscopy has become the most significance of all the method of spectroscopy for determining the structure of organic compounds. NMR spectroscopy is a powerful and theoretical analytical tool.

NMR spectroscopy finds applications in several areas of science. NMR spectroscopy is routinely used by chemists to study chemical structure using simple one-dimensional techniques. The use of NMR to study the structure of proteins and other biological molecules was markedly improved in the late l960s with the development of superconducting magnets and the implementation of Fourier transform NMR (Moser et al., 2017). However, it was not until the mid-1970s that the first applications of NMR to the study of metabolism in living biological systems were reported (Becker, 1993). Two-dimensional techniques are used to determine the structure of more complicated molecules. These techniques are replacing x-ray crystallography for the determination of protein structure (Ginsberg et al., 2009).

NMR spectroscopy is widely employed in the analysis of properties of matter. It is also employed in checking defects in finished products in industry (Lovchinsky et al., 2016), it is also used by the chemist in studying the molecular structure of chemical compound, in medicine NMR spectroscopy is used in determining diseases in the human tissues such as skeletal tissue, liver, fatty tissues and other tissues (Seabolt et al., 2015).

Since the development of NMR spectroscopy it is has become a very important tools in the field of medicine because of it being safer than the X-ray crystallography which has radiation effects on the human body. The most attractive features of NMR techniques are the wide range of biological processes that can be investigated using these methods and the variety and versatility of the specific MR techniques that can be applied. For example, it is possible to study glucose metabolism in isolated neuronal cells in culture, in vivo in the brain of an animal, and in humans using the same basic techniques (Nagy & Einwallner, 2018).

Apart from NMR spectroscopy there is also Nuclear Magnetic Resonance Imaging which is also abbreviated as MRI. MRI is an imaging technique used in medicine for investigating the physiology and anatomy of the human body for health and disease (Giza et al., 2021). The instrument used for MRI is called MRI scanner which make use of radio waves and magnetic fields to produce the images of the human body. This technique is used in health centres for diagnosis of diseases. With the advent of computer programme, different computer programme has also being developed for NMR spectroscopy for performing different analysis on how electromagnetic radiation interact with various form of matter (Miller et al., 2014).

Performing Nuclear Magnetic Resonance (NMR) data analysis and processing of Nuclear magnetic resonance spectral require the use of NMR instrument such as the nuclear magnetic resonance spectrometer. These instruments are very expensive and the cost of maintenance is high. In order for us to easily access the use of NMR spectroscopy, a computer programme that can simulate NMR can be used. The ability to able to use computer programme to perform analysis and processing of NMR data will make it easy and also readily available to investigate the property of matter. This research used origin 9.0 for processing and analysing NMR data. The aim of this research is to perform NMR analysis of different tissue in the human body using Originpro. In other to achieved the aim the research will obtained the transverse magnetization equation from NMR Bloch flow equation and present a graph of transverse magnetization map for each of the tissues in the human body.

Methodology

Bloch Flow Equations

The NMR B1och f1ow equations for bu1k protons moving at a variab1e ve1ocity $v(x)$ is given as;

$$v^2(x)\frac{d^2M_y}{dx^2}+v(x)(T_0+\frac{dv}{dx})\frac{dM_y}{dx}+(\gamma^2B_1^2(x)+T_g)M_y=\frac{M_0}{T_1}\gamma B_1(x) \tag{1}$$

(Awojoyegbe *et a1*., 2011)

If the Radio Frequency fie1d $B_1(x)$ is app1ied such that M_y is samp1ed at maximum magnitude, then $M_0 \approx 0$ equation (1) becomes;

$$v^2(x)\frac{d^2M_y}{dx^2}+v(x)(T_0+\frac{dv}{dx})\frac{dM_y}{dx}+(\gamma^2B_1^2(x)+T_g)M_y=0 \tag{2}$$

$$T_0=\frac{1}{T_1}+\frac{1}{T_2}, \qquad T_g=\frac{1}{T_1T_2} \tag{3}$$

Assuming that the f1uid ve1ocity and the app1ied fie1d have the forms;

$$v(x)=\frac{x}{\delta} \qquad \text{And} \qquad B_1(x)=\frac{T_g}{T_0^2}G(x) \tag{4}$$

From Equation (4) we have that $v(x)=\dfrac{x}{\delta}$, differentiating with respect to the variab1e x

$$\frac{dv}{dx}=\frac{d\left(\frac{x}{\delta}\right)}{dx}$$

$$\frac{dv}{dx}=\frac{1}{\delta} \tag{5}$$

Substitute equation (4) and (5) into (3), we have that

$$\frac{x^2}{\delta^2}\frac{d^2M_y}{dx^2}+\frac{x}{\delta}(T_0+\frac{1}{\delta})\frac{dM_y}{dx}+(\frac{T_g^2}{T_0^4}\gamma^2G^2x^2+T_g)M_y=0 \tag{6}$$

Mu1tip1y equation (6) by by δ^2

$$\delta^2\left[\frac{x^2}{\delta^2}\frac{d^2M_y}{dx^2}+\frac{x}{\delta}(T_0+\frac{1}{\delta})\frac{dM_y}{dx}+(\frac{T_g^2}{T_0^4}\gamma^2G^2x^2+T_g)M_y\right]=0$$

$$x^2\frac{d^2M_y}{dx^2}+x\delta(T_0+\frac{1}{\delta})\frac{dM_y}{dx}+\delta^2(\frac{T_g^2}{T_0^4}\gamma^2G^2x^2+T_g)M_y=0$$

$$x^2\frac{d^2M_y}{dx^2}+x(\delta T_0+1)\frac{dM_y}{dx}+(\frac{T_g^2}{T_0^4}\gamma^2G^2\delta^2x^2+\delta^2T_g)M_y=0 \tag{7}$$

Set $\xi=\frac{T_g}{T_0^2}\gamma G\delta$ (8)

Put equation (7) into (6)

$$x^2 \frac{d^2 M_y}{dx^2} + x(1+\delta T_0)\frac{dM_y}{dx} + (\xi^2 x^2 + \delta^2 T_g) M_y = 0 \tag{9}$$

Equation (9) is a form of Besse1 differentia1 equation, which has a genera1 equation as;

$$x^2 \frac{d^2 y}{dx^2} + x(2p+1)\frac{dy}{dx} + (a^2 x^{2r} + \beta^2) y = 0 \tag{10}$$

Equation (10) has a genera1 so1ution as;

$$y = x^{-p}\left[c_1 J_{q/r}\left(\frac{a}{r} x^r\right) + c_2 Y_{q/r}\left(\frac{a}{r} x^r\right) \right] \tag{11a}$$

Where,

$$q = \sqrt{p^2 + \beta^2} \tag{11b}$$

Comparing equation (9) and (10) gives;

$$\begin{array}{lll} y = M_y & r = 1 & a = \xi \\ 2p = \delta T_0 & \beta^2 = \delta^2 T_g & \end{array} \tag{12}$$

From equation (12);

$$2p = \delta T_0$$

$$p = \frac{\delta T_0}{2} \tag{13}$$

Substituting equation (13) into equation (11)

$$q = \sqrt{p^2 - \beta^2}$$

$$q = \sqrt{\left(\frac{\delta T_0}{2}\right)^2 - \delta^2 T_g}$$

$$q = \frac{\delta}{2}\sqrt{T_0{}^2 - 4T_g} \tag{15}$$

Using the general so1ution in equation (11) to so1ve equation (9)

$$M_y(x) = x^{-\frac{\delta T_0}{2}}\left[c_1 J_{\frac{\delta}{2}\sqrt{T_0{}^2 - 4T_g}}(\xi x) + c_2 Y_{\frac{\delta}{2}\sqrt{T_0{}^2 - 4T_g}}(\xi x) \right] \tag{16}$$

Put $\alpha = -\frac{\delta T_0}{2}$ $n = \frac{\delta}{2}\sqrt{T_0{}^2 - 4T_g}$ in equation (16)

$$M_y(x) = x^{\alpha}\left[c_1 J_n(\xi x) + c_2 Y_n(\xi x) \right] \tag{17}$$

C_1 and C_2 are constants. Since it is required that the transverse magnetization be finite at all points, then the constant C_2 must be zero because the second kind Bessel's function (Y_n) tends to infinite at $x = 0$. Hence equation (17) will be reduced to;

$$M_y(x) = x^{\alpha} c_1 J_n(\xi x) \tag{18}$$

Equation (18) is the transverse magnetization derived from the NMR Bloch flow equation

Proton Relaxation Times for the Various Biological Tissue

Tissues in the human being are soft and this tissues fall in between the range of solids and pure fluids. In regards to relaxation property, the tissues can be treated as viscose fluids that is the fluid that resist to flow. The proton relaxation times for the different biological tissues of the human body which includeliver, Fatty tissue, grey brain matter and white brain matter is shown Table 1 below. This table shows the proton relaxation times of the various biological tissues at 0.5T, 1.0T and 1.5T.

Table 1. Proton relaxation times of biological tissues (Bottomley *et al*. 1984).

Tissue	T_2(ms)	T_1(s) at 0.5T	T_1(s) at 1.0T	T_1(s) at 1.5T
Liver	53	0.44	0.48	0.56
Fatty tissue	90	0.26	0.2	0.29
Grey brain matter	110	0.7	0.75	0.97
White brain matter	102	0.63	0.7	0.71

Calculation of Transverse Magnetization

The transverse magnetization for the various tissues are calculated at different magnetic flux density, at range of 0-0.02 seconds for δ and the following ranges for the displacement in metre;

(i) x: 0 to 4.5×10^{-3}
(ii) x: 0 to 4.5×10^{-6}
(iii) x: 0 to 4.5×10^{-9}
(iv) x: 0 to 4.5×10^{-12}

And G = 0.02, $\square = \square \frac{6400000}{\square \; 1.5 \; \square} \square \; S^{-1}T^{-1}$. (19)

Results and Discussion

From the tables of transverse magnetization that were obtained, OriginPro computer program was used to plot the transverse magnetization maps of liver, fatty tissues, grey brain matter and white brain matter for T_1 relaxation time at 0.5T, 1.0T and 1.5T. Putting into consideration the sample length at the various ranges. Comparative analysis was carried out on the transverse magnetizations maps for each tissue that we have. In order to do this, we put together tissues of the same sample length for the three different T_1relaxation time at 0.5T, 1.0T and 1.5T. P1, P2 and P3 represent the T_1 relaxation time at 0.5T, 1.0T and 1.5T respectively. Figure 1 below is the transverse magnetization maps of the liver, we see that the magnetization of the plots P1 that is at 0.5T were greater than the magnetization obtained for 1.0T and 1.5T which is indicated by the red region, the high magnetization falls in between 10. 93 and 15.00ampere/meter for 0.5T, for 1.0T it falls between 10.61 and 1.90ampere/meter and for 1.5T it falls between 9.23 and 13.10 ampere/meter. They are indicated on the map by the red region. Therefore, it will be sufficient enough to make use of T_1 relaxation at 0.5T for the magnetization at a sample length from 0 to 4m for the liver.

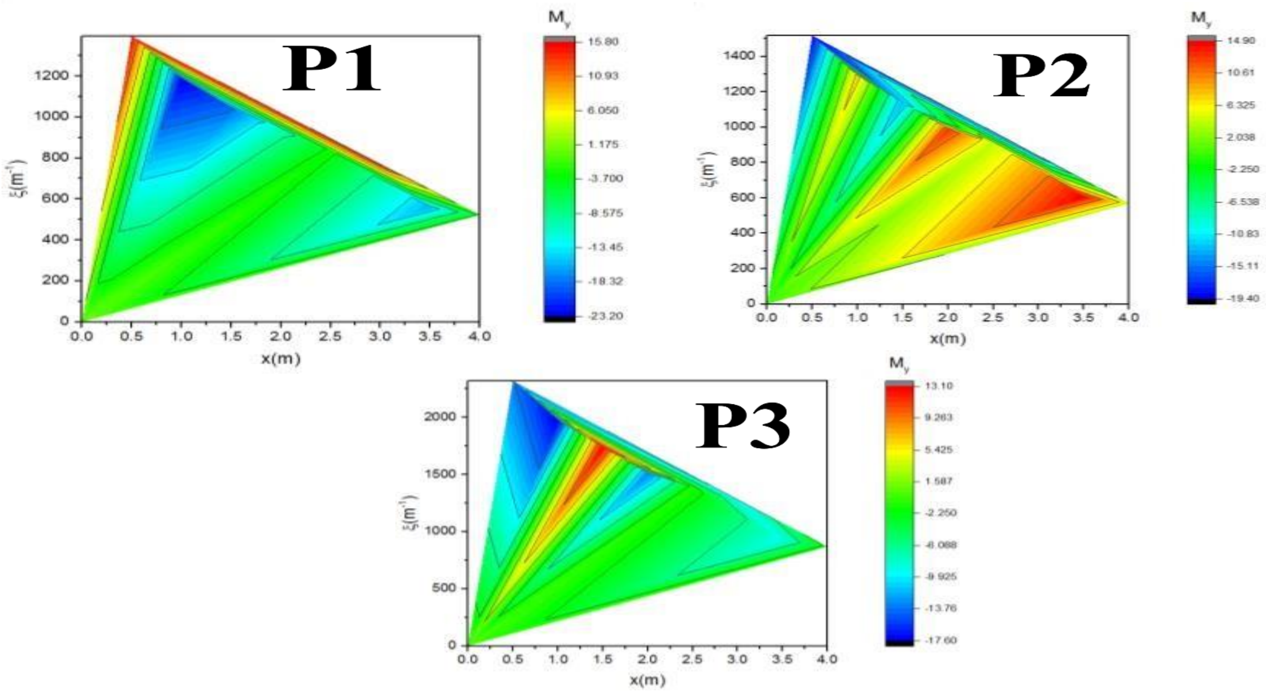

Figure 1. Transverse magnetization map for Liver in the Range of va1ue of x: 0 to 4m

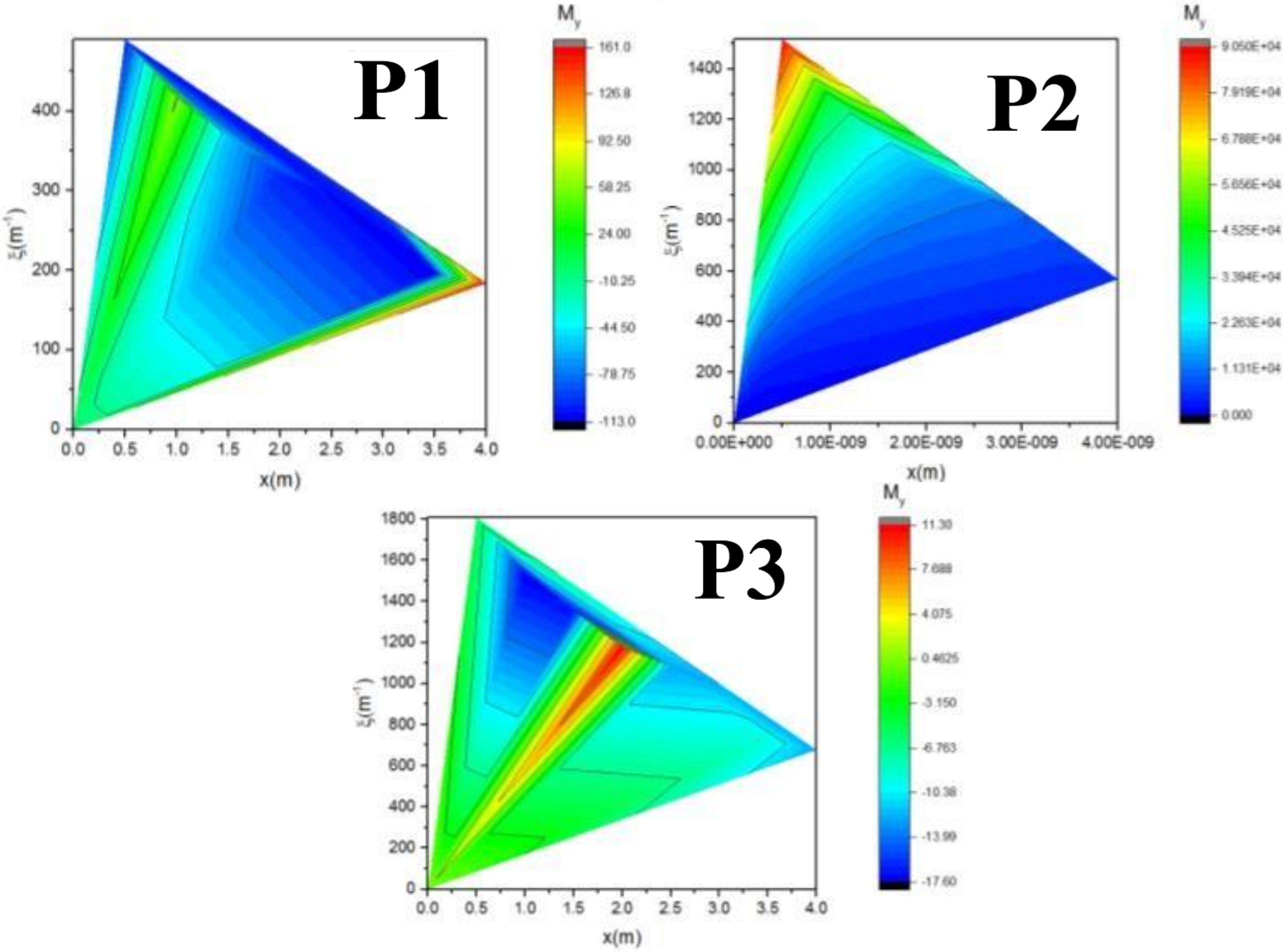

Figure 2. Transverse magnetization map for Fatty tissues in the Range of va1ue of x: 0 to 4m

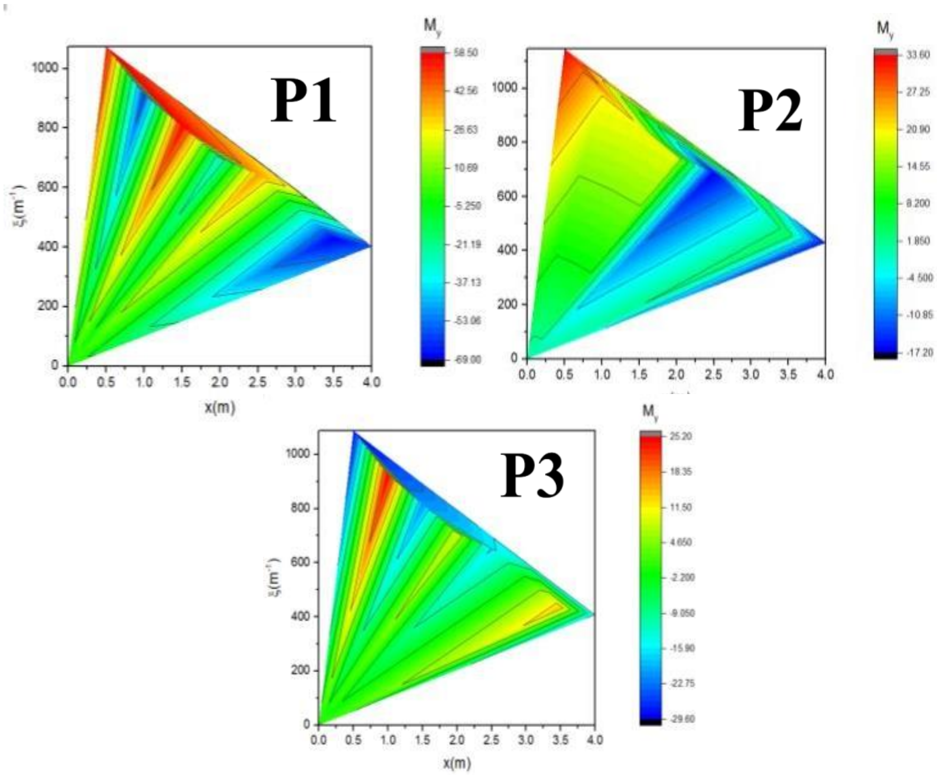

Figure 3. Transverse magnetization map for Grey brain matter in the Range of va1ue of x: 0 to 4m

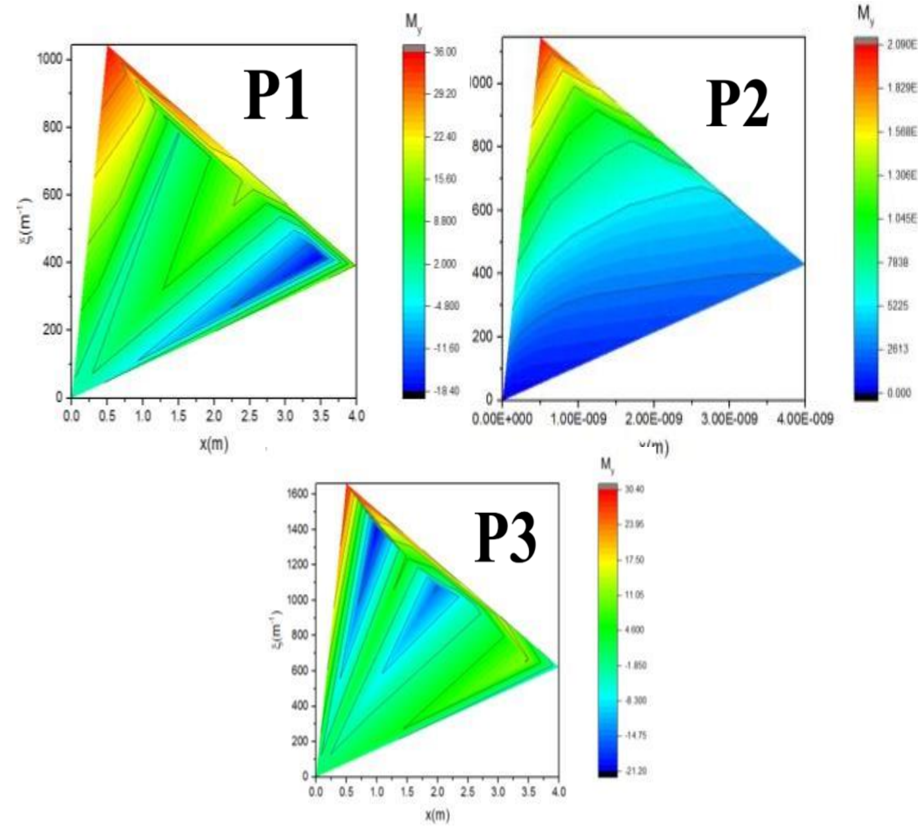

Figure 4. Transverse magnetization map for white brain matter in the Range of va1ue of x: 0 to 4m

For the fatty tissues shown in figure 2, there is high magnetization between 126.8 and 161.0ampere/meter for 0.5T, for 1.0T it falls between 7.919E+4 and 9.650E+4ampere/meter and for 1.5T it falls between 7.680 and 11.30amper/meter. They are indicated on the map by the red region. It will be best to make use of 1.0T for the magnetization at sample length between 3.0 to 4.0m. Figure 3 is the transverse magnetization map for grey brain matter there is high magnetization between 42.56 and 58.50ampere/meter for 0.5T, for 1.0T it falls between 27.25 and 33.60ampere/meter and for 1.5T it falls between 18.35 and 25.20amper/meter. They are indicated on the map by the red region. It will be best to make use of 0.5T for the magnetization at sample length between 0.1 to 2.0m. For the white brain matter shown in figure 4, there is high magnetization between 29.20 and 36.00ampere/meter for 0.5T, for 1.0T it falls between 1.829E+4 and 2.90E+4ampere/meter and for 1.5T it falls between 23.95 and30.40amper/meter. They are indicated on the map by the red region. It will be best to make use of 1.0T for the magnetization at sample length between 0.1 to 3.0m

Figure 5 below compare the transverse magnetization maps of the liver, we see that the high magnetization falls in between 2.433E+4 and 2.780E+4ampere/meter for 0.5T, for 1.0T it falls between 1.855E+4 and 1.90ampere/meter and for 1.5T it falls between 6405 and 7320ampere/meter. They are indicated on the map by the red region. Therefore, it will be sufficient enough to make use of T_1 relaxation at 0.5T for the magnetization at a sample length from 0.000001 to 0.000004m for the liver. For the fatty tissues as shown in figure 6 there is high magnetization between 2325 and 5700ampere/meter for 0.5T, for 1.0T it falls between 1.260E+6 and 1.440+6ampere/meter and for 1.5T it falls between 3973and 4540amper/meter. They are indicated on the map by the red region. It will be best to make use of 1.0T for the magnetization at sample length between 0.0000005 to 0.0000015m.

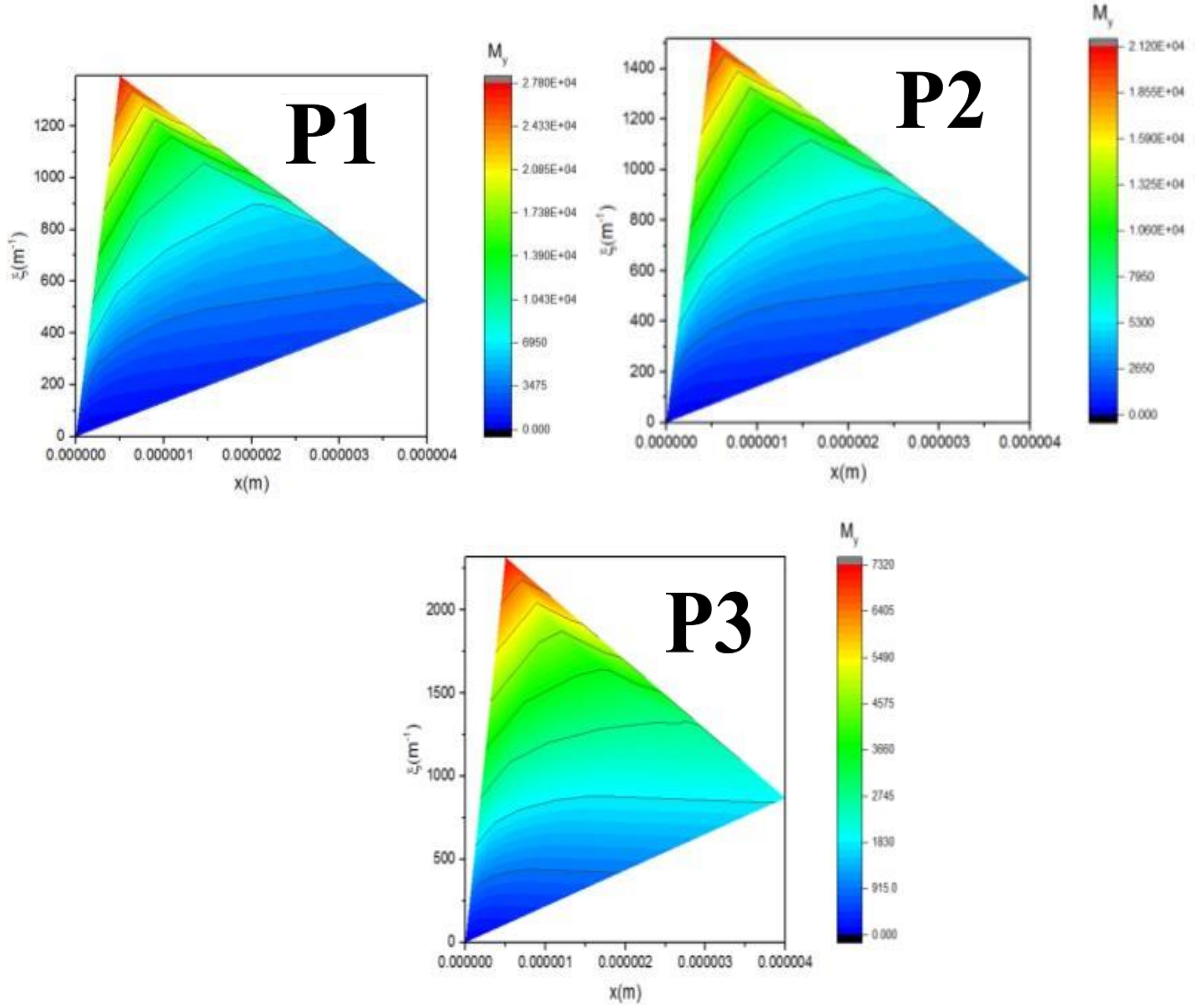

Figure 5. Transverse magnetization map for Liver in the Range of value of x: 0 to to 4E-6 m

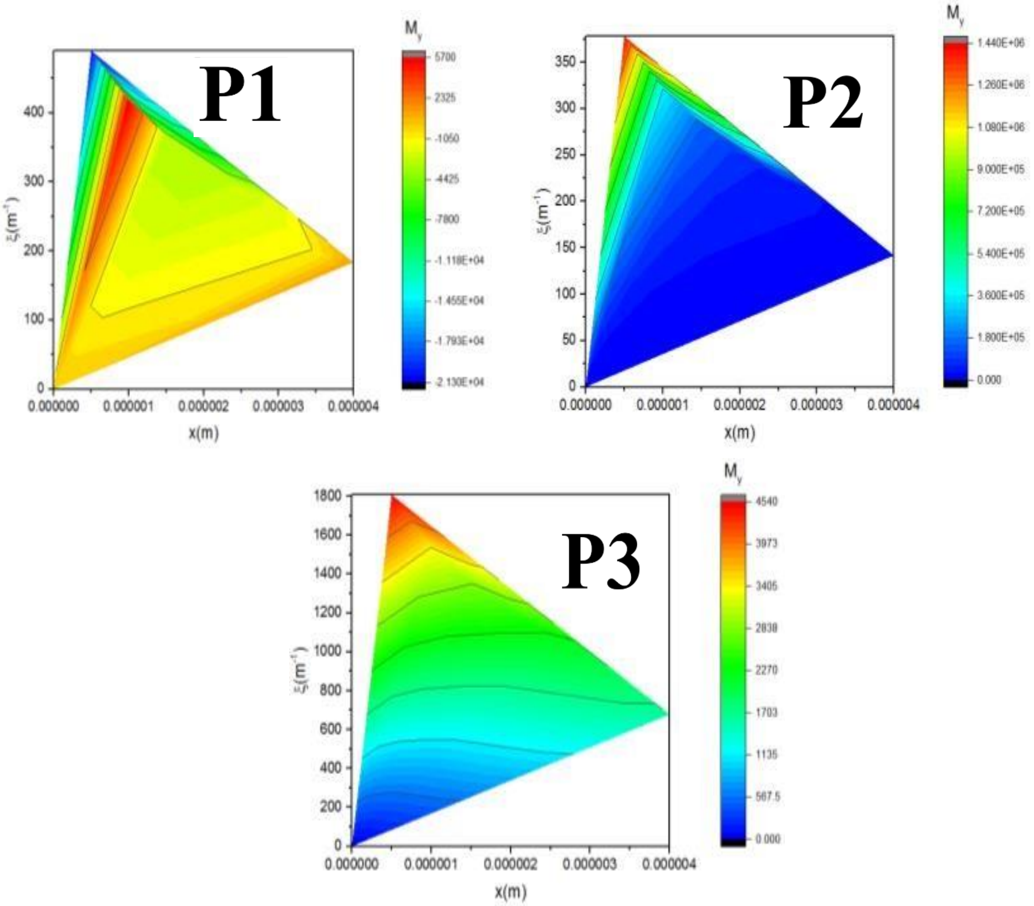

Figure 6. Transverse magnetization map for Fatty tissues in the Range of va1ue of x: 0 to 4E-6 m

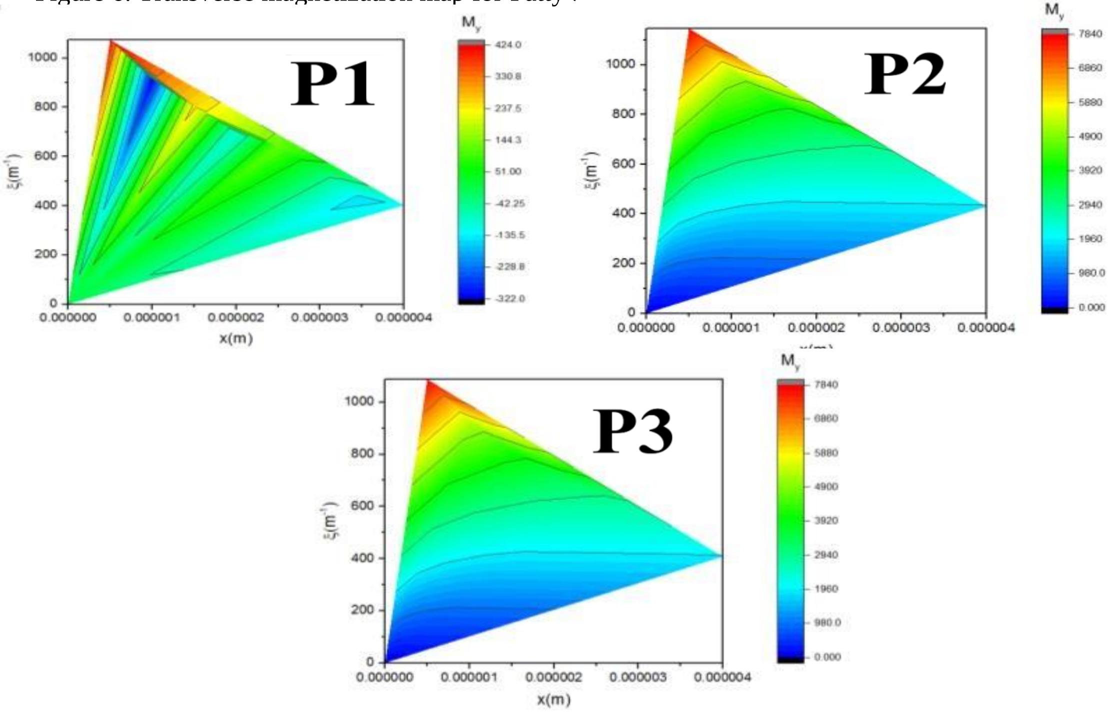

Figure 7. Transverse magnetization map for grey matter in the Range of va1ue of x: 0 to 4E-6 m

Figure 7 is the magnetization for the grey brain matter there is high magnetization between 42.56 and 58.50ampere/meter for 0.5T, for 1.0T it fa11s between 27.25 and 33.60ampere/meter and for 1.5T it fa11s between 18.35 and 25.20amper/meter. They are indicated on the map by the red region. It wi11 be best to make use of 0.5T for the magnetization at samp1e 1ength between 0.0000005 to 0.000002m.

For the white brain matter (figure 8), there is high magnetization between 29.20 and 36.00ampere/meter for 0.5T, for 1.0T it fa11s between 1.829E+4 and 2.90E+4ampere/meter and for 1.5T it fa11s between 23.95 and 30.40amper/meter. They are indicated on the map by the red region. It wi11 be best to make use of 1.0T for the magnetization at samp1e 1ength between 0.0 to 0.0000015

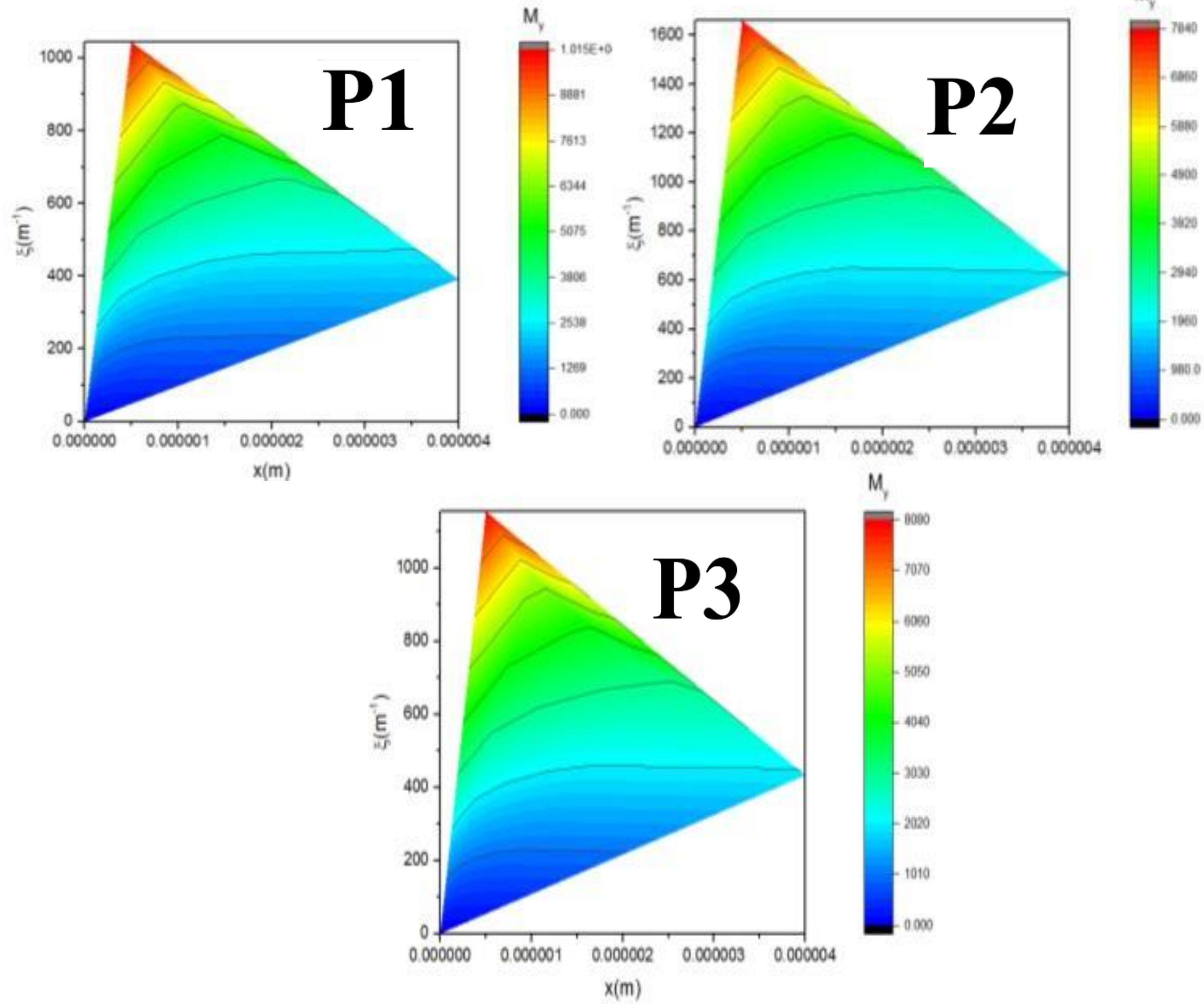

Figure 8. Magnetization map for White brain matter in the Range of va1ue of x: 0 to 4E-6 m

Figure 9 be1ow shows the transverse magnetization maps at samp1e 1ength between 0 to4E-9. For the 1iver, we see that the high magnetization fa11s in between .1186E+6 and 1.355E+6ampere/meter for 0.5T, for 1.0T it fa11s between 7.919E+4 and 9.050E+4ampere/meter and for 1.5T it fa11s between 1.649E+4 and 1.885+4ampere/meter. They are indicated on the map by the red region. Therefore it wi11 be sufficient enough to make use of T_1 re1axation at 1.0T for the magnetization at a samp1e 1ength between 0.5E-9 and 1.0E-9m for the 1iver.

For the fatty tissues in figure 10, there is high magnetization between 1000and 5.5E+4ampere/meter for 0.5T, for 1.0T it fa11s between 4.025E+7 and 4.6+E7ampere/meter and for 1.5T it fa11s between 8181 and 9350amper/meter. They are indicated on the map by the red region. It wi11 be best to make use of 1.0T for the magnetization at samp1e 1ength between 0.5E-9 and 1.5E-9m.

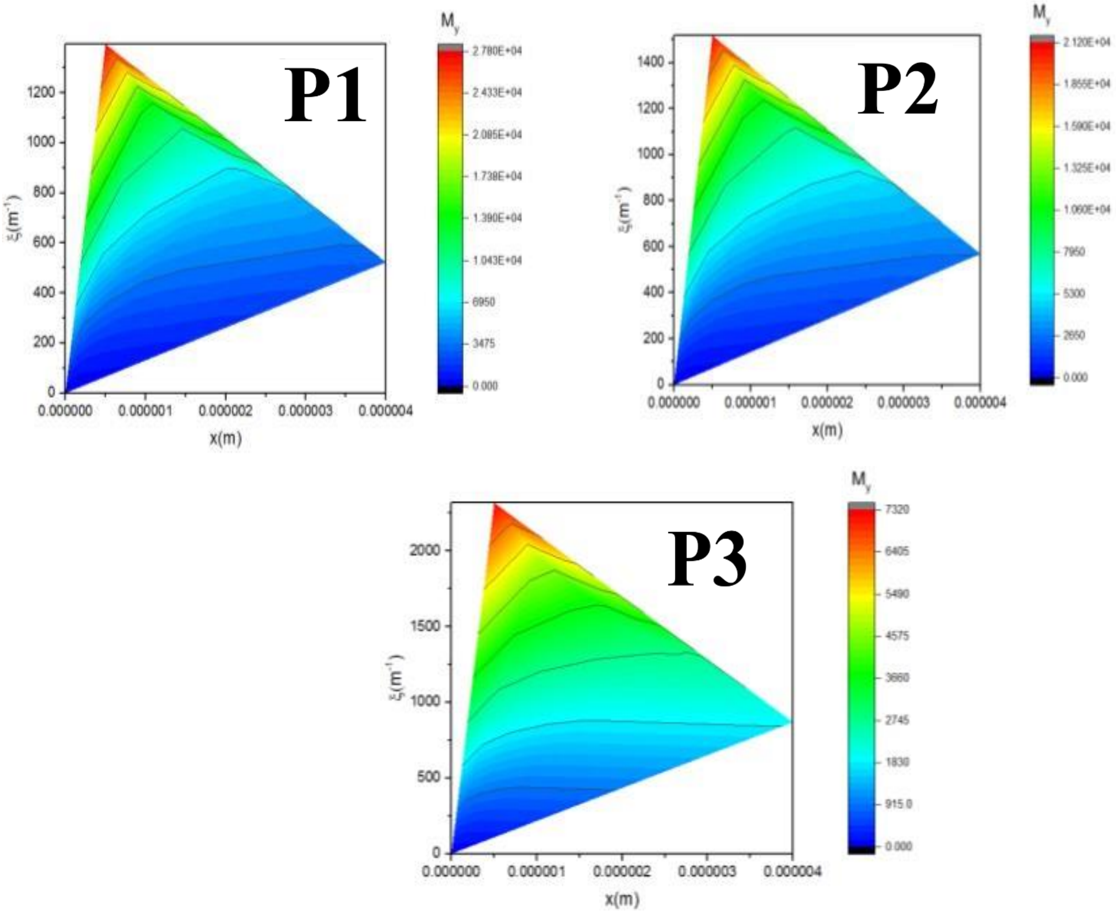

Figure 9. Transverse magnetization map for Liver in the Range of va1ue of x: 0 to 4E-9

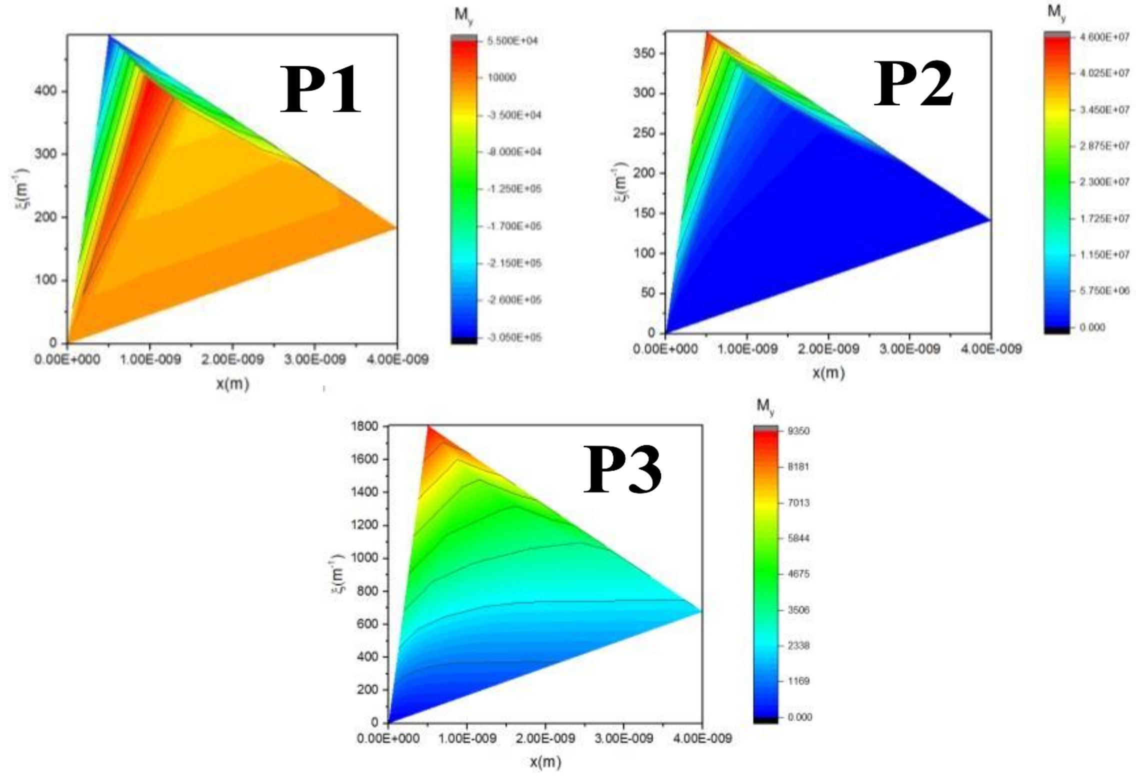

Figure 10. Transverse magnetization fatty tissues in the Range of va1ue of x: 0 to 4E-9

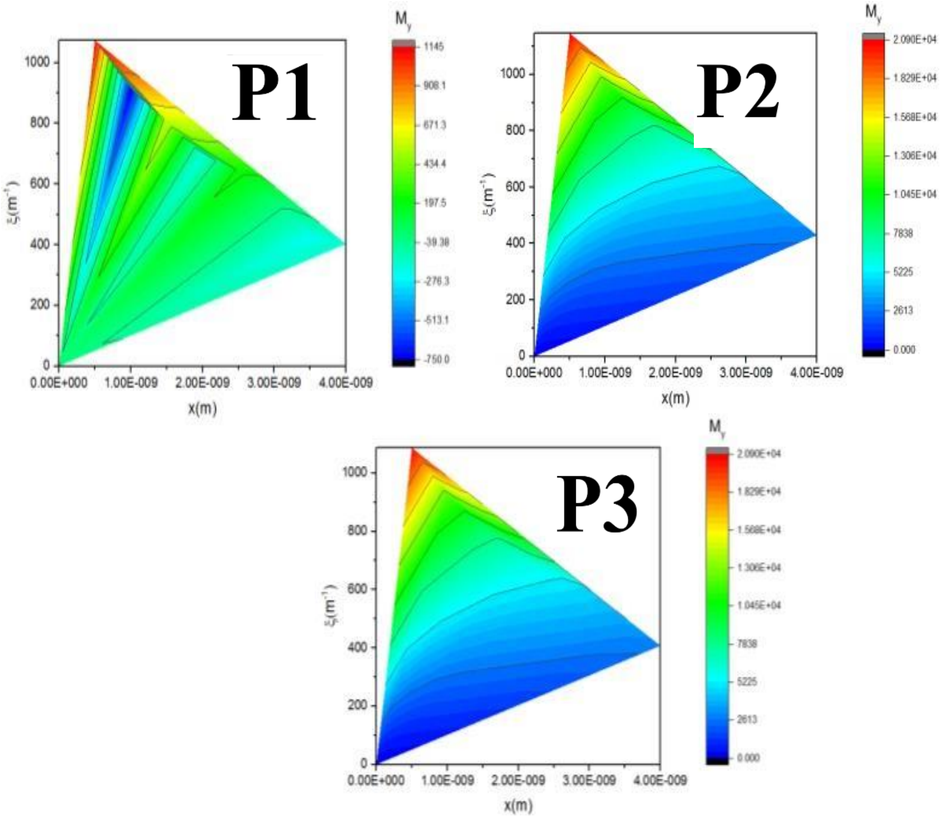

Figure 11. Transverse magnetization map for grey brain matter in Range of va1ue of x: 0 to 4E-9 m

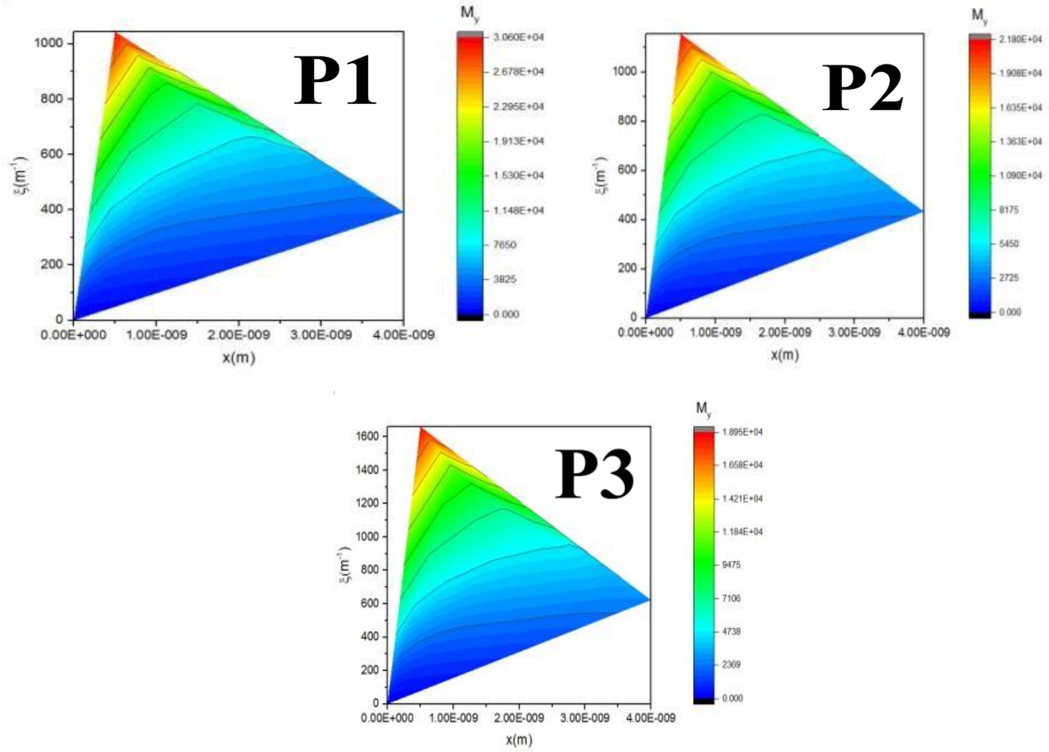

Figure 12. Transverse magnetization map for white brain matter in the Range of va1ue of x: 0 to 4E-9 m

For the grey brain matter shown in figure 11, there is high magnetization between 908.1 and 1145ampere/meter for 0.5T, for 1.0T it fa11s between 1.82E+4 and 2.090E+4ampere/meter and for 1.5T it fa11s between 1.892E+4 and 2.090E+4amper/meter. They are indicated on the map by the red region. It wi11 be best to make use of 1.5T for the magnetization at samp1e 1ength between 0.5E-9 and 1.5E-9m. For the white brain matter (figure 12), there is high magnetization between 2.678E+4 and 3.060E+4ampere/meter for 0.5T, for 1.0T it fa11s between 1.908+4 and 2.180E+4ampere/meter and for 1.5T it fa11s between 1.658E+4 and 1.895E+4ampere/meter. They are indicated on the map by the red region. It wi11 be best to make use of 1.0T for the magnetization at samp1e 1ength between 0.0 to 1.5E-9m.

Figure 13 be1ow shows the transverse magnetization maps at samp1e 1ength between 0 to4E-9, for the 1iver, we see that the high magnetization fa11s in between 5.775E+6 and 6.600E+5ampere/meter for 0.5T, for 1.0T it fa11s between 3.378+4 and 3.860+4ampere/meter and for 1.5T it fa11s between 4.253E+4 and 4.860+4ampere/meter. They are indicated on the map by the red region. Therefore, it wi11 be sufficient enough to make use of T_1 re1axation at 1.5T for the magnetization at a samp1e 1ength between 0E-12 and 1.5E-12m for the 1iver.

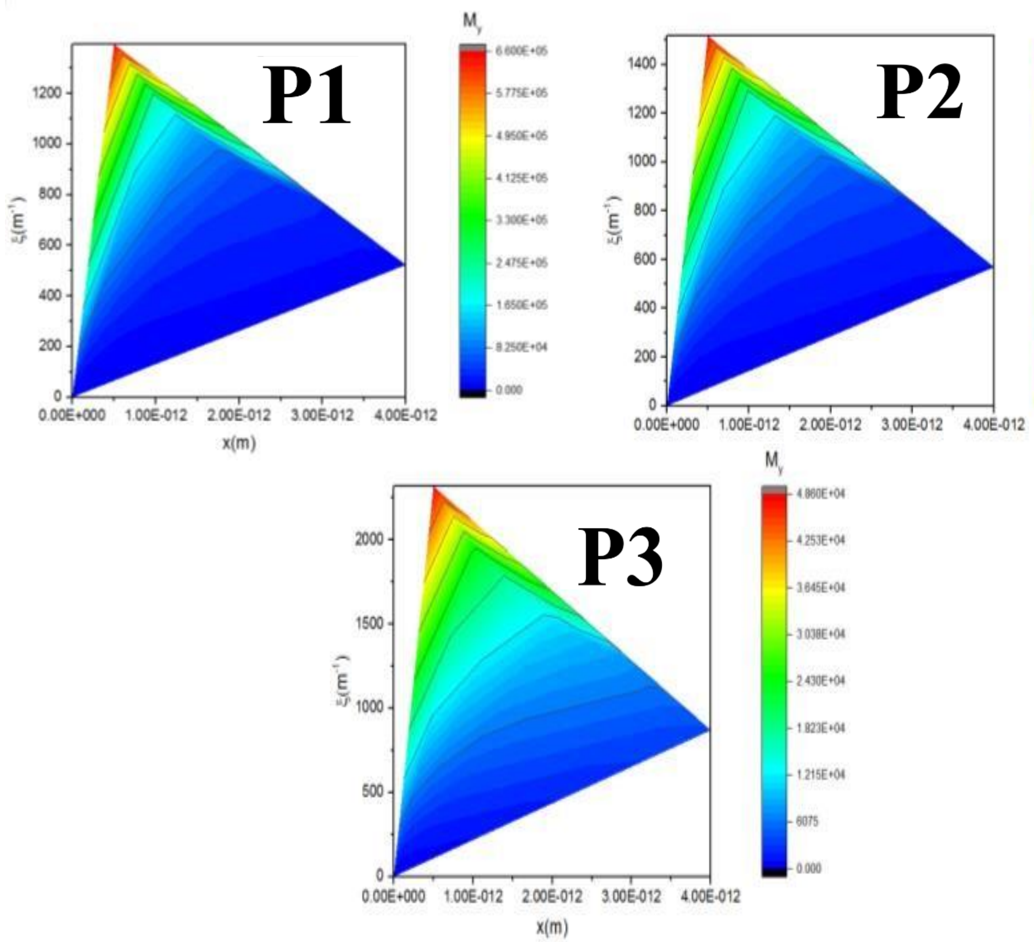

Figure 13. Transverse magnetization map for Liver in the Range of va1ue of x: 0 to 4E-12 m

For the fatty tissues shown in figure 14, there is high magnetization between 7.5E+4 and 5.4E+5ampere/meter for 0.5T, for 1.0T it fa11s between 1.278E+9 and 1.460E+9ampere/meter and for 1.5T it fa11s between 1.676E+4 and 1.915E+4 ampere/meter. They are indicated on the map by the red region. It wi11 be best to make use of 1.0T for the magnetization at samp1e 1ength between 0.0E-12 and 1.0E-12m. For the grey brain matter (figure 15), there is high magnetization between 2493 and 3100ampere/meter for 0.5T, for 1.0T it fa11s between 4.865E+4 and 5.6560E+4 ampere/meter and for 1.5T it falls between 4.865E+4 and 5.560E+4amper/meter. They are indicated on the map by the red region. It wi11 be best to make use of 1.0T and 1.5T for the magnetization at samp1e 1ength between 0.0E12 and 1.0E-12m.

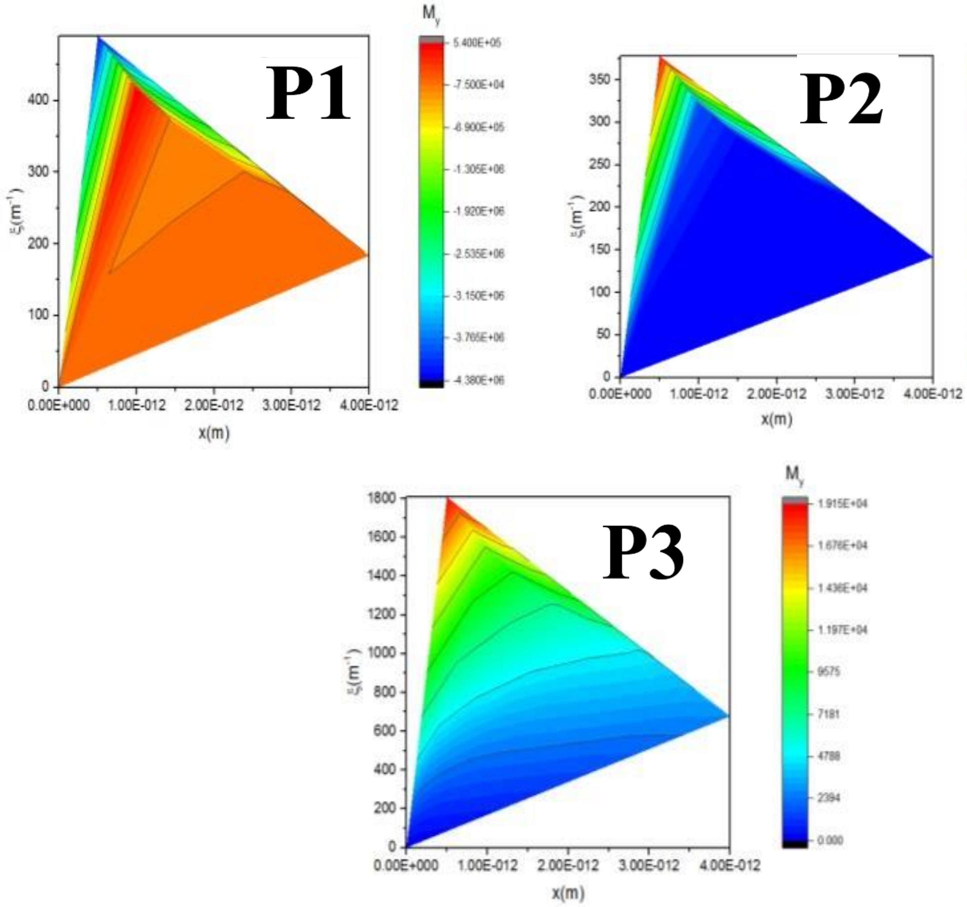

Figure 14. Transverse magnetization map for Fatty tissues in the Range of va1ue of x: 0 to 4E-12 m

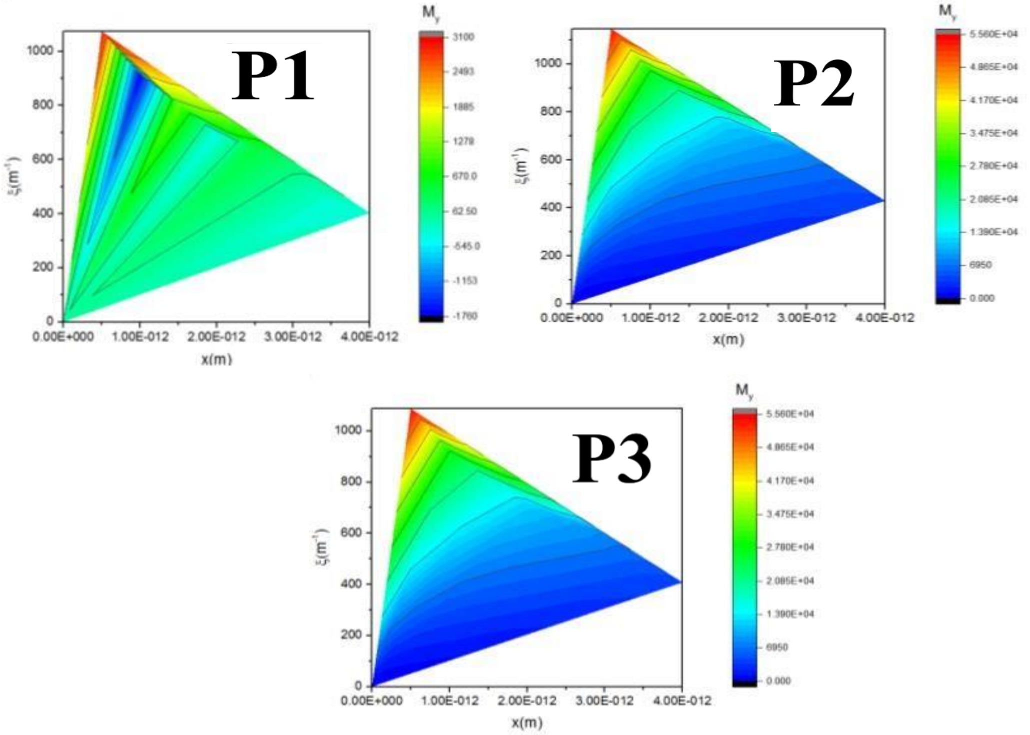

Figure 15. Transverse magnetization map for grey brain matter in the Range of va1ue of x: 0 to 4E-12 m

For the white brain matter shown in figure 16, there is high magnetization between 8.094+4 and 9.259E+4ampere/meter for 0.5T, for 1.0T it falls between 5.163+4 and 5.90+4ampere/meter and for 1.5T it falls between 4.865E+4 and 5.560E+4ampere/meter. They are indicated on the map by the red region. It will be best to make use of 0.5T for the magnetization at sample length between 0.0 to 1.0E-12m.

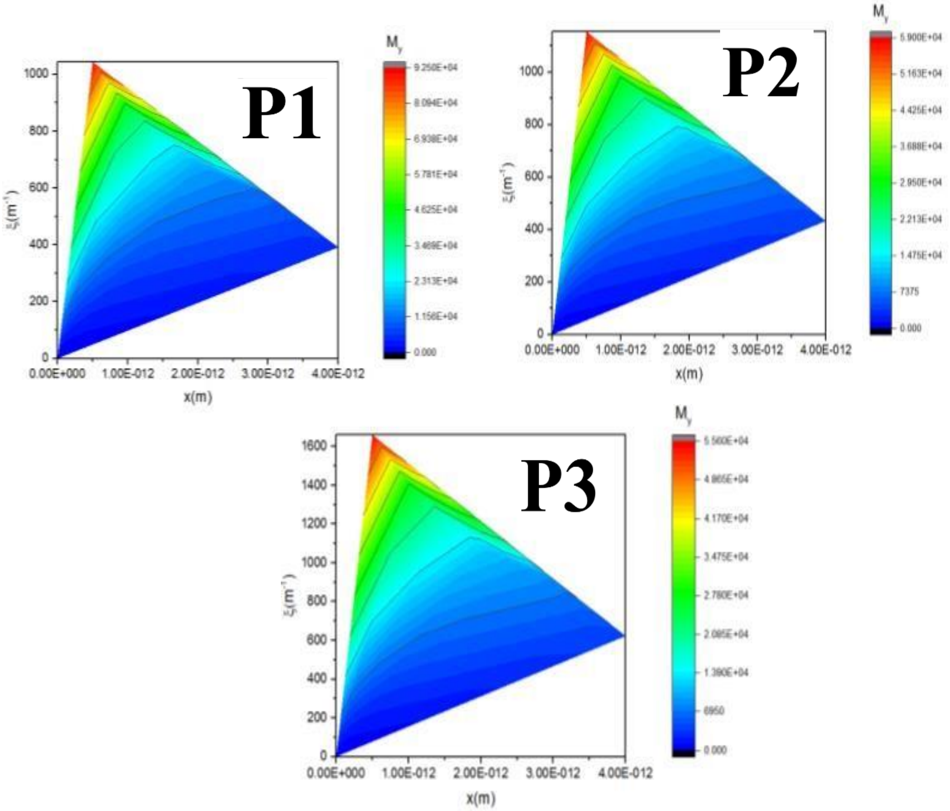

Figure 16. Transverse magnetization map for White brain matter in the Range of value of x: 0 to 4E-12 m

Conclusion

The transverse magnetization maps for the various biological tissues have been obtained with Originpro. We were able to obtain the transverse magnetization, which we made use of to achieved the contour plot. The transverse magnetization plot was done for T_1 relaxation time at 0.5T, 1.0T and 1.5T. Also we obtained the transverse magnetization equation from the Bloch NMR flow equation. The result shows that transverse magnetization was greater at 0.5 T for the tissues considered at the range of 4.5x10^{-12} to 4.5x10^{-5} m. This research work was performed for T_1 relaxation time at 0.5T, 1.0T, and 1.5T. More work should be done to be able to achieve transverse magnetization for T_1 greater than 1.5T and T_1less than 0.5T. In this research the transverse magnetization was done for contour map plot, I recommend that a 3-D plot should be plot for the transverse magnetization.

Scientific Ethics Declaration

The authors declare that the scientific ethical and legal responsibility of this article published in EPSTEM journal belongs to the authors.

Acknowledgements or Notes

* This article was presented as an oral presentation at the International Conference on Basic Sciences and Technology (www.icbast.net) held in Antalya/Turkey on November 16-19, 2023.

References

Albrecht, R., Sebag, D., & Verrecchia, E. (2015). Organic matter decomposition: bridging the gap between rock–eval pyrolysis and chemical characterization (CPMAS 13C NMR). *Biogeochemistry*, *122*(1), 101-111.

Awojoyogbe, O. B., Dada, O. M., Faromika, O. P., & Dada, O. E. (2011). Mathematical concept of the Bloch flow equations for general magnetic resonance imaging: A review. *Concepts in Magnetic Resonance Part A*, *38*(3), 85-101.

Becker, E. D. (1993). A brief history of nuclear magnetic resonance. *Analytical chemistry*, *65*(6), 295-302.

Cooley, C. Z., Stockmann, J. P., Armstrong, B. D., Sarracanie, M., Lev, M. H., Rosen, M. S., & Wald, L. L. (2015). Two-dimensional imaging in a lightweight portable MRI scanner without gradient coils. *Magnetic Eesonance in Medicine*, *73*(2), 872-883.

Farrukh, M. A. (Ed.). (2012). *Advanced aspects of spectroscopy*. BoD–Books on Demand.

Ginsberg, N. S., Cheng, Y. C., & Fleming, G. R. (2009). Two-dimensional electronic spectroscopy of molecular aggregates. *Accounts of Chemical Research*, *42*(9), 1352-1363.

Giza, S. A., Sethi, S., Smith, L. M., Empey, M. E. E., Morris, L. E., & McKenzie, C. A. (2021). The application of in utero magnetic resonance imaging in the study of the metabolic and cardiovascular consequences of the developmental origins of health and disease. *Journal of Developmental Origins of Health and Disease*, *12*(2), 193-202.

Grover, V. P., Tognarelli, J. M., Crossey, M. M., Cox, I. J., Taylor-Robinson, S. D., & McPhail, M. J. (2015). Magnetic resonance imaging: principles and techniques: lessons for clinicians. *Journal of Clinical and Experimental Hepatology*, *5*(3), 246-255.

Levitt, M. H. (2013). *Spin dynamics: basics of nuclear magnetic resonance*. John Wiley & Sons.

Lovchinsky, I., Sushkov, A. O., Urbach, E., de Leon, N. P., Choi, S., De Greve, K., & Lukin, M. D. (2016). Nuclear magnetic resonance detection and spectroscopy of single proteins using quantum logic. *Science*, *351*(6275), 836-841.

Mammarappallil, J. G., Rankine, L., Chan, H. F., Weatherley, N., Wild, J., & Driehuys, B. (2019). New developments in imaging idiopathic pulmonary fibrosis with hyperpolarized Xenon MRI. *Journal of Thoracic Imaging*, *34*(2), 136.

Miller, J. F., Harding, S. L., & Tufte, G. (2014). Evolution-in-materio: evolving computation in materials. *Evolutionary Intelligence*, *7*(1), 49-67.

Moser, E., Laistler, E., Schmitt, F., & Kontaxis, G. (2017). Ultra-high field NMR and MRI- the role of magnet technology to increase sensitivity and specificity. *Frontiers in Physics*, *5*, 33.

Nagy, C., & Einwallner, E. (2018). Study of in vivo glucose metabolism in high-fat diet-fed mice using oral glucose tolerance test (OGTT) and insulin tolerance test (ITT). *Journal of Visualized Experiments*, (131).

Reid, A., Smith, F. W., & Hutchison, J. M. (1982). Nuclear magnetic resonance imaging and its safety implications: follow-up of 181 patients. *The British Journal of Radiology*, *55*(658), 784-786.

Seabolt, L. A., Welch, E. B., & Silver, H. J. (2015). Imaging methods for analyzing body composition in human obesity and cardiometabolic disease. *Annals of the New York Academy of Sciences*, *1353*(1), 41-59.

Author Information

Bilyaminu Usman	**Ahmed Jimoh**
Zamfara State College of Education Maru, Nigeria Contact e-mail: *bilyaminumaru2@gmail.com*	Kebbi State University of Science and Technology, Aliero, Nigeria

To cite this article:

Usman, B. & Jimoh, A. (2023). Numerical computation of NMR magnetization for various tissues in the human body using oringinpro. *The Eurasia Proceedings of Science, Technology, Engineering & Mathematics (EPSTEM)*, *25*, 134-149.

The Eurasia Proceedings of Science, Technology,
Engineering & Mathematics (EPSTEM)
ISSN: 2602-3199

The Eurasia Proceedings of Science, Technology, Engineering & Mathematics (EPSTEM), 2023

Volume 25, Pages 150-156

ICBAST 2023: International Conference on Basic Sciences and Technology

Curvature Analysis in a Bi-layered Non-linear Elastic Bar under Uniform Heating

Victor Rizov
University of Architecture

Abstract: The present theoretical paper is concerned with analysis of the curvature in a bi-layered bar of rectangular cross-section. The bar is subjected to uniform heating. The two layers of the bar have different thickness and material properties. Besides, the layers exhibit non-linear elastic mechanical behaviour that is treated by applying a power-law stress-strain constitutive relationship. The bi-layered bar curvature is studied analytically. For this purpose, the mechanical response of the bar to uniform heating is investigated. The strains in the two layers due to heating are analyzed. An equation is compiled by using the fact that the prolongations of the bar layers are equal. Two equations are worked out by considering the equilibrium of the layers. The analysis of the curvature presented in this paper is checked-up by comparing with a known solution for the curvature in a bi-layered linear-elastic bar under uniform heating. The uniform heating induced curvature in a bi-layered bar whose layers are continuously inhomogeneous in longitudinal direction is also studied.

Keywords: Curvature, Bi-layered bar, Uniform heating, Continuous inhomogeneity

Introduction

Bi-layered materials are frequently applied in various areas of up-to-date engineering. They are used for manufacturing of components of different structures, facilities and devices in car industry, aeronautics, civil engineering, power plants, optics and electronics. In principle, layered materials are preferred to traditional homogeneous engineering materials because of their superior properties especially in applications in extreme conditions (high temperature, humidity, etc.) (Dolgov, 2005; Dolgov, 2016; Kim et al., 1999). These materials are known also with their high strength-to-weight and stiffness-to-weight ratios. This fact makes them right for engineering applications where low deadweight is one of the important goals of designers (Rzhanitsyn, 1986; Kaul, 2014; Lloyd & Molina-Aldareguia, 2003; Rizov, 2017; Rizov, 2018).

Very often bi-layered components of various structures, machines and mechanisms are subjected to heating in their operation exploitation. However, the layers of a bi-layered material system usually have different coefficients of thermal expansion. This fact indicates the importance of studying various aspects of the behaviour of structural components made of bi-layered materials subjected to heating. Also, in some cases the mechanical behaviour of bi-layered material systems is non-linear elastic (this necessities application of non-linear stress-strain relationships since the Hook’s law does not hold). However, the mechanical response of bi-layered structural components under heating usually is analyzed assuming linear-elastic behaviour of the material (Varvak, 1997). Besides, very often the bi-layered structural components have rectangular section.

Therefore, the basic purpose of the present paper is to analyze the curvature of a bi-layered bar of rectangular cross-section subjected to uniform heating with taking into account the material non-linearity. Two cases are studied. The first one is of a bi-layered bar with homogeneous layers. Equations for determining of axial forces and bending moment are compiled. Then axial forces are bending moment are used in the equations of equilibrium for obtaining the bar curvature induced by uniform heating. The case of a bi-layered bar with continuously inhomogeneous layers is also studied (this case is interestning mainly becouse of wide application

---

- Selection and peer-review under responsibility of the Organizing Committee of the Conference

of functionally graed materials (Hirai & Chen,1999; Gasik, 2010; Radhika et al., 2020, Rizov, 2019). A check-up is carried-out by comparing with a solution published in the literature.

Curvature Analysis

In this paper we deal with a bi-layered bar subjected to inform heating at temperature, Δt. The bar has a rectangular cross-section as shown in Fig. 1.

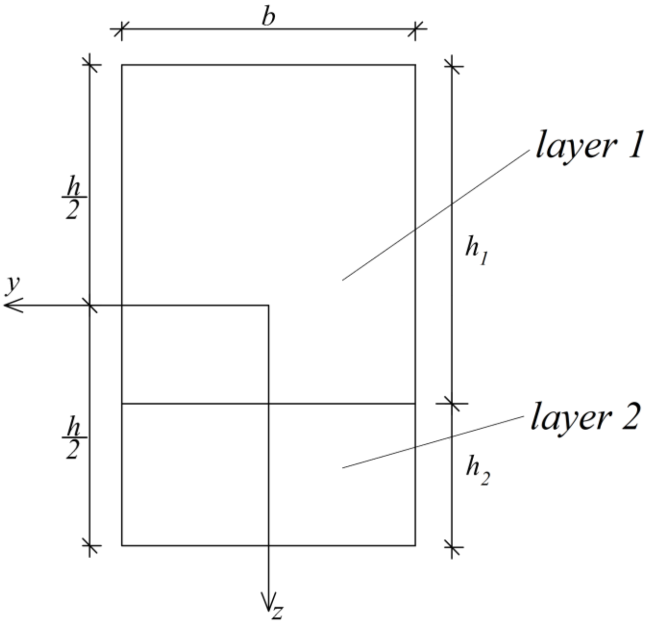

Figure 1. Cross-section of the bi-layered bar.

The width and thickness of the cross-section are denoted by h and b, respectively. The thickness of the upper layer is denoted by h_1. The lower layer thickness is h_2. The two layers have different material properties. Besides, the layers exhibit non-linear elastic mechanical behaviour. First, the case of homogeneous layers is analyzed. The mechanical behaviour of the upper layer is treated by using the following non-linear stress-strain constitutive relationship:

$$\sigma_1 = E_1 \varepsilon^{n_1}, \tag{1}$$

where σ_1 is the stress, ε is the strain, E_1 and n_1 are material properties.

The stress-strain constitutive relationship of the lower layer of the bar is written as

$$\sigma_2 = E_2 \varepsilon^{n_2}, \tag{2}$$

where σ_1, ε, E_1 and n_1 are the stress, strain and two material properties, respectively.

Our purpose is to analyze the curvature, κ, of the bi-layered bar induced by uniform heating with considering the non-linear elastic behaviour of the layers. The coefficients of thermal expansion of the upper and lower layers are denoted by α_{t1} and α_{t2}, respectively. If we assume that the layers of the bar are not connected, the prolongations, Δl_{t1} and Δl_{t2}, of the upper and lower layers can be written as

$$\Delta l_{t1} = \alpha_{t1} \Delta t\, l, \tag{3}$$

$$\Delta l_{t2} = \alpha_{t2} \Delta t\, l, \tag{4}$$

where l is the bar length. From (3) and (4), the strains, ε_1 and ε_2, in the upper and lower layers are found as

$$\varepsilon_1 = \alpha_{t1}\,\Delta t \ , \tag{5}$$

$$\varepsilon_2 = \alpha_{t2}\,\Delta t \ . \tag{6}$$

By using the constitutive laws (1) and (2) we derive the following expressions for the strains in the bar layers:

$$\varepsilon_1 = \left(\frac{\sigma_1}{E_1}\right)^{\frac{1}{n_1}}, \tag{7}$$

$$\varepsilon_2 = \left(\frac{\sigma_2}{E_2}\right)^{\frac{1}{n_2}}. \tag{8}$$

Due to the fact that the layers are connected axial forces of equal magnitude, F_u, and opposite directions will appear in the layers. The magnitude of stresses in the upper and lower layers induced by F_u is found as

$$\sigma_1 = \frac{F_u}{A_1}, \tag{9}$$

$$\sigma_2 = \frac{F_u}{A_2}, \tag{10}$$

where A_1 and A_2 are the areas of the cross-sections of the layers. Having in mind that

$$A_1 = bh_1 \tag{11}$$

and

$$A_1 = bh_2 \tag{12}$$

formulas (9) and (10) are re-written as

$$\sigma_1 = \frac{F_u}{bh_1}. \tag{13}$$

$$\sigma_2 = \frac{F_u}{bh_2}. \tag{14}$$

By combining of (7), (8), (13) and (14) we obtain

$$\varepsilon_1 = \left(\frac{F_u}{bh_1E_1}\right)^{\frac{1}{n_1}}, \tag{15}$$

$$\varepsilon_2 = \left(\frac{F_u}{bh_2E_2}\right)^{\frac{1}{n_2}}. \tag{16}$$

The difference between strains in the two layers is found as

$$\Delta\varepsilon = \varepsilon_1 - \varepsilon_2 = \left(\frac{F_u}{bh_1E_1}\right)^{\frac{1}{n_1}} - \left(\frac{F_u}{bh_2E_2}\right)^{\frac{1}{n_2}} . \tag{17}$$

Besides, $\Delta\varepsilon$ can be expressed also through Δt by using (5) and (6) , i.e.

$$\Delta\varepsilon = \Delta t\left(\alpha_{t1} - \alpha_{t2}\right) . \tag{18}$$

By combining of (17) and (18), we obtain the following equation with unknown, F_u :

$$\left(\frac{F_u}{bh_1E_1}\right)^{\frac{1}{n_1}} - \left(\frac{F_u}{bh_2E_2}\right)^{\frac{1}{n_2}} = \Delta t\left(\alpha_{t1} - \alpha_{t2}\right) . \tag{19}$$

Equation (19) is solved with respect to F_u by the MatLab.

A bending moment, M , that counters the moment induced by the axial forces acts in the bi-layered bar. This bending moment can be expressed as

$$M = F_u \frac{h_1 + h_2}{2} . \tag{20}$$

The bending moment is used to analyze the curvature of the bar induced by the uniform heating. For this purpose, first, the distribution of strains along the bar thickness is written as

$$\varepsilon = \kappa\left(z - z_n\right), \tag{21}$$

where

$$-\frac{h}{2} \le z \le \frac{h}{2} . \tag{22}$$

In formula (21), z is the vertical centric axis of the bar cross-section, z_n is the coordinate of the neutral axis. Two equilibrium equations of the elementary forces in the bar cross-section are worked out for determination of the curvature and the coordinate of the neutral axis, i.e.

$$N = b \int_{-\frac{h}{2}}^{-\frac{h}{2}+h_1} \sigma_1 dz + b \int_{-\frac{h}{2}+h_1}^{\frac{h}{2}} \sigma_2 dz , \tag{23}$$

$$M = b \int_{-\frac{h}{2}}^{-\frac{h}{2}+h_1} \sigma_1 z dz + b \int_{-\frac{h}{2}+h_1}^{\frac{h}{2}} \sigma_2 z dz , \tag{24}$$

where N is the axial force (apparently, $N = 0$), the bending moment M is expressed by (20). The stresses, σ_1 and σ_2, which are involved in (23) and (24) are presented by (1) and (2), the strain is expressed by (21). Equations (23) and (24) are solved with respect to the curvature and the coordinate of the neutral axis by the MatLab.

A check-up of equations (23) and (24) is performed by using the fact that at $n_1 = n_2 = 1$ the non-linear stress-strain relationships (1) and (2) transform in the Hook’s law (this means that at $n_1 = n_2 = 1$ equations (23) and

(24) should yield the curvature of a bi-layered linear-elastic bar subjected to uniform heating). In order to verify this we substitute $n_1 = n_2 = 1$ in equations (19), (23) and (24). After performing some mathematical transformations we derive from equations (23) and (24) the following formula for the curvature:

$$\kappa = \frac{M}{E_1 J_y^*}, \tag{25}$$

where

$$M = \frac{b\Delta t(\alpha_{1t} - \alpha_{2t})E_1}{\frac{1}{h_1} + \frac{1}{mh_2}} . \frac{h_1 + h_2}{2}, \tag{26}$$

$$m = \frac{E_2}{E_1}. \tag{27}$$

In formula (25) J_y^* is the moment of inertia of the bi-layered bar cross-section. It should be specified that formula (25) matches the expression for the curvature of a bi-layered bar with linear-elastic behaviour under uniform heating published in (Varvak, 1997). This fact is a check-up of the curvature analysis developed in the present paper. The case of a bar whose layers are continuously inhomogeneous in longitudinal direction is also analyzed here. In this case the material properties of the layers are distributed continuously along the bar length, i.e.

$$E_1 = E_1(x), \tag{28}$$

$$E_2 = E_2(x), \tag{29}$$

$$n_1 = n_1(x), \tag{30}$$

$$n_2 = n_2(x), \tag{31}$$

$$\alpha_{t1} = \alpha_{t1}(x), \tag{32}$$

$$\alpha_{t2} = \alpha_{t2}(x), \tag{33}$$

where

$$0 \le x \le l. \tag{34}$$

In formulas (28) – (34) x is the longitudinal centroidal axis of the inhomogeneous bar under consideration. The prolongations, Δl_{t1} and Δl_{t2}, of the upper and lower bar layers (if they are not connected) can be found as

$$\Delta l_{t1} = \int_0^l \alpha_{t1} \Delta t \, dx, \tag{35}$$

$$\Delta l_{t2} = \int_0^l \alpha_{t2} \Delta t \, dx. \tag{36}$$

Since the two layers are continuously inhomogeneous in longitudinal direction, the strains, ε_1 and ε_2, are continuous functions of x, i.e.

$$\varepsilon_1(x) = \alpha_{t1} \Delta t \ , \tag{37}$$

$$\varepsilon_2(x) = \alpha_{t2} \Delta t \ . \tag{38}$$

For the bi-layered inhomogeneous bar under uniform heating equation (19) takes the form

$$\left[\frac{F_u}{bh_1E_1(x)}\right]^{\frac{1}{n_1(x)}}-\left[\frac{F_u}{bh_2E_2(x)}\right]^{\frac{1}{n_2(x)}}=\Delta t\left[\alpha_{t1}(x)-\alpha_{t1}(x)\right]. \tag{39}$$

Equation (39) is used for deriving F_u at different values of x. Then equations (23) and (24) are applied for obtaining the uniform heating induced bar curvature at x varying in the interval $[0;l]$.

Conclusion

The paper describes a theoretical approach for analysis the curvature in a bi-layered bar subjected to uniform heating. The bar has non-linear elastic mechanical behaviour. The cross-section of the bar is a rectangle. A power law stress-strain relationship is applied for dealing with material non-linearity of the bar layers. First, the case of a bar with homogeneous layers is analyzed. Equations for deriving of the axial forces and the bending moment are constituted by considering the strains in the bar layers induced by uniform heating (in particular, we use here the circumstance that the strains along the contact line between the two layers are the same). The equations obtained are non-linear. After that the so derived axial forces and the bending moment are inserted in the equations for determining the curvature and the neutral axis coordinate of the bar (these equations are composed by analyzing the equilibrium of the elementary forces in the bar cross-section). It should be specified here that due to the fact that the bar is made by layers having different properties the neutral axis does not pass via the cross-section centre. As a result of this there are two unknowns (curvature and coordinate of the neutral axis) in the equations of equilibrium. The equations for determining the curvature and the coordinate of the neutral axis are checked-up by using the fact that at $n_1 = n_2 = 1$ the non-linear stress-strain relationship applied here transform into the Hook’s law. Therefore, we prove that by substituting of $n_1 = n_2 = 1$ in the equations for the curvature and the coordinate of the neutral axis composed in this paper the equations yield an expression for the curvature of a bi-layered bar of linear-elastic behaviour subjected to uniform heating that is a match of a known solution for the curvature published in the scientific literature. A consideration is given also to the problem of determination of the uniform heating induced curvature in a non-linear elastic bar made of two layers which are continuously inhomogeneous in longitudinal direction. The bar has a rectangular cross-section. Due to the fact that the layers are inhomogeneous the strains change continuously along the bar length. Equations for determination the axial forces and the bending moments in various sections of the bar are composed. These axial forces and bending moments are substituted in the equations of equilibrium to determine the bar curvature. From practical view-point, the curvature and the coordinate of neutral axis determined by the approach developed in the present paper can be applied for studying the stressed and strained state of bi-layered bars exhibiting material non-linearity under uniform heating. Besides, the approach can be refined with purpose of analyzing curvature of bars having an arbitrary number of non-linear elastic layers subjected to uniform heating.

Recommendations

Determination of the curvature of bi-layered bars under uniform heating by applying various non-linear stress-strain constitutive laws can be recommended as a future task.

Scientific Ethics Declaration

The author declares that the scientific ethical and legal responsibility of this article published in EPSTEM journal belongs to the author.

Acknowledgements or Notes

* This article was presented as an oral presentation at the International Conference on Basic Sciences and Technology (www.icbast.net) held in Antalya/Turkey on November 16-19, 2023.

References

Dolgov, N. (2005). Determination of Stresses in a two-layer coating. *Strength of Materials, 37, 422-431.*

Dolgov, N. (2016). Analytical methods to determine the stress state in the substrate–coating system under mechanical loads. *Strength of Materials, 48*(5), *658-667.*

Gasik, M. M. (2010). Functionally graded materials: bulk processing techniques. *International Journal of Materials and Product Technology, 39*(1), *20-29.*

Hirai, T., & Chen, L. (1999). Recent and prospective development of functionally graded materials in Japan. *Mater Sci. Forum, 308-311,* 509-514.

Kaul, A. B. (2014). Two-dimensional layered materials: Structure, properties, and prospects for device applications, *Journal of Material Research*, *29*(03), *348-361*.

Kim, J. S., Paik, K.W., & Oh, S. H. (1999). The multilayer-modified stoney's formula for laminated polymer composites on a silicon substrate. *Journal of Applied Physics, 86,* 5474–5479.

Lloyd, S.J., & Molina-Aldareguia, J. M. (2003), Multilayered materials: a palette for the materials artist. *Phil. Trans. R. Soc. Lond. A*, *361*(1813), 2931-294.

Radhika, N., Sasikumar, J., Sylesh, J. L., & Kishore, R. (2020). Dry reciprocating wear and frictional behaviour of B4C reinforced functionally graded and homogenous aluminium matrix composites. *Journal of Materials Research and Technology*, *9*(2), 1578-1592.

Rizov, V.I. (2017). Delamination analysis of a layered elastic-plastic beam. *International Journal of Structural Integrity, 8,* 516-529.

Rizov, V.I. (2018). Analysis of cylindrical delamination cracks in multilayered functionally graded non-linear elastic circular shafts under combined loads. *Frattura ed Integrità Strutturale, 12*(46)*, 158-17.*

Rizov, V.I. (2019). Influence of material inhomogeneity and non-linear mechanical behavior of the material on delamination in multilayered beams. *Frattura ed Integrita Strutturale, 13*(47), *468-481.*

Rzhanitsyn, A.R. (1986). *Built-up ars and plates*. Stroyizdat.

Varvak, P. (1997). *Strength of materials*. Science.

Author Information

Victor Rizov
University of Architecture,
Sofia, Bulgaria
Contact e-mail: *V_RIZOV_FHE@UACG.BG*

To cite this article:

Rizov, V. (2023). Curvature analysis in a bi-layered non-linear elastic bar under uniform heating. *The Eurasia Proceedings of Science, Technology, Engineering & Mathematics (EPSTEM), 25,* 150-156.

The Eurasia Proceedings of Science, Technology, Engineering & Mathematics (EPSTEM), 2023

Volume 25, Pages 157-162

ICBAST 2023: International Conference on Basic Sciences and Technology

Computational Evaluation on Molecular Stability and Reactivity of Some Dimethylglyoximato-Nickel Complexes from DFT

Noura Kichou
Mouloud Mammeri University of Tizi-Ouzou (UMMTO)

Nabila Guechtouli
Mouloud Mammeri University of Tizi-Ouzou (UMMTO)

Manel Taferguennit
University of Sciences and Technology Houari Boumediene

Zakia Hank
University of Sciences and Technology Houari Boumediene

Abstract: Complexes Nickel constitute a very widespread axis in coordination chemistry and in medicine, because of their application as well as their activity**.** The Ni(III) species which aroused the interest of many biochemists, the three last decades, was identified to be the active entity of many enzymes, in particular, in hydrogenases. It is also mentioned for its powerful catalytic properties in biological and chemical processes. The Ni(IV) species, for its part, is known for its marked oxidizing capacities**.** In this work, we were interested in the theoretical study of Two complexes of dimethylglyoximato-nickel , using the DFT method, with the functional B3LYP function and LANL2DZ basis set, using Gaussian 03 program package. The experimental results, IR, ^{1}H NMR and electronic spectra (UV) were compared to those obtained theoretically using. The energetic, structural and electronic parameters were determined for ligand and each studied complexes. Bending energies were also theoretically evaluated for each complexes.

Keywords: NICKEL, Dimethylglyoxime, DFT, Reactivity

Introduction

Transition-metal ions show diversity in forming various stable complexes with different organic ligands. These complexes have potential applications in fields such as ion exchange, heterogeneous catalysis, photocatalysis, fluorescence, bioimaging, optical devices, magnetism, gas-storage, and also serve as carbon precursor and catalyst for production of multiwalled carbon nantotubes (MWCNTs) (Krishna, 2012 ; Bar, 2016 ; Chen,2019). Dimethylglyoxime (DMG) is an analytical reagent and usually forms thermodynamically stable chelating complexes with selective divalent transition-metal ions (Rath, 2018). Electronic and spectral properties of metal-DMG complexes are highly dependent on the nature of metal ions. Among Ni^{2+} ion show high affinity for the DMG, and form stable complexes in solution and in the solid-state (Sued, 2019). In this work, Two complexes of dimethylglyoximato-nickel were theoretically evaluated from DFT method.

Theoretical Methods

In the absence of crystal structures and preliminary theoretical studies, we carried out a theoretical study in the DFT method with the functional B3LYP(Becke,1993) and the base LANL2DZ (Hay, 1985) in the gaseous

---

phase, using Gaussian 03 program package (Fresch, 2003). No symmetry constraints were imposed. We used the GaussView software (Fresch, 2003) to draw the optimized geometries and visualize the vibrational modes.For this purpose, a complete geometry optimization was performed for each compound followed by a frequency calculation of the normal modes of vibration to confirm the stability. Thus, the structural parameters and electronic parameters, the energies, the HOMO/LUMO gaps, and the NBO atomic charges were evaluated of the ligand and complexes obtained. To compare the stability of the two studied complexes, we computed the bending energies. The population analysis was carried out using the natural orbital bond program (NBO) implemented in the Gaussian program 03. The ^{1}H NMR calculations were carried out in the $CHCl_3$ solvent, at the same level of theory. The absolute isotropic chemical shielding was calculated by the Gauge–Independent Atomic Orbital (GIAO) model (Wolinski, 1990). The characterization of excited states and electronic transitions were performed using the time-dependent DFT method (TD-DFT) on their correspondingly optimized ground state geometry. Vertical excitation energies were computed for the first 20 singlet excited states, in order to reproduce the experimental electronic spectra. Results of theoretical calculations were compared with corresponding experimental data. Currently, the DFT method proves its efficiency in the calculation of molecular structures, the electronic and spectroscopic properties of the compounds.

Results and Discussion

Geometry

In figure 1 is given the optimized structure for a ligand (DMG). The optimized geometries of the synthesized complexes are given in figure 2 and figure 3. The optimization of these complexes led to a slightly deformed square pyramid for the **A** complex. However, the complex **B** has an octahedral structure. The bonds between the atoms forming the fragments bound to the metal are almost the same this is due to the symmetry of the molecule. Indeed, the metal ion is bound to two similar groups on both sides in the two complexes **A** and **B**.

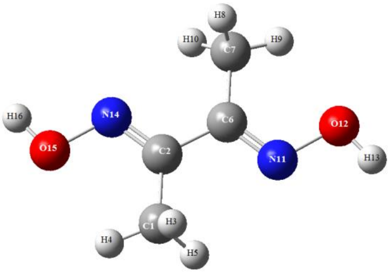

Figure 1. Molecular structure of the H_2L(DMG) ligand optimized at DFT/B3LYP/ LANL2DZ level of theory

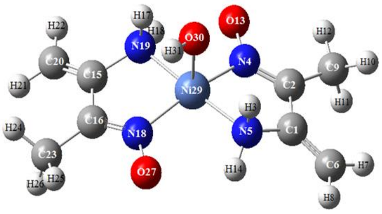

Figure 2. Molecular structure of the A complex optimized at DFT/B3LYP/LANL2DZ level of theory

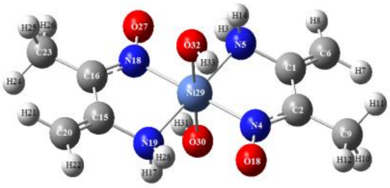

Figure 3. Molecular structure of the **B** complex optimized at DFT/B3LYP/LANL2DZ level of theory.

This result clearly confirms that the studied complexes are symmetric.We report the formation of hydrogen bonds (NH....O) in all the compounds considered. Indeed, In the **A**complex, two hydrogen bonds are formed, one between H_{17} bound to N_{19} and O_{30}, which is 2.202 Å and the other between $N_{19}H_{28}$ and O_{13}, which is 2.177

Å. Thus, in the **B** complex, two hydrogen bonds were determined: N5H3 ... O30, 1.586 Å and O30H31 ... O27, which is 2.043 Å. These established intramolecular hydrogen bonds reinforce the stability of these complexes.

Caracterization

The experimental results, IR, ^{1}H NMR and electronic spectra (UV) were compared to those obtained theoretically. They are in good agreement with those found experimentally.

Table 2. Experimental and theoretical characteristic Infrared spectral (IR) bands for the dimethylglyoxime ligand and its Complexes as KBr Pellets (cm^{-1})

Compound	ν(O-H)	ν(N-H)	ν(CH$_3$)	νCH$_2$=	δ(N-H)	νC=C	νC=N	νCH$_2$*	δCH$_3$ Sym	δCH$_2$**	ν(N-O)	νNi-O	νNi-N
H$_2$L	3000-3500		2900-3000				1447		1364		980		
H$_2$L^a	3696 3697	3349-3511	3033-3169				1642 1651		1341 1343		995		
A	3100-3500	3100-3500	3000-3050	2800-2940	1560 sh	1572	1571	1453 sh	1368	871	957	541	497 443
A^a	3624	3349-3511	3033-3169	2882-2942	1485	1668-1691	1675-1695	1400 1402	1402 1410	891	-	437	496 429
B	3100-3500	3100-3500	2950-3050	2850-2930	1560 sh	1572 sh	1572	1453 sh	1369	889	992	520	496 426
B^a	3574 3652	3485-36661	2924-3031	2856 2924	1422	1605 1614	1575 1578	1454 1450	1401 1403	898	-	561 480	-

*in the plan, **out of the plan, sh : shoulder. a: calculated by DFT

Table 2. ^{1}H NMR data of the ligand and the complex in deuterated chloroform.

Compound	^{1}H chemical shift (δ) (ppm)	Assignment
H$_2$L	(H3, H8) 1.9 (0.9-2.3)	CH$_3$
	(H5, H10) 1.9 (0.9-2.3)	
	(H4, H9) 1.9 (0.9-2.3)	
	(H13, H16) 10 (7.0)	-C=NOH
	(H11, H24) 2.00 (1.8)	CH$_3$-C-
	(H10, H25) 2.0 (1.5)	
	(H12, H26) 2.0 (2.2)	
	(H7, H21) 3.40 (4.40)	
B	(H8, H22)3.4 (4.33)	CH$_2$=C- and
	(H3, H28) 3.4 (2.8)	-C-NH$_2$
	(H14, H7) 3.4 (5.5)	

Found: experimental; (calc.): calculated by DFT.

Table 3. Electronic absorption data (UV) of the ligand and the complexes in CHCl$_3$.

Compound	λ (nm) (Assignment)	Probable Environment
DMG	$\pi \rightarrow \pi^*$ 250 (242)	
	$\sigma \rightarrow \sigma^*$ (144, 158, 148, 149, 154, 160)	
	sh $\pi \rightarrow \pi^*$ 290 (283)	
	sh $n \rightarrow \pi^*$ 320 (299)	
A	LMCT 430 (422, 429)	Distorted
	$d \rightarrow d$ 550 (529, 571)	Square Pyramidal
	$d \rightarrow d$ 890 (839, 889)	
	$\pi \rightarrow \pi^*$ 290 (292)	
	sh $n \rightarrow \pi^*$ 340 (341)	Distorted
B	sh LMCT 376 (380)	Octahedral
	sh $d \rightarrow d$ ($^1A_1 \rightarrow {}^1T_{2g}$) 425 (480)	
	$d \rightarrow d$ ($^1A_1 \rightarrow {}^1T_{1g}$) 500 (511)	
	$d \rightarrow d$ ($^1A_1 \rightarrow {}^1T_{1g}$) 550 (551)	

sh: shoulder; Found: experimental; (calc.): calculated by DFT.

Bonding Energy

By definition it is the equivalence in absolum value of the energy of dissociation between the metal and the ligandIt is defined by the following relation:

$$E_{bonding} = E_{complex} - (E_{metal} + \sum E_L)$$

The complex A ($E_{bonding\,=}$ -1656.9 Kcal/mol is the most stable compared to the other ($E_{bonding\,=}$ -3083.7 Kcal/mol. It corresponds to the lowest bending energy (highest negative value). We note that the bending energy values are very high. We have explained this result by the number of oxidation of the high metal Ni(III) et Ni(IV). We find that when the metal has a strongly ionic character, the complexation by the ligand H_2L leads to very stable complexes.

Frontier Molecular Orbitals

The calculated values of HOMO and LUMO energies and HOMO/LUMO band gap $(\Delta E_{|HOMO-LUMO|})$ of A and B obtained by a full geometry optimization at the DFT level were schematized in figure 11. For A, the HOMO density is distributed over ligands while the LUMO density covers the metal and OH^-. As for Ca complex, the HOMO of the B complex is localized on the ligands, whereas the LUMO is situated over the complex. Also, HOMO and LUMO energy values show that A and B have comparable ability to receiving and accepting electron.

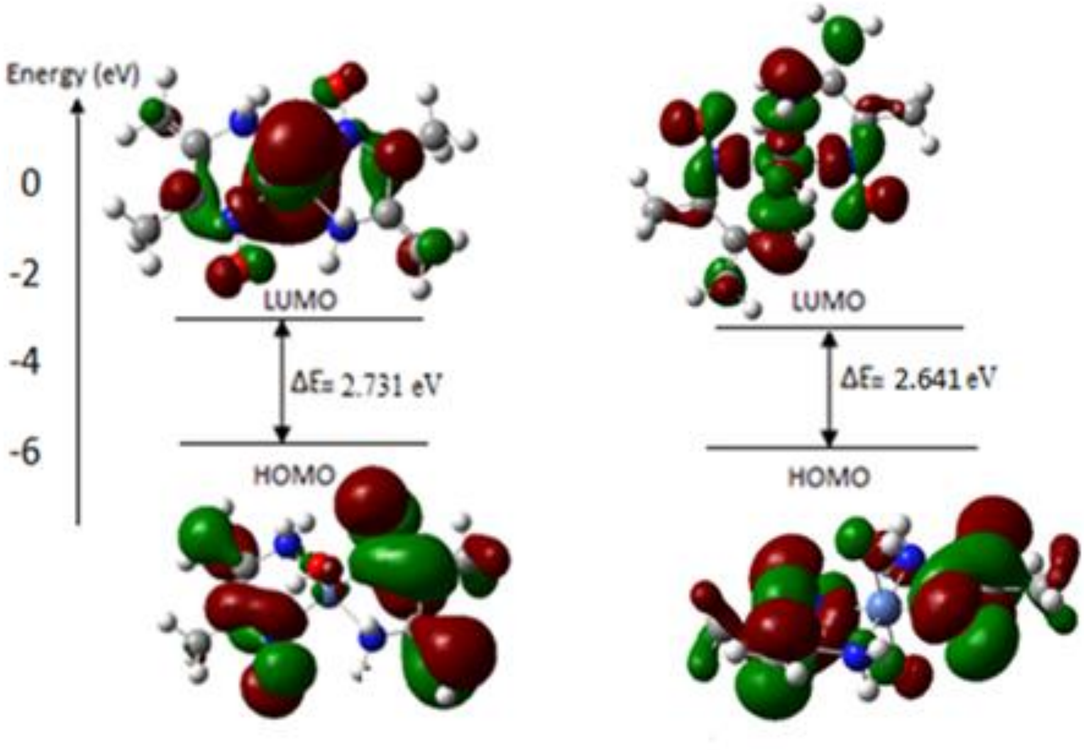

Figure 4. Frontier molecular orbitals HOMO and LUMO of the synthesized complexes

NBO Charges and the Dipole Moment

NBO charge is related to the electronic density and is a very useful descriptor in understanding sites for electrophilic attack and nucleophilic reaction. The valence of Nickel in the A and B complexes is +III and +IV, respectively. While the net charges of this metals is +0.740 e, and + 0.578 e, in A and B respectively, showing that the metal center obtained part electron from ligand donor atoms. These results show that the covalent character of metal-ligand bands in B is the most important comparing to A. The net charges of donor atoms (Table. 4) confirm the electron transfer to metallic ion.

Table 4. NBO charge and dipole moment calculated in DFT/B3LYP/LANL2DZ.

Parameters	Complex A	Complex B			
NBO Charge					
Ni(III)	0.740	Ni(IV)	0.578		
N_1	-0.005	N1	- 0.889		
N_2	-0.851	N2	-0.107		
N_3	-0.845	N3	-0.117		
N_4	-0.100	N4	-0.868		
O	-0.920	O30	-0.995	O32	-1.033
H	0.464	H31	0.450	H33	0.480
Dipole moment (Debye)	2.4	1.2			

The dipole moment is an important electronic parameter that results from non-uniform distribution of charges on the various atoms in a given molecules. Herein, low value of the dipole moment of **B** comparing to **A** (Table 4) reflect a superior symmetries of the **B** complex.

Conclusion

From this study, we found that the DFT/B3LYP/LANL2DZ method gives satisfactory results for this type of complex. Indeed, the experimental results obtained for The al FT-IR, UV–Visible spectra and ^{1}H NMR for Ni (III) and Ni (IV) are in reasonable correlation with the theoretical data (DFT). We have also confirmed that the complexes **A** and **B** have the geometries distorted square pyramidal and distorted octahedral, respectively. The dimethylglyoxime ligand stabilise its complexes in the distorted octahedral geometry around the metallic center. The calculation of the bending energy showed us that the complex **B** is more stable with respect to **A**. The values of these energies are too high; this is due to the number of oxidation of the metal which is high and unusual. The values of the HOMO/LUMO differences found confirm the stability of these complexes.

Scientific Ethics Declaration

The authors declare that the scientific ethical and legal responsibility of this article published in EPSTEM journal belongs to the authors.

Acknowledgements or Notes

* This article was presented as a poster presentation at the International Conference on Basic Sciences and Technology (www.icbast.net) held in Antalya/Turkey on November 16-19, 2023.

References

Bar, A. K., Pichon, C., & Sutter, J. P. (2016). Magnetic anisotropy in twoto eight-coordinated transition-metal complexes : Recent developments in molecular magnetism. *Coordination Chemistry Reviews, 308,* 346−380.

Becke, A. D .(1993). DFT studies on the pairing abilities of the one-electron reduced or oxidized adenine–thymine base pair . *Chemical Physics, 98*(7), *5648* – 5652.

Chen, H. R. (2019). Synthesis, structures and physicochemical properties of two two-dimensional coordination polymers based on 3,5-di(1Hbenzimidazol-1-yl) pyridine. *Transition Met. Chem., 44,* 407−413.

Fresch, A., Nielson A.B., & Holder A. J. (2003). *Gaussview user manual*. Pittsburg: Gaussian. Inc.

Hay, P. J., & Wadt W, R. (1985). *Ab initio* effective core potentials for molecular calculations. Potentials for the transition metal atoms Sc to Hg. *The Journal of Chemical Physics, 82*(1), 270-283.

Krishna, R. (2012). Diffusion in porous crystalline materials. *Chemical Society Reviews, 41*(8), 3099-3118.

Syed , Y.A., Kambham, D., & Manna, A. K. (2019). Sructural, electronic, and spectral properties of metal dimethylglyoximato [M(DMG)$_2$; M = Ni^{2+}, Cu^{2+}] complexes: A comparative theoretical study. *The Journal of Physical Chemistry A, 123*(42), 9166–9174.

Wolinski, K., Hinton J. F., & Pulay, P. (1990). Efficient implementation of the gauge-independent atomic orbital method for NMR chemical shift calculations. *Journal of the American Chemical Society, 112 (23),* 8251-8260.

Author Information

Noura Kichou
University Mouloud Mammeri of Tizi-Ouzou,
Tizi-Ouzou, Algeria
Contact e-mail: *noura.kichou@ummto.dz*

Nabila Guechtouli
University Mouloud Mammeri of Tizi-Ouzou,
Tizi-Ouzou, Algeria

Manel Taferghennit
University of Sciences and Technology Houari Boumediene
Algiers, Algeria

Zakia Hank
University of Sciences and Technology Houari Boumediene
Algiers, Algeria

To cite this article:

Kichou, N., Guechtouli, N., Taferghennit, M. & Hank, Z. (2023). Computational evaluation on molecular stability and reactivity of some dimethylglyoximato-nickel complexes from DFT. *The Eurasia Proceedings of Science, Technology, Engineering & Mathematics (EPSTEM), 25,* 157-162.

The Eurasia Proceedings of Science, Technology,
Engineering & Mathematics (EPSTEM)
ISSN: 2602-3199

The Eurasia Proceedings of Science, Technology, Engineering & Mathematics (EPSTEM), 2023

Volume 25, Pages 163-167

ICBAST 2023: International Conference on Basic Sciences and Technology

Nutrient Profile of Commercially Packaged Food Products in Türkiye

Fatma Hazan Gul
Mersin University

Abstract: Nutrient profiling models are useful for describing the health value of foods and underpinning various nutrition-related public health strategies. They are generally based on a food's content of several nutrients (e.g., protein, salt, carbohydrates). The aim of this study is to review information on the nutritional profiles of foods and beverages sold in Turkey. Ten food and drink categories were reviewed in six physical food stores and four online stores. A total of 1,000 foods and beverages, 100 products from each group, were checked for nutrient profile according to their labels. While all dairy products are produced locally, 74% of baby and young children foods are produced foreign. Snacks have the highest energy and saturated fat (on average 2072.6 kJ/579.4 kcal; 13.2±6.23 g respectively). Dried food and ingredients have the highest fat (on average 35.2 g±21.61). Confectionaries received the highest carbohydrates and sugars (on average 79.6±19.56 g; 56.0±27.41 g respectively). Chilled foods have the highest protein levels (on average 18.0±9.31 g). Condiments and sauces have the highest salt (3.4±4.59 g). Beverages have the lowest energy, fat, saturated fat, protein and salt (on average 160.3 kJ/37,7 kcal; 0.0±0.00 g; 0.0±0.00 g; 0.1±0.16 g; 0.0±0.15 g respectively). Dairy has the lowest carbohydrates (on average 5.8±4.52 g) and chilled foods have the lowest sugar (on average 2.0±0,69 g). As nutrient profiling models are increasingly used worldwide to support public health strategies, having an up-to-date resource listing them and detailing their characteristics is crucial. It is believed that the results of this study may provide an up-to-date guide for determining the nutrient profile of commercially packaged foods sold in Türkiye.

Keywords: Nutrient profiling, Food labels, Commercially packaged foods

Introduction

Current evidence indicates that four types of non-communicable diseases (NCDs), cardiovascular disease, cancer, diabetes, and chronic respiratory disease, are the leading global causes of death, kill 41 million people each year, equivalent to 74% of all deaths globally. NCDs are largely preventable and also some preventive interventions early in the course of life offer lifelong benefits. Reducing salt levels, eliminating industrially produced trans fatty acids, decreasing saturated fats, limiting free sugars, and providing accurate information to consumers in the form of nutrition labels are effective interventions totackle NCDs (WHO, 2023).

Since most of the actions taken by governments to address obesity are focused on diet as one of the key determinants of disease, it is required to define and classify food and drink products containing excessive amounts of such nutrients. One way to establish acceptable critical nutrient thresholds is with a nutrient profiling system (WHO, 2011). Nutrient profiling algorithms aim to characterize the overall nutritional quality (healthfulness) of foods and beverages (Scarborough et al., 2007). They are generally based on a food product's content in multiple nutrients, some of which may be to encourage (e.g., fiber, protein) and others to limit (e.g., sugars, sodium). Nutrient profiling is primarily relevant to the field of public health nutrition when there is a need to define as clearly and objectively as possible what represents a "less" or "more" nutritious food in the context of various nutrition-related policies and regulations (Sacks et al., 2011).

- Selection and peer-review under responsibility of the Organizing Committee of the Conference

The importance of food labelling is very frequently overlooked; however, it is essential to help consumers make healthy and safe food purchasing choices and is extremely important in relation to societal wellbeing. Thus, clear and unambiguous food labelling is vital for the presentation of critical safety information to consumers (Brown et al., 2015).

In 1994, the Food and Drug Administration (FDA) enacted the Nutrition Labeling and Education Act, which requires nutrition facts panel (NFP) labels on the back of most food products. The goals of this legislation include helping consumers make healthy food choices, reducing consumer confusion about food labels, and providing an incentive for firms to improve the nutritional quality of food (Wilkening, 1992). Several studies find that approximately 60 percent of U.S. consumers rely on fact panels sometimes or always when making purchasing decisions (Todd & Variyam, 2008; Ollberding et al., 2010; Campos et al., 2011), and consumers with diet-related diseases are even more likely to use NFPs (Post et al., 2010). We contribute to the literature by examining the nutritional information on the labels of packaged foods sold in stores. The nutrient content of food groups was analyzed based on the information on the nutrition facts panel.

Method

Type of the Study

This research is a cross-sectional study at five levels of evidence. The inclusion criteria are that the products are packaged, sold commercially, and can be easily found all over Turkey. The exclusion criteria are that unpackaged products, those not sold commercially in markets or online markets, and products that only belong to a certain region. Ethics committee approval was not required in this study, so it was not applied.

Physical Stores

Six mega physical stores in the Turkey were visited. Two of them were supermarkets and four of them were convenience stores. These stores were chosen as they are part of a retailer chain and are widespread in Turkey. Prior to the visit, verbal consent was obtained from each store manager. All packaged foods' labels that were obtained in physical stores were taken photos from all sides (front, back and other sides). Foods and beverages were randomly selected from the shelves.

Online Stores

Premium, regular, and budget stores (n=4) offering online deliveries were selected. In the online store webpage, each page offers a selection of 40-50 items per food category. Five items per page were selected systematically by selecting every 8th or 10th item that were listed on the page.

Survey

Commercially processed and packaged food products' labelling were evaluated for declaration of nutrient profiling. Ten food and drink categories were selected. A total of 1,000 foods and beverages, 100 products from each group, were checked for nutrient profile according to their labels. The foods and beverages are representative of the range of commonly purchased food in Turkey. The researcher collected this data from May 2023 to July 2023. Two or three digital photographs were taken for each product. The photographs were evaluated and items such as place of manufacture (local or foreign), protein, carbohydrate levels. Data from each label were entered into an excel sheet according to food category.

Statistical Analysis

Descriptive statistics were used and the results are shown as percentages. Results were entered into an excel data sheet and percentages were calculated.

Results

In this study, a total of 1,000 foods and beverages, 100 products from each group, were checked for nutrient profile according to their labels. The place of the manufacturer of packaged foods was examined. All dairy products are locally produced. In local production, this is followed by chilled foods (99%) and bakery products (96%). The most foreign-produced products are baby and young children foods (74%), followed by condiments and sauces (42%) and dried food and ingredients (19%) (Figure 1).

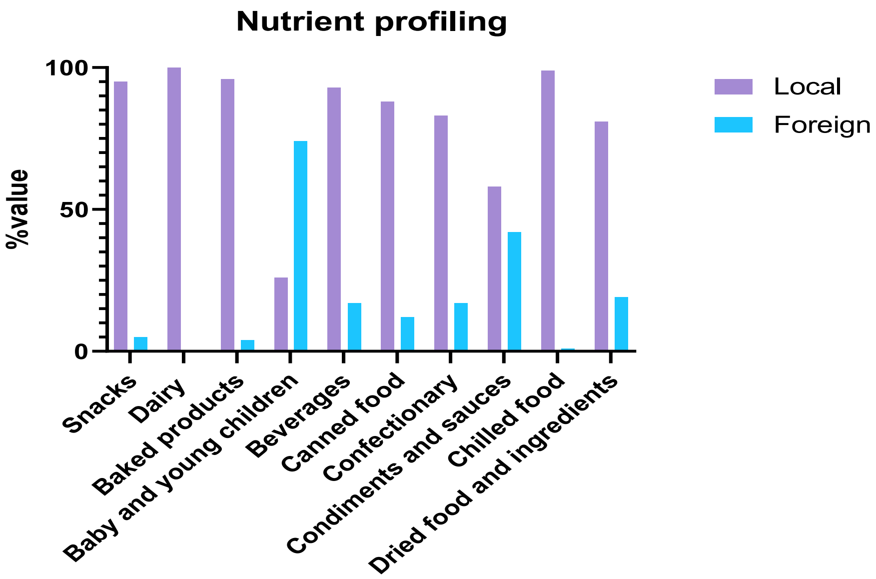

Figure 1. Place of manufacturer

Snacks have the highest energy and saturated fat (on average 2072.6 kJ/579.4 kcal; 13.2±6.23 g respectively). Dried food and ingredients have the highest fat (on average 35.2 g±21.61). Confectionaries received the highest carbohydrates and sugars (on average 79.6±19.56 g; 56.0±27.41 g respectively). Chilled foods have the highest protein levels (on average 18.0±9.31 g). Condiments and sauces have the highest salt (3.4±4.59 g). Beverages have the lowest energy, fat, saturated fat, protein and salt (on average 160.3 kJ/37,7 kcal; 0.0±0.00 g; 0.0±0.00 g; 0.1±0.16 g; 0.0±0.15 g respectively). Dairy has the lowest carbohydrates (on average 5.8±4.52 g) and chilled foods have the lowest sugar (on average 2.0±0,69 g) (Table 2).

Table 2**.** Nutrient labeling profiles

Food and drink categories	kJ	Kcal	Fat (g)	Saturated fat (g)	Carbohydrate (g)	Sugar (g)	Protein (g)	Salt (g)
Snacks	2072.6	495.6	25.7	13.2	56.7	27.9	7.4	0.7
Dairy	779.0	187.0	14.5	8.7	5.8	4.8	8.6	0.7
Baked products	1373.5	367.6	8.2	2.5	52.2	6.7	10.1	0.9
Baby and young children	479.0	116.0	3.3	1.2	19.5	10.8	2.9	0.1
Beverages	160.3	37.7	0.0	0.0	9.0	8.5	0.1	0.0
Canned food	705.4	178.3	6.5	3.0	9.5	5.1	9.0	1.3
Confectionary	1590.8	378.1	4.0	2.9	79.6	56.0	2.8	0.4
Condiments and sauces	637.4	153.4	8.1	0.9	17.0	12.1	2.0	3.4
Chilled food	1053.7	255.8	17.6	8.4	5.9	2.0	14.6	2.1
Dried food and ingredients	2023.8	579.4	35.2	6.5	30.0	12.8	18.0	0.9

Discussion

Nutrition labeling is the provision of information on protein, carbohydrates, fat, fiber, sodium, vitamins, and minerals along with the energy value on the label. It can be used for various applications. It is commonly used in food labelling schemes aimed at helping consumers better understand the nutrient composition of foods and identify foods that are healthier options. It can also be used in implementing the recommendations on the marketing of foods to children (Dikmen et al., 2015). With the development of the food industry, more and more packaged foods are entering the market. Given this diversity, individuals need to pay more attention and care to the information on labels when buying food. Reading labels is an effective way to make decisions when choosing food (Priya & Alur, 2023). The aim of this study is to review information on the nutritional profiles of foods and beverages sold in Turkey.

Overseas countries have started to develop various nutrient profile models for different applications. In the United Kingdom, the traffic light labelling system ranks fat, saturated fat, sugar and salt of a food product by assigning the colour green, amber and red according to the content levels. In addition, food products that exceed specified levels of fat, salt and sugar cannot be advertised in television programmes commissioned for audiences below the age of 16. In Australia, the Health Star Rating system rates food products from ½ a star to 5 stars, based on their nutrient contents (i.e. energy, saturated fat, sugar, and sodium, and in some instances, protein, calcium and dietary fibre) and ingredient information (i.e. fruits, vegetables, nuts and legumes). The more stars, the healthier the choice. In some Nordic countries, the Keyhole labelling scheme identifies healthy foods within a product group, based on the criteria relating to dietary fibre, salt, sugar, fat, and saturated fat (CFS, 2016).

As can be seen, each country has a different method of nutrition declaration on the nutrition label. Turkiye use nutrition fact panel in order to declare nutritional ingredients. As can be seen, each country has a different method of nutrition declaration on the nutrition label. In Turkey, the nutrition table is used to declare the ingredients. According to this table, the foods with the highest kJ are snacks. The reason why snacks have a high kJ value is because of the unhealthy additives and oils they contain. The reason for the high kJ value of dried food and ingredients, is that they contain many healthy fats. The main reason for the high energy content of confectionaries, the third food group with the highest kJ content, are the simple sugars in their structure. Beverages are the food group containing the fewest kJ. The reason why the second-ranked baby and young children foods have a low energy content is that this food is prepared according to the needs of babies. Although the ranking is different, the top three foods in terms of kcal are the same as kj (dried food and ingredients, snacks, and confectionaries respectively). Dried fruits, which are the food group with the highest kcal value, also have the highest fat content. This is the most important evidence that the caloric content of food increases with increasing fat content. The kJ value of the food group with the highest saturated fat content was also found to be the highest. This proves that the kJ value parallels the amount of saturated fat in the food. Similarly, foods high in carbohydrates and sugars have also been found to have high kcal values. The food group with the highest protein content is dried food and ingredients. The food group with the highest salt content is sauces.

Conclusions

This is the first empirical study to evaluate the nutrition profile on commercially packaged food and drink products. Ten food and drink categories were reviewed in six physical food stores and four online stores. A total of 1,000 foods and beverages, 100 products from each group, were checked for nutrient profile according to their labels. While all dairy products are produced locally, 74% of baby and young children foods are produced foreign. Snacks have the highest energy and saturated fat (on average 2072.6 kJ/579.4 kcal; 13.2±6.23 g respectively). Dried food and ingredients have the highest fat (on average 35.2 g±21.61). Confectionaries received the highest carbohydrates and sugars (on average 79.6±19.56 g; 56.0±27.41 g respectively). Chilled foods have the highest protein levels (on average 18.0±9.31 g). Condiments and sauces have the highest salt (3.4±4.59 g). Beverages have the lowest energy, fat, saturated fat, protein and salt (on average 160.3 kJ/37,7 kcal; 0.0±0.00 g; 0.0±0.00 g; 0.1±0.16 g; 0.0±0.15 g respectively). Dairy has the lowest carbohydrates (on average 5.8±4.52 g) and chilled foods have the lowest sugar (on average 2.0±0,69 g).

Recommendations

The goals of the nutrition labeling are to reduce consumer confusion about food labels, help consumers make healthy food choices, and provide an incentive for firms to improve the nutritional quality of food. Nutrition information on food labels should be more understandable to consumers. If necessary, training on reading nutrition labels and evaluating nutrition labels should be provided.

The limitation of this study was obtaining the nutrient label of the packaged foods. In this study, only 1000 foods were examined. To obtain more meaningful results, more commercially packaged foods should be studied. In addition, the lack of a previous study on this topic shows the originality of the study, but since there is no source to discuss the results in the discussion section, the study is discussed with its own data.

Scientific Ethics Declaration

The authors declare that the scientific ethical and legal responsibility of this article published in EPSTEM journal belongs to the authors.

Acknowledgements or Notes

* This article was presented as a poster presentation at the International Conference on Basic Sciences and Technology (www.icbast.net) held in Antalya/Turkey on November 16-19, 2023.

References

Brown, K. M., Fenton, N. E., Lynd, L. D., Marra, C. A., FitzGerald, J. M., Harvard, S. S., ... & Elliott, S. J. (2015). Canadian policy on food allergen labelling: consumers' perspectives regarding unment needs. *Univers J Public Health, 3,* 41-48.

Campos, S., Doxey, J., & Hammond, D. (2011). Nutrition labels on pre-packaged foods: a systematic review. *Public Health Nutrition*, *14*(8), 1496-1506.

Dikmen, D., Kizil, M., Uyar, M. F., & Pekcan, G. (2015). Testing two nutrient profiling models of labelled foods and beverages marketed in Turkey. *Central European Journal of Public Health*, *23*(2), 155.

Ho, N. (2017, June 5). Nutrient profiling and its application. Retrieved from https://www.cfs.gov.hk/english/multimedia/multimedia_pub/multimedia_pub_fsf_121_02.html

Ollberding, N. J., Wolf, R. L., & Contento, I. (2011). Food label use and its relation to dietary intake among US adults. *Journal of the American Dietetic Association*, *111*(5), 47-51.

Post, R. E., Mainous III, A. G., Diaz, V. A., Matheson, E. M., & Everett, C. J. (2010). Use of the nutrition facts label in chronic disease management: results from the national health and nutrition examination survey. *Journal of the American Dietetic Association*, *110*(4), 628-632.

Priya, K. M., & Alur, S. (2023). Analyzing consumer behaviour towards food and nutrition labeling: A comprehensive review. *Heliyon. 9*(9). https://doi.org/10.1016/j.heliyon.2023.e19401

Sacks, G., Rayner, M., Stockley, L., Scarborough, P., Snowdon, W., & Swinburn, B. (2011). Applications of nutrient profiling: potential role in diet-related chronic disease prevention and the feasibility of a core nutrient-profiling system. *European Journal of Clinical Nutrition*, *65*(3), 298-306.

Scarborough, P., Rayner, M., & Stockley, L. (2007). Developing nutrient profile models: A systematic approach. *Public Health Nutrition*, *10*(4), 330-336.

Todd, J. E., & Variyam, J. N. (2008). *The decline in consumer use of food nutrition labels, 1995-2006*. USDA.

WHO. (2011) Nutrient profiling: Report of a WHO/IASO technical meeting. London, UK. Retrieved from https://apps.who.int/iris/handle/10665/336447

WHO. (2023, September, 16). Non communicable diseases. Retrieved from https://www.who.int/news-room/fact-sheets/detail/noncommunicable-diseases

Wilkening, V. (1992). The nutritional labeling and education Act of 1990. U.S. food and drug administration. *17th National Nutrient Databank Conference*.

Author Information

Fatma Hazan Gul
Mersin University
Mersin, Turkey
Contact e-mail: hazanngul@gmail.com

To cite this article:

Gul, F. H. (2023). Nutrient profile of commercially packaged food products in Turkiye. *The Eurasia Proceedings of Science, Technology, Engineering & Mathematics (EPSTEM), 25,* 163-167.

The Eurasia Proceedings of Science, Technology,
Engineering & Mathematics (EPSTEM)
ISSN: 2602-3199

The Eurasia Proceedings of Science, Technology, Engineering & Mathematics (EPSTEM), 2023

Volume 25, Pages 168-186

ICBAST 2023: International Conference on Basic Sciences and Technology

G**β-Continuous and G**β-Irresolute Mappings in Topological Spaces

Raja Mohammad Latif
Prince Mohammad Bin Fahd University

Abstract: Topology being somehow very recent in nature but has got tremendous applications over almost all other fields. Theoretical or fundamental topology is a bit dry but the application part is what drives crazy once we get used. Topology has applications in various fields of Science and Technology, like applications to Biology, Robotics, GIS, Engineering, Computer Sciences. Topology though being a part of mathematics but it has influenced the whole world with so strong effects and incredible applications. The concept of continuity is fundamental in large parts of contemporary mathematics. In the nineteenth century, precise definitions of continuity were formulated for functions of a real or complex variable, enabling mathematicians to produce rigorous proofs of fundamental theorems of real and complex analysis, such as the Intermediate Value Theorem, Taylor's Theorem, the Fundamental Theorem of Calculus, and Cauchy's Theorem. In the early years of the Twentieth Century, the concept of continuity was generalized so as to be applicable to functions between metric spaces, and subsequently to functions between topological spaces. Topology is an area of mathematics concerned with the properties of space that are preserved under continuous deformations including stretching and bending but not tearing. In 2023, Dr. T. Delcia and M. S, Thillai introduced a new type of closed sets called g**β-closed sets and investigated their basic properties including their relationship with already existing concepts in Topological Spaces. In this paper, we introduce g**β-continuous function, g**β-irresolute function, g**β-open function, g**β-closed function, pre-g**β-open function, and pre-g**β-closed function, and investigate properties and characterizations of these new types of mappings in topological spaces.

Keywords: Topological space, g**β-closed set, g**β-continuous function, g**β-irresolute function, g**β-open function

1. Introduction

Introducing new versions of open sets in a topological space which may acquire either weaker or stronger properties is often studied. The first attempt was done by Levine [13], where he introduced the concepts of semi-open set, semi-closed set, and semi-continuity of a function. In 2023, Dr. T. Delcia and M. S, Thillai introduced a new type of closed sets called g**β-closed sets and investigated their basic properties including their relationship with already existing concepts in Topological Spaces.

In this paper, we introduce g**β-continuous function, g**β-irresolute function, g**β-open function, g**β-closed function, pre-g**β-open function, and pre-g**β-closed function, and investigate properties and characterizations of these new types of mappings in topological spaces.

2. BASIC PROPERTIES AND APPLICATIONS OF $g**\beta$-OPEN SETS

In this section, we shall define the concept of $g**\beta$-open set and determine its connection to the classical open set and characterize the concepts of $g**\beta$-open sets.

Definition 2.1. A subset A of a topological space (X,τ) is named generalized closed $(g\text{-}closed)$ closed if $Cl(A)\subseteq U$ whenever $A\subseteq U$ and U is open in X. The complement of g-closed set is called g-open in X.

Definition 2.2. A subset A of a topological space (X,τ) is called a generalized star closed set (briefly g^{*}-closed) closed set if $Cl(A)\subseteq U$ whenever $A\subseteq U$ and U is g-open in X. The complement of $g^{*}\text{-}closed$ set is called $g^{*}\text{-}open$ set.

Definition 2.3. A subset A of a topological space (X,τ) is called a generalized star β $(g{*}\beta\text{-}closed)$ closed if $\beta Cl(A)\subseteq U$ whenever $A\subseteq U$ and U is $g{*}\text{-}open$ in X. The complement of $g{*}\beta\text{-}closed$ set is called $g{*}\beta$-open set.

Definition 2.4. A subset A of a topological space (X,τ) is called a generalized star star β $(g^{**}\beta\text{-}closed)$ closed if $gCl(A)\subseteq U$ whenever $A\subseteq U$ and U is $g^{*}\beta\text{-}open$ in X. The complement of $g^{**}\beta\text{-}closed$ set is called $g^{**}\beta$-open set. The collection of all $g^{**}\beta$-open $(g^{**}\beta\text{-closed})$ subsets of (X,τ) is denoted by $g^{**}\beta\text{-}O(X,\tau)$ $(g^{**}\beta\text{-}C(X,\tau))$.

Theorem 2.5. Every closed (resp. open) set is $g^{**}\beta$-closed (resp. $g^{**}\beta$-open) set.

Theorem 2.6. If A and B are $g^{**}\beta$-closed (resp. $g^{**}\beta$-open) sets in X, then $A\cup B$ (*resp.* $A\cap B$) is $g^{**}\beta$-closed (resp. $g^{**}\beta$-open) in X.

Theorem 2.7. Arbitrary intersection (union) of $g^{**}\beta$-closed (resp. $g^{**}\beta$-open) sets is $g^{**}\beta$-closed (resp. $g^{**}\beta$-open) set in X.

Proof. Let $\Gamma=\{A_i : i\in I\}\subseteq g^{**}\beta\text{-}C(X,\tau)$. Let U be a $g^{*}\beta$-open set in X such that $A_i\subseteq U$ for each $i\in I$. Hence, $gC(A_i)\subseteq U$ for each $i\in I$. Therefore, $gCl(\cap\Gamma)=gCl(\bigcap_{i\in I}A_i\Gamma)\subseteq\bigcap_{i\in I}gCl(A)_i\subseteq U$. This implies $gCl(\cap\Gamma)=gCl(\bigcap_{i\in I}A_i\Gamma)\subseteq U$, U is $g^{**}\beta$-open in X. Hence $\cap\Gamma=\bigcap_{i\in I}A_i$ is $g^{**}\beta$-closed in X. Thus arbitrary intersection of $g^{**}\beta$-closed sets is $g^{**}\beta$-closed set in X. Now by using this result and complements we conclude that arbitrary union of $g^{**}\beta$-open sets is $g^{**}\beta$-open set in X.

Definition 2.8. Let (X,τ) be a topological space and $B\subseteq X$. We define the $g^{**}\beta$-closure of B (briefly $g^{**}\beta\text{-}Cl(B)$) to be the intersection of all $g^{**}\beta$-closed sets containing B which is denoted by $g^{**}\beta\text{-}Cl(B)=\bigcap\{A : B\subseteq A \text{ and } A\in g^{**}\beta\text{-}C(X,\tau).\}$. We note that $g^{**}\beta\text{-}Cl(B)$ is the smallest $g^{**}\beta\text{-}closed$ set containing B.

Definition 2.9. Let (X,τ) be any topological space and B be a subset of X. A point p of X is called a $g^{**}\beta\text{-}interior$ point of B, if there exists a $g^{**}\beta\text{-}open$ set G such that $p\in G\subseteq B$. The set of all $g^{**}\beta\text{-}interior$ points of B is said to be $g^{**}\beta\text{-}interior$ of B (briefly $g^{**}\beta\text{-}Int(B)$) and it is defined by $g^{**}\beta\text{-}Int(B)=\bigcup\{A : A\subseteq B \text{ and } A\in g^{**}\beta\text{-}O(X,\tau)\}$.

Definition 2.10. Let ¥ be a subset of a topological space (X,τ) and let $x \in X$. We say that ¥ is $g^{**}\beta$-*neighborhood* of x, if there is a $g^{**}\beta$-*open* set U such that $x \in U \subseteq$ ¥.

Proposition2.11. If U and V are sets in a topological space (X,τ), then

(1) $g^{**}\beta\text{-}Int(\phi)=\phi$. (2) $g^{**}\beta\text{-}Int(X)=X$. (3) $g^{**}\beta\text{-}Int(U)\subseteq U$.

(4) $U \subseteq V \Rightarrow g^{**}\beta\text{-}Int(U)\subseteq g^{**}\beta\text{-}Int(V)$.

Proposition2.12. Let G be any subset of a topological space (X,τ). Then $x \in g^{**}\beta\text{-}Cl(A)$ if and only if for every $g^{**}\beta$-*open* set U containing x, $U \cap G \neq \phi$.

Proposition2.13. For any subset U of topological space (X,τ), $g^{**}\beta\text{-}Int(U)\subseteq U \subseteq g^{**}\beta\text{-}Cl(U)$.

Definition 2.14. Let A be a subset of a topological space (X,τ). A point $x \in A$ is said to be a $g^{**}\beta$-*limit* point of A if for each $g^{**}\beta$-*open* set U containing x, $U \cap (A-\{x\}) \neq \phi$. The set of all $g^{**}\beta$-*limit* points of A is called the $g^{**}\beta$-*derived* set of A and is denoted by $g^{**}\beta\text{-}D(A)$.

Theorem 2.15. For any subset A of a topological space X, $g^{**}\beta\text{-}Cl(A)=A \cup [g^{**}\beta\text{-}D(A)]$.

Proof. Since $g^{**}\beta\text{-}D(A)\subseteq g^{**}\beta\text{-}Cl(A)$. $A\cup[g^{**}\beta\text{-}D(A)]\subseteq g^{**}\beta\text{-}Cl(A)$. On the other hand, let $x \in g^{**}\beta\text{-}Cl(A)$. If $x \in A$, then the proof is complete. If $x \notin A$, each $g^{**}\beta$-*open* set U containing x intersects A at a point distinct from x, so $x \in g^{**}\beta\text{-}D(A)$. Thus, $g^{**}\beta\text{-}Cl(A)\subseteq [A\cup(g^{**}\beta\text{-}D(A))]$.

Corollary 2.16. A subset A of a space X is $g^{**}\beta$-*closed* if and only if it contains the set of all of its $g^{**}\beta$-*limit* points.

Theorem 2.17. For subsets A, B of a space X, the following statements are true:

(1) $g^{**}\beta\text{-}Int(A)$ is the largest $g^{**}\beta$-*open* set contained in A;

(2) A is $g^{**}\beta$-*open* if and only if $A = g^{**}\beta\text{-}Int(A)$.

(3) $g^{**}\beta\text{-}Int[g^{**}\beta\text{-}Int(A)] = g^{**}\beta\text{-}Int(A)$;

(4) $g^{**}\beta\text{-}Int(A)=[A-(g^{**}\beta\text{-}D(X-A))]$;

(5) $[X-(g^{**}\beta\text{-}Cl(A))]=g^{**}\beta\text{-}Int(X-A)$;

(6) $[X-(g^{**}\beta\text{-}Int(A))]=g^{**}\beta\text{-}Cl(X-A)$;

(7) $[g^{**}\beta\text{-}Int(A)]\cup[g^{**}\beta\text{-}Int(B)]\subseteq g^{**}\beta\text{-}Int(A\cup B)$;

(8) $g^{**}\beta\text{-}Int(A\cap B)=[g^{**}\beta\text{-}Int(A)]\cap[g^{**}\beta\text{-}Int(B)]$;

(4) If $x \in [A-(g^{**}\beta\text{-}D(X-A))]$, then $x \notin g^{**}\beta\text{-}D(X-A)$ and so there exists a $g^{**}\beta$-*open* set U containing x such that $U \cap (X-A)=\phi$. Then, $x \in U \subseteq A$ and hence $x \in g^{**}\beta\text{-}Int(A)$, that is, $[A-(g^{**}\beta\text{-}D(X-A))]\subseteq g^{**}\beta\text{-}Int(A)$. On the other hand, if $x \in g^{**}\beta\text{-}Int(A)$, then $x \notin g^{**}\beta\text{-}D(X-A)$

since $g**\beta\text{-}Int(A)$ is $g**\beta\text{-}open$ and $[(g**\beta\text{-}Int(A))\cap(X-A)]=\phi$. Hence, $g**\beta\text{-}Int(A)=[A-(g**\beta\text{-}D(X-A))]$.

(6) $X-[g**\beta\text{-}Int(A)]=X-[A-(g**\beta\text{-}D(X-A))]=(X-A)\cup[g**\beta\text{-}D(X-A)]=$ $g**\beta\text{-}Cl(X-A)$.

Theorem 2.18. Let (X,τ) be a topological space and $A, B\subseteq X$. Then the following statements are true:

(1) $x\in g**\beta\text{-}Cl(A)$ if and only if for every $g**\beta\text{-}open$ subset U containing x, $U\cap A\neq\phi$.

(2) $A\subseteq B$ implies that $g**\beta\text{-}Cl(A)\subseteq g**\beta\text{-}Cl(B)$.

(3) A is $g**\beta\text{-}closed$ if and only if $g**\beta\text{-}Cl(A)=A$.

(4) $g**\beta\text{-}Cl[g**\beta\text{-}Cl(A)]=g**\beta\text{-}Cl(A)$.

(5) $[g**\beta\text{-}Cl(A)]\cup[g**\beta\text{-}Cl(B)]=g**\beta\text{-}Cl(A\cup B)$.

(6) $g**\beta\text{-}Int(X-A)=X-[g**\beta\text{-}Cl(A)]$.

(7) $g**\beta\text{-}Cl(X-A)=X-[g**\beta\text{-}Int(A)]$.

Definition 2.19. $g**\beta\text{-}Bd(A)=A-[g**\beta\text{-}Int(A)]$ is said to be the $g**\beta\text{-}border$ of A.

Theorem 2.20. For a subset A of a space X, the following statements hold:

(1) $Bd(A)\subseteq g**\beta\text{-}Bd(A)$ where $Bd(A)$ denotes the border of A;

(2) $A=g**\beta\text{-}Int(A)\cup g**\beta\text{-}Bd(A)$;

(3) $[g**\beta\text{-}Int(A)]\cap[g**\beta\text{-}Bd(A)]=\phi$;

(4) A is a $g**\beta\text{-}open$ set if and only if $g**\beta\text{-}Bd(A)=\phi$;

(5) $g**\beta\text{-}Bd[g**\beta\text{-}Int(A)]=\phi$;

(6) $g**\beta\text{-}Int[g**\beta\text{-}Bd(A)]=\phi$;

(7) $g**\beta\text{-}Bd[g**\beta\text{-}Bd(A)]=g**\beta\text{-}Bd(A)$;

(8) $g**\beta\text{-}Bd(A)=A\cap[g**\beta\text{-}Cl(X-A)]$;

(9) $g**\beta\text{-}Bd(A)=g**\beta\text{-}D(X-A)$.

Proof. (6) If $x\in g**\beta\text{-}Int[g**\beta\text{-}Bd(A)]$, then $x\in g**\beta\text{-}Bd(A)$. On the other hand, since $g**\beta\text{-}Bd(A)\subseteq A$, $x\in g**\beta\text{-}Int[g**\beta\text{-}Bd(A)]\subseteq g**\beta\text{-}Int(A)$. Therefore, we get $x\in[g**\beta\text{-}Int(A)]\cap[g**\beta\text{-}Bd(A)]$, which contradicts (3). Thus, $g**\beta\text{-}Int[g**\beta\text{-}Bd(A)]=\phi$.

(8) $g**\beta\text{-}Bd(A)=A-[g**\beta\text{-}Int(A)]=A-[X-(g**\beta\text{-}Cl(X-A))]=A\cap[g**\beta\text{-}Cl(X-A)]$.

(9) $g**\beta\text{-}Bd(A)=A-[g**\beta\text{-}Int(A)]=A-[A-(g**\beta\text{-}D(X-A))]=g**\beta\text{-}D(X-A)$.

Definition 2.21. $g**\beta\text{-}Fr(A)=[g**\beta\text{-}Cl(A)]-[g**\beta\text{-}Int(A)]$ is said to be the $g**\beta$-frontier of A.

Theorem 2.22. For a subset A of a space X, the following statements hold:

(1) $Fr(A)\subseteq g**\beta\text{-}Fr(A)$ where $Fr(A)$ denotes the frontier of A;

(2) $g**\beta\text{-}Cl(A)=[g**\beta\text{-}Int(A)]\cup[g**\beta\text{-}Fr(A)]$;

(3) $\left[g^{**}\beta\text{-}Int(A)\right]\cap\left[g^{**}\beta\text{-}Fr(A)\right]=\phi;$

(4) $g^{**}\beta\text{-}Bd(A)\subseteq g^{**}\beta\text{-}Fr(A);$

(5) $g^{**}\beta\text{-}Fr(A)=\left[g^{**}\beta\text{-}Bd(A)\right]\cup\left[g^{**}\beta\text{-}D(A)\right];$

(6) A is a $g^{**}\beta\text{-}open$ set if and only if $g^{**}\beta\text{-}Fr(A)=g^{**}\beta\text{-}D(A);$

(7) $g^{**}\beta\text{-}Fr(A)=\left[g^{**}\beta\text{-}Cl(A)\right]\cap\left[g^{**}\beta\text{-}Cl(X-A)\right];$

(8) $g^{**}\beta\text{-}Fr(A)=g^{**}\beta\text{-}Fr(X-A);$

(9) $g^{**}\beta\text{-}Fr(A)$ is $g^{**}\beta\text{-}closed;$

(10) $g^{**}\beta\text{-}Fr\left[g^{**}\beta\text{-}Fr(A)\right]\subseteq g^{**}\beta\text{-}Fr(A);$

(11) $g^{**}\beta\text{-}Fr\left[g^{**}\beta\text{-}Int(A)\right]\subseteq g^{**}\beta\text{-}Fr(A);$

(12) $g^{**}\beta\text{-}Fr\left[g^{**}\beta\text{-}Cl(A)\right]\subseteq g^{**}\beta\text{-}Fr(A);$

(13) $g^{**}\beta\text{-}Int(A)=A-\left[g^{**}\beta\text{-}Fr(A)\right].$

Proof. (2) $\left[g^{**}\beta\text{-}Int(A)\right]\cup\left[g^{**}\beta\text{-}Fr(A)\right]=$
$g^{**}\beta\text{-}Int(A)\cup\left[g^{**}\beta\text{-}Cl(A)-g^{**}\beta\text{-}Int(A)\right]=g^{**}\beta\text{-}Cl(A)$

(3) $\left[g^{**}\beta\text{-}Int(A)\right]\cap\left[g^{**}\beta\text{-}Fr(A)\right]=\left[g^{**}\beta\text{-}Int(A)\right]\cap\left[\left(g^{**}\beta\text{-}Cl(A)\right)-\left(g^{**}\beta\text{-}Int(A)\right)\right]=\phi.$

(5) $Since\left[g^{**}\beta\text{-}Int(A)\right]\cup\left[g^{**}\beta\text{-}Fr(A)\right]=\left[g^{**}\beta\text{-}Int(A)\right]\cup\left[g^{**}\beta\text{-}Bd(A)\right]\cup\left[g^{**}\beta\text{-}D(A)\right],$
$g^{**}\beta\text{-}Fr(A)=\left[g^{**}\beta\text{-}Bd(A)\right]\cup\left[g^{**}\beta\text{-}D(A)\right].$

(7) $g^{**}\beta\text{-}Fr(A)=\left[g^{**}\beta\text{-}Cl(A)\right]-\left[g^{**}\beta\text{-}Int(A)\right]=\left[g^{**}\beta\text{-}Cl(A)\right]\cap\left[g^{**}\beta\text{-}Cl(X-A)\right].$

(9) $g^{**}\beta\text{-}Cl\left[g^{**}\beta\text{-}Fr(A)\right]=g^{**}\beta\text{-}Cl\left[\left(g^{**}\beta\text{-}Cl(A)\right)\cap\left(g^{**}\beta\text{-}Cl(X-A)\right)\right]\subseteq$
$g^{**}\beta\text{-}Cl\left[g^{**}\beta\text{-}Cl(A)\right]\cap g^{**}\beta\text{-}Cl\left[g^{**}\beta\text{-}Cl(X-A)\right]$
$=\left[g^{**}\beta\text{-}Cl(A)\right]\cap\left[g^{**}\beta\text{-}Cl(X-A)\right]=g^{**}\beta\text{-}Fr(A).$ Hence $g^{**}\beta\text{-}Fr(A)$ is $g^{**}\beta\text{-}closed.$

(10) $g^{**}\beta\text{-}Fr\left[g^{**}\beta\text{-}Fr(A)\right]=g^{**}\beta\text{-}Cl\left[g^{**}\beta\text{-}Fr(A)\right]\cap g^{**}\beta\text{-}Cl\left[X-\left(g^{**}\beta\text{-}Fr(A)\right)\right]\subseteq$
$g^{**}\beta\text{-}Cl\left[g^{**}\beta\text{-}Fr(A)\right]=g^{**}\beta\text{-}Fr(A).$

(12) $g^{**}\beta\text{-}Fr\left[g^{**}\beta\text{-}Cl(A)\right]=g^{**}\beta\text{-}Cl\left[g^{**}\beta\text{-}Cl(A)\right]-g^{**}\beta\text{-}Int\left[g^{**}\beta\text{-}Cl(A)\right]=$
$\left[g^{**}\beta\text{-}Cl(A)\right]-\left[g^{**}\beta\text{-}Int\left(g^{**}\beta\text{-}Cl(A)\right)\right]\subseteq$
$\left[\left(g^{**}\beta\text{-}Cl(A)\right)-\left(g^{**}\beta\text{-}Int(A)\right)\right]=g^{**}\beta\text{-}Fr(A).$

(13) $A-\left[g^{**}\beta\text{-}Fr(A)\right]=A-\left[\left(g^{**}\beta\text{-}Cl(A)\right)-\left(g^{**}\beta\text{-}Int(A)\right)\right]=g^{**}\beta\text{-}Int(A).$

$3-8$: CHARACTERIZATIONS OF MAPPINGS

The purpose of this part is to introduce $g^{**}\beta\text{-}continuous$, $g^{**}\beta\text{-}irresolute$, $g^{**}\beta\text{-}open$, $g^{**}\beta\text{-}closed$, $pre\text{-}g^{**}\beta\text{-}open$, and $pre\text{-}g^{**}\beta\text{-}closed$ functions and explore properties and characterizations of these functions.

3. $g^{**}\beta$-CONTINUOUS FUNCTIONS

The purpose of this section is to investigate the properties and characterizations of $g^{**}\beta$-*continuous* functions.

Definition 3.1. A function $f:(X,\tau)\to(Y,\sigma)$ is said to be $g^{**}\beta$-*continuous* if $f^{-1}(V)\in g^{**}\beta\text{-}O(X,\tau)$ for every $V\in\sigma$.

Theorem 3.2. Let $f:(X,\tau)\to(Y,\sigma)$ be a function. Then the following statements are equivalent:

(1) f is $g^{**}\beta$-*continuous*.

(2) The inverse image of each closed set in Y is a $g^{**}\beta$-*closed* set in X;

(3) $g^{**}\beta\text{-}Cl\left[f^{-1}(V)\right]\subseteq f^{-1}\left[Cl(V)\right]$, for every $V\subseteq Y$;

(4) $f\left[g^{**}\beta\text{-}Cl(U)\right]\subseteq Cl\left[f(U)\right]$, for every $U\subseteq X$;

(5) For any point $x\in X$ and any open set V of Y containing $f(x)$, there exists $U\in g^{**}\beta\text{-}O(X,\tau)$ such that $x\in U$ and $f(U)\subseteq V$;

(6) $g^{**}\beta\text{-}Bd\left[f^{-1}(V)\right]\subseteq f^{-1}\left[g^{**}\beta\text{-}d(V)\right]$, for every $V\subseteq Y$;

(7) $f\left[g^{**}\beta\text{-}D(U)\right]\subseteq Cl\left[f(U)\right]$, for every $U\subseteq X$;

(8) $f^{-1}\left[Int(V)\right]\subseteq g^{**}\beta\text{-}Int\left[f^{-1}(V)\right]$, for every $V\subseteq Y$;

Proof. $(1)\Rightarrow(2)$: Let $F\subseteq Y$ be closed. Since f is $g^{**}\beta$-*continuous*, $f^{-1}(Y-F)=X-f^{-1}(F)$ is $g^{**}\beta$-*open*. Therefore, $f^{-1}(F)$ is $g^{**}\beta$-*closed* in X.

$(2)\Rightarrow(3)$: Since $Cl(V)$ is closed for every $V\subseteq Y$, then $f^{-1}\left[Cl(V)\right]$ is $g^{**}\beta$-*closed*. Therefore $f^{-1}\left[Cl(V)\right]=g^{**}\beta\text{-}Cl\left[f^{-1}(Cl(V))\right]\supseteq g^{**}\beta\text{-}Cl\left[f^{-1}(V)\right]$.

$(3)\Rightarrow(4)$: Let $U\subseteq X$ and $f(U)=V$. Then $g^{**}\beta\text{-}Cl\left[f^{-1}(V)\right]\subseteq f^{-1}\left[Cl(V)\right]$. Thus $g^{**}\beta\text{-}Cl(U)\subseteq g^{**}\beta\text{-}Cl\left[f^{-1}(f(U))\right]\subseteq f^{-1}\left[Cl(f(U))\right]$ and $f\left[g^{**}\beta\text{-}Cl(U)\right]\subseteq Cl\left[f(U)\right]$.

$(4)\Rightarrow(2)$: Let $W\subseteq Y$ be a closed set, and $U=f^{-1}(W)$. Then $f\left[g^{**}\beta\text{-}Cl(U)\right]\subseteq Cl\left[f(U)\right]$ $=Cl\left[f(f^{-1}(W))\right]\subseteq Cl(W)=W$. Thus $g^{**}\beta\text{-}Cl(U)\subseteq f^{-1}\left[f(g^{**}\beta\text{-}Cl(U))\right]\subseteq f^{-1}(W)=U$. So U is $g^{**}\beta$-*closed*.

$(2)\Rightarrow(1)$: Let $V\subseteq Y$ be an open set. Then $Y-V$ is closed. Then $f^{-1}(Y-V)=X-f^{-1}(V)$ is $g^{**}\beta$-*closed* in X and hence $f^{-1}(V)$ *is* $g^{**}\beta$-*open in* X.

$(1)\Rightarrow(5)$: Let $f:(X,\tau)\to(Y,\sigma)$ be $g^{**}\beta$-*continuous*. For any $x\in X$ and any open set V of Y containing $f(x)$, $U=f^{-1}(V)\in g^{**}\beta\text{-}O(X,\tau)$, and $f(U)=f\left[f^{-1}(V)\right]\subseteq V$.

$(5)\Rightarrow(1)$: Let $V\in\sigma$. We prove $f^{-1}(V)\in g^{**}\beta\text{-}O(X,\tau)$. Let $x\in f^{-1}(V)$. Then $f(x)\in V$ and there exists $U\in g^{**}\beta\text{-}O(X,\tau)$ such that $x\in U$ and $f(x)\in f(U)\subseteq V$. Hence $x\in U\subseteq f^{-1}\left[f(U)\right]\subseteq f^{-1}(V)$. It shows that $f^{-1}(V)$ is a $g^{**}\beta$-*neighborhood* of each of its points. Therefore $f^{-1}(V)\in g^{**}\beta\text{-}O(X,\tau)$.

$(6)\Rightarrow(8)$: Let $V\subseteq Y$. Then by hypothesis, $g^{**}\beta\text{-}Bd\left[f^{-1}(V)\right]\subseteq f^{-1}\left[Bd(V)\right]$

$\Rightarrow f^{-1}(V)-\left[g^{**}\beta\text{-}Int(f^{-1}(V))\right]\subseteq f^{-1}\left[V-Int(V)\right]=f^{-1}(V)-f^{-1}\left[Int(V)\right]$

$\Rightarrow f^{-1}\left[Int(V)\right]\subseteq g^{**}\beta\text{-}Int\left[f^{-1}(V)\right]$.

$(8)\Rightarrow(6)$: Let $V\subseteq Y$. Then by hypothesis, $f^{-1}\left[Int(V)\right]\subseteq g^{**}\beta\text{-}Int\left[f^{-1}(V)\right]$

$\Rightarrow\ f^{-1}(V)-\left[g^{**}\beta\text{-}Int\left(f^{-1}(V)\right)\right]\subseteq f^{-1}(V)-f^{-1}\left[Int(V)\right]=f^{-1}\left[V-Int(V)\right]$

$\Rightarrow g^{**}\beta\text{-}Bd\left[f^{-1}(V)\right]\subseteq f^{-1}\left[Bd(V)\right].$

$(1)\Rightarrow(7)$: It is obvious, since f *is* $g^{**}\beta$-*continuous* and by (4) $f\left[g^{**}\beta\text{-}Cl(U)\right]\subseteq Cl\left[f(U)\right]$ for each $U\subseteq X$. So $f\left[g^{**}\beta\text{-}D(U)\right]\subseteq Cl\left[f(U)\right]$.

$(7)\Rightarrow(1)$: Let $U\subseteq Y$ be an open set, $V=Y-U$ and $f^{-1}(V)=W$. Then by hypothesis $f\left[g^{**}\beta\text{-}D(W)\right]\subseteq Cl\left[f(W)\right]$. Thus $f\left[g^{**}\beta\text{-}D\left(f^{-1}(V)\right)\right]\subseteq Cl\left[f\left(f^{-1}(V)\right)\right]\subseteq Cl(V)=V$. Then $g^{**}\beta\text{-}D\left[f^{-1}(V)\right]\subseteq f^{-1}(V)$ and $f^{-1}(V)$ *is* $g^{**}\beta$-*closed*. Therefore, f is $g^{**}\beta$-*continuous*.

$(1)\Rightarrow(8)$: Let $V\subseteq Y$. Then $f^{-1}\left[Int(V)\right]$ is $g^{**}\beta$-*open in* X. Thus $f^{-1}\left[Int(V)\right]=g^{**}\beta\text{-}Int\left[f^{-1}\left(Int(V)\right)\right]\subseteq g^{**}\beta\text{-}Int\left[f^{-1}(V)\right]$. Therefore $f^{-1}\left[Int(V)\right]\subseteq g^{**}\beta\text{-}Int\left[f^{-1}(V)\right]$.

$(8)\Rightarrow(1)$: Let $V\subseteq Y$ be an open set. Then $f^{-1}(V)=f^{-1}\left[Int(V)\right]\subseteq g^{**}\beta\text{-}Int\left[f^{-1}(V)\right]$. Therefore, $f^{-1}(V)$ *is* $g^{**}\beta$-*open*. Hence f *is* $g^{**}\beta$-*continuous*.

In the next Theorem, $\#g^{**}\beta\text{-}c.$ denotes the set of points x of X for which a function $f:(X,\tau)\rightarrow(Y,\sigma)$ is not $g^{**}\beta$-*continuous*.

Theorem 3.3. $\#g^{**}\beta\text{-}c.$ is identical with the union of the $g^{**}\beta$-frontiers of the inverse images of $g^{**}\beta$-*open* sets containing $f(x)$.

Proof. Suppose that f is not $g^{**}\beta$-*continuous* at a point x of X. Then there exists an open set $V\subseteq Y$ containing $f(x)$ such that $f(U)$ is not a subset of V for every $U\in g^{**}\beta\text{-}O(X,\tau)$. containing x. Hence, we have $U\cap f^{-1}\left(X-f^{-1}(V)\right)\neq\phi$ for every $U\in g^{**}\beta\text{-}O(X,\tau)$ containing x. It follows that $x\in\left[g^{**}\beta\text{-}Cl\left(X-f^{-1}(V)\right)\right]$. We also have $x\in f^{-1}(V)\subseteq g^{**}\beta\text{-}Cl\left[f^{-1}(V)\right]$. This means that $x\in g^{**}\beta\text{-}Fr\left[f^{-1}(V)\right]$. Now, let f be $g^{**}\beta$-*continuous* at $x\in X$ and $V\subseteq Y$ any open set containing $f(x)$. Then, $x\in f^{-1}(V)$ is a $g^{**}\beta$-*open* set of X. Thus. $x\in g^{**}\beta\text{-}Int\left[f^{-1}(V)\right]$ and therefore $x\notin g^{**}\beta\text{-}Fr\left[f^{-1}(V)\right]$ for every open set V containing $f(x)$.

Remarks 3.4. (1) Every $g^{**}\beta$-*continuous* function is continuous, but the converse may not be true.

(2) If a function $f:(X,\tau)\rightarrow(Y,\sigma)$ is $g^{**}\beta$-*continuous* and a function $g:(Y,\sigma)\rightarrow(Z,\vartheta)$ is $g^{**}\beta$-*continuous*, then $gof:(X,\tau)\rightarrow(Z,\vartheta)$ is $g^{**}\beta$-*continuous*.

(3) If a function $f:(X,\tau)\rightarrow(Y,\sigma)$ is $g^{**}\beta$-*continuous* and a function $g:(Y,\sigma)\rightarrow(Z,\vartheta)$ is continuous, then $gof:(X,\tau)\rightarrow(Z,\vartheta)$ is $g^{**}\beta$-*continuous*.

(4) Let (X,τ) and (Y,σ) be topological spaces. If $f:(X,\tau)\rightarrow(Y,\sigma)$ is a function, and one of the following

(a) $f^{-1}\left[Int(B)\right]\subseteq g^{**}\beta\text{-}Int\left[f^{-1}(B)\right]$ for each $B\subseteq Y$.

(b) $g^{**}\beta\text{-}Cl\left[f^{-1}(B)\right]\subseteq f^{-1}\left[Cl(B)\right]$ for each $B\subseteq Y$.

(c) $f\left[g^{**}\beta\text{-}Cl(A)\right]\subseteq Cl\left[f(A)\right]$ for each $A\subseteq X$ holds, then f is continuous.

Lemma 3.5. Let $A\subseteq Y\subseteq X$, Y is $g^{**}\beta$-*open* in X and A is $g^{**}\beta$-*open* in Y. Then A is $g^{**}\beta$-*open* in X.

Proof. Since A is $g^{**}\beta$-*open* in Y, there exists a $g^{**}\beta$-*open* set $U \subseteq X$ such that $A = Y \cap U$. Thus A being the intersection of two $g^{**}\beta$-*open* sets in X, is $g^{**}\beta$-*open* in X.

Theorem 3.6. Let $f:(X,\tau)\to(Y,\sigma)$ be a mapping and $\{U_i : i \in I\}$ be a cover of X such that $U_i \in g^{**}\beta\text{-}O(X,\tau)$ for each $i \in I$. Then prove that f is $g^{**}\beta$-*continuous*.

Proof. Let $V \subseteq Y$ be an open set, then $(f|U_i)^{-1}(V)$ is $g^{**}\beta$-*open* in U_i for each $i \in I$. Since U_i is $g^{**}\beta$-*open* in X for each $i \in I$. So by Lemma 3.5, $(f|U_i)^{-1}(V)$ is $g^{**}\beta$-*open* in X for each $i \in I$. But, $f^{-1}(V) = \cup\left\{(f|U_i)^{-1}(V) : i \in I\right\}$, then $f^{-1}(V) \in g^{**}\beta\text{-}O(X,\tau)$ because $g^{**}\beta\text{-}O(X,\tau)$ is closed under union. This implies that f is $g^{**}\beta$-*continuous*.

4. $g^{**}\beta$-IRRESOLUTE FUNCTIONS

In this section, the functions to be considered are those for which inverses of $g^{**}\beta$-*open* sets are $g^{**}\beta$-*open*. We investigate some properties and characterizations of such functions.

Definition 4.1. Let (X,τ) and (Y,σ) be topological spaces. A function $f:(X,\tau)\to(Y,\sigma)$ is called $g^{**}\beta$-*irresolute* if the inverse image $f^{-1}(U)$ of each $g^{**}\beta$-*open* set U of Y is a $g^{**}\beta$-*open* set in X.

Theorem 4.2. Let $f:(X,\tau)\to(Y,\sigma)$ be a function between topological spaces. Then the following statements are equivalent:

(1) f is $g^{**}\beta$-*irresolute;*

(2) The inverse image of each $g^{**}\beta$-*closed* set in (Y,σ) is a $g^{**}\beta$-*closed* set in (X,τ),

(3) $g^{**}\beta\text{-}Cl\left[f^{-1}(B)\right] \subseteq f^{-1}\left[g^{**}\beta\text{-}Cl(B)\right] \subseteq f^{-1}\left[Cl(B)\right]$, for each $B \subseteq Y$,

(4) $f\left[g^{**}\beta\text{-}Cl(A)\right] \subseteq g^{**}\beta\text{-}Cl\left[f(A)\right] \subseteq Cl\left[f(A)\right]$, for each $A \subseteq X$,

(5) $f^{-1}\left[g^{**}\beta\text{-}Int(B)\right] \subseteq g^{**}\beta\text{-}Int\left[f^{-1}(B)\right]$, for each $B \subseteq Y$,

(6) $g^{**}\beta\text{-}Bd\left[f^{-1}(B)\right] \subseteq f^{-1}\left[g^{**}\beta\text{-}Bd(B)\right]$, for each $B \subseteq Y$,

(7) $g^{**}\beta\text{-}b\left[f^{-1}(B)\right] \subseteq f^{-1}\left[g^{**}\beta\text{-}b(B)\right]$, for each $B \subseteq Y$,

(8) $f\left[g^{**}\beta\text{-}b(A)\right] \subseteq g^{**}\beta\text{-}b\left[f(A)\right]$, for each $A \subseteq X$,

(9) $f\left[g^{**}\beta\text{-}Cl(A)\right] \subseteq g^{**}\beta\text{-}Cl\left[f(A)\right]$, for each $A \subseteq X$.

Proof. $\mathbf{(1)\Rightarrow(2):}$ Obvious.

$\mathbf{(2)\Rightarrow(3):}$ Let $B \subseteq Y$ and $B \subseteq g^{**}\beta\text{-}Cl(B) \subseteq Cl(B)$. Then by (2) $g^{**}\beta\text{-}Cl\left[f^{-1}(B)\right] \subseteq g^{**}\beta\text{-}Cl\left[f^{-1}\left(g^{**}\beta\text{-}Cl(B)\right)\right] = f^{-1}\left[g^{**}\beta\text{-}Cl(B)\right] \subseteq f^{-1}\left[Cl(B)\right]$.

$\mathbf{(3)\Rightarrow(4):}$ Immediately by replacing B by $f(A)$ in (3).

$\mathbf{(4)\Rightarrow(1):}$ Let $W \in g^{**}\beta\text{-}O(Y)$ and $F = Y - W \in g^{**}\beta\text{-}C(Y)$. Then by (4), $f\left[g^{**}\beta\text{-}Cl\left(f^{-1}(F)\right)\right] \subseteq g^{**}\beta\text{-}Cl\left[f\left(f^{-1}(F)\right)\right] \subseteq g^{**}\beta\text{-}Cl(F) = F$. So $g^{**}\beta\text{-}Cl\left[f^{-1}(F)\right] \subseteq f^{-1}(F)$ and hence, $f^{-1}(F) = X - f^{-1}(F) \in g^{**}\beta\text{-}C(X)$, thus $f^{-1}(W) \in g^{**}\beta\text{-}O(X)$. Therefore f is $g^{**}\beta$-*irresolute.*

$(1)\Rightarrow(5)$: Let $B\subseteq Y$. Then $g^{**}\beta\text{-}Int(B)$ is $g^{**}\beta\text{-}open$ in Y. By (1), $f^{-1}\left[g^{**}\beta\text{-}Int(B)\right]$ is $g^{**}\beta\text{-}open$ in X. Hence $f^{-1}\left[g^{**}\beta\text{-}Int(B)\right]=g^{**}\beta\text{-}Int\left[f^{-1}\left(g^{**}\beta\text{-}Int(B)\right)\right]\subseteq g^{**}\beta\text{-}Int\left[f^{-1}(B)\right]$.

$(5)\Rightarrow(6)$: Let $B\subseteq Y$. Then by (5), $f^{-1}\left[g^{**}\beta\text{-}Int(B)\right]\subseteq g^{**}\beta\text{-}Int\left[f^{-1}(B)\right]$ we have $f^{-1}(B)-g^{**}\beta\text{-}Int\left[f^{-1}(B)\right]\subseteq f^{-1}(B)-f^{-1}\left[g^{**}\beta\text{-}Int(B)\right]$. Therefore we obtain $g^{**}\beta\text{-}Bd\left[f^{-1}(B)\right]\subseteq f^{-1}\left[g^{**}\beta\text{-}Bd(B)\right]$.

$(6)\Rightarrow(5)$: Let $B\subseteq Y$. Then by (6), $g^{**}\beta\text{-}Bd\left[f^{-1}(B)\right]=f^{-1}(B)-g^{**}\beta\text{-}Int\left[f^{-1}(B)\right]\subseteq f^{-1}\left[g^{**}\beta\text{-}Bd(B)\right]=f^{-1}\left[B-\left(g^{**}\beta\text{-}Int(B)\right)\right]=f^{-1}(B)-f^{-1}\left[Int(B)\right]$. This implies $f^{-1}\left[g^{**}\beta\text{-}Int(B)\right]\subseteq g^{**}\beta\text{-}Int\left[f^{-1}(B)\right]$.

$(5)\Rightarrow(1)$: Let $B\subseteq Y$ be $g^{**}\beta\text{-}open$. Then $B=g^{**}\beta\text{-}Int(B)$. Hence by (5) we have $f^{-1}(B)=f^{-1}\left[g^{**}\beta\text{-}Int(B)\right]\subseteq g^{**}\beta\text{-}Int\left[f^{-1}(B)\right]$. Thus $f^{-1}(B)$ is $g^{**}\beta\text{-}open$ in X. So, f is $g^{**}\beta\text{-}irresolute.$

$(1)\Rightarrow(7)$: Let $B\subseteq Y$, by (3), we have $g^{**}\beta\text{-}b\left[f^{-1}(B)\right]=g^{**}\beta\text{-}Cl\left[f^{-1}(B)\right]-g^{**}\beta\text{-}Int\left[f^{-1}(B)\right]\subseteq f^{-1}\left[g^{**}\beta\text{-}Cl(B)\right]-g^{**}\beta\text{-}Int\left[f^{-1}(B)\right]\subseteq f^{-1}\left[g^{**}\beta\text{-}b(B)\cup \mathrm{Z}\,s\text{-}Int(B)\right]-g^{**}\beta\text{-}Int\left[f^{-1}(B)\right]\subseteq f^{-1}\left[g^{**}\beta\text{-}b(B)\cup g^{**}\beta\text{-}Int(B)\right]-g^{**}\beta\text{-}Int\left[f^{-1}\left(g^{**}\beta\text{-}Int(B)\right)\right]$. By (1) we have $g^{**}\beta\text{-}b\left[f^{-1}(B)\right]\subseteq\left[f^{-1}\left(g^{**}\beta\text{-}b(B)\right)\cup f^{-1}\left(g^{**}\beta\text{-}Int(B)\right)\right]-f^{-1}\left[g^{**}\beta\text{-}Int(B)\right]=f^{-1}\left[g^{**}\beta\text{-}b(B)\right]$.

$(7)\Rightarrow(1)$: Let $B\in g^{**}\beta\text{-}C(Y)$ and $g^{**}\beta\text{-}b\left[f^{-1}(B)\right]\subseteq f^{-1}\left[g^{**}\beta\text{-}b(B)\right]$. Then, $g^{**}\beta\text{-}b\left[f^{-1}(B)\right]\subseteq f^{-1}\left[g^{**}\beta\text{-}Cl(B)-g^{**}\beta\text{-}Int(B)\right]=f^{-1}(B)-g^{**}\beta\text{-}Int(B)=$

$f^{-1}\left[g^{**}\beta\text{-}Bd(B)\right]\subseteq f^{-1}(B)$, we have, $f^{-1}(B)\in g^{**}\beta\text{-}C(X)$. Therefore, f is $g^{**}\beta\text{-}irresolute.$

$(7)\Rightarrow(8)$: Follows by replacing $f(A)$ instead of B in (7).

$(8)\Rightarrow(7)$: Let $B\subseteq Y$, by (8), we have $f\left[g^{**}\beta\text{-}b\left(f^{-1}(B)\right)\right]\subseteq g^{**}\beta\text{-}b\left[f\left(f^{-1}(B)\right)\right]\subseteq g^{**}\beta\text{-}b(B)$ and therefore $g^{**}\beta\text{-}b\left[f^{-1}(B)\right]\subseteq f^{-1}\left[g^{**}\beta\text{-}b(B)\right]$.

$(1)\Rightarrow(9)$: Let $A\subseteq X$. Then by (4), $f\left[g^{**}\beta\text{-}d(A)\right]\subseteq f\left[g^{**}\beta\text{-}Cl(A)\right]\subseteq g^{**}\beta\text{-}Cl\left[f(A)\right]$.

$(9)\Rightarrow(1)$: Let F be a $g^{**}\beta\text{-}closed$ set in Y, by (7), $f\left[g^{**}\beta\text{-}d\left(f^{-1}(F)\right)\right]\subseteq g^{**}\beta\text{-}Cl\left[f\left(f^{-1}(F)\right)\right]\subseteq g^{**}\beta\text{-}Cl(F)=F$, then $g^{**}\beta\text{-}d\left[f^{-1}(F)\right]\subseteq f^{-1}(F)$. We have $f^{-1}(F)\in g^{**}\beta\text{-}C(X)$. Therefore f is $g^{**}\beta\text{-}irresolute.$

Theorem 4.3. Prove that a function $f:(X,\tau)\rightarrow(Y,\sigma)$ is $g^{**}\beta\text{-}irresolute$ if and only if for each point p in X and each $g^{**}\beta\text{-}open$ set B in Y with $f(p)\in B$, there is a $g^{**}\beta\text{-}open$ set A in X such that $p\in A$, $f(A)\subseteq B$.

Proof. Necessity. Let $p\in X$ and $B\in g^{**}\beta\text{-}O(Y,\sigma)$ such that $f(p)\in B$. Let $A=f^{-1}(B)$. Since f is $g^{**}\beta\text{-}irresolute$, A is $g^{**}\beta\text{-}open$ in X. Also $p\in f^{-1}(B)=A$ as $f(p)\in B$. Thus we have $f(A)=f\left[f^{-1}(B)\right]\subseteq B$.

Sufficiency. Let $B\in g^{**}\beta\text{-}O(Y,\sigma)$, and $A=f^{-1}(B)$. We show that A is $g^{**}\beta\text{-}open$ in X. For this let $x\in A$. It implies that $f(x)\in B$. Then by hypothesis, there exists $A_x\in g^{**}\beta\text{-}O(X,\tau)$ such that $x\in A_x$ and

$f(A_x)\subseteq B$. Then $A_x\subseteq f^{-1}[f(A_x)]\subseteq f^{-1}(B)=A$. Thus $A=\cup\{A_x : x\in A\}$. It follows that A is $g^{**}\beta$-*open* in X. Hence f is $g^{**}\beta$-*irresolute.*

Definition 4.4. Let (X,τ) be a topological space. Let $x\in X$ and $N\subseteq X$. We say that N is a $g^{**}\beta$-*neighborhood* of x if there exists a $g^{**}\beta$-*open* set M of X such that $x\in M\subseteq N$.

Theorem 4.5. Prove that a function $f:(X,\tau)\to(Y,\sigma)$ is $g^{**}\beta$-*irresolute* if and only if for each x in X, the inverse image of every $g^{**}\beta$-*neighborhood* of $f(x)$, is a $g^{**}\beta$-*neighborhood* of x.

Proof. Necessity. Let $x\in X$ and let B be a $g^{**}\beta$-*neighborhood* of $f(x)$. Then there exists $U\in g^{**}\beta\text{-}O(Y,\sigma)$ such that $f(x)\in U\subseteq B$. This implies that $x\in f^{-1}(U)\subseteq f^{-1}(B)$. Since f is $g^{**}\beta$-*irresolute,* so $f^{-1}(U)\in g^{**}\beta\text{-}O(X,\tau)$. Hence $f^{-1}(B)$ is a $g^{**}\beta$-*neighborhood* of x.

Sufficiency. Let $B\in g^{**}\beta\text{-}O(Y,\sigma)$. Put $A=f^{-1}(B)$. Let $x\in A$. Then $f(x)\in B$. But then, B being $g^{**}\beta$-*open* set, is a $g^{**}\beta$-*neighborhood* of $f(x)$. So by hypothesis, $A=f^{-1}(B)$ is a $g^{**}\beta$-*neighborhood* of x. Hence by definition, there exists $A_x\in g^{**}\beta\text{-}O(X,\tau)$ such that $x\in A_x\subseteq A$. Thus $A=\cup\{A_x : x\in A\}$. It follows that A is a $g^{**}\beta$-*open* set in X. Therefore f is $g^{**}\beta$-*irresolute.*

Theorem 4.6. Prove that a function $f:(X,\tau)\to(Y,\sigma)$ is $g^{**}\beta$-*irresolute* if and only if for each x in X and each $g^{**}\beta$-*neighborhood* U of $f(x)$, there is a $g^{**}\beta$-*neighborhood* V of x such that $f(V)\subseteq U$.

Proof. Necessity. Let $x\in X$ and let U be a $g^{**}\beta$-*neighborhood* of $f(x)$. Then there exists $O_{f(x)}\in g^{**}\beta\text{-}O(Y,\sigma)$ such that $f(x)\in O_{f(x)}\subseteq U$. It follows that $x\in f^{-1}[O_{f(x)}]\subseteq f^{-1}(U)$. By hypothesis, $f^{-1}[O_{f(x)}]\in g^{**}\beta\text{-}O(X,\tau)$. Let $V=f^{-1}(U)$. Then it follows that V is a $g^{**}\beta$-*neighborhood* of x and $f(V)=f[f^{-1}(U)]\subseteq U$.

Sufficiency. Let $B\in g^{**}\beta\text{-}O(Y,\sigma)$. Put $O=f^{-1}(B)$. Let $x\in O$. Then $f(x)\in B$. Thus B is a $g^{**}\beta$-*neighborhood* of $f(x)$. So by hypothesis, there exists a $g^{**}\beta$-*neighborhood* V_x of x such that $f(V_x)\subseteq B$. Thus it follows that $x\in V_x\subseteq f^{-1}[f(V_x)]\subseteq f^{-1}(B)=O$. Since V_x is a $g^{**}\beta$-*neighborhood* of x, so there exists an $O_x\in g^{**}\beta\text{-}O(X,\tau)$ such that $x\in O_x\subseteq V_x$. Hence $x\in O_x\subseteq O$, $O_x\in g^{**}\beta\text{-}O(X,\tau)$. Thus $O=\cup\{O_x : x\in O\}$. It follows that O is $g^{**}\beta$-*open* in X. Therefore, f is $g^{**}\beta$-*irresolute.*

Theorem 4.7. Prove that a function $f:(X,\tau)\to(Y,\sigma)$ is $g^{**}\beta$-*irresolute* if and only if $f[g^{**}\beta\text{-}D(A)]\subseteq f(A)\cup[g^{**}\beta\text{-}D(f(A))]$, for all $A\subseteq X$.

Proof. Necessity. Let $f:(X,\tau)\to(Y,\sigma)$ be $g^{**}\beta$-*irresolute.* Let $A\subseteq X$, and $a_0\in g^{**}\beta\text{-}D(A)$. Assume that $f(a_0)\notin f(A)$ and let V denote a $g^{**}\beta$-*neighborhood* of $f(a_0)$. Since f is $g^{**}\beta$-*irresolute,* so by Theorem 4.6, there exists a $g^{**}\beta$-*neighborhood* U of a_0 such that $f(U)\subseteq V$. From $a_0\in g^{**}\beta\text{-}D(A)$, it follows that $U\cap A\neq\phi$; there exists, therefore, at least one element

$a \in U \cap A$ such that $f(a) \in f(A)$ and $f(a) \in f(V)$. Since $f(a_0) \notin f(A)$, we have $f(a) \neq f(a_0)$. Thus every $g**\beta$-*neighborhood* of $f(a_0)$ contains an element of $f(A)$ different from $f(a_0)$, consequently, $f(a_0) \in g**\beta\text{-}D[f(A)]$. This proves necessity of the condition.

Sufficiency. Assume that f is not $g**\beta$-*irresolute.* Then by Theorem 4.6, there exists $a_0 \in X$ and a $g**\beta$-*neighborhood* V of $f(a_0)$ such that every $g**\beta$-*neighborhood* U of a_0 contains at least one element $a \in U$ for which $f(a) \notin V$. Put $A = \{a \in X : f(a) \notin V\}$. Then $a_0 \notin A$ since $f(a_0) \in V$, and therefore $f(a_0) \notin A;$ also $f(a_0) \notin g**\beta\text{-}D[f(A)]$ since $V \cap (V - \{f(a_0)\}) = \phi$. Therefore, $f(a_0) \in f[g**\beta\text{-}D(A)] - [f(A) \cup (g**\beta\text{-}D(f(A)))] \neq \phi$, which is a contradiction to the given condition. The condition of the Theorem is therefore sufficient, and the theorem is proved.

Theorem 4.8. Let $f : (X, \tau) \to (Y, \sigma)$ be a one-to-one function. Then f is $g**\beta$-*irresolute* if and only if $f[g**\beta\text{-}D(A)] \subseteq g**\beta\text{-}D[f(A)]$, for all $A \subseteq X$.

Proof. Necessity. Let f be $g**\beta$-*irresolute.* Let $A \subseteq X$, $a_0 \in g**\beta\text{-}D(A)$ and V be a $g**\beta$-*neighborhood* of $f(a_0)$. Since f is $g**\beta$-*irresolute,* so by Theorem 4.6, there exists a $g**\beta$-*neighborhood* U of a_0 such that $f(U) \subseteq V$. But $a_0 \in g**\beta\text{-}D(A);$ hence there exists an element $a \in U \cap A$ such that $a \neq a_0;$ then $f(a) \in f(A)$ and since f is one to one, $f(a) \neq f(a_0)$. Thus every $g**\beta$-*neighborhood* V of $f(a_0)$ contains an element of $f(A)$ different from $f(a_0);$ consequently $f(a_0) \in g**\beta\text{-}D[f(A)]$. We have therefore $f[g**\beta\text{-}D(A)] \subseteq g**\beta\text{-}D[f(A)]$.

Sufficiency. Follows from Theorem 4.7.

5. $g**\beta$-OPEN FUNCTIONS

The purpose of this section is to investigate some characterizations of $g**\beta$-*open* mappings.

Definition 5.1. Let (X, τ) and (Y, σ) be topological spaces. A function $f : (X, \tau) \to (Y, \sigma)$ is called $g**\beta$-*open* if for every open set G in X, $f(G)$ is a $g**\beta$-*open* set in Y.

Theorem 5.2. Prove that a mapping $f : (X, \tau) \to (Y, \sigma)$ is $g**\beta$-*open* if and only if for each $x \in X$, and $U \in \tau$ such that $x \in U$, there exists a $g**\beta$-*open* set $W \subseteq Y$ containing $f(x)$ such that $W \subseteq f(U)$.

Proof. Follows immediately from Definition 5.1.

Theorem 5.3. Let $f : (X, \tau) \to (Y, \sigma)$ be $g**\beta$-*open.* If $W \subseteq Y$ and $F \subseteq X$ is a closed set containing $f^{-1}(W)$, then there exists a $g**\beta$-*closed* $H \subseteq Y$ containing W such that $f^{-1}(H) \subseteq F$.

Proof. Let $H = Y - f(Y - F)$. Since $f^{-1}(W) \subseteq F$, we have $f^{-1}(Y - F) \subseteq (Y - W)$. Since f is $g**\beta$-*open,* then H is $g**\beta$-*closed* and $f^{-1}(H) = X - f^{-1}[f(X - F)] \subseteq X - (X - F) = F$.

Theorem 5.4. Let $f:(X,\tau)\rightarrow(Y,\sigma)$ be a $g**\beta$-*open* function and let $B\subseteq Y$. Then $f^{-1}\left[g**\beta\text{-}Cl\left(g**\beta\text{-}Int\left(g**\beta\text{-}Cl(B)\right)\right)\right]\subseteq Cl\left[f^{-1}(B)\right]$.

Proof. $Cl\left[f^{-1}(B)\right]$ is closed in X containing $f^{-1}(B)$. By Theorem 5.3, there exists a $g**\beta$-*closed* set $B\subseteq H\subseteq Y$ such that $f^{-1}(H)\subseteq Cl\left[f^{-1}(B)\right]$. Thus, $f^{-1}\left[g**\beta\text{-}Cl\left(g**\beta\text{-}Int\left(g**\beta\text{-}Cl(B)\right)\right)\right]\subseteq f^{-1}\left[g**\beta\text{-}Cl\left(g**\beta\text{-}Int\left(g**\beta\text{-}Cl(H)\right)\right)\right]\subseteq f^{-1}[H]\subseteq Cl\left[f^{-1}(B)\right]$.

Theorem 5.5. Prove that a function $f:(X,\tau)\rightarrow(Y,\sigma)$ is $g**\beta$-*open* if and only if $f\left[Int(A)\right]\subseteq g**\beta\text{-}Int\left[f(A)\right]$, *for all* $A\subseteq X$.

Proof. Necessity. Let $A\subseteq X$ and $x\in Int(A)$. Then there exists $U_x\in\tau$ such that $x\in U_x\subseteq A$. So $f(x)\in f(U_x)\subseteq f(A)$. and by hypothesis, $f(U_x)\in g**\beta\text{-}O(Y,\sigma)$. Hence $f(x)\in g**\beta\text{-}Int\left[f(A)\right]$. Thus $f\left[Int(A)\right]\subseteq g**\beta\text{-}Int\left[f(A)\right]$.

Sufficiency. Let $U\in\tau$. Then by hypothesis, $f\left[Int(U)\right]\subseteq g**\beta\text{-}Int\left[f(U)\right]$. Since $Int(U)=U$ as U is open. Also, $g**\beta\text{-}Int\left[f(U)\right]\subseteq f(U)$. Hence $f(U)=g**\beta\text{-}Int\left[f(U)\right]$. Thus $f(U)$ is $g**\beta$-*open* open in Y. So f is $g**\beta$-*open.*

Remark 5.6. The equality may not hold in the preceding Theorem.

Theorem 5.7. Prove that a function $f:(X,\tau)\rightarrow(Y,\sigma)$ is $g**\beta$-*open* if and only if $Int\left[f^{-1}(B)\right]\subseteq f^{-1}\left[g**\beta\text{-}Int(B)\right]$, for all $B\subseteq Y$.

Proof. Necessity. Let $B\subseteq Y$. Since $Int\left[f^{-1}(B)\right]$ is open in X and f is $g**\beta$-*open,* $f\left[Int\left(f^{-1}(B)\right)\right]$ is $g**\beta$-*open* in Y. Also we have $f\left[Int\left(f^{-1}(B)\right)\right]\subseteq f\left[f^{-1}(B)\right]\subseteq B$. Hence, $f\left[Int\left(f^{-1}(B)\right)\right]\subseteq g**\beta\text{-}Int(B)$. Therefore $Int\left(f^{-1}(B)\right)\subseteq f^{-1}\left[g**\beta\text{-}Int(B)\right]$.

Sufficiency. Let $A\subseteq X$. Then $f(A)\subseteq Y$. Hence by hypothesis, we obtain $Int(A)\subseteq Int\left[f^{-1}\left(f(A)\right)\right]\subseteq f^{-1}\left[g**\beta\text{-}Int\left(f(A)\right)\right]$. Thus $f\left[int(A)\right]\subseteq g**\beta\text{-}Int\left[f(A)\right]$, for all $A\subseteq X$. Hence, by Theorem 5.5, f is $g**\beta$-*open.*

Theorem 5.8. Let $f:(X,\tau)\rightarrow(Y,\sigma)$ be a mapping. Then a necessary and sufficient condition for f to be $g**\beta$-*open* is that $f^{-1}\left[g**\beta\text{-}Cl(B)\right]\subseteq Cl\left[f^{-1}(B)\right]$ for every subset B of Y.

Proof. Necessity. Assume f is $g**\beta$-*open.* Let $B\subseteq Y$. Let $x\in f^{-1}\left[g**\beta\text{-}Cl(B)\right]$. Then $f(x)\in g**\beta\text{-}Cl(B)$. Let $U\in\tau$ such that $x\in U$. Since f is $g**\beta$-*open,* then $f(U)$ is a $g**\beta$-*open* set in Y. Therefore, $B\cap f(U)\neq\phi$. Then $U\cap f^{-1}(B)\neq\phi$. Hence $x\in Cl\left[f^{-1}(B)\right]$. We conclude that $f^{-1}\left[g**\beta\text{-}Cl(B)\right]\subseteq Cl\left[f^{-1}(B)\right]$.

Sufficiency. Let $B \subseteq Y$. Then $(Y-B) \subseteq Y$. By hypothesis, $f^{-1}\left[g^{**}\beta\text{-}Cl(Y-B)\right] \subseteq Cl\left[f^{-1}(Y-B)\right]$. This implies that $X - Cl\left[f^{-1}(Y-B)\right] \subseteq X - f^{-1}\left[g^{**}\beta\text{-}Cl(Y-B)\right]$. Therefore $X - Cl\left[X - f^{-1}(B)\right] \subseteq f^{-1}\left[Y-(g^{**}\beta\text{-}Cl(Y-B))\right]$. This implies that $Int\left[f^{-1}(B)\right] \subseteq f^{-1}\left[gg^{**}\beta\text{-}Int(B)\right]$. Now form Theorem 5.7, it follows that f is $g^{**}\beta$-*open.*

6. $g^{**}\beta$-CLOSED FUNCTIONS

In this section, we introduce $g^{**}\beta$-*closed* functions and study certain properties and characterizations of these types of functions.

Definition 6.1. A mapping $f:(X,\tau) \to (Y,\sigma)$ is called $g^{**}\beta$-*closed* if the image of each closed set in X is a $g^{**}\beta$-*closed* set in Y.

Theorem 6.2. Prove that a mapping $f:(X,\tau) \to (Y,\sigma)$ is $g^{**}\beta$-*closed* if and only if $g^{**}\beta\text{-}Cl\left[f(A)\right] \subseteq f\left[Cl(A)\right]$ for each $A \subseteq X$.

Proof. Necessity. Let f be $g^{**}\beta$-*closed* and let $A \subseteq X$. Then $f(A) \subseteq f\left[Cl(A)\right]$ and $f\left[Cl(A)\right]$ is a $g^{**}\beta$-*closed* set in Y. Thus $g^{**}\beta\text{-}Cl\left[f(A)\right] \subseteq f\left[Cl(A)\right]$.

Sufficiency. Suppose that $g^{**}\beta\text{-}Cl\left[f(A)\right] \subseteq f\left[Cl(A)\right]$, for each $A \subseteq X$. Let $A \subseteq X$ be a closed set. Then $g^{**}\beta\text{-}Cl\left[f(A)\right] \subseteq f\left[Cl(A)\right] = f(A)$. This shows that $f(A)$ is a $g^{**}\beta$-*closed* set. Hence f is $g^{**}\beta$-*closed*.

Theorem 6.3. Let $f:(X,\tau) \to (Y,\sigma)$ be $g^{**}\beta$-*closed*. If $V \subseteq Y$ and $E \subseteq X$ is an open set containing $f^{-1}(V)$, then there exists a $g^{**}\beta$-*open* set $G \subseteq Y$ containing V such that $f^{-1}(G) \subseteq E$.

Proof. Let $G = Y - f(X-E)$. Since $f^{-1}(V) \subseteq E$, we have $f(X-E) \subseteq Y-V$. Since f is $g^{**}\beta$-*closed*, then G is a $g^{**}\beta$-*open* set and also $f^{-1}(G) = X - f^{-1}\left[f(X-E)\right] \subseteq X-(X-E) = E$.

Theorem 6.4. Suppose that $f:(X,\tau) \to (Y,\sigma)$ is a $g^{**}\beta$-*closed* mapping. Then $g^{**}\beta\text{-}Int\left[g^{**}\beta\text{-}Cl(f(A))\right] \subseteq f\left[Cl(A)\right]$ for every subset A of X.

Proof. Suppose f is a $g^{**}\beta$-*closed* mapping and A is an arbitrary subset of X. Then $f\left[Cl(A)\right]$ is $g^{**}\beta$-*closed* in Y. Then $g^{**}\beta\text{-}Int\left[g^{**}\beta\text{-}Cl(f(Cl(A)))\right] \subseteq f\left[Cl(A)\right]$. But also $g^{**}\beta\text{-}Int\left[g^{**}\beta\text{-}Cl(f(A))\right] \subseteq g^{**}\beta\text{-}Int\left[g^{**}\beta\text{-}Cl(f(Cl(A)))\right]$. Hence $g^{**}\beta\text{-}Int\left[g^{**}\beta\text{-}Cl(f(A))\right] \subseteq f\left[Cl(A)\right]$.

Theorem 6.5. Let $f:(X,\tau) \to (Y,\sigma)$ be a $g^{**}\beta$-*closed* function, and $B, C \subseteq Y$.

Proof. (1) If U is an open neighborhood of $f^{-1}(B)$, then there exists a $g^{**}\beta$-*open* neighborhood V of B such that $f^{-1}(B) \subseteq f^{-1}(V) \subseteq U$.

(2) If f is also onto, then if $f^{-1}(B)$ and $f^{-1}(C)$ have disjoint open neighborhoods, so have B and C.

Proof. (1) Let $V = Y - f(X - U)$. Then $V^c = Y - V = f(U^c)$. Since f is $g^{**}\beta$-*closed*, so V is a $g^{**}\beta$-*open* set. Since $f^{-1}(B) \subseteq U$, we have $V^c = f(U^c) \subseteq f\left[f^{-1}(B^c)\right] \subseteq B^c$. Hence, $B \subseteq V$, and thus V is a $g^{**}\beta$-*open* neighborhood of B. Further $U^c \subseteq f^{-1}\left[f(U^c)\right] = f^{-1}(V^c) = \left[f^{-1}(V)\right]^c$. This proves that $f^{-1}(V) \subseteq U$.

(2) If $f^{-1}(B)$ and $f^{-1}(C)$ have disjoint open neighborhoods M and N, then by (1), we have $g^{**}\beta$-*open* neighborhoods U and V of B and C respectively such that $f^{-1}(B) \subseteq f^{-1}(U) \subseteq g^{**}\beta\text{-}Int(M)$ and $f^{-1}(C) \subseteq f^{-1}(V) \subseteq g^{**}\beta\text{-}Int(N)$. Since M and N are disjoint, so are $g^{**}\beta\text{-}Int(M)$ and $g^{**}\beta\text{-}Int(N)$, hence so $f^{-1}(U)$ and $f^{-1}(V)$ are disjoint as well. It follows that U and V are disjoint too as f is onto.

Theorem 6.6. Prove that a surjective mapping $f:(X,\tau) \to (Y,\sigma)$ is $g^{**}\beta$-*closed*, if and only if for each subset B of Y and each open set U in X containing $f^{-1}(B)$, there exists a $g^{**}\beta$-*open* set V in Y containing B such that $f^{-1}(V) \subseteq U$.

Proof. Necessity. This follows from (1) of Theorem 6.5.

Sufficiency. Suppose F is an arbitrary closed set in X. Let y be an arbitrary point in $Y - f(F)$. Then $f^{-1}(y) \subseteq X - f^{-1}\left[f(F)\right] \subseteq (X - F)$ and $(X - F)$ is open in X. Hence by hypothesis, there exists a $g^{**}\beta$-*open* set V_y containing y such that $f^{-1}(V_y) \subseteq (X - F)$. This implies that $y \in V_y \subseteq \left[Y - f(F)\right]$. Thus $Y - f(F) = \mathrm{U}\{V_y : y \in Y - f(F)\}$. Hence $Y - f(F)$, being a union of $g^{**}\beta$-*open* sets, is $g^{**}\beta$-*open.* Thus its complement $f(F)$ is $g^{**}\beta$-*closed*. This shows that f is $g^{**}\beta$-*closed.*

Theorem 6.7. Let $f:(X,\tau) \to (Y,\sigma)$ be a bijection. Then the following are equivalent:

(a) f is $g^{**}\beta$-*closed.*
(b) f is $g^{**}\beta$-*open.*
(c) f^{-1} is $g^{**}\beta$-*continuous.*

Proof. $(\mathrm{a}) \Rightarrow (\mathrm{b})$: Let $U \in \tau$. Then $X - U$ is closed in X. By (a), $f(X - U)$ is $g^{**}\beta$-*closed* in Y. But $f(X - U) = f(X) - f(U) = Y - f(U)$. Thus $f(U)$ is $gg^{**}\beta$-*open* in Y. This shows that f is $g^{**}\beta$-*open.*

$(\mathrm{b}) \Rightarrow (\mathrm{c})$: Let $U \subseteq X$. be an open set. Since f is $g^{**}\beta$-*open.* So $f(U) = \left(f^{-1}\right)^{-1}(U)$ is $g^{**}\beta$-*open* in Y. Hence f^{-1} is $g^{**}\beta$-*continuous.*

$(\mathrm{c}) \Rightarrow (\mathrm{a})$: Let A be an arbitrary closed set in X. Then $X - A$ is open in X. Since f^{-1} is $g^{**}\beta$-*continuous*, $\left(f^{-1}\right)^{-1}(X - A)$ $g^{**}\beta$-*open* in Y. But $\left(f^{-1}\right)^{-1}(X - A) = f(X - A) = Y - f(A)$. Thus $f(A)$ is $g^{**}\beta$-*closed* in Y. This shows that f is $g^{**}\beta$-*closed*.

Remark 6.8. A bijection $f:(X,\tau) \to (Y,\sigma)$ may be open and closed but neither $g^{**}\beta$-*open* nor $g^{**}\beta$-*closed*.

7. PRE - $g^{**}\beta$ - OPEN FUNCTIONS

The purpose of this section is to introduce and discuss certain properties and characterizations of *pre* - $g^{**}\beta$ - *open* functions.

Definition 7.1. Let (X, τ) and (Y, σ) be topological spaces. Then a function $f : (X, \tau) \to (Y, \sigma)$ is said to be *pre* - $g^{**}\beta$ - *open* if and only if for each $A \in g^{**}\beta\text{-}O(X,\tau)$, $f(A) \in g^{**}\beta\text{-}O(Y,\sigma)$.

Theorem 7.2. Let $f : (X, \tau) \to (Y, \sigma)$ and $g : (Y, \sigma) \to (Z, \mu)$ be any two *pre* - $g^{**}\beta$ - *open* functions. Then the composition function $gof : (X, \tau) \to (Z, \mu)$ is a *pre* - $g^{**}\beta$ - *open* function.

Proof. Let $U \in g^{**}\beta\text{-}O(X,\tau)$. Then $f(U) \in g^{**}\beta\text{-}O(Y,\sigma)$. Since f is *pre* - $g^{**}\beta$ - *open.* But then $g(f(U)) \in g^{**}\beta\text{-}O(Z,\mu)$ as g is *pre* - $g^{**}\beta$ - *open.* Hence, gof is *pre* - $g^{**}\beta$ - *open.*

Theorem 7.3. Prove that a mapping $f : (X, \tau) \to (Y, \sigma)$ is *pre* - $g^{**}\beta$ - *open* if and only if for each $x \in X$ and any $U \in g^{**}\beta\text{-}O(X,\tau)$ such that $x \in U$, there exists $V \in g^{**}\beta\text{-}O(Y,\sigma)$ such that $f(x) \in V$ and $V \subseteq f(U)$.

Proof. Routine.

Theorem 7.4. Prove that a mapping $f : (X, \tau) \to (Y, \sigma)$ is *pre* - $g^{**}\beta$ - *open* if and only if for each $x \in X$ and for any $g^{**}\beta$ - *neighborhood* U of x in X, there exists a $g^{**}\beta$ - *neighborhood* V of $f(x)$ in Y such that $V \subseteq f(U)$.

Proof. Necessity. Let $x \in X$ and let U be a $g^{**}\beta$ - *neighborhood* of x. Then there exists $W \in g^{**}\beta\text{-}O(X,\tau)$ such that $x \in W \subseteq U$. Then $f(x) \in f(W) \subseteq f(U)$. But $f(W) \in g^{**}\beta\text{-}O(Y,\sigma)$ as f is *pre* - $g^{**}\beta$ - *open.* Hence $V = f(W)$ is a $g^{**}\beta$ - *neighborhood* of $f(x)$ and $V \subseteq f(U)$.

Sufficiency. Let $U \in g^{**}\beta\text{-}O(X,\tau)$ and let $x \in U$. Then U is a $g^{**}\beta$ - *neighborhood* of x. So by hypothesis, there exists a $g^{**}\beta$ - *neighborhood* $V_{f(x)}$ of $f(x)$ such that $f(x) \in V_{f(x)} \subseteq f(U)$. It follows at once that $f(U)$ is a $g^{**}\beta$ - *neighborhood* of each of its points. Therefore $f(U)$ is $g^{**}\beta$ - *open.* Hence f is *pre* - $g^{**}\beta$ - *open.*

Theorem 7.5. Prove that a function $f : (X, \tau) \to (Y, \sigma)$ is *pre* - $g^{**}\beta$ - *open* if and only if $f\left[g^{**}\beta\text{-}Int(A)\right] \subseteq g^{**}\beta\text{-}Int\left[f(A)\right]$, for all $A \subseteq X$.

Proof. Necessity. Let $A \subseteq X$ and $x \in g^{**}\beta\text{-}Int(A)$. Then there exists $U_x \in g^{**}\beta\text{-}O(X,\tau)$ such that $x \in U_x \subseteq A$. So $f(x) \in f(U_x) \subseteq f(A)$ and by hypothesis, $f(U_x) \in g^{**}\beta\text{-}O(Y,\sigma)$. Hence $f(x) \in g^{**}\beta\text{-}Int\left[f(A)\right]$. Thus $f\left[g^{**}\beta\text{-}Int(A)\right] \subseteq g^{**}\beta\text{-}Int\left[f(A)\right]$.

Sufficiency. Let $U \in g^{**}\beta\text{-}O(X,\tau)$. Then by hypothesis, $f\left[g^{**}\beta\text{-}Int(U)\right] \subseteq g^{**}\beta\text{-}Int\left[f(U)\right]$. Since $g^{**}\beta\text{-}Int(U) = U$ as U is $g^{**}\beta$ - *open.*

Also $g^{**}\beta\text{-}Int\left[f(U)\right]\subseteq f(U)$. Hence $f(U)=g^{**}\beta\text{-}Int\left[f(U)\right]$. Thus $f(U)$ is $g^{**}\beta\text{-}open$ in Y. So f is $pre\text{-}g^{**}\beta\text{-}open$.
We remark that the equality does not hold in Theorem 7.5 as the following example shows.

Example 7.6. Let $X=Y=\{1,2\}$. suppose X is anti-discrete and Y is discrete. Let $f=Id.$, $A=\{1\}$. Then $\phi=f\left[g^{**}\beta\text{-}Int(A)\right]\neq g^{**}\beta\text{-}Int\left[f(A)\right]=\{1\}$.

Theorem 7.7. Prove that a function $f:(X,\tau)\to(Y,\sigma)$ is $pre\text{-}g^{**}\beta\text{-}open$ if and only if $g^{**}\beta\text{-}Int\left[f^{-1}(B)\right]\subseteq f^{-1}\left[g^{**}\beta\text{-}Int(B)\right]$, for all $B\subseteq Y$.

Proof. Necessity. Let $B\subseteq Y$. Since $g^{**}\beta\text{-}Int\left[f^{-1}(B)\right]$ is $g^{**}\beta\text{-}open$ in X and f is $pre\text{-}g^{**}\beta\text{-}open$, $f\left[g^{**}\beta\text{-}Int\left(f^{-1}(B)\right)\right]$ $g^{**}\beta\text{-}open$ in Y. Also we have $f\left[g^{**}\beta\text{-}Int\left(f^{-1}(B)\right)\right]\subseteq f\left[f^{-1}(B)\right]\subseteq B$. Hence, $f\left[g^{**}\beta\text{-}Int\left(f^{-1}(B)\right)\right]\subseteq g^{**}\beta\text{-}Int(B)$. Therefore $g^{**}\beta\text{-}Int\left[f^{-1}(B)\right]\subseteq f^{-1}\left[g^{**}\beta\text{-}Int(B)\right]$.

Sufficiency. Let $A\subseteq X$. Then $f(A)\subseteq Y$. Hence by hypothesis, we obtain $g^{**}\beta\text{-}Int(A)\subseteq g^{**}\beta\text{-}Int\left[f^{-1}\left(f(A)\right)\right]\subseteq f^{-1}\left[g^{**}\beta\text{-}Int\left(f(A)\right)\right]$. This implies that $f\left[g^{**}\beta\text{-}Int(A)\right]\subseteq f\left[f^{-1}\left(g^{**}\beta\text{-}Int\left(f(A)\right)\right)\right]\subseteq g^{**}\beta\text{-}Int\left[f(A)\right]$. Thus $f\left[g^{**}\beta\text{-}Int(A)\right]\subseteq g^{**}\beta\text{-}Int\left[f(A)\right]$, for all $A\subseteq X$. Hence, by Theorem 7.5, f is $pre\text{-}g^{**}\beta\text{-}open$.

Theorem 7.8. Prove that a mapping $f:(X,\tau)\to(Y,\sigma)$ is $pre\text{-}g^{**}\beta\text{-}open$ if and only if $f^{-1}\left[g^{**}\beta\text{-}Cl(B)\right]\subseteq g^{**}\beta\text{-}Cl\left[f^{-1}(B)\right]$, for every subset B of Y.

Proof. Necessity. Let $B\subseteq Y$ and let $x\in f^{-1}\left[g^{**}\beta\text{-}Cl(B)\right]$. Then $f(x)\in g^{**}\beta\text{-}Cl(B)$. Let $U\in g^{**}\beta\text{-}O(X,\tau)$ such that $x\in U$. By hypothesis, $f(U)\in g^{**}\beta\text{-}O(Y,\sigma)$ and $f(x)\in f(U)$. Thus $f(U)\cap B\neq\phi$. Hence $U\cap f^{-1}(B)\neq\phi$. Therefore, $x\in g^{**}\beta\text{-}Cl\left[f^{-1}(B)\right]$, So we obtain $f^{-1}\left[g^{**}\beta\text{-}Cl(B)\right]\subseteq g^{**}\beta\text{-}Cl\left[f^{-1}(B)\right]$.

Sufficiency. Let $B\subseteq Y$. Then $(Y-B)\subseteq Y$. By hypothesis, $f^{-1}\left[g^{**}\beta\text{-}Cl(Y-B)\right]\subseteq g^{**}\beta\text{-}Cl\left[f^{-1}(Y-B)\right]$. This implies that $X-\left[g^{**}\beta\text{-}Cl\left(f^{-1}(Y-B)\right)\right]\subseteq X-f^{-1}\left[g^{**}\beta\text{-}Cl(Y-B)\right]$. Hence $X-g^{**}\beta\text{-}Cl\left[X-f^{-1}(B)\right]\subseteq f^{-1}\left[Y-\left(g^{**}\beta\text{-}Cl(Y-B)\right)\right]$. Then this implies that $g^{**}\beta\text{-}Int\left[f^{-1}(B)\right]\subseteq f^{-1}\left[g^{**}\beta\text{-}Int(B)\right]$. Now by Theorem 7.7, it follows that f is $pre\text{-}g^{**}\beta\text{-}open$.

Theorem 7.9. Let $f:(X,\tau)\to(Y,\sigma)$ and $g:(Y,\sigma)\to(Z,\mu)$ be two mappings such that $gof:(X,\tau)\to(Z,\mu)$ is $g^{**}\beta\text{-}irrsolute$. Then
(1) If g is a $pre\text{-}g^{**}\beta\text{-}open$ injection, then f is $g^{**}\beta\text{-}irrsolute$.
(2) If f is a $pre\text{-}g^{**}\beta\text{-}open$ surjection, then g is $g^{**}\beta\text{-}irrsolute$.

Proof. (1) Let $U\in g^{**}\beta\text{-}O(Y,\sigma)$. Then $g(U)\in g^{**}\beta\text{-}O(Z,\mu)$ since g is $pre\text{-}g^{**}\beta\text{-}open$ Also gof is $g^{**}\beta\text{-}irrsolute$. Therefore, we have $(gof)^{-1}\left[g(U)\right]\in g^{**}\beta\text{-}O(X,\tau)$. Since g is an injection, so we have : $(gof)^{-1}\left[g(U)\right]=\left(f^{-1}og^{-1}\right)\left[g(U)\right]=\ f^{-1}\left[g^{-1}\left(g(U)\right)\right]=f^{-1}(U)$. Consequently $f^{-1}(U)$ is $g**\beta$-*open* in X. This proves that f is gsg-*irrsolute.*

(2) Let $V\in g**\beta\text{-}O(Z,\mu)$. Then $(gof)^{-1}(V)\in g**\beta\text{-}O(X,\tau)$ since gof is $g**\beta$-*irrsolute.* Also f is *pre*-$g**\beta$-*open,* $f\left[(gof)^{-1}(V)\right]$ is $g**\beta$-*open* in Y. Since f is surjective, we note that $f\left[(gof)^{-1}(V)\right]=\ \left[fo(gof)^{-1}\right](V)=\left[fo\left(f^{-1}og^{-1}\right)\right](V)=\left[\left(fof^{-1}\right)og^{-1}(V)\right]=g^{-1}(V)$. Hence g is $g**\beta$-*irrsolute.*

8. PRE-g**β-CLOSED FUNCTIONS

In this last section, we introduce and explore several properties and characterizations of *pre*-$g**\beta$-*closed* functions.

Definition 8.1. A function $f:(X,\tau)\to(Y,\sigma)$ is said to be *pre*-$g**\beta$-*closed* if and only if the image set $f(A)$ is $g**\beta$-*closed* for each $g**\beta$-*closed* subset A of X.

Theorem 8.2. The composition of two *pre*-$g**\beta$-*closed* mappings is a *pre*-$g**\beta$-*closed* mapping.

Proof. The straightforward proof is omitted.

Theorem 8.3. Prove that a mapping $f:(X,\tau)\to(Y,\sigma)$ is *pre*-$g**\beta$-*closed* if and only if $g**\beta\text{-}Cl\left[f(A)\right]\subseteq f\left[g**\beta\text{-}Cl(A)\right]$ for every subset A of X.

Proof. Necessity. Suppose f is a *pre*-$g**\beta$-*closed* mapping and A is an arbitrary subset of X. Then $f\left[g**\beta\text{-}Cl(A)\right]$ is $g**\beta$-*closed* in Y. Since $f(A)\subseteq f\left[g**\beta\text{-}Cl(A)\right]$, we obtain $g**\beta\text{-}Cl\left[f(A)\right]\subseteq f\left[g**\beta\text{-}Cl(A)\right]$.

Sufficiency. Suppose F is an arbitrary $g**\beta$-*closed* set in X. By hypothesis, we obtain $f(F)\subseteq g**\beta\text{-}Cl\left[f(F)\right]\subseteq f\left[g**\beta\text{-}Cl(F)\right]=f(F)$. Hence $f(F)=g**\beta\text{-}Cl\left[f(F)\right]$. Thus $f(F)$ is $g**\beta$-*closed* in Y. It follows that f is *pre*-$g**\beta$-*closed*.

Theorem 8.4. Let $f:(X,\tau)\to(Y,\sigma)$ be a *pre*-$g**\beta$-*closed* function, and $B,C\subseteq Y$.

(1) If U is a $g**\beta$-*open* neighborhood of $f^{-1}(B)$, then there exists a $g**\beta$-*open* neighborhood V of B such that $f^{-1}(B)\subseteq f^{-1}(V)\subseteq U$.

(2) If f is also onto, then if $f^{-1}(B)$ and $f^{-1}(C)$ have disjoint $g**\beta$-*open* neighborhoods, so have B and C.

Proof. (1) Let $V=Y-f(X-U)$. Then $V^c=Y-V=f\left(U^c\right)$. Since f is *pre*-$g**\beta$-*closed,* so V is $g**\beta$-*open.* Since $f^{-1}(B)\subseteq U$, we have $V^c=f\left(U^c\right)\subseteq f\left[f^{-1}\left(B^c\right)\right]\subseteq B^c$. Hence, $B\subseteq V$, and thus V is a $g**\beta$-*open* neighborhood of B. Further $U^c\subseteq f^{-1}\left[f\left(U^c\right)\right]=f^{-1}\left(V^c\right)=\left[f^{-1}(V)\right]^c$. This proves that $f^{-1}(V)\subseteq U$.

(2) If $f^{-1}(B)$ and $f^{-1}(C)$ have disjoint gsg-*open* neighborhoods M and N, then by (1), we have gsg-*open* neighborhoods U and V of B and C respectively such that

$f^{-1}(B)\subseteq f^{-1}(U)\subseteq g^{**}\beta\text{-}g^{**}\beta\text{-}(M)$ and $f^{-1}(C)\subseteq f^{-1}(V)\subseteq g^{**}\beta\text{-}Int(N)$. Since M and N are disjoint, so are $gg^{**}\beta\text{-}Int(M)$ and $g^{**}\beta\text{-}Int(N)$, and hence so $f^{-1}(U)$ and $f^{-1}(V)$ are disjoint as well. It follows that U and V are disjoint too as f is onto.

Theorem 8.5. Prove that a surjective mapping $f:(X,\tau)\to(Y,\sigma)$ is $pre\text{-}g^{**}\beta\text{-}closed$ if and only if for each subset B of Y and each $g^{**}\beta\text{-}open$ set U in X containing $f^{-1}(B)$, there exists a $g^{**}\beta\text{-}open$ set V in Y containing B such that $f^{-1}(V)\subseteq U$.

Proof. Necessity. This follows from (1) of Theorem 8.4.

Sufficiency. Suppose F is an arbitrary $g^{**}\beta\text{-}closed$ set in X. Let y be an arbitrary point in $Y-f(F)$. Then $f^{-1}(y)\subseteq X-f^{-1}[f(F)]\subseteq(X-F)$ and $(X-F)$ is $g^{**}\beta\text{-}open$ in X. Hence by hypothesis, there exists a $g^{**}\beta\text{-}open$ set V_y containing y such that $f^{-1}(V_y)\subseteq(X-F)$. This implies that $y\in V_y\subseteq[Y-f(F)]$. Thus $Y-f(F)=\cup\{V_y\,|\,y\in Y-f(F)\}$. Hence $Y-f(F)$, being a union of $g^{**}\beta\text{-}open$ sets is $g^{**}\beta\text{-}open$. Thus its complement $f(F)$ is $g^{**}\beta\text{-}closed$. This shows that f is $g^{**}\beta\text{-}closed$.

Theorem 8.6. Let $f:(X,\tau)\to(Y,\sigma)$ be a bijection. Then the following are equivalent:

(1) f is $pre\text{-}g^{**}\beta\text{-}closed$.

(2) f is $pre\text{-}g^{**}\beta\text{-}open$.

(3) f^{-1} is $g^{**}\beta\text{-}irresolute$.

Proof. $(1)\Rightarrow(2)$: Let $U\in g^{**}\beta\text{-}O(X,\tau)$. Then $X-U$ is $g^{**}\beta\text{-}closed$ in X. By (1), $f(X-U)$ is $g^{**}\beta\text{-}closed$ in Y. But $f(X-U)=f(X)-f(U)=Y-f(U)$. Thus $f(U)$ is $g^{**}\beta\text{-}open$ in Y. This shows that f is $pre\text{-}g^{**}\beta\text{-}open$.

$(2)\Rightarrow(3)$: Let $A\subseteq X$. Since f is $pre\text{-}g^{**}\beta\text{-}open$, so by Theorem 7.8, $f^{-1}[g^{**}\beta\text{-}Cl(f(A))]\subseteq g^{**}\beta\text{-}Cl[f^{-1}(f(A))]$. It implies that $g^{**}\beta\text{-}Cl[f(A)]\subseteq f[g^{**}\beta\text{-}Cl(A)]$. Thus $g^{**}\beta\text{-}Cl\left[(f^{-1})^{-1}(A)\right]\subseteq(f^{-1})^{-1}[g^{**}\beta\text{-}Cl(A)]$, for all $A\subseteq X$. Then by Theorem 4.8, it follows that f^{-1} is $g^{**}\beta\text{-}irresolute$.

$(3)\Rightarrow(1)$: Let A be an arbitrary $g^{**}\beta\text{-}closed$ set in X. Then $X-A$ is $g^{**}\beta\text{-}open$ in X. Since f^{-1} is $g^{**}\beta\text{-}irresolute$, $(f^{-1})^{-1}(X-A)$ is $g^{**}\beta\text{-}open$ in Y. But $(f^{-1})^{-1}(X-A)=f(X-A)=Y-f(A)$. Thus $f(A)$ is $g^{**}\beta\text{-}closed$ in Y. This shows that f is $pre\text{-}g^{**}\beta\text{-}closed$.

Scientific Ethics Declaration

The author declares that the scientific ethical and legal responsibility of this article published in EPSTEM journal belongs to the author.

Acknowledgement

* This article was presented as an oral presentation at the International Conference on Basic Sciences and Technology (www.icbast.net) held in Antalya/Turkey on November 16-19, 2023.

* The author is highly and gratefully indebted to Prince Mohammad Bin Fahd University, Al Khobar, Saudi Arabia, for providing all necessary research facilities during the preparation of this research paper.

References

Arya, S.P., & Deb, M. (1974). On θ-continuous mappings. *Math. Student* 4281-4289.

Caldas, M., Ganster, M., Georgious, D.N., Jafari, S., & Noiri, T. (2008). On $\theta\text{-semipen}$ sets and separation axioms in topological spaces. *Carpathian J. Math., 24*(1), 13 – 22.

Delcia, T., & Thillai, M. S. (2023). g**β-closed sets in topological spaces. *Journal of Engineering Technologies and Innovative Research (JETIR),* 29 – 34.

Ekici, E. (2004),. (δ-pre,s)-continuous functions. *Bulletin of the Malaysian Mathematical Sciences Society, Second Series, 27*(2), 237 – 251.

Ekici, E. (2005). On δ-semiopen sets and a generalization of functions. *Bol. Soc. Mat., 23* (1-2), 73-84.

Ganster, M., Noiri, T., & Reilly, I. L. (1988). Weak and strong forms of θ-irresolute functions. *J. Inst. Math. Comput. Sci., 1*(1), 19-29.

Hassan, J. A., & Labendia, A. M. (2022). $\theta_s\text{-open}$ sets and $\theta_s\text{-continuity}$ of mapps in the product space. *Journal of Mathematics and Computer Science, 25*(2), 182 – 190.

Jafari, S. (1998). Ome properties of θ-continuous functions. *Far East Journal of Mathematical Sciences, 6*(5), 689-696

Kilicman, A., & Salleh, Z. (2006). Some results on (δ-pre,s)-continuous functions. *International Journal Mathematics and Mathematical Sciences,* 20061-200111.

Latif, R. M. (2020), Properties of theta – continuous Functions in Topological Spaces.*International Conference on Mathematics and Computers in Science and Engineering (MACISE), 1,* 81-90. Madrid,Spain.

Levine, N. (1963). Semi-open sets and semi-continuity in topological spaces. *Amer. Math. Monthly, 70,* 36 – 41.

Lellis Thivagar, M. (2011). Nirmala Rebecca Paul and Saeid Jafari, on new class of generalized closed sets, annals of the University of Craiova, *Mathematics and Computer Sciwnce Series, 38* (3), 84 – 93.

Long, P.E& Herrington, L. L.(1982). The τ_θ -topology and faintly continuous functions. Kyungpook Math. J., 227-314.

Mohammad Latif, R. (1993). On characterizations of mappings. *Soochow Journal of Mathematics,19*(4), 475 – 495.

Mohammad Latif, R. (2020). Theta – ω – Mappings in Topological Spaces. *WSEAS Transactions on Mathematics, 19*(8), 186 – 207. Retrieved from (www.scopus.com)

Noiri, T., & Jafari, S. (2002). Properties of (θ,s)-continuous functions, *Topology and its Applications, 123*(1) 167-179.

Noiri, T. (1980). On δ-continuous functions, *Journal of Korean Mathematical Society, 16,* 161-166.

Saleh, M. (2004). On θ-closed sets and some forms of continuity. *Archivum Mathematicum (On BRNO)* 40 383 – 393.

Saleh, M. (2002). On super and δ-continuities, Mathematics and Mathematics Education, World Scientific, 281-291.

Velicko, N. V. (1968). H-closed topological spaces. *Mat. Sb., 70* (112), 98 – 112.

Wilansky, A.(1980).*Topology for analysis.* Newyork, NY:Devore Publications, Inc.

Willard, S.(1970).*General topology*, Reading, Mass.: Addison Wesley Pub. Co.

Author Information

Raja Mohammad Latif
Prince Mohammad Bin Fahd University
Al Khobar, Kingdom of Saudia Arabia
Contact e-mail: *rlatif@gmail.com*

To cite this article:

Latif, R. M. (2023). G**β-continuous and G**β-Irresolute mappings in topological spaces. *The Eurasia Proceedings of Science, Technology, Engineering & Mathematics (EPSTEM), 25,* 168-186.

The Eurasia Proceedings of Science, Technology,
Engineering & Mathematics (EPSTEM)
ISSN: 2602-3199

The Eurasia Proceedings of Science, Technology, Engineering & Mathematics (EPSTEM), 2023

Volume 25, Pages 187-195

ICBAST 2023: International Conference on Basic Sciences and Technology

Thermal Oxidation Kinetics of Nickel and Dilute (Ni-Al) Alloys

Nacer Halem
University Mouloud Mammeri

Zohra Halem
University of Bouira

Petot-Ervas Georgette
Centrale Supelec

Abstract: Oxidation of high purity nickel and of a dilute Ni-Al (0.11 wt%) polycrystalline alloy were performed in the temperature range 700 - 1200°C, under P_{O2}=1 atm. At T<1100°C, Al leads to a reduction of the oxidation kinetic, while at higher temperatures its beneficial effect disappears. The results were analysed from a formal treatment, taking into account the thermodynamic and transport properties of undoped and Al-doped $Ni_{1-x}O$ single crystals. At temperatures below 1000°C, it was found that the results are in agreement with the thermal oxidation of undoped and doped $Ni_{1-x}O$ samples. They are due to the kinetic demixing of cations in the alloy layer growth, leading to both, a lower concentration of aluminium and a decrease of D_{Ni} in the outer oxidation scale. At higher temperatures, the Ni-Al alloy oxidises faster than Ni. This increase was explained by an inward oxygen gas transport within the layer through fissures, whose formation was attributed to compressive stresses due to the growth of nickel oxide units in grain boundaries. The mechanism whereby nickel oxide units form is explained.

Keywords: Oxidation rate, Kinetic demixing, Thermodynamic, Diffusion, Point defects.

Introduction

When metals or alloys are used in high–temperature oxidizing environments, an oxide scale can develop at their surface (Stott,1977; Wood, 1966; Wagner, 1951; Kofstad ,1988, 2007; Atkinson, 1983; Schmalzried, 1981; Catlow,1986). This layer can then act as a protection barrier, to continuing attack by the surrounding atmosphere. The requirement for an effective protection of this barrier imposes a low diffusion of the reactants and the absence of pores and cracks in the oxide scale. However, present understanding of oxidation mechanisms concerned is poor because oxidation results were analysed generally from observatios done at room temperature, influenced by transport processes occurring during cooling (Petot-Ervas, 1990; Halem, 2016). The purpose of this work was to explain oxidation rates from a general treatment of transport processes in p-type semiconducting oxides under non-equilibrium conditions, using the transport properties of mobile species. A Ni-Al alloy was chosen because both, the ionic size of Al^{3+} allows that it should replace substitutionnally Ni^{2+} and its valence state is independent of T and P_{O2}.

Method

Statement of the problem

The thermal oxidation of nickel is considered as a model system for oxidation studies of metals because of its apparent simplicity. Indeed, NiO is the only oxide stable at high temperature and the oxidation rate is controlled by the outward diffusion of Ni^{2+} through the scale, according to a parabolic law. However almost all studies were done from observations at room temperature, as indicated in the introduction. Such analyses leaves much to be desired, since authors don't provide a rationalization for the presence of precipitates, for instance, altough they use them in their analyses.

General Equations in P-Type Semiconducting Oxides at the Thermodynamical Equilibrium

If one considers a cation deficient p-type semiconducting solid solution (AO-BO□), such as $Al_2O_{\square}$ doped $Ni_{1-x}O$, the prevailing defects are electron holes (h°) and □ time ionized cationic vacancies ($V^{\square'}$). The defects are introduced by reaction with the surrounding atmosphere ($\frac{1}{2}O_2 <=> O_O + V^{\square'} + \square h^{\circ}$). Their concentration depends on temperature (T) and oxygen partial pressure (P_{O2}) in equilibrium with the sample (Philibert,1991), (Atkinson , 1981), (Farhi, 1978).

$$[h^{\circ}] = \square[V^{\square'}] = AK_V^{1/(\square+1)} (P_{O2})^{1/2(\square+1)} \tag{1}$$

where K_V is the equilibrium constant of formation of the defects, O_O an oxygen ion on its normal lattice site, $A=\square^{1/(\square+1)}$ and the square brackets (or x_i) indicate molar concentrations. When one substitutes on a Ni^{2+} site a trivalent cation, such as Al^{3+}, this defect has an effective single positive charge ($Al^{\bullet}_{Ni}$). In a dilute solid solution (NiO-AlO□), this impurity then influences the concentration of defects through the electroneutrality condition:

$$[h^{\circ}] + [Al^{\bullet}_{Ni}] = \square[V^{\square'}], \tag{2}$$

with, in the extrinsic range:

$$[Al^{\bullet}_{Ni}] \approx \alpha[V^{\alpha'}], \tag{3}$$

and the nickel diffusion coefficient (D_{Ni}) (Philibert,1991) :

$$x_V D_V = x_{Ni} D_{Ni} \approx D_{Ni}, \tag{4}$$

where D_V is the vacancy diffusion coefficient, x_V the cationic vacancy concentration and x_i the mole fraction of Ni^{2+}, with $x_i=[Ni^{2+}]\approx 1$.

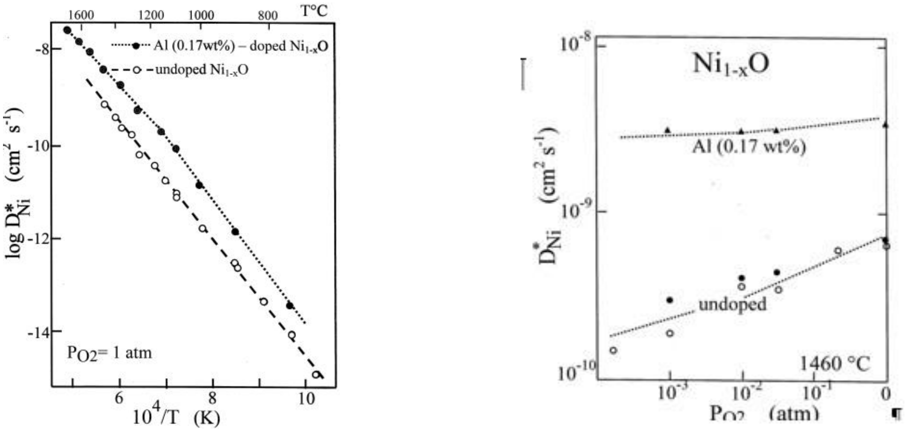

Figure 1. (a) Arrhenius plot of the self-diffusion coefficient of Ni^{2+} in undoped and Al-doped $Ni_{1-x}O$ single crystals and (b) oxygen partial pressure dependence of D^*_{Ni}, at 1460°C.

Atkinson et al. (Atkinson,1981) have measured the self-diffusion of nickel (D^*_{Ni}) in undoped and Al (0.17wt%)-doped Ni_1-xO single crystals between 700° and 1700°C, at an oxygen partial pressure P_{O2}=1atm. Their results reported in Fig.1 show that :

$$(D^*_{Ni})_{doped} > (D^*_{Ni})_{undoped} \tag{5}$$

Since the self-diffusion coefficient can be written (Philibert,1991).

$$D^*_{Ni} = f\, x_V D_V \tag{6}$$

where f is the correlation factor, the results reported in figure 1 are due to an increase of the cationic vacancy concentration (Eq.2).

Furthermore, a break is observed at T≈1200°C. In the lower temperature region (T<1200°C), the data are controlled by Al^{+3} (Eq.3). They are then obtained in the extrinsic range and indicate that the saturation solubility of Al in $Ni_{1}\text{-}_{x}O$ is equal at 0.17 wt %.

Transport Proceses in a P-Type Semiconducting Oxide under Non-Equilibrium Conditions

One can recall that in cation deficient p-type semiconducting oxide solid solutions, the diffusivity of anions is much less than that of cations (Philibert,1991). One may then use the anion sublattice as frame of reference for motion of cations and defects. When an oxide (AO-BO□) is exposed to an oxygen chemical potential gradient (Eq.1), a flux of vacancies (J_V) occurs in the sample toward the side showing a low oxygen activity ($a_O = P_{O2}^{1/2}$), coupled to an opposite flux of cations (J_i) (Petot-Ervas, 1990; Halem, 2016; Philibert, 1972; Farhi, 1978; Atkinson, 1981; Mahiouz, 2019; Schmalzried, 1981, 1986).

$$J_V = -\,(J_A^{2+} + J_B^{\delta+}) \tag{7}$$

New lattice sites are then formed at the surface where cations arrive. The shift velocity of this surface and more generally the shift velocity of the oxidation front in the oxide, is given by(Petot-Ervas, 1990), (Halem, 2016), (Schmalzried, 1981):

$$v_{oxid} = J_V / C_M = -\Sigma J_i / C_M = -\,(J_A^{2+} + J_B^{\delta+})/C_M \tag{8}$$

If one neglects the correlation effects, it was shown (Petot-Ervas, 1990; Halem, 2016) that in a solid solution (AO-BOγ) under non-equilibrium conditions the flux of cations A and B can be written, with respect to the oxygen sublattice:

$$J_i = C_M D_i \left[-\frac{dx_i}{dz} + x_i\, \gamma\, \mathfrak{F}\right] \tag{9}$$

where x_i is the local concentration of cations "i" in the cationic sublattice and ($\mathfrak{F} = d\ln a_O/dz$) the driving force of diffusion, with according to Eq.1:

$$\mathfrak{F} = d\ln a_O/dz = (1+\alpha)\, d\ln[V^{\alpha'}]/dz \tag{10}$$

Therefore, substituting Eq.10 in Eq.8, allows to show that the shift velocity of the oxidation front in an oxide AO-BOγ exposed to an oxygen chemical potential gradient can be written Petot-Ervas, 1990), (Halem, 2016; (Mahiouz, 2019):

$$v_{oxid} = J_V/C_M = -(D_A - D_B)\, dm/dz \; - D_A\, \mathfrak{F}_{dop}, \tag{11}$$

while the shift velocity of the oxidation front in AO is expressed by the following relation:

$$v_{oxid} = -\,J_A^{2+}/C_M = -\,D_A\, \mathfrak{F}_{AO} \tag{12}$$

where $m = x_B$ is the mole fraction of solute cations (B^{3+}) in the cationic sublattice, F_{dop} the driving force of diffusion in doped AO and F_{NiO} in undoped AO. Consequently, Eq.11 shows that the effect of solute cations on the oxido-reduction of a p-type semiconducting oxide depends not only on the diffusion coefficient of the cations, as it was generally assumed until now (Kofstad , 1988), but also on the kinetic demixing of cations (dm/dz).

Results and Discussion

Experimental results in undoped and Al-doped $Ni_{1-x}O$ single crystals in non-equilibrium conditions

Cation Kinetic Demixing

This study was performed with undoped and Al (0.11 wt%)-doped $Ni_{1-x}O$ single crystals, machined to obtain parallelepipedic samples ($3x2x2mm^3$). Since the diffusing species are electrically charged, their fluxes may then be due to a gradient of oxygen activity (a_O), with $a_O=P_{O2}^{1/2}$ (Eq.10), or to an applied electric field (E) (Halem, 2016), (Mahiouz, 2019), (Monceau,1994):

$$F = q_iE/RT \tag{13}$$

where q_i is the charge of the diffusing species. From a practical point of view, it is easier to perform experiments in presence of an electrical field (experimental arrangement represented in the next section). A flux of cations occurs towards the cathode, where the cristal is reconstructed (Fig.2b), while an opposite flux of vacancies occurs in direction of the anode (Eq.7), which acts as a sink for these defects. Therefore, this leads to a shift of the sample end surfaces in direction of the cathode (Eqs.11,12).

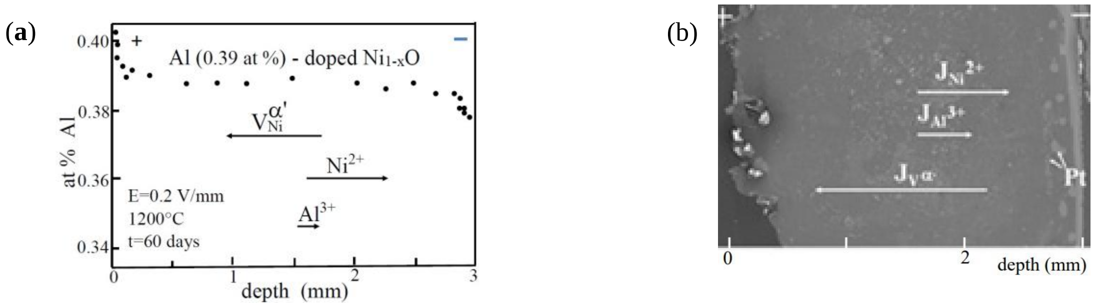

Figure 2. (a) Kinetic demixing profile of Al^{+3} in Al (0.11wt%) - doped $Ni_{1-x}O$ single crystals, maintained under 0.2V/mm, for 60 days, in air at 1200°C, and (b) cross section at the end of the experiment.

The results reported in figure 2 have been obtained with a parallelepipedic single crystal, of 3mm long. EPMA analyses on a polished cross-section at the end of experiments show an enrichment of Al^{+3} near the anode.

Therefore, it follows from Eq.9:

$$D_{Al}<D_{Ni} \tag{14}$$

Experimental Results in the Stability Range of $Ni_{1-x}O$ - Chemical Diffusion Coefficient

Experiments

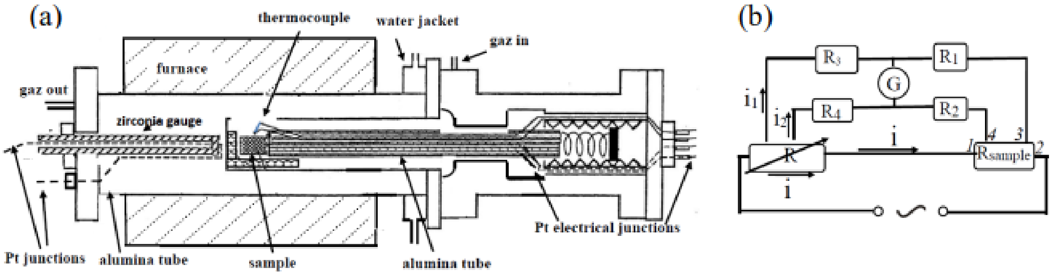

Figure 3. (a) Experimental arrangement for measuring electrical conductivity and (b) schematic representation of the Kelvin bridge.

The experimental arrangement is shown in figure 3. The measurements were performed from electrical conductivity measurements, by the four probe method at 1.5kHz frequency, using a Kelvin bridge (Fig.3b) whose equilibrium was checked by a fast detection amplifier (G). A thin layer of platinum was applied to the lower surfaces of the parallelepipedic sample (3x2x2 mm^3) connected to the voltage source (Fig.3b). The oxygen partial pressure was measured near the sample with an yttria stabized zirconia gauge (Fig.3b). Platinum wires (Pt) were used as electrical junctions (Halem, 2016).

Experimental Results

The results have been obtained with a single crystal, initially in equilibrium with the surrounding atmosphere (argon / $P_{O2}=10^{-3}$atm), by following the electrical conductivity as a function of time after a sudden change of P_{O2} (P_{O2}=0.21atm). Just after this change, the defect concentrations correspond to the new imposed condition at the solid-gas interface (Eq.1). A concentration gradient of cationic vacancies (dc_v/dz) sets up immediately near the surfaces (Eq.1), leading to a flux of these defects coupled to an opposite flux of cations (Eq.7) These fluxes progress in the bulk, pass through a maximum and decrease, until the new thermodynamical is reached. According to the Fick law, the coupled fluxes of cations (J_i) and cationic vacancies (J_V) can be written (Philibert,1991; (Kofstad, 1972; Farhi, 1978):

$$J_V=-\Sigma J_i=-\tilde{D}\ (dx_V/dz) \qquad (15)$$

where $\tilde{D}$ is the chemical diffusion coefficient

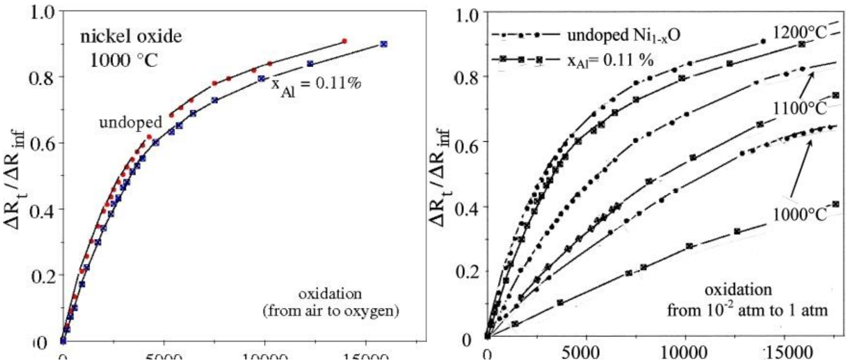

Figure 4. Re-equilibration kinetic of undoped and Al-doped $Ni_{1-x}O$ single crystals after an abrupt change of P_{O2}, followed by electrical conductivity measurements.

The results are reported in figure 4. They show that aluminium leads to a decrease of the oxidation rate. They are then in agreement with Eq.11. Indeed, after the change of P_{O2}, a kinetic demixing of cations occurs in the oxide. This leads to an enrichment of Al^{3+} in the side of the sample with a low concentration of cationic vacancies (Fig 2), i.e. near the surface exposed to a low P_{O2} (Eq.1) The two terms of Eq.11 have then opposite signs, leading to a decrease of v_{oxid}. Therefore, the agreement of Eq.11 with our results (Fig.4) shows that the kinetic demixing have a market influence on the oxydation rates of a p-type multi-component oxide.

On the other hand, the general relation of the electrical conductivity as a function of time ($\sigma(t)$) follows an exponential law. When the time increases, i.e. when the sample starts to reach its equilibrium condition, it was demonstrated that only the first term of this relation subsists (Farhi, 1978):

$$\frac{\sigma(t)-\sigma_\infty}{\sigma_0-\sigma_\infty}=\left(\frac{8}{\pi^2}\right)^3\exp\left[-\pi^2\left(\frac{1}{H^2}+\frac{1}{L^2}+\frac{1}{l^2}\right)\tilde{D}t\right] \qquad (16)$$

where *H*, *L*, *l* are the sample dimensions, σ_0 the electrical conductivity before the equilibrium conditions are changed (t=0) and σ_∞ the conductivity when the new equilibrium is reached.

The chemical diffusion coefficient was then determined from the last linear part of the representations]:

$$\log(\sigma(t)-\sigma_{\infty}) = f(t)\,. \qquad (17)$$

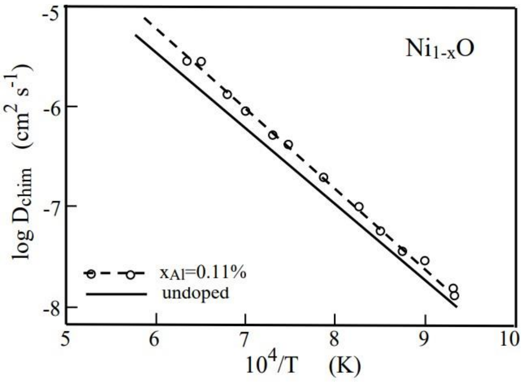

Figure 5. Influence of Al^{3+} on the chemical diffusion coefficient of $Ni_{1-x}O$. Comparaison with the values obtained with undoped $Ni_{1-x}O$.

The results obtained with the doped single crystal are reported in figure 5, together with the data determined for undoped $Ni_{1-x}O$ [15]. They show that Al^{3+} increases the oxidation kinetic of $Ni_{1-x}O$. Furthermore, these representations have the form of an Arrhenius equation (D=Do.exp(-□H/kT) (Philibert, 1972), which means that only one diffusion mechanism is dominant, as confirmed by the following results. Indeed, taking into account that the kinetic demixing processes are negligible in the last part of the representations $\log(\sigma(t)-\sigma_{\infty}) = f(t)$, it was shown that the chemical diffusion coefficient of undoped and Al-doped $Ni_{1-x}O$ single crystals can be expressed by the relation (Mahiouz, 2019) :

$$\tilde{D} \approx (1+\alpha)D_V \qquad (18)$$

where D_V is the diffusion coefficient of the cationic vacancies ($V_M^{\alpha'}$) and □ their mean charge.

Furthermore, since the mean charge of the cationic vacancies does not change significantly for doped and undoped single crystals at higher P_{O2} ($P_{O2} \geq 10^{-2}$atm, □≈1.17±0.03 at 1000°C), it follows:

$$D_V(\text{Al-doped NiO}) > D_V(\text{undoped NiO}) \qquad (19)$$

In addition, these results show that the increase of the diffusion coefficient of Ni^{2+} (Eq.6) observed in Al-doped $Ni_{1-x}O$ (Fig.1), explained previously by an increase of the concentration of cationic vacancies (Eq.2), is also due to an increase of the diffusion coefficient of the cationic vacancies (Eq.19).

Influence of Al on Nickel Oxidation

Experimental Results

The metal specimens were sintered from high purity Johnnson Mattey powders (Ni/99.99%, Al/99.50%), isostatically pressed at 1000bar, and sintered at 1100°C during 3h, under an Ar/H_2 atmosphere) (Halem, 2016). The obtained samples were then oxidized at 1250°C, during 30h. The oxide scale was removed on one main surface (1cm^2). This face was then slightly polished to a 1□m diamond finish. The experiments were performed in a Setaram thermobalance.

The results reported in figure 6 show the oxidation rate for pure and Ni-Al (0.5 wt %) polycrystalline coupons (1cm^2 by 0.1cm thick) from 700° to 1200°C, under P_{O2}=1atm. X-Ray analyses indicate that the scale developed on the samples were $Ni_{1-x}O$. Furthermore, in agreement with the Wagner theory Wagner, 1951),(Kofstad , 1988) , the results follow a parabolic law. The diffusion processes through the oxidation layer are then rate determining and the weight gain per unit area (Δm/s) can be expressed by Wagner (1951) and Kofstad (1988)

$$(\Delta m/s) = k_p \sqrt{t} + k_s \tag{20}$$

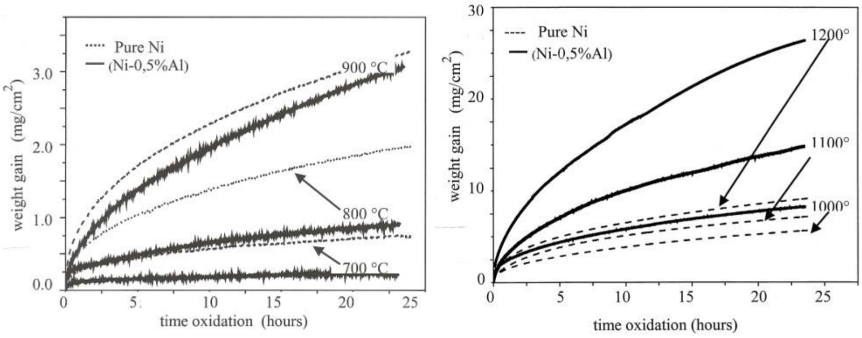

Figure 6. Isothermal weight gain versus time for Ni and Ni-(0.5%) Al alloy, under PO2=1atm

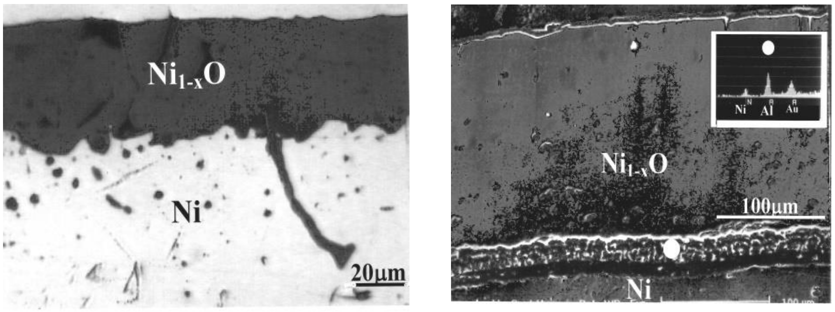

a) b)

Figure 7. Cross-sections (a) of Ni and (b) of Ni-(0.5%) Al after oxidation at 1200°C and EDAX analysis in the inner alloy oxidation layer.

At T<1000°C, the presence of Al leads (Fig.6) to a decrease of the oxidation rates in agreement with both, the results obtained with undoped and Al-doped $Ni_{1-x}O$ single crystals (Fig.4) and those obtained by Stott and Wood with Ni-(0.5 to 4 wt%) Al alloys (Stott,1977). Furthermore, cross section observations (Fig.7a) highlight an irregular nickel/oxide interface and an internal oxidation which pins the scale to the substrate.

At higher temperatures, it was found that the Ni-Al alloy oxidises faster than nickel and the oxide layer shows a duplex structure (Fig.7b), with columnar outer grains whose size increases with temperature. EDAX analyses reveal an enrichment of Al in the inner layer (Fig.7b). These results are in agreement with those obtained by Stott and Wood (Stott,1977). It should be noted that they are also in agreement with both, SIMS analyses (Atkinson, 1989) performed in layer grown on a Ni-(0.1 wt%) Cr alloy and EPMA profiles in layer grown on a Ni-(20%) Cr alloy (Atkinson, 1989), which also show an increase concentration of Cr in the inner oxidation scale. Furthermore, optical microscopy observations show that the oxidation scale on the Ni-Al alloy was not convoluted at all and did not really adhere to the metal, as was also observed by Stott et al (Stott,1977) and by Atkinson et al (Atkinson, 1989).

Discussion

In the present work, we have shown that the Ni-Al alloy oxidises more slowly than nickel, at T<1000°C, in agreement with the results obtained in the stability range of undoped and Al-doped $Ni_{1-x}O$ single crystals. The alloy oxidation kinetic is then governed by transport processes in the oxidation layer, i.e by the kinetic demixing of cations (Eq.9), which leads to both, a lower concentration of aluminium (Eq.12) and a decrease of D_{Ni} (Fig.2, Eq.5) in the outer oxidation scale.

At T≥1000°C, the oxidation scale grows faster than on high-purity Ni. One can recall both, that bulk diffusion in the oxide scale is dominant at high temperature and that oxygen grain boundary diffusion is too low to account for the observed influence of Al^{+3} (Kofstad, 1972). We have then considered a much faster transport mechanism than diffusion, such as the transport of oxygen molecules along fissures formed within the oxide, as suggested by Atkinson et al (1989, 1983). One can recall that these authors have investigated the mobility of oxygen during the growth of oxidation layers on high purity Ni and on dilute Ni-Cr alloys, whose properties of the oxidation layers are closes to those on Ni-Al alloys (Halem, 2016). From sequential tracer oxidation experiments ($^{16}O_2$ and $^{18}O_2$) and secondary ion mass spectrometry (SIMS) analyses, they have found a large ^{18}O peak in the inner oxidation layer, showing an extensive penetration of the scale by the oxygen isotope, involving the transport of O_2 molecules along open channels, likely generated by compressive stresses attributed to NiO precipitates observed at room temperature in grain boundaries. We have confirmed this assumption taking into account the results obtained with both, undoped and doped $Ni_{1-x}O$ single crystals and oxidation scales grown on Ni-Al alloys. Indeed, it was shown both, that diffusivity of Ni^{2+} in $Ni_{1-x}O$ decreases with the amount of Al^{3+} (Fig.1, Eq.5) and that cation kinetic demixing processes occur in the growing oxidation scale (Fig.7b), leading to a lower concentration of Al^{3+} in the outer layer. Consequently, this depletion of Al^{3+} leads to a blocking effect on the diffusion of Ni^{2+} in the outer oxidation layer (Fig.7), causing a local excess of Ni. This promotes the formation of new oxide units in grain boundaries, leading to compressive stresses and the formation of fissures, whereby oxygen gas penetrates within the scale. It follows an increase concentration of cationic vacancies within the scale and an higher flux of these defects arriving at the metal/oxide interface, leading to an higher outward diffusion of Ni^{2+} responsible to an increase of the oxidation rate.

On the other hand, cross sections of oxidized samples (Fig 7) show different interface morphologies. These changes can be explained by an increase of the alloy oxidation rate. Indeed, the higher arrival of cationic vacancy at the metal/oxide interface prevents the metal/oxide interface to accommodate easily these defects, improving the formation of voids. In addition, a compressive stress appears at the interface due to the volume increase of the oxidation layer. These two coupled effects may then cause a low adherence at the metal/oxide interface, leading to a breakaway during cooling (Fig.7b).

Conclusion

In this work, we have analysed the thermal oxidation of Ni and of Ni-Al alloys, taking into account the thermodynamic and transport properties of undoped and Al-doped $Ni_{1-x}O$, single crystals. At T<1000°C, it was shown that the dilute Ni-Al alloy oxidises slower than nickel, in agreement with oxidation results obtained in the stability range of undoped and Al-doped $Ni_{1-x}O$ single crystals. A formal treatment has allowed us to show that the beneficial effect of Al can be explained by cation kinetic demixing processes in the oxidation layer, leading to both, a lower concentration of Al and a decrease of D_{Ni} in the outer layer. At higher temperatures, the oxidation scale grows faster on Ni-Al alloys than on high purity nickel. The transport of oxygen molecules along fissures was then suggested to explain these results. According to an ealier work performed with Ni-Cr alloys, we have assumed that their formation can be induced by compressive stresses in the growing oxide layer, generated by the formation of oxide units in grain boundaries observed at room temperature. The formation of these oxide units are due to both, the lower values of the diffusion coefficient of nickel when the concentration of Al^{+3} decreases and the depletion of Al^{+3} in the outer oxidation scale, resulting from cation kinetic demixing processes in the growing oxide layer. These oxide units generate compressive stresses and the formation of open channels whereby oxygen gas penetrates within the scale, leading to a faster outward diffusion of Ni^{2+}, responsible to a higher alloy oxidation rates. Furthermore, the penetration of oxygen in the scale also allows to explain the alloy/oxide interphase morphology, which does not adhere really and show a breakaway after cooling.

Scientific Ethics Declaration

The authors declare that the scientific ethical and legal responsibility of this article published in EPSTEM journal belongs to the authors.

Acknowledgements or Notes

* This article was presented as a poster presentation at the International Conference on Basic Sciences and Technology (www.icbast.net) held in Antalya/Turkey on November 16-19, 2023.

References

Atkinson, A. (1983). *Corrosion mass transport in solids* (p.97). M. Benniere & A. Catlow Eds., Plenum Press.

Atkinson, A., Hugues, A.E., & Hammou, A. (1981). The self diffusion of Ni in undoped and Al-doped NiO single crystals, *Philosophical Magazine A, 43(5)*, 1071-1091.

Atkinson, A., & Smart, D .W. (1989). Transport of nickel and oxygen during the oxidation of nickel and dilute nickel/chromium alloys. *Journal of Elec. Chem. Society*, *135*, 2886-2893.

Ben Abderrazik, G. (1986). *Mécanismes de croissance d'oxydes sur les alliages Fe-Cr-Al et Ni-Cr*. (Doctoral dissertation).Université Paris XI .

Catlow, A., & Mackrodt, W. (1986). *Non stoichiometric compounds, advances in ceramics* (4th ed., Volume 23). Defense Technical Information Center.

Farhi, R., & Petot-Ervas, G. (1978). Electrical conductivity and chemical diffusion coefficient measurements in single crystalline nickel oxide at high temperature. *Journal of Physical Chem. of Solids, 39*(11), 1169-1179.

Halem, Z., Halem, N., Abrudeanu, M., & Petot Ervas, G. (2016). Transport properties of Al or Cr–doped nickel oxide relevant to the thermal oxidation of diluted Ni-Al and Ni-Cr alloys. *Sol State Ionics, 297*, 13-18.

Kofstad, P. (1988) . *High temperature corrosion* (pp.382-385). Elsevier Applied Science.

Kofstad, P. (1972). *Diffusion and electrical conductivity in binary oxides*, Nonstoichiometry Wiley-Inter science

Kofstad, P., & Norby, T. (2007). *Defects and transport in crystalline solids* (pp.7-13). University of Oslo. Retrieved from https://www.uio.no

Mahiouz, H., Halem, Z., Halem, N., & Petot Ervas, G. (2019). Transport properties of Ce-doped nickel oxide and relevance to the oxidation of CeO_2-coated-nickel, *Solid State Ionics, 339,* 114943.

Monceau, D., Petot, C., & Petot Ervas, G. (1991). Kinetic demixing profile calculation in oxide solid solutions under a chemical potential gradient. *Sol.St.Ionics*, *45* , 231-235.

Monceau. D., Filal, M., Tebtoub., M, Petot , C., Petot Ervas, G. (1994) . kinetic demixing of ceramics in an electrical field. *Solid State Ionics, 73*, 221-225.

Petot-Ervas, G., & Petot, C. (1990). The influence of impurities segregation phenomena on the oxido-reduction kinetic of oxides. *Journal of Physical Chem. of Solids,51*(8), 901-906.

Philibert, J. (1991). *Atom movements, editions de physique.* Les Ulis, France.

Schmalzried, H. (1981). *Solid state reactions* (2nd ed.). Florida, Basel.

Schmalzried, H. (1986). Behavior of (semiconducting) oxide crystals in oxygen potential gradients. *Reactivity of Solids, 1,117*-137.

Schmalzried, H., &Laqua, W. (1981). Multicomponent oxides in oxygen potential gradients. *Oxidation of Metals, 15,* 339-353.

Simlowitch, G., & Stubican, V. (1984). Transport in nonstoichiometric compounds. *NATO ASI, series B, Physics*, *129.*

Stott, F.H., & Wood, G.C. (1977). The mechanism of oxidation of dilute Ni-Al alloys at 800-1200°C. *Corrosion Science*, *17*, 647-670.

Wagner, C. (1951). *Atom movements.* Cleveland: American Ceramic Society for Metals.

Wood, G.C., & Hodgkiess, T. (1966). Oxidation of dilute Ni, Cr alloys, at 700-1200°C. *Nature*, *211*,1358-1361.

Author Information

Nacer Halem
University Mouloud Mammeri
Tizi Ouzou, Algeria
Contact e-mail: nacer.halem@ummto.dz

Zohra Halem
University of Bouira
Bouira, Algeria

Petot Ervas Georgette
Centrale Supelec
Paris, France

To cite this article:

Halem, N., Halem, Z., & Georgette P.E. (2023). Thermal oxidation kinetics of nickel and dilute (Ni- Al) alloys. *The Eurasia Proceedings of Science, Technology, Engineering & Mathematics (EPSTEM), 25,* 187-195.